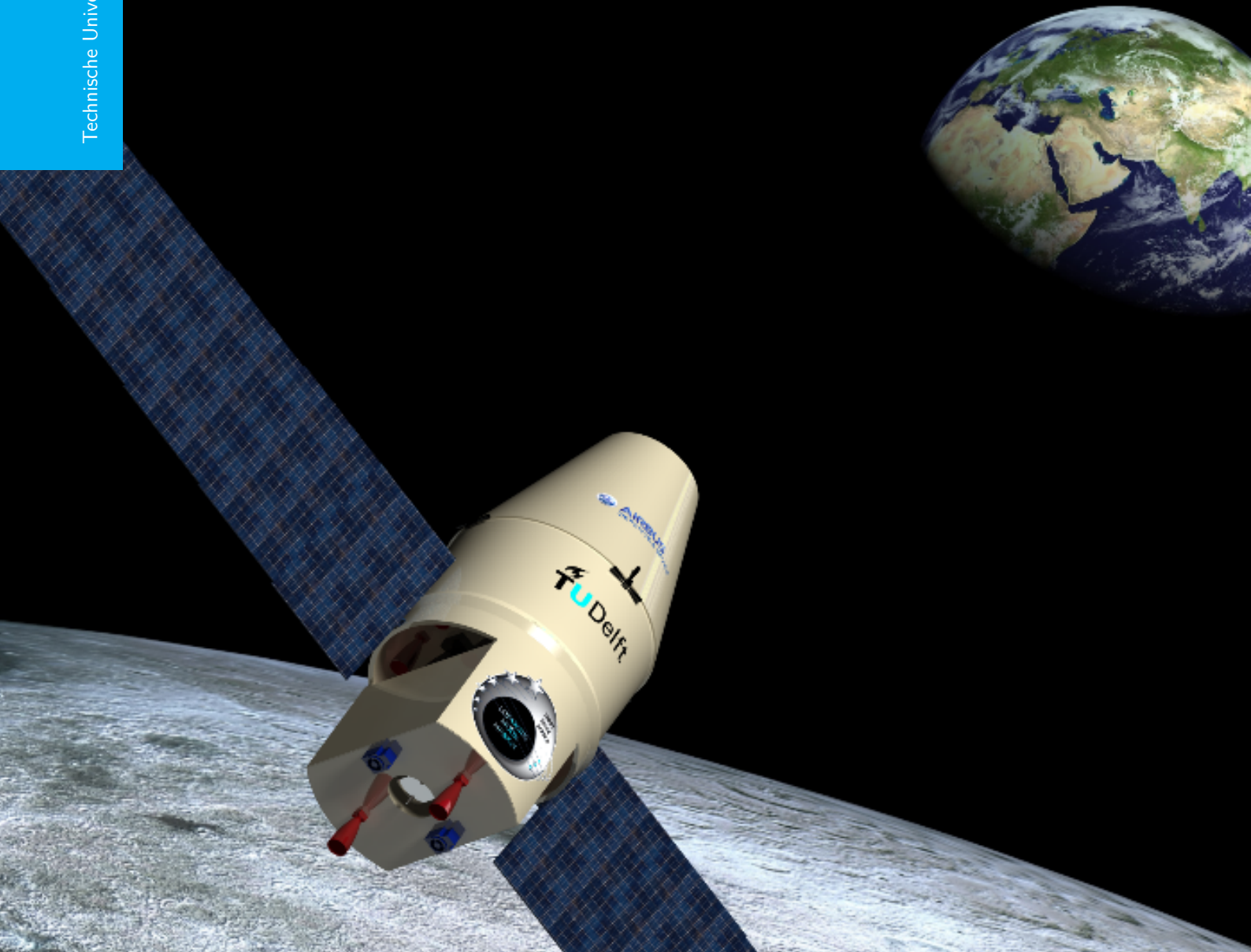


# LOFARside

## Final Report - Version 3.1

K. Bossenbroek	1515411	F. Hogervorst	4134486
W. Bouma	4023803	O. Mazouz	4147146
A. Dorozsmai	4152778	M. Ortega	4152409
A. Gorbatenko	4159888	T. Vergoossen	4089626
N. Hadžisejdić	4190785		

Technische Universiteit Delft





# LOFARSIDE

FINAL REPORT - VERSION 3.1

by

**K. Bossenbroek, W. Bouma, A. Dorozsmai, A. Gorbatenko, N. Hadžisejdić, F. Hogervorst, O. Mazouz, M. Ortega, T. Vergoossen**

as part of the

**Design Synthesis Exercise (DSE)**

in BSc. Aerospace Engineering

at Delft University of Technology

Tutor:	Ir. M. C. Naeije	TU Delft/AS
Coaches:	Ir. K. J. Cowan	TU Delft/SSE
	Dr. M. Gallo	TU Delft/FPP
Client:	Ir. H. J. Cruijssen	Airbus D&S

# CHANGE RECORD

<b>Issue</b>	<b>Date</b>	<b>Pages affected</b>	<b>Brief description of change</b>
1.0	16-12-2014	all	Draft version
2.0	16-01-2015	all	Changed report structure
3.0	21-01-2015	all	All chapters
3.1	27-01-2015	Front cover, 19, 63,109-112, 125-127	Front cover, Electric propulsion, Telecommunications, Cost Estimation, Recommendations

# SUMMARY

The Delft Space Agency (DSA) has secured a contract with Airbus Defence & Space to place a Low Frequency radar Array (LOFAR) system on the far side of the Moon. Using the moon as a shield against Earth's ionosphere enables measuring low frequency radiation dating from the Dark Ages of the Universe. Primary scientific interests are 21 [cm] cosmology and extragalactic surveys. Apart from this, reflections of radiation by the lunar regolith using a Langmuir probe, mass flow and energy balance characteristics of the top layer of lunar soil and the possibility of conducting other scientific research are offered to companies or educational institutions in return for funding. The most important top-level constraints are the use of the VEGA launcher, a budget of 500 [M€], a transfer time of maximum 1 year and an array baseline of at least 10 [km]. This report presents the final design for a mission concept as part of the Design Synthesis Exercise of the Bachelor Aerospace Engineering at the Delft University of Technology. It is preceded by a project plan, baseline report and midterm report. The different subsystems of the mission concept are designed in detail, the performance of the concept is analysed and the mission's viability and feasibility is assessed.

The satellite will be launched using ESA's VEGA launcher. The structural subsystem is designed to withstand launch loads and vibrations while complying with the specified frequency domain. After launch the satellite will use an electrical propulsion system to spiral out from its 300 [km] low earth orbit with an inclination of 16° to the Moon's sphere of influence. 46 [m<sup>2</sup>] solar panels will provide the system with power during the transfer. Active and passive thermal control systems will regulate the temperature within the spacecraft and 8 control momentum gyroscopes and 16 chemical thrusters will control its orientation. During the transfer phase two helical antennas mounted on opposite sides of the body will provide continuous communication with Ground Control. Using a chemical thruster the satellite will be inserted into a lunar orbit, where it will spiral down with low thrust propulsion to a polar orbit at 100 [km]. The lander will decouple from the transfer orbiter Spilaio, which will be crashed in a controlled manner on the near side of the Moon. The lander Noor will land on the rim of the Shackleton crater at the south pole of the Moon using chemical propulsion. The accuracy to be able to land on the crater rim of about 100x100 [m<sup>2</sup>] is achieved using terrain relative navigation in combination with multiple sensors. Landing struts designed for a drop from 3 [m] will be deployed for landing.

The lander, situated at a position of almost continuous illumination and visibility with Earth, will deploy a tethered rover based on NASA's Axel rover design that will descend into the crater's eternal darkness. It will deploy 10 [km] of cable and 21 antennas over unequal distances powered by the lander's solar panels of 6.9 [m<sup>2</sup>]. Using a thermal knife the crossed dipole antennas will deploy and after calibration can start their surveys. The deployed antennas will form a virtual array with a baseline of 10 [km] using aperture synthesis. The data will be sent via a direct radar communications link to Earth for processing and analysis. A high-gain parabolic antenna with a diameter of 0.7 [m] operating in X-band will be used for the downlink data transmission of 84 [Mbit/s]. Uplink transmission for commands will be received using a helical antenna with a 0.055 [m] diameter and 0.1 [m] length operating in S-band.

Cost analysis has indicated that the project can be completed for a budget of 400.9 [M€]. Up to 60 [M€] could be supplied by companies and educational institutions in return for taking their instruments to the Moon. Recommendations about the effect of top level requirements conclude mainly that a shared launch using Ariane 6 into a Geostationary Transfer Orbit (GTO) could reduce the mass of the electric power system needed for electrical propulsion because a large part of the Van Allen belts would be skipped. This could also allow for a longer transfer time, as the damage to system components due to space exposure is reduced.



# PREFACE

This is the Final Report (FR) for the project *LOFAR on the far side of the Moon* as part of the Design Synthesis Exercise (DSE) from TU Delft. Here, a detailed design process is presented. The group would like to express their appreciation to Marc Naije, Henk Cruijssen, Kevin Cowan and Mauro Gallo for their collaboration and guidance. They have always advised the group towards the correct design attitude. We would also like to acknowledge the advice provided by Ron Noomen, Dominic Dirx, Leonid Gurvits, Lucas Antignac and Remco van der Heijden. Their input was very valuable in finishing the preliminary design process and further development.

*Delft, January 2015*



# CONTENTS

<b>List of Symbols</b>	<b>xi</b>
<b>List of Abbreviations</b>	<b>xii</b>
<b>1 Introduction</b>	<b>1</b>
<b>2 LOFARside Mission Overview</b>	<b>2</b>
2.1 Mission Need and Purpose Statement . . . . .	2
2.2 Constraints . . . . .	2
2.3 Mission Overview . . . . .	2
2.4 Functional Analysis . . . . .	3
2.4.1 Functional Flow Diagram . . . . .	3
2.4.2 Functional Breakdown Structure . . . . .	3
<b>3 Mission Characteristics</b>	<b>6</b>
3.1 Launch and Transfer . . . . .	6
3.1.1 Launch . . . . .	6
3.1.2 Orbit . . . . .	6
3.2 Decoupling and Disposal of Spílaio . . . . .	8
3.3 Two stage landing reconsideration . . . . .	8
3.4 Deployment and Rover Design . . . . .	9
3.4.1 Antenna and Baseline configuration . . . . .	9
3.4.2 Scientific Payload . . . . .	10
3.4.3 Location of LOFAR . . . . .	10
3.4.4 Rover . . . . .	10
3.5 Operation . . . . .	11
3.6 Summary . . . . .	11
<b>4 Astrodynamic characteristics and Simulation tools</b>	<b>13</b>
4.1 Astrodynamic Characteristics . . . . .	13
4.1.1 Keplerian Elements . . . . .	13
4.1.2 Eclipse definitions . . . . .	13
4.2 Simulation tool . . . . .	14
<b>5 Landing site</b>	<b>15</b>
5.1 Determination of landing site . . . . .	15
5.2 Illumination conditions . . . . .	16
5.2.1 Illumination Pattern . . . . .	16
5.2.2 Variations in Illumination Profile over Time . . . . .	17
<b>6 Propulsion Subsystems</b>	<b>19</b>
6.1 Electrical Propulsion . . . . .	19
6.2 Chemical propulsion . . . . .	19
6.2.1 Chemical propulsive system . . . . .	19
6.2.2 Landing . . . . .	21
6.2.3 Hovering . . . . .	27
6.2.4 Mass and time budgets . . . . .	28
6.2.5 Volume Tanks . . . . .	28
6.2.6 Validation & Verification . . . . .	29
<b>7 Electrical Power Subsystem</b>	<b>30</b>
7.1 Power Budgets . . . . .	30
7.1.1 Transfer Phase . . . . .	30
7.1.2 Landing, Deployment and Operation Phase . . . . .	31
7.2 Generation . . . . .	31
7.2.1 Transfer Phase . . . . .	31
7.2.2 Landing, Deployment and Operation Phase . . . . .	32

7.2.3	Solar Cell and Efficiency . . . . .	32
7.2.4	Solar Flux . . . . .	33
7.2.5	Incidence Angle . . . . .	34
7.2.6	Inherent Degradation . . . . .	35
7.2.7	Life Degradation . . . . .	35
7.2.8	Temperature Effect. . . . .	37
7.2.9	Power Production Capability: BOL and EOL . . . . .	39
7.2.10	Area, Mass and Cost of Solar Array . . . . .	40
7.3	Energy Storage . . . . .	40
7.3.1	Battery Types . . . . .	40
7.3.2	Battery Sizing . . . . .	41
7.3.3	Regenerative Fuel Cells . . . . .	42
7.4	Power Management and Distribution . . . . .	43
7.4.1	Power Distribution. . . . .	43
7.4.2	Power Regulation . . . . .	44
7.5	Structural Element of Noor's Solar Array . . . . .	45
7.5.1	Location and Configuration of the Solar Cells on Noor . . . . .	45
7.5.2	Protection of the Solar Cells on Noor. . . . .	46
7.6	Verification and Validation . . . . .	46
<b>8</b>	<b>Attitude Determination and Control Subsystem</b>	<b>47</b>
8.1	ADCS Requirements . . . . .	47
8.2	Equations of Motion . . . . .	47
8.3	S/C Geometric Properties . . . . .	48
8.4	Disturbance Torques . . . . .	49
8.4.1	Gravity Torque . . . . .	49
8.4.2	Solar Pressure Torque . . . . .	49
8.4.3	Magnetic Torque . . . . .	50
8.4.4	Total Torque . . . . .	50
8.5	Transfer Phase ADCS Design . . . . .	50
8.5.1	Simplified Equations of Motion . . . . .	51
8.5.2	Actuators. . . . .	52
8.5.3	Sensors . . . . .	53
8.6	ADCS Block Diagram . . . . .	54
8.7	Verification & Validation . . . . .	54
<b>9</b>	<b>Telecommunication Subsystem</b>	<b>55</b>
9.1	Analysis for different the mission phases . . . . .	55
9.1.1	Telemetry . . . . .	55
9.1.2	Command . . . . .	55
9.1.3	Tracking . . . . .	56
9.1.4	Elements of Communication system. . . . .	56
9.2	Approach . . . . .	56
9.3	Transfer phase . . . . .	56
9.3.1	Antenna design options . . . . .	56
9.3.2	Setting up the budget link . . . . .	57
9.3.3	Closing the budget link . . . . .	59
9.4	Mission phase. . . . .	59
9.5	System overview . . . . .	62
9.6	Verification and Validation . . . . .	63
<b>10</b>	<b>Command and Data Handling Subsystem</b>	<b>65</b>
10.1	Command and Data Handling . . . . .	65
10.2	On-Board Computer . . . . .	68
<b>11</b>	<b>Guidance and Navigation Subsystem</b>	<b>70</b>
11.1	Transfer navigation . . . . .	70
11.2	Transfer guidance. . . . .	70
11.3	Landing navigation . . . . .	70
11.4	Terrain relative navigation methods. . . . .	71
11.5	TRN trade-off . . . . .	71
11.6	Navigation architecture . . . . .	74

11.7	Hazard detection and avoidance . . . . .	74
11.8	TRN implications on trajectory . . . . .	75
11.9	Verification and validation . . . . .	75
<b>12</b>	<b>Moon Rover Subsystem</b>	<b>76</b>
12.1	Power required for deployment and end-of-life disposal . . . . .	76
12.1.1	Lagrange equations of motion for single wheel on slope . . . . .	76
12.1.2	Validation of the model . . . . .	77
12.1.3	Application to Shackleton crater . . . . .	77
12.2	Cable design and tension considerations . . . . .	77
12.2.1	Power and data rate implications . . . . .	78
12.2.2	Cable tension considerations . . . . .	78
12.2.3	Cable environment . . . . .	78
12.3	Sizing of the Rover . . . . .	78
12.3.1	Rover navigation and control . . . . .	79
12.3.2	Thermal control . . . . .	79
12.3.3	Rover Configuration . . . . .	80
<b>13</b>	<b>Thermal Control Subsystem</b>	<b>81</b>
13.1	Required Operating Temperature Range . . . . .	81
13.2	Transfer Phase Thermal Control . . . . .	81
13.2.1	Thermal Environment . . . . .	81
13.2.2	Thermal Equilibrium . . . . .	83
13.2.3	Thermal Strategy. . . . .	84
13.3	Lunar Station Thermal Control . . . . .	86
13.3.1	Lunar Thermal Environment. . . . .	86
13.3.2	Thermal Strategy. . . . .	88
13.4	Verification & Validation . . . . .	88
<b>14</b>	<b>Structures and Mechanisms Subsystem</b>	<b>89</b>
14.1	Spacecraft. . . . .	89
14.1.1	S/C Configuration . . . . .	89
14.1.2	Material . . . . .	90
14.1.3	Structural parameters . . . . .	90
14.1.4	Loads . . . . .	93
14.1.5	Verification and Validation procedures. . . . .	96
14.2	Solar panels. . . . .	97
14.3	Landing struts. . . . .	97
<b>15</b>	<b>Performance analysis</b>	<b>100</b>
15.1	Performance parameters . . . . .	100
15.2	Compliance matrix & Feasibility analysis . . . . .	100
15.3	Sensitivity analysis . . . . .	102
15.3.1	Sensitivity towards transfer time . . . . .	102
15.3.2	Sensitivity towards array baseline . . . . .	102
15.3.3	Sensitivity towards number of antennas . . . . .	102
15.3.4	Sensitivity towards location on the Moon . . . . .	103
<b>16</b>	<b>Future developments</b>	<b>104</b>
16.1	Project design & development logic . . . . .	104
16.2	Production Plan. . . . .	104
<b>17</b>	<b>Project Management</b>	<b>108</b>
17.1	Resource Allocation . . . . .	108
17.2	Cost Analysis . . . . .	109
17.2.1	TRANSCOST Cost Estimation Method . . . . .	109
17.2.2	Unmanned Space Vehicle Cost Model . . . . .	109
17.2.3	NASA Instrument Cost Model . . . . .	112
17.2.4	Cost Estimation Overview . . . . .	112
17.3	RAMS . . . . .	112
17.4	Risk Management. . . . .	113
17.4.1	Midterm Risk management evaluation. . . . .	113
17.4.2	Risk assessment . . . . .	115

---

17.4.3 Project risk analysis . . . . .	115
17.4.4 Project risk mitigation . . . . .	116
17.4.5 System Risk analysis . . . . .	116
17.4.6 System risk mitigation . . . . .	117
<b>18 Market Analysis</b>	<b>119</b>
18.1 Secondary Instruments . . . . .	119
18.2 Additional instruments trade-off . . . . .	120
18.3 Required financial contribution. . . . .	121
<b>19 Sustainable Development Strategy</b>	<b>122</b>
19.1 Sustainable project management . . . . .	122
19.2 Economic & Social development . . . . .	122
19.3 Sustainable design choices . . . . .	123
<b>20 Conclusions and Recommendations</b>	<b>124</b>
20.1 Conclusions. . . . .	124
20.2 Evaluation of Top Level Requirements . . . . .	125
20.3 Recommendations on Future Work. . . . .	125
<b>A Configuration</b>	<b>128</b>
<b>Bibliography</b>	<b>133</b>

# LIST OF SYMBOLS

Symbol	Definition	Unit	Symbol	Definition	Unit
$\alpha$	Thermal expansion coefficient	$K^{-1}$	$L_d$	Life degradation	–
$\alpha_{1/2}$	Antenna half-power beamwidth	$^\circ$	$L_{fs}$	Loss for wireless propagation	$dB$
$\gamma$	Temperature coefficient	$mW/K$	$L_{pr}$	Antenna pointing loss	$dB$
$\eta$	Efficiency	–	$L_l$	Loss factor of the transmitter	$dB$
$\theta$	Sun incidence angle	$^\circ$	$L_r$	Reception feeder loss	$dB$
$\lambda$	Wavelength	$m$	$L_s$	Space loss	$dB$
$\mu$	Standard gravitational parameter	$km^3s^{-2}$	$L_t$	Loss factor of the receiver	$dB$
$\rho$	Density	$kg/m^3$	$m$	Mass	$kg$
$\sigma$	Stress	$Pa$	$\dot{m}$	Mass flow	$kg/s$
$\Phi$	Solar constant	$W/m^2$	$P$	Transmitted power	$W$
$\omega$	Argument of periapsis	$rad$	$P$	Pressure	$Pa$
$\omega$	Angular velocity	$rad/s$	$P_{cr}$	Critical buckling load	$N$
$\Omega$	Right ascension of ascending node	$rad$	$R$	Radius	$m$
$A$	Surface area	$m^2$	$R$	Data rate	$bits/s$
$A$	Amplitude	$m$	$R$	Universal gas constant	$kJ/kg \cdot K$
$a$	Semi-major axis of an orbit	$km$	$S$	Solar flux	$W/m^2$
$C$	Battery capacity	$Whr$	$SNR$	Signal to Noise ratio	$dB$
$C$	Cost	€	$s$	Slant height	$m$
$c_{sa}$	Specific cost	€/W	$T$	Thrust	$N$
$c$	Speed of light in vacuum	$ms^{-1}$	$T$	Temperature	$K$
$D$	Antenna diameter	$m$	$t$	Skin thickness	$m$
$E$	Young's modulus	$Pa$	$t$	Time	$s$
$e$	Orbital eccentricity	–	$V$	Volume	$m^3$
$F$	Force	$N$	$V$	Potential energy	$J$
$f$	Frequency	$Hz$	$v$	Velocity	$m/s$
$F.S.$	Factor of safety	–	$\mathcal{L}$	Lagrangian	$m^2/s^3$
$G_r$	Gain of the receiving antenna	$dB$			
$G_t$	Gain of the transmitting antenna	$dB$			
$g$	Gravitational acceleration on Earth	$m/s^2$			
$H$	Angular momentum	$kg \cdot m^2/s$			
$H$	Height of the cylinder	$m$			
$h$	Height	$m$			
$I$	Area Moment of inertia	$m^4$			
$I$	Mass moment of inertia	$kg \cdot m^2$			
$I_{sp}$	Specific Impulse	$s$			
$i$	Orbital inclination	$^\circ$			
$K$	Kinetic energy	$J$			
$k$	Boltzmann constant	$m^2kg/s^2/K$			
$k$	Stiffness	$N/m$			
$L$	Length	$m$			

# LIST OF ABBREVIATIONS

<b>AGE</b>	Aerospace Ground Equipment	<b>LLCD</b>	Lunar Laser Communication Demonstration
<b>AOCS</b>	Attitude Orientation and Control System	<b>LLO</b>	Low Lunar Orbit
<b>BER</b>	Bit Error Rate	<b>LNA</b>	Low Noise Amplifier
<b>BOL</b>	Beginning-of-Life	<b>LO</b>	Local Oscillator
<b>BPSK</b>	Binary Phase Shift Keying	<b>LOFAR</b>	LOW Frequency ARray
<b>C&amp;DH</b>	Command & Data Handling	<b>LOOS</b>	Launch Operations & Orbital Support
<b>CERs</b>	Cost Estimating Relationships	<b>LP</b>	Long Period
<b>CMG</b>	Control Momentum Gyroscope	<b>LP1</b>	Leibnitz- $\beta$ Plateau
<b>CNES</b>	The Centre National d'Études Spatiales	<b>MANS</b>	Microcosm Autonomous Navigation System
<b>CoG</b>	Centre of Gravity	<b>MIMU</b>	Miniature Inertial Measurement Unit
<b>CPU</b>	Central Processing Unit	<b>MLI</b>	Multi Layer Insulator
<b>CR1</b>	Connecting Ridge	<b>MMH</b>	Monomethylhydrazine
<b>CSC</b>	Computer Software Component	<b>MP1</b>	Malapert Mountain 1
<b>CSH</b>	Centre Spatial Guyanais (Guiana Space Centre)	<b>MP2</b>	Malapert Mountain 2
<b>D-BPSK</b>	Differential Binary Phase Shift Keying	<b>MUPUS</b>	Multi Purpose Sensor Package
<b>DACU</b>	Data Acquisition and Control Unit	<b>NASA</b>	National Aeronautics and Space Administration
<b>DC</b>	Downconverter	<b>NiCd</b>	Nickel Cadmium
<b>DET</b>	Direct-Energy-Transfer	<b>NICM</b>	NASA Instrument Cost Model
<b>DOD</b>	Depth of Discharge	<b>NiH2</b>	Nickel Hydrogen
<b>DSA</b>	Delft Space Agency	<b>NiMH</b>	Nickel Metal Hybrid
<b>DSP</b>	Digital Signal Processing	<b>OBDH</b>	On-Board Data Handling
<b>ECC</b>	Eccentricity	<b>OCB</b>	On-Board Computer
<b>EDRS</b>	European Data Relay System	<b>OSR</b>	Optical Solar Reflector
<b>EMS</b>	Electromagnetic Sounding	<b>PCI</b>	Peripheral Component Interconnect
<b>EOL</b>	End-of-Life	<b>PPT</b>	Peak-Power Tracker
<b>EPS</b>	Electrical Power Subsystem	<b>RAAN</b>	Right ascension of the ascending node
<b>ESA</b>	European Space Agency	<b>RAR</b>	Radio Astronomy Receiver
<b>FPGA</b>	Field Programmable Gate Array	<b>RF</b>	Radio Frequency
<b>GaAs</b>	Gallium Arsenide	<b>RFCS</b>	Regenerative Fuel Cells
<b>GaInP</b>	Gallium indium Phosphide	<b>RFDU</b>	Radio Frequency Distribution Unit
<b>GCRs</b>	Galactic Cosmic Rays	<b>RMS</b>	Root-mean-square
<b>Ge</b>	Germanium	<b>RTG</b>	Radioisotope Thermoelectric Generator
<b>GMAT</b>	General Mission Analysis Tool	<b>S/C</b>	Spacecraft
<b>GNC</b>	Guidance and Navigation Control	<b>SEP</b>	Solar Energetic Proton
<b>GPS</b>	Global Positioning System	<b>SLOC</b>	Source Lines of Code
<b>GRI</b>	de Gerlache crater	<b>SLR</b>	Satellite laser ranging
<b>H/K</b>	Housekeeping	<b>SP</b>	Short Period
<b>HDA</b>	Hazard Detection and Avoidance	<b>SPENVIS</b>	SPace ENVironment Information System
<b>HPA</b>	High Power Amplifier	<b>SR1</b>	Shackleton Rim
<b>HPBW</b>	Half Peak Beamwidth	<b>SSPA</b>	Solid State Power Amplifier
<b>HRN</b>	Hazard Relative Navigation	<b>SSR</b>	Solid State Recorder
<b>I/O</b>	Input/Output	<b>STK</b>	System Tool Kit
<b>IA&amp;T</b>	Integration, Assembly and Testing	<b>SWPs</b>	Solar Wind Particles
<b>IMU</b>	Inertial Measurement Unit	<b>TA</b>	True Anomaly
<b>INC</b>	Inclination	<b>TRL</b>	Technology Readiness Level
<b>INS</b>	Inertial Navigation System	<b>TRN</b>	Terrain Relative Navigation
<b>IPGP</b>	Institut de Physique du Globe de Paris	<b>TT&amp;C</b>	Telemetry, Tracking and Command
<b>LADEE</b>	Lunar Atmosphere and Dust Environment Explorer	<b>TWTA</b>	Traveling Wave Tube Amplifier
<b>LEO</b>	Low Earth Orbit	<b>USCM8</b>	Unmanned Space Vehicle Cost Model
<b>Li-ion</b>	Lithium ion	<b>UTC</b>	Coordinated Universal Time
<b>LIDAR</b>	Light Detection And Ranging	<b>VEGA</b>	Vettore Europeo di Generazione Avanzata

# 1

## INTRODUCTION

This report presents the final design for a mission concept as part of the Design Synthesis Exercise of the Bachelor Aerospace Engineering at the Delft University of Technology. In this introduction some background information, the system design approach and the structure of the report are explained.

### BACKGROUND INFORMATION

As a rising star in commercial space flight, the Delft Space Agency (DSA) has secured a contract by Airbus Defence & Space to place a LOW Frequency ARray (LOFAR) radar system on the far side of the Moon. Using the Moon as a shield against Earth's ionosphere enables measuring low frequency radiation dating to the early stages of the Universe. Primary scientific interests are 21 [cm] cosmology and extragalactic surveys. Apart from this, reflections of radiation by the lunar regolith using a Langmuir probe, mass flow and energy balance characteristics of the top layer of lunar soil and the possibility to conduct other scientific research are offered to companies or educational institutions in return for funding. This report is preceded by a project plan, baseline report and midterm report. In the project plan the team's structure was set up and the project outline and planning derived. The baseline report presented the Team's efforts to understand the scientific background as well as the derivation of system level requirements from top level constraints and their implications on the mission. In the midterm report the different design options were analyzed and after trade-offs a mission concept was presented. This final report presents the detailed design of this concept, conclusions thereof and recommendations for future work.

### SYSTEM DESIGN APPROACH AND RESTRICTIONS

The systems design approach over the whole project started with the derivation of system level requirements from the mission need and top level constraints. Based on these requirements different design options were found and analyzed such that a trade-off to select the most optimal mission concept could be conducted. Now, the different subsystems of this concept are analyzed in enough detail to prove feasibility of the overall design. Each member of the team has designed a specific technical aspect of this mission. Project management allocates resources and implements deadlines to ensure that each team member works effectively and any bottlenecks are identified quickly and managed accordingly. All resource restrictions with respect to the work force and time scheduling must always be controlled by the project manager, who will ensure that deadlines are met. The systems engineer is responsible for the integration of the different subsystems and makes sure that concurrently designed subsystems are using the right values. The iterative nature of the design process is facilitated by the systems engineer.

### STRUCTURE OF THE REPORT

The report gives an overview of the LOFARside mission in Chapter 2, including mission need and project statement, constraints, project design and development logic and functional analysis, flow diagrams and breakdown structure. The characteristics of the mission in the form of a detailed breakdown of the different mission phases are given in Chapter 3. Information on astrodynamics characteristics and the simulation of the transfer are described in Chapter 4 and the decision on landing site is explained in Chapter 5. The detailed design of the different subsystems is presented in the next chapters. Chapter 6 details the propulsion subsystems, both electric and chemical. The power system used for the electrical propulsion, as well as the landing, deployment and operations phase is designed in Chapter 7. The Telecommunication systems and the Command & Data handling subsystem are presented in Chapter 9 and Chapter 10, respectively. Chapter 8 and Chapter 11 present the design of the Attitude Determination and Control and the Guidance and Navigation subsystems. The design of the rover which is used to deploy the antennas on the Moon is explained in Chapter 12 followed by the design of the Thermal Control and Structures subsystems in Chapter 13 and Chapter 14, respectively. A performance analysis of the mission concept is conducted in Chapter 15. Based on the design detail, future developments are given in Chapter 16. The complete project management, from resource allocation to risk management is given in Chapter 17. A market analysis aimed at generating funds for the project is described in Chapter 18, followed by the sustainable development strategy applied throughout the project in Chapter 19. Conclusions and recommendations, including an evaluation of the top level requirements and their effect on the mission design are detailed in Chapter 20. Finally, the appendices and a bibliography are included.

## LOFAR SIDE MISSION OVERVIEW

In this chapter an overview of the mission is presented which aims to place a LOw Frequency radar ARray (LOFAR) on the far side of the Moon. First the mission need and purpose statement are given (Section 2.1), after which the mission overview is discussed (Section 2.3). The chapter concludes with a description of the functional analysis of the LOFAR side mission (Section 2.4).

### 2.1. MISSION NEED AND PURPOSE STATEMENT

The electromagnetic spectrum has been observed at almost all wavelengths, which has supplied mankind with a wealth of information. Observations on Earth are limited by the absorption of certain wavelengths by Earth's atmosphere. Even outside the atmosphere measurements are limited by Earth's ionosphere. Low frequency electromagnetic radiation can not be observed under these conditions. Understanding the origins of the Universe requires analyzing signals emitted in that time. These signals over time have been red-shifted towards low to very low frequencies. Thus, in order to understand these Dark Ages of the Universe, low frequency radio astronomy is required. The Moon is tidally locked with Earth and so its far side is always protected from Earth's disturbing influence by the Moon. It also provides a very stable surface on which to measure. Therefore, the ideal place for low frequency radio astronomy is the far side of the Moon. The LOFAR side mission's purpose is to:

'Place a LOFAR antenna system on the far side of the Moon to avoid interference of the Earth's ionosphere and unwanted electromagnetic waves to observe low frequency radiation from the Dark Ages of the Universe'

### 2.2. CONSTRAINTS

A number of constraints are given by the client, Airbus Defense & Space, for which the mission is designed. The most important top level constraints are:

- Use of ESA's VEGA launcher
- 500M € Budget
- Transfer time of maximum 1 year, mission lifetime of 5 years
- Baseline of 10-100 [km] and a maximum amount of antennas distributed in a favourable fashion
- Primary propulsion preferably based on Electrical Propulsion
- Use of off-the-shelf technology and hardware with a Technology Readiness Level (TRL)  $\geq 5$

The effect of these constraints on the mission design is defining. Use of the VEGA launcher limits the mass that can be launched in a Low Earth Orbit (LEO) to about 2300 [kg] and makes using a Geostationary Transfer Orbit (GTO) impossible. In combination with desired large baselines and number of antennas this means that the payload mass on the surface of the moon must be maximized. As such, these are identified as driving requirements, and their effect is monitored to ensure it is not a killer requirement. The use of electrical propulsion facilitates this mass optimization, while use of off-the-shelf technology and hardware and the use of the VEGA launcher are implemented to keep the cost of the mission as low as possible. A complete list of system requirements and their respective effects is given in the baseline report of this project [1]. Proof of compliance of the mission concept with system requirements is given in Section 15.2.

### 2.3. MISSION OVERVIEW

The mission concept that was derived from system requirements at the midterm level is explained in this section. After launch by the VEGA launcher the satellite will use its electric propulsion system to spiral out from its 300 [km] low earth orbit with inclination of 16° to the Moon's sphere of influence. It will use thermal control and physical protection to protect the system from space exposure like temperature extremes and the Van Allen radiation belts.

Using a chemical thruster it will insert into a lunar orbit, after which it will switch back to electric propulsion and spiral down to a polar orbit at 100 [km]. The lander will land on the rim of the Shackleton crater at the south pole of the moon with a very high accuracy of 100 by 100 [m] using Terrain Relative Navigation. The lander, situated at a position of almost continuous illumination and visibility with Earth, will deploy a tethered rover based on NASA's Axel rover design that descends into the crater's eternal darkness. It will deploy 10 [km] of cable and 21 antennas over unequal distances powered by the lander's solar panels. Using a thermal knife the crossed dipole antennas will deploy and after calibration can start their surveys. The data gathered will be used through radar interferometry and aperture synthesis to create a virtual very large radar array. The data is sent via a direct radar communications link to Earth for processing and analysis.

Based upon the Allegory of the Plato's Cave names have chosen for the Mother-ship, the Lander and the Rover. The names are Spílaio (cave), Noor (enlightenment) and Colbí (citizen of the town of darkness), respectively. Throughout the report these names will be used to refer to the specific mission segment.

## 2.4. FUNCTIONAL ANALYSIS

The mission has to be decomposed into different phases in order to have a planned, timed and structured flow of the activities and actions that need to be undertaken. These activities and the constraints set on these activities will set requirements on the system for which design options have to be found. In this section these functions are determined using two tools; the functional flow diagram and the functional breakdown structure.

### 2.4.1. FUNCTIONAL FLOW DIAGRAM

The functional flow provides a schematic view of the actions that need to be performed during the mission. It is a chronological flow of the functions of the system and helps evaluate and design the required subsystems. In Figure 2.1 the LOFAR functional flow is presented.

### 2.4.2. FUNCTIONAL BREAKDOWN STRUCTURE

Another view on the work to be performed can be presented in the form of a functional breakdown structure. The identified elements are based on the functional flow diagram and are ordered hierarchically. The functional breakdown structure can be found in Figure 2.2.

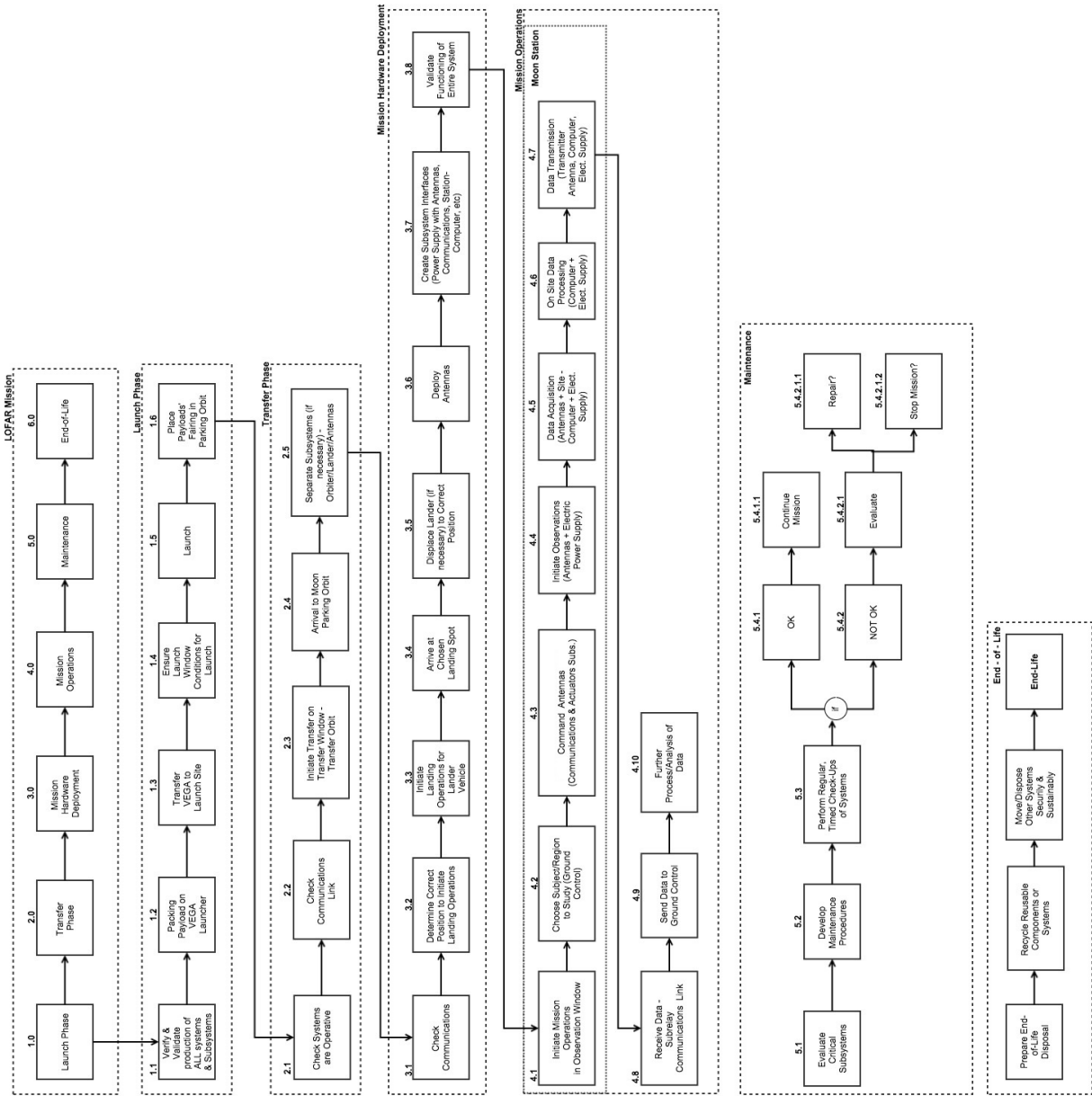


Figure 2.1: Functional Flow Diagram LOFAR

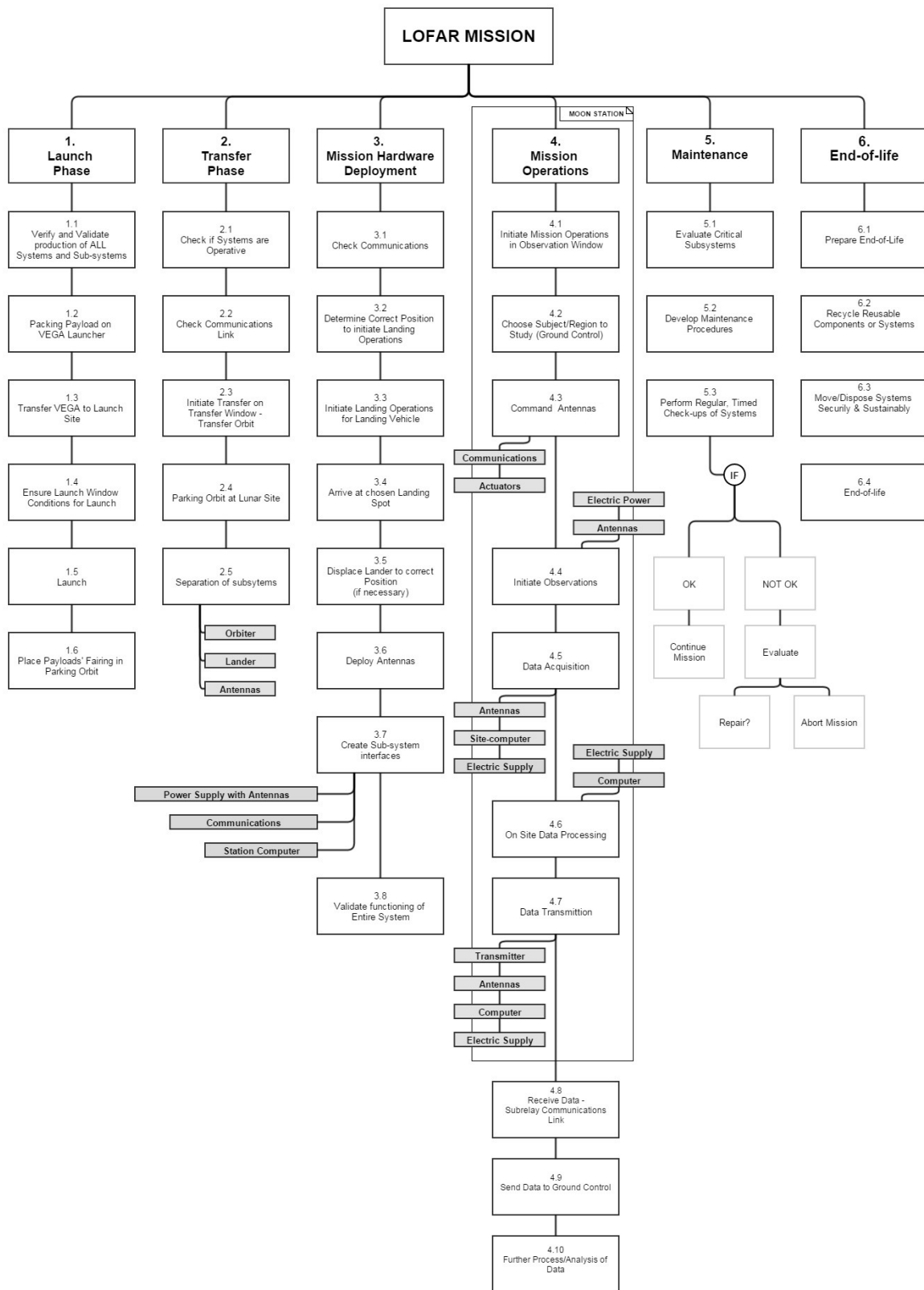


Figure 2.2: Functional Breakdown Structure LOFAR

## MISSION CHARACTERISTICS

This chapter gives an overview of the mission concept and its most important characteristics. An overview of the launch and transfer (Section 3.1) decoupling and disposal of the Spílaio (Section 3.2), two staged landing (Section 3.3), deployment and rover design (Section 3.4), and operations phase (Section 3.5) is given. The chapter ends with a summary of all important mission characteristics (Section 3.6).

### 3.1. LAUNCH AND TRANSFER

In this section the design for the mission from launch to Low Lunar Orbit is described. First the launch will be described and then the orbit will be explained.

#### 3.1.1. LAUNCH

The spacecraft (S/C) is launched on 26 November 2021 11:59, Coordinated Universal Time (UTC), from the Guinana Space Centre (French Guiana). It is launched with the Vettore Europeo di Generazione Avanzata (VEGA) launch vehicle into a Low Earth Orbit (LEO) at an altitude of 300 [km]. The orbit has an inclination of  $16.7^\circ$  with the equator. The combination of inclination and altitude gives an S/C mass of 2280 [kg] [2, pp.2-7].

#### 3.1.2. ORBIT

The mission is simulated in two parts; Phase 1 and Phase 2. A simulation in two phases has the advantage that a change in parameters for Lunar capture can be simulated quicker. This saves simulation time compared to a simulation where the full orbit is simulated on each iteration. More information on the simulation can be found in Chapter 4.

The simulation of Phase 1 includes the transfer from LEO at an altitude of 300 [km] up to an altitude of 200,000 [km] with respect to Earth. At this altitude the perturbations of the orbit due to the Moon are negligible as can be seen in Figure 3.1, this makes the shape of the orbit independent from the launch date and can therefore be simulated independently from Phase 2. Figure 3.1 shows a 100 day propagation of satellites in circular orbit at 3 different altitudes. It can be seen that higher altitudes have much higher perturbations due to the Moon and cannot be simulated independently.

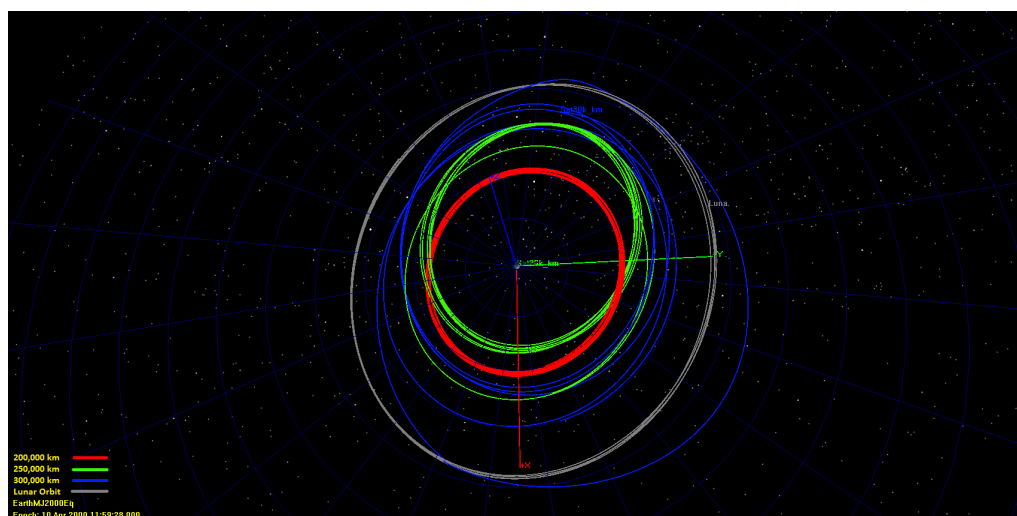


Figure 3.1: Orbit perturbation for a 100 day propagation of Earth Orbits at different altitudes

Phase 2 starts at a 200,000 [km] altitude from Earth and ends at Low Lunar Polar orbit. In the simulation the burn time of the low thrust engine, the inclination ( $i$ ), true anomaly (TA) and the right ascension of the ascending node ( $\Omega$ ) at 200,000 [km] altitude are varied. The trajectory is targeted at  $20,000 \pm 1,000$  [km] Lunar altitude and an inclination of  $90 \pm 0.1^\circ$  with the Lunar equator. Higher target altitudes will encounter more perturbations for the low thrust braking spiral which can be seen in Figure 3.2. However lower altitudes will increase the Delta-V of the Lunar capture burn. An altitude of around 20,000 [km] showed the best results for the final mass and eccentricity.

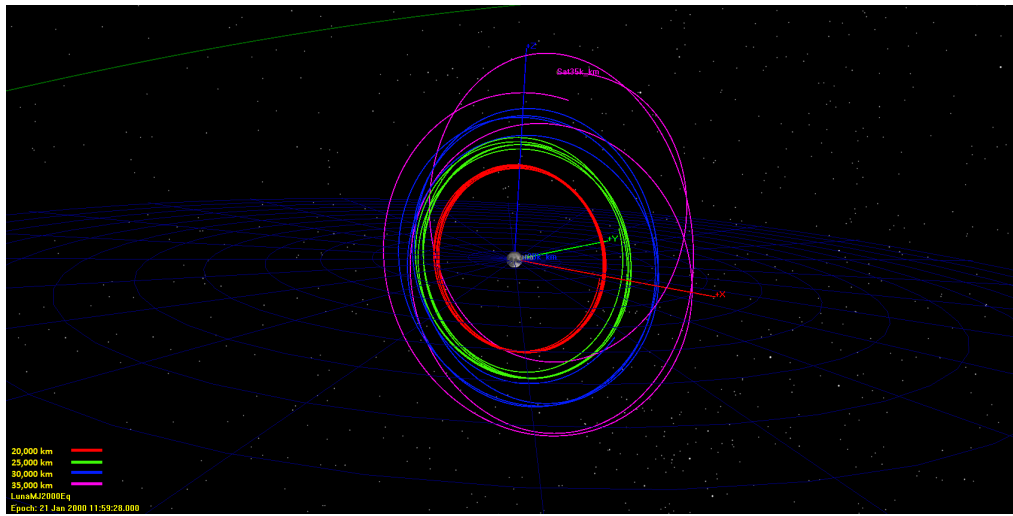


Figure 3.2: Orbit perturbation for a 20 day propagation of Lunar Polar Orbits at different altitudes

When the S/C arrives at  $20,000 \pm 1,000$  [km] Lunar altitude and an inclination of  $90 \pm 0.1^\circ$  a Lunar capture manoeuvre is performed with an additional chemical thruster with a thrust of 350 [N]. Using an additional thruster for the capture manoeuvre simplifies the Lunar capture during simulation. Low thrust captures are too complicated and are out of the scope of this study. A low thrust capture should be investigated in the future since it could increase the S/C mass in Low Lunar Orbit. However, it will probably limit the launch window since the configuration of the Earth, Moon and S/C becomes more important.

Different starting dates for Phase 2 were evaluated to find the best launch date. The starting dates are distributed over the last five months of 2022, this will result in a launch date somewhere at the end of 2021 or begin 2022 and is assumed to provide enough time for the development of the mission. The results of the different starting dates are shown in Table 3.1.

Date	5-8-22	3-8-22	2-8-22	1-10-2022	2-10-2022	10-10-2022	9-11-22	12-11-2022	13-11-22	15-11-22	10-12-22
Final Mass (kg)	1613	1622	1578	1606	1614	1581	1588	1592	1596	1598	1611
LEO INC (deg)	16.619	14.555	12.670	16.490	13.899	16.588	13.729	17.437	14.304	13.607	16.625
LEO RAAN (deg)	14.00	14.00	14.00	14.00	14.00	14.00	14.00	14.00	14.00	14.00	14.00
LEO TA (deg)	-122.11	-126.49	-107.25	-91.42	-71.03	-81.24	-108.93	-63.40	-39.11	-39.45	-82.94
Delta V Burn (km/s)	-0.095	-0.088	-0.165	-0.093	-0.102	-0.136	-0.149	-0.131	-0.134	-0.141	-0.087
Time (Days) (no eclipse)	70.48	58.78	56.80	73.14	62.78	80.48	40.36	45.76	43.43	43.58	57.03
LLO INC (deg)	88.502	77.424	87.434	87.071	88.173	88.851	87.252	86.227	87.156	88.530	86.315
LLO RAAN (deg)	25.58	266.33	306.96	322.88	100.15	143.32	298.28	219.16	210.76	214.66	335.49
LLO ECC (-)	0.305	0.391	0.397	0.148	0.357	0.154	0.393	0.320	0.377	0.466	0.236
Altitude Perilune (km)	101.09	97.80	101.22	100.95	104.33	107.73	100.30	100.95	94.98	95.49	-22.15

Table 3.1: Transfer options for Phase 2,  $I_{sp} = 2350$  [s],  $T = 0.55$  [N]

The starting date for Phase 2 is chosen to be the first of October 2022. This date showed the lowest eccentricity and a small Delta-V for the capture manoeuvre. It should be noted that all options are suitable for the mission and the mission could be launched at any day in the year.

### ECLIPSES

During eclipse the S/C is designed to shut down its engines to reduce the weight of the batteries. To calculate the total transfer time an estimation for the eclipse duration is needed. The eclipse duration is calculated and is subsequently added to the transfer time results of the simulation for Phase 1 and 2. This can be done since the orbit of the S/C during a spiraling transfer is approximately circular at all times [3]. Therefore, if the S/C is in eclipse, it continues a circular orbit until it is illuminated again and it continues its outwards spiral.

For the calculation of the eclipse duration of Phase 1 and Phase 2 use is made of AGI's System Tool Kit (STK) 10. In

NASA's General Mission Analysis Tool (GMAT), orbital data was exported as an ephemeris file and loaded into STK. Here it was analyzed for lighting times of the S/C. For Phase 1 it resulted in a Penumbra time of 0.8194 [days] and an Umbra time of 35.9377 [days]. For Phase 2 the results were 0.1225 and 0.1945 [days] for Penumbra and Umbra times respectively. (For the definition of Penumbra and Umbra see Chapter 4)

### COMPLETE TRANSFER ORBIT

The orbital parameters of the S/C in LEO and in LLO are given in Table 3.2. Furthermore, the mass of the S/C during its transfer can be found in Table 3.3. It also shows the propellant mass used in the segments of the transfer. A graphical representation of the complete transfer can be seen in Figures 3.3, 3.4a and 3.4b.

	$i$ [deg]	$e$ [-]	$\Omega$ [deg]	$\omega$ [deg]	$a$ [km]
LEO	16.7	0.00	14.0	0.0	6679
LLO	85.6	0.18	195.0	355.0	2230

Table 3.2: Orbital Parameters for initial LEO orbit and final LLO

	LEO	Start Phase 2	Start Capture burn	End Capture burn	LLO
Mass S/C [kg]	2280	1659	1647	1575	1497
$M_{propellant}$ [kg]	-	621	12	72	78
Epoch	26 Nov 2021	1 Oct 2022	27 Oct 2022	30 Oct 2022	26 Nov 2022

Table 3.3: Masses during transfer

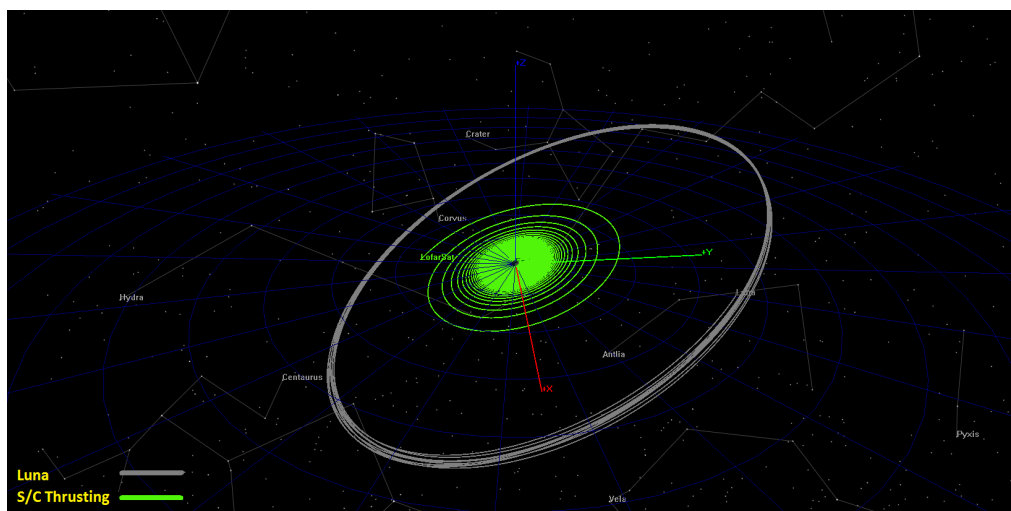


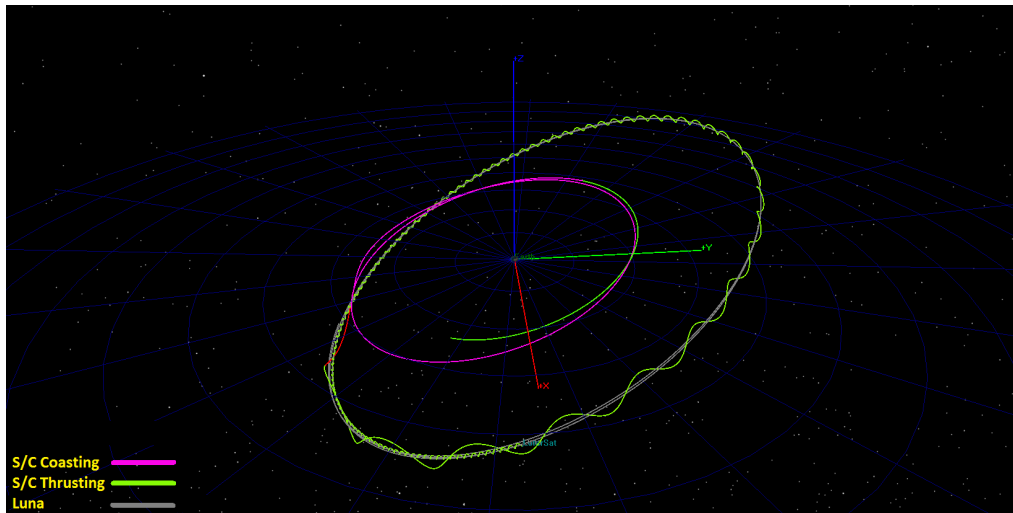
Figure 3.3: Graphical representation Phase 1

## 3.2. DECOUPLING AND DISPOSAL OF SPÍLAIO

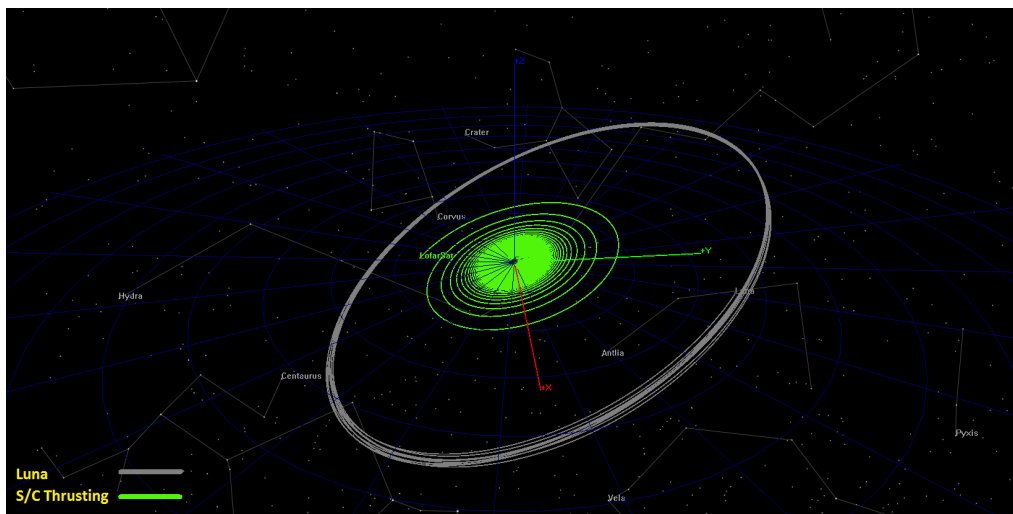
When the spacecraft (S/C) arrives at a 100 [km] circular Low Lunar Orbit Spílaio is decoupled from Noor. Noor then initiates its de-orbital burn and Spílaio is kept in a 100 [km] circular Lunar orbit. After Noor has landed and the system is deployed, Spílaio starts its de-orbital burn using low thrust propulsion and is targeted to crash on the near side of the Moon which is not an interesting place for future missions [4]. Spílaio is de-orbited to clear the Lunar orbit for future missions. The crash could also be used for investigating the lunar surface if seismographs are taken on-board Noor. The de-orbit manoeuvre commands are predetermined before decoupling and will be executed at a predetermined time. This is done since Spílaio itself doesn't feature sensors for real time attitude determination.

## 3.3. TWO STAGE LANDING RECONSIDERATION

In the Mid-term report a trade-off was presented regarding a single stage and two stage landing. The latter won, however at the start of the detailed design phase an overlooked error was found in the code on which this trade-off



(a) Earth Reference Frame



(b) Moon Reference Frame

Figure 3.4: Graphical representation Phase 2

was based. A wrong constant was filled into a statistical Mass Estimating Relation (MER) resulting in an undersized estimate of S/C mass without fuel and payload (in this case called dry mass). Correcting the error decreased the available payload. Further limitations on payload mass were set by a smaller S/C mass in lunar parking orbit as a result from the transfer orbit determination. The benefits on payload mass for two stage landing become relatively worse at lower overall S/C masses. Re-running the MER code resulted in a payload mass of 190 [kg] for single stage landing and 220 [kg] for two stage landing. This benefit on payload mass with a two stage landing was considered to be too small compared to the system complexity and risk it would induce into the design. Therefore the concept was dropped and a single stage landing was chosen for further analysis.

### 3.4. DEPLOYMENT AND ROVER DESIGN

The low frequency radar array will be deployed in the Shackleton crater on the South Pole of the Moon using a rover based on NASA's Axel rover. An analysis of possible science topics and talks with radio astronomy experts has led to an antenna and baseline configuration. The location and nature of the array and the deployment method are explained in this section.

#### 3.4.1. ANTENNA AND BASELINE CONFIGURATION

Different antenna and baseline configurations correspond to different scientific topics. The choice of configuration is dependent on technical and radio astronomical constraints.

A fundamental constraint in radio observations comes from the presence of free electrons in the Interplanetary

Medium (IPM) and in the Interstellar Medium (ISM). The plasma frequencies of these mediums do not exceed 20-30 [KHz] [5]. The most serious consequences of these free electrons are foreground mission, free-free absorption and scattering of waves in turbulent regions [5]. Furthermore, the resolution of the array has to be matched to the density of sources at the instrument's sensitivity to avoid confusion [5]. The baseline is determined by ratio between the detected wavelength and the required angular resolution. The number of antennas depends on the desired integration time, the surface brightness of the source and the sky temperature. The sensitivity is constrained by the surface brightness temperature of the sky. Based on these relations, the requirements in terms of baseline, required integration time and number of antennas can be derived for each possible science mission [5].

The payload mass that is available on the surface of the Moon gives an upper constraint on the number of antennas that can be brought along. However, distributing the antennas over larger baselines will likely lead to a heavier solution. The maximum payload mass of 216 [kg], which includes all other systems necessary for mission operation, means that it is not likely that more than 100 antennas can be taken along. Taking into account technical constraints such as mass and power and discussions with Professor Gurvits about the scientific benefits a baseline of 10 [km] and 21 antennas were chosen. With respect to scientific topics, there was no clear benefit of taking 100 antennas instead of 21.

Primary scientific goals are:

- to measure the red-shifted 21 cm hydrogen line from the Dark Ages of the Universe and from the Epoch of Reionization (EoR).
- to conduct extragalactic surveys.

A secondary objective is to determine the conditions for 21 cm cosmology observations (such as foreground noise and the effect of lunar Regolith reflections on the signal). These results will provide invaluable information for a very large lunar observatory.

### 3.4.2. SCIENTIFIC PAYLOAD

The main scientific payload of the LOFARside mission are low frequency antennas. Additional scientific instruments as well as the possibility of taking payloads in return for funding are explored.

#### LOW FREQUENCY ANTENNA

For the extragalactic surveys and detection of the 21 [cm] hydrogen line from the Dark Ages, the tripole antenna designed by L. Chen [6] will be used as a crossed dipole antenna. It consists of two orthogonally placed dipole antennas, which can be deployed by a thermal knife in a tape-measure like fashion.

#### ADDITIONAL INSTRUMENTS

By taking additional instruments to the lunar surface the mission's scientific output is increased while securing additional funding. Additional instruments that could be brought to the Moon if interested companies are found are a Langmuir probe, which measures plasma parameters, and a MUPUS package, which measures physical parameters in the near-surface layers. A market analysis and the process by which the instruments were chosen is detailed in Chapter 18.

### 3.4.3. LOCATION OF LOFAR

It was decided in the midterm-report [7] that the LOFAR system will be placed in the eternally dark Shackleton crater at the South Pole on the far side of the Moon. The main considerations for this decision are

- Constant visibility with Earth or Earth-orbiting satellites enables a direct data-relay and so no relay satellite is required.
- The rim of the crater on the South pole has almost constant illumination, which means that the power unit on the rim of the crater is able to generate power almost continuously.
- The calibration of the array is very difficult. Placing the antennas in an eternally dark crater means that the calibration does not need to be repeated and is limited in difficulty. Also, the antennas do not require thermal protection against high temperatures.

### 3.4.4. ROVER

Using a trade-off the rover was selected as the most optimal deployment method. The design of the rover used is based on NASA's Axel rover, which uses a "rappelling robot concept" consisting "of two wheels connected by a central cylindrical body, a caster arm, and an actively controlled tether passing through the caster arm... The caster arm provides a reaction force against the terrain needed to generate forward motion when traveling on flat ground" [8, pp. 16]. In Chapter 12 an analysis is made of how this rover must be adapted for the LOFARside mission.

### 3.5. OPERATION

Mission operations consist of collecting data, modulating and compressing it, and sending/receiving data to/from ground control. Depending on the scientific research topics the radar array will perform different measurements. These can differ greatly in their integration time and scope. The primary scientific objectives are 21 [cm] cosmology and extra-galactic surveys. Ground control uplinks commands to the lunar station to perform surveys of the desired part of the sky with the specified integration time. The 21 antennas operate under 10 [Mhz] and after sampling and correlation this results in a data rate of 84 [Mbit/s]. This is sent to ground control stations of ESTRACK via a high-gain parabolic antenna with a diameter of 0.7 [m] using X-band frequencies. The uplink is formed using a different, smaller helical antenna with a diameter of 0.055 [m] operating in S-band. Ground control will process the received data using a supercomputer.

### 3.6. SUMMARY

A summary of the mass budgets is presented in Table 3.4. Here the subsystems have been subdivided into the three segments; the transfer segment, landing segment and the deployment segment. The subsystems that will be acting in each phase are included under their respective section in the table. Gathering with the different departments within the project, more reasonable contingency values were implemented for each subsystem. For the components whose masses were given from the suppliers, only a 1% contingency was adopted since this value is unlikely to change. On the other hand, for the calculations made by the project team members, a greater contingency was adopted. The current values of the subsystems are presented in the left column whereas the maximum values that these will ever have are given in the right column.

From the total mass of all systems, it is visible that since the VEGA launcher can only take 2280 [kg] the current launcher will not be able to carry all the components. Currently, there is an excess of 64.31 [kg] whereas it could increase up to 408.50 [kg] if contingencies are taken into account (other components that still have not been included in the mass budget). On the other hand, the DSA is confident that after optimizing the design through iteration techniques these values can be decreased to meet the VEGA launcher requirements.

Nonetheless, it is given that the VEGA-C will have a 15% increase in performance with respect to the current VEGA and a total of 2622 [kg] could be carried as payload. Therefore, there is currently an allowable extra margin of 277.68 [kg] in case things are launched with their current state. On the other hand, if the contingency is taken into account for the VEGA-C there is an excess of 66.5 [kg] that should be further optimized. This launcher would be ideal for LOFAR purposes since all components that have been analysed to be necessary would fit and even extra components that still have not been taken into account could be carried on-board.

SYSTEM	Mass [kg]			
	Allocation	Specification Value	Contingency	Maximum Value
<b>Transfer Segment</b>				
<b>Propulsion</b>				
Propellant	711.6		20%	853.92
Propellant Tank	71.16		20%	85.39
2 × E. Thrusters	23.2		5%	24.36
Total Propulsion	805.96			963.67
<b>Power</b>				
9 × Battery	9.6		15%	11.04
Solar Arrays	253		15%	290.95
Total Power	262.6			301.99
<b>Structures</b>				
Transport Vehicle	25.5		20%	30.6
Noor lander	64.4		20%	77.28
Total Structures	89.9			107.88
<b>Thermal Control</b>				
Total Passive Control	10		20%	12
<b>AOCS</b>				
10 × 22 [N] Thruster	6.5		10%	7.15
Fuel Transfer AOCS	20.63		20%	24.75

2× 200 [N] Thruster	4	10%	4.4
Fuel Braking	71.9	20%	86.28
8× CMG	147.2	10%	161.92
2× Sun Sensor	0.13	5%	0.136
2× Star Tracker	7.97	5%	8.36
MIMU	4.44	5%	4.66
Total AOCS	258.77		297.67
<b>TT&amp;C</b>			
Total TT&C	25	10%	27.5
<b>CD&amp;H</b>			
Total CD&H	5	10%	5.5
<b>GNC</b>			
Total GNC	11	20%	13.2
<b>Total Mass Before Decouple</b>	1540.18		1726.93
<b>Landing Segment</b>			
<b>Total Mass After Decouple</b>	1010.52		1110.67
<b>Propulsion</b>			
Propellant	570.7	10%	627.77
Propellant Tank	66.32	20%	79.58
4× 200 [N] Thruster	8	5%	8.4
5× 500 [N] Thruster	25	5%	26.25
Helium Pressurizer	3	20%	3.6
Total Propulsion	673.02		745.60
<b>GNC</b>			
Camera + Gimble	20	5%	21
<b>Total Landed S/C</b>	436.82		487.91
<b>Deployment Segment</b>			
<b>Allocation Specification Value</b>		<b>Contingency</b>	<b>Estimate Target</b>
<b>Payload</b>			
AXEL Rover	25	20%	30
21× Antenna	11.76	5%	12.34
10[km]×Cable	63.6	10%	69.96
Additional Payload	30	10%	33
Total Payload	205.36		145.30
<b>Power</b>			
Solar Panels	38.5	10%	42.35
2 × Battery	2.2	10%	2.42
Total Power	40.7		44.77
<b>On-Site Computer</b>			
Total	10	20%	12
<b>Thermal Control</b>			
Heater	2	20%	2.4
<b>Total Mass</b>	2344.313		2688.50
<b>Available Mass VEGA</b>	-64.31		-408.50
<b>Available Mass VEGA-C</b>	277.68		-66.50

Table 3.4: Mass Budget

# 4

## ASTRODYNAMIC CHARACTERISTICS AND SIMULATION TOOLS

Understanding the astrodynamic characteristics is essential for designing the transfer orbit. In this chapter these astrodynamic characteristics used for the simulation of the Earth Moon transfer (Section 4.1) and the simulation tool (Section 4.2) are described.

### 4.1. ASTRODYNAMIC CHARACTERISTICS

In this section the Keplerian elements are explained which will be used in the simulation. Then some information about eclipses is provided.

#### 4.1.1. KEPLERIAN ELEMENTS

Every orbit can be described with the Keplerian elements as shown in Figure 4.1. The basic elements for an orbit are the semi-major axis ( $a$ ) describing the size of the orbit and eccentricity ( $e$ ) describing the shape of the orbit, these can be seen in Figure 4.1a. The inclination ( $i$ ), is the angle between the plane of reference (in the simulations the equator) and the orbital plane and can be seen in Figure 4.1b. The argument of periapsis ( $\omega$ ), is the angle from the ascending node to the vector pointing from the centre of the central body to the periapsis of the orbit. The right ascension of ascending node ( $\Omega$ ), is the angle between the Vernal Equinox and the ascending node. The true anomaly ( $TA$ ), is the angle between the vector pointing from the centre of the central body to the periapsis and the spacecraft (S/C). The elements  $i$ ,  $\omega$ ,  $\Omega$  and  $TA$  can be seen in Figure 4.1 [3].

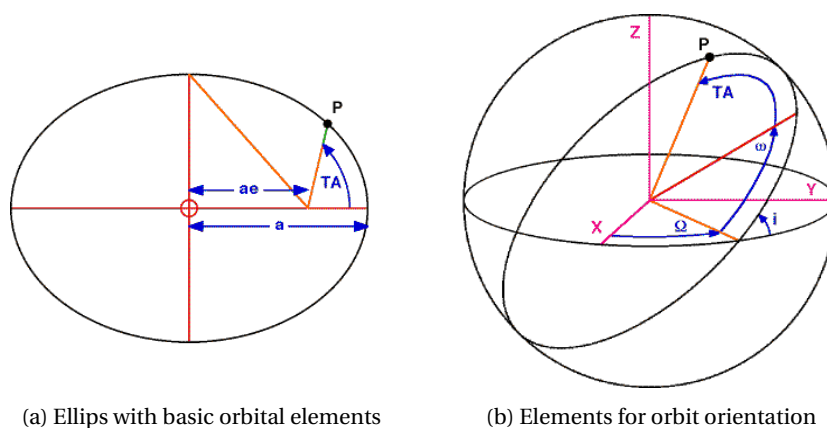


Figure 4.1: Orbital elements

#### 4.1.2. ECLIPSE DEFINITIONS

Eclipses are an important factor for a transfer with electric propulsion. The power demand of the S/C can not be satisfied during eclipse. Therefore the S/C can not thrust at full power all the time since this would require very large energy storage and this would in turn increase the weight of the S/C. Eclipses are divided into two parts, the Penumbra and the Umbra. During Penumbra the S/C is partly lit by the Sun, e.g. in Figure 4.2 if a S/C is located in the top part of the grey area near the Earth, sunlight from the top part of the sun is able to illuminate the S/C. However sunlight from the bottom part is blocked by the Earth. During Umbra the S/C has no illumination of the Sun at all. This can be seen in Figure 4.2

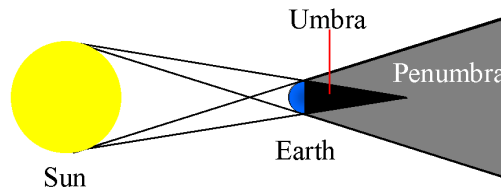


Figure 4.2: Graphical representation of (Pen)Umbral

## 4.2. SIMULATION TOOL

The transfer orbit is simulated using NASA's General Mission Analysis Tool (GMAT). This tool works similar to AGI's System Tool Kit (STK) and is open-source. GMAT is extensively verified and validated by experts from the Goddard Space Flight Center [9]. It is also flight qualified to support operational maneuver planning for the Advanced Composition Explorer (ACE) mission which is orbiting the Sun-Earth L1 point[10]. Thus it is assumed accurate enough for the simulation of the mission in this stage of the design process.

For Phase 1 the S/C is modelled in GMAT as a S/C of 2280 [kg] with a thruster attached with a thrust of 0.55 [N]. Different thrusts were investigated and showed that this is the minimum thrust needed for meeting the 1 year transfer time requirement. The engine is modelled with a specific impulse of 2024 [s] which corresponds with two SNECMA's PPS 5000 Xenon Hall Thruster at 84% thrust level as described in Section 6.1. Its initial altitude is 300 [km] as described in Section 3.1.2 and propagates until an altitude of 200,000 [km].

For Phase 2 the S/C is modelled with the same thruster as for Phase 1 and has an additional 350 [N] thruster required for the capture manoeuvre. This thruster is simulated with a specific impulse of 270 [s]. It has an initial mass of 1659 [kg] corresponding to the mass of the S/C at the end of Phase 1 and an circular orbit with an altitude of 200,000 [km]. It then targets the Moon at 20,000  $\pm$  1,000 [km] altitude and an inclination with the Moon's equator of 90  $\pm$  0.1 [deg], this is done by varying the burn time of the low thrust engine and by varying TA,  $\Omega$  and  $i$  of the initial orbit at 200,000 [km]. When this target is achieved, a high thrust burn is performed at lunar periapsis. The burn time is varied to achieve a lunar orbit eccentricity of 0  $\pm$  0.001 [deg]. From thereon the altitude is decreased by thrusting against flight direction with the low thrust propulsion until the orbit achieves an altitude of 100 [km] above the lunar surface.

For the propagation of the S/C in GMAT two propagators are used. One with the Earth as the central body, this is used for Phase 1 and the first part of Phase 2. From the lunar capture manoeuvre up to the final Low Lunar Orbit (LLO) a propagator with the Moon as central body is used. The properties of these propagators are given in Table 4.1.

	Central body Earth	Central body Luna
<b>Integrator Type</b>	RungeKutta89	RungeKutta89
<b>Accuracy</b>	1.0000e-011	1.0000e-011
<b>Error Control</b>	RSSStep	RSSStep
<b>Primary Body</b>	Earth	Luna
<b>Gravity Model</b>	JGM-2	LP-165
<b>Point Masses</b>	Luna, Sun	Earth, Sun

Table 4.1: Propagator properties used during simulation

## LANDING SITE

In this chapter the exact landing site is pinpointed (Section 5.1). Also, the illumination conditions (Section 5.2) of this landing site and their implications on the mission are discussed.

### 5.1. DETERMINATION OF LANDING SITE

The mission landing site was narrowed down to the Lunar South Pole in the Mid-term report based on considerations on lighting conditions and communication. In this section the actual landing site is determined. In [11] several regions were investigated in terms of illumination conditions, the most promising regions can be seen in Figure 5.1 also from [11]. The regions are named: Shackleton Rim (SR1), Connecting Ridge (CR1), de Gerlache crater (GR1), Malapert Mountain (MP1 and MP2) and Leibnitz- $\beta$  Plateau (LP1). For the LOFAR mission, as much sunlight as possible for the power system is preferred. However, the antennas have to be in permanent darkness. So a good site to do science is lit for most of the time and has a region a permanent darkness in the vicinity. For the landing, the landing ellipse has to be considered, it must fit within the illuminated area. In Figure 5.2 a map is shown of the Lunar South Pole with the considered locations. Red and yellow areas are permanently shadowed from the Sun. The only region that is close to an area with permanent darkness is SR1. CR1 and GR1 are approximately 20 [km] from such an area and the rest is much further.

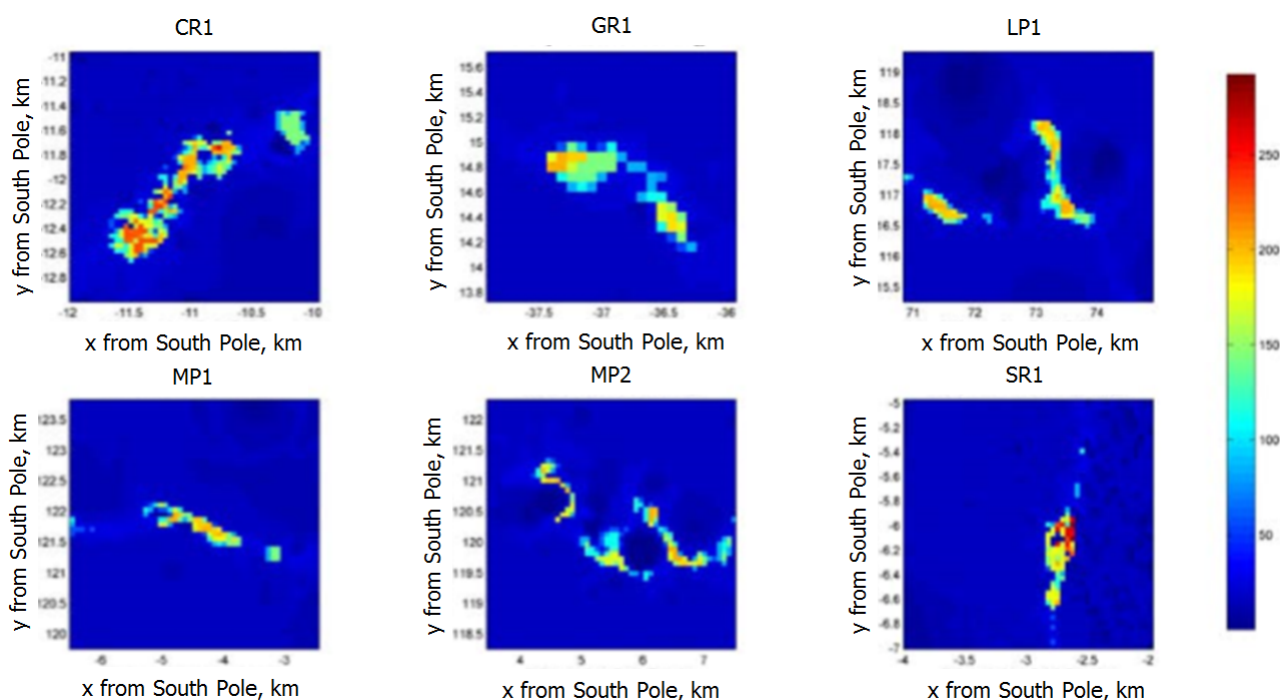


Figure 5.1: Promising locations in the South Pole region with high amounts of illumination during the Lunar year. The color code is in days.

Based on this information the Shackleton Rim is chosen as the landing site. The Connecting Ridge is an alternative that could be considered but the range of the rover would have to be high. A reason to consider CR1 is the more lenient landing requirement. However, looking at Figure 5.1 SR1 gives a required landing ellipse of approximately 600 [m] x 200 [m] which is deemed plausible from literature studies on planned future missions [12]. In Section 11.3 the actual landing is elaborated in more depth.

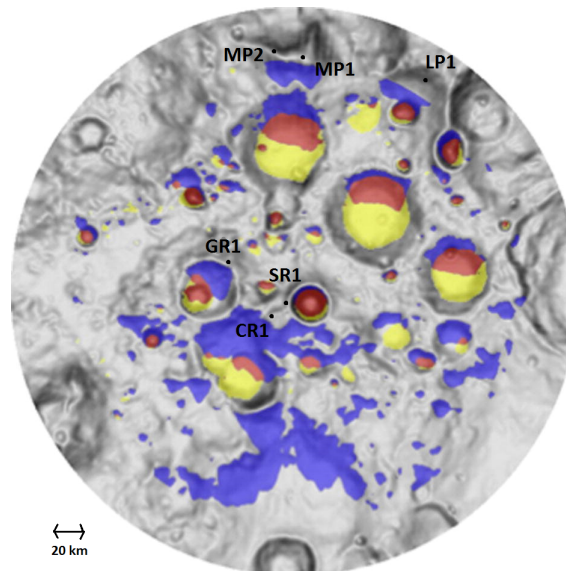


Figure 5.2: Map of Lunar South Pole showing the locations from Figure 5.1, red and yellow areas are permanently shadowed from the sun (blue and red areas are also permanently shadowed from Earth)

## 5.2. ILLUMINATION CONDITIONS

The desired landing location is on the Lunar South pole. Due to the terrain of this region, high mountains and crater rims, some locations with very long continuous light exist. To proper design the power subsystem for the Noor lander it is necessary to have a clear and precise overview of the alternation between daylight and eclipse moments. These light and darkness moments will drive the size and mass of the solar array, as well as the additional battery capacity and its associated mass. The design of the power subsystem of the Noor lander will be discussed in Chapter 7. The discussion of illumination pattern is followed by an explanation of the implications of seasonal changes.

### 5.2.1. ILLUMINATION PATTERN

The Noor lander should be designed to fully operate during eclipse periods. The best landing location is the Shackelton Rim, as discussed in Section 5.1 where the amount of days with continuous illumination is 274 [11].

At the elevated polar site, the solar illumination profile is governed by the horizon terrain instead of the orbital mechanics of the Sun-Earth-Moon system. Typically the Sun is near the horizon where it can be blocked by mountains, hills and boulders from a significant distance away [13]. This will cause irregular illumination for which the power subsystem must be designed. Therefore the amount of illumination and eclipse days per Lunar year is not enough to design the power subsystem of the Noor lander. A detailed and precise pattern of the daylight and eclipse periods is needed. For this detailed topographical maps and elevation models are necessary.

In [14] topographic information provided by the Kaguya laser altimeter was used to evaluate the illumination conditions at the Lunar South pole. The Kaguya topography was valid to use for the determination of realistic illumination conditions, because the topographical information was compared to simulated data and actual Clementine images [14]. For the year 2020 illumination maps were computed for the Lunar South pole. Furthermore the map includes the detailed locations and durations of eclipse periods for the Lunar South pole region.

The illumination profile, given in Figure 5.3, shows if the landing location, site A, is lit or dark for a variety of illumination conditions. This polar plot shows the sub-solar longitude as the angle and sub-solar latitude as the radius. From this it can be derived that the Lunar summer period is given in the center of the spiral. These data points have the most negative sub-solar latitudes. In Figure 5.3 half a lunar year is given, but because of Solar symmetry the other part of the lunar year will have the same profile [14]. Therefore it is sufficient to evaluate this illumination profile. Every small block represents half a day and the yellow and red blocks represent the Shackelton Rim. To determine the worst case that the power subsystem of the Noor lander must sustain, all eclipse moments were indicated and are also given in Figure 5.3. For every eclipse period the amount of daylight days before that specific eclipse period were obtained, as well as the amount of days of that particular eclipse. These values are given in Table 5.1. Eclipse period 1 until 4 are not of interest since there are enough illuminated days before them. To find the worst case during one Lunar year the amount of days in eclipse were divided by the amount of days of illumination.

There are three eclipse periods that are critical during the Lunar year. These are eclipse period 5, 12 and 17. These periods are the worst case the Noor lander is supposed to survive. However, when designing for these period the

Eclipse period	Eclipse [days]	Daylight [days]	Eclipse/Daylight [-]	$P_{sa}$ [W]	$A_{sa}$ [m <sup>2</sup> ]	$A_{cone}$ [m <sup>2</sup> ]
<b>5</b>	<b>3.5</b>	<b>0.5</b>	<b>7</b>	<b>1919.4</b>	<b>7.4</b>	<b>23.4</b>
6	1	5	0.2	235.3	0.9	2.9
7	0.5	2.5	0.2	235.3	0.9	2.9
8	1.5	5.5	0.27	253.3	1	3.1
9	1	1	1	433.4	1.7	5.3
10	0.5	4	0.13	216.7	0.8	2.6
11	1.5	1.5	1	433.4	1.7	5.3
<b>12</b>	<b>4</b>	<b>0.5</b>	<b>8</b>	<b>2167.1</b>	<b>8.4</b>	<b>26.4</b>
13	3	3.5	0.86	398	1.5	4.8
14	1.5	1	1.50	557.3	2.2	6.8
15	4.5	4.5	1	433.4	1.7	5.3
16	0.5	3.5	0.14	221.1	0.9	2.7
<b>17</b>	<b>6.5</b>	<b>1</b>	<b>6.5</b>	<b>1795.6</b>	<b>7</b>	<b>21.8</b>
<b>Assumptions</b>						
Eclipse Period 12	7	4.5	1.56	410.9	1.6	5.0
<b>Eclipse Period 17</b>	<b>4.5</b>	<b>1.5</b>	<b>3</b>	<b>571</b>	<b>2.2</b>	<b>6.9</b>

Table 5.1: Table with eclipse periods and the corresponding required power during daylight ( $P_{sa}$ ), the area of the solar array ( $A_{sa}$ ) and the total area of the solar array due to the configuration of the Noor lander ( $A_{cone}$ ).

solar array will be highly oversized, using the calculation approach explained in Chapter 7. The value of the required solar array area is also given in Table 5.1. Most of the time about 80% - 90% of the solar panels will not be used. This is a waste of resources. Moreover, it would be unnecessary to size for these three situations because there are long periods of illumination and only small eclipse moments before the days with illumination that are supposed to charge for the difficult eclipse periods (5, 12 and 17). This means that the worst case situations are not necessarily as bad as the previous calculation might indicate. Therefore the solar array should be sized to better fit the operations during the entire year. For this reason three assumptions were made considering the three eclipse periods.

- **Eclipse period 5**

Assume that the half day of eclipse between eclipse period 4 and 5 is also a dark period. This means that eclipse period 5 will account for 4.5 days of darkness. Although the eclipse period increases, this will not create problems because there are enough days with daylight before the eclipse periods.

- **Eclipse period 12**

When assuming that the daylight period between eclipse 11 and 12 is also a period of darkness, then power must be provided for an eclipse period of 4.5 days during an illuminated period of 1.5 days. This will still cause an over estimation of the solar array. Therefore another assumption was made. Eclipse period 10 is attached to the period 11 and 12, because the amount of days in eclipse are few and the days of illumination are higher for this period. This will give 6.5 days of darkness that have to be provided for in 5.5 days of illumination. This case is given at the bottom of Table 5.1.

- **Eclipse period 17**

This case will use the same approach as the previous one. Assume that eclipse period 16 is attached to eclipse period 17. Now the total amount of days in eclipse is 7 and the days in daylight are 4.5. The results for this scenario are also provided in Table 5.1. Eclipse period 17 becomes now the worst case for which the power subsystem must be designed.

### 5.2.2. VARIATIONS IN ILLUMINATION PROFILE OVER TIME

The analysis of the illumination profiles were conducted over a period of one year in the year 2020 [14]. The results can not be exactly applied to other years due to the complex combination of the rotation and sidereal periods of the Moon, the regression of the Moon's orbit ascending node and the Earth orbit around the Sun. This means that a precise rule to transpose the results of one year to another is impossible to determine. However, in more detailed phases of the design it is possible and recommended to create illumination profiles by for the exact time of the mission. In [14] and [13] analysis on different years between 2020 to 2030 were conducted and they show a slight change in the longest illumination period duration as well as the detailed pattern of eclipse periods. Although the illumination conditions change [15] concludes that illumination cycles for a site are fairly repetitive each year. For this reason it is assumed that the illumination and eclipse periods in 2020 are similar to the conditions in 2022, when the Noor lander reaches the Moon, and stay constant through the 5 years of operations.

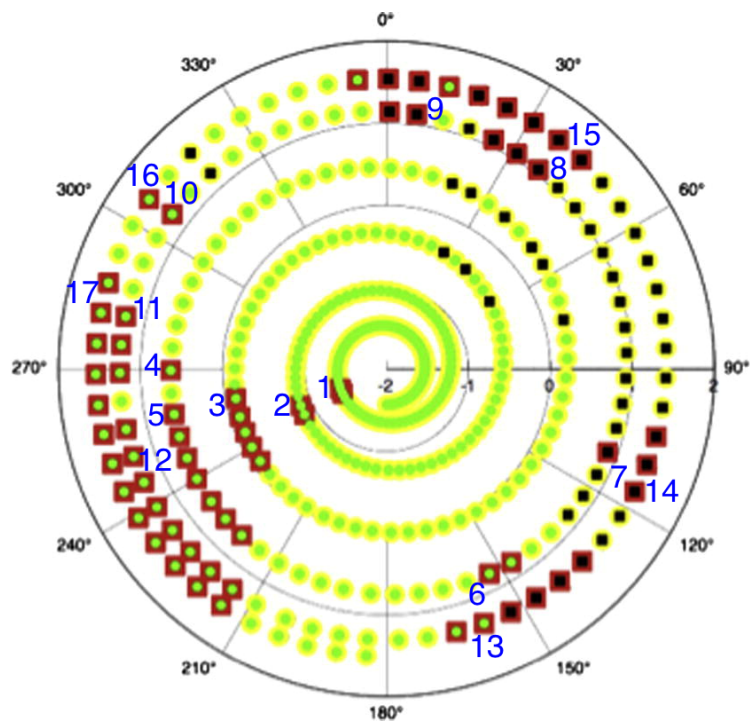


Figure 5.3: A detailed illumination profile for Points A and B. Point A corresponds to the Shackelton Rim. One block represents half a day [14]. Each number corresponds to an eclipse period.

# 6

## PROPULSION SUBSYSTEMS

The propulsion subsystem will provide the spacecraft (S/C) with the necessary thrust to reach the Moon and land safely on the lunar surface at the desired landing location. In the following sections the electrical propulsion (Section 6.1) is described and the chemical propulsion (Section 6.2) subsystem is evaluated.

### 6.1. ELECTRICAL PROPULSION

For the low-thrust trajectory of the transfer orbit, electric engines will be used. In Table 6.1 a list of specifications of European manufactured electric engines is given. The electric propulsion subsystem will consist of two Snecma PPS-5000 Xenon Hall Thrusters. This is in terms of vacuum thrust, required power, mass and lifetime the most optimal combination. The maximum operating power of 10 [kW] corresponds to 0.650 [N] thrust. To meet the 1-year transfer time requirement, the lowest possible thrust the engines should produce equals 0.55 [N]. Hence, the engines will operate at 85% of their maximum power. At this power level the engines have a specific impulse of 2024 [s] and require a total amount of power equal to 8500 [W]. In Section 6.1 and Section 6.1 a schematic drawing and a more detailed overview on the specifications<sup>1</sup> of the PPS-5000 is depicted respectively.

Engine	Manufacturer	Stage	Vacuum $T$ [N]	Vacuum $I_{sp}$ [s]	Power [kW]	Mass [kg]	Lifetime [days]
PPS-5000	Snecma	Hall thruster	0.325	2350	5	11.16	625
HEMP-T 30250	Thales-D	Ion thruster	0.25	3000	7.5	14.5	N/A
RIT-22	AD&S	Ion thruster	0.15	4500	5	7	417
RIT-XT	AD&S	Ion thruster	0.15	4500	4.7	N/A	625
PPS-1350-E	Snecma	Hall thruster	0.14	1800	2.5	4.8	208
PPS-1350-G/-S	Snecma	Hall thruster	0.09	1660	1.5	5.3	439
HEMP-T 3050	Thales-D	Ion thruster	0.05	3000	1.5	N/A	200
PPS-500	Snecma	Hall thruster	0.03	1330	0.5	4	188
UK-10	DERA-UK	Ion thruster	0.018	3510	0.483	15.2	417
RIT-10	AD&S	Ion thruster	0.015	3300	0.56	1.8	833

Table 6.1: List of specifications of European manufactured electric engines.

As summarized in Table 3.2, the electric engines will require a total amount of 711 [kg] xenon propellant. The required power will be generated by solar arrays, of which the sizing is evaluated in . During eclipse the engines will be shut down.

### 6.2. CHEMICAL PROPULSION

Liquid propulsion systems, due to high densities, have lower volume tanks and higher specific impulses compared to solid/hybrid rockets<sup>2</sup>. In this section, the use of liquid propulsion to control the attitude of Spilaio during the transfer, for orbit insertion at the Moon, for orbit maintenance and for landing Noor is discussed.

#### 6.2.1. CHEMICAL PROPULSIVE SYSTEM

The choice of thrusters is limited to re-ignitable systems because thrusters will be used at different stages of the mission. Bi-propellant liquid thrusters ignite upon mixing fuel with an oxidizer at the right pressure. The toxic monomethyl hydrazine ( $CH_3NHNH_2$ , MMH) and dinitrogen tetroxide ( $N_2O_4$ ) are commonly used as fuel and oxidizer. Their hypergolic characteristics enable ignition without an ignition source. The fuels are combined in the combustion chamber under pressure from the tanks which is shown in Figure 6.2<sup>3</sup>.

<sup>1</sup>[http://www.snecma.com/IMG/files/gammeplasmiqueen\\_modulvoir\\_file\\_fr.pdf](http://www.snecma.com/IMG/files/gammeplasmiqueen_modulvoir_file_fr.pdf)

<sup>2</sup>Higher specific impulse for liquid propelled systems - <http://history.nasa.gov/conghand/propelnt.htm>

<sup>3</sup>Schematic of liquid-propellant rocket - <http://history.nasa.gov/conghand/propulsn.htm>

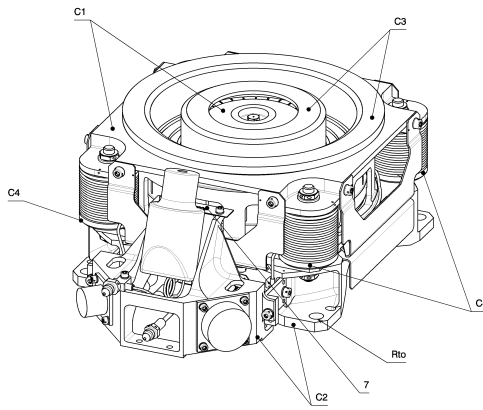


Figure 6.1: Schematic drawing of Snecma PPS-5000.

PPS-5000	
Power [W]	2500-5000
Thrust [mN]	230-325
Specific Impulse [s]	1730-2350
Specific Thrust [mN/kW]	46-60
Lifetime [days]	625
Mass [kg]	11.16

Table 6.2: Detailed specifications of Snecma PPS-5000

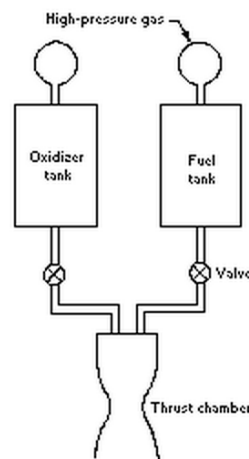
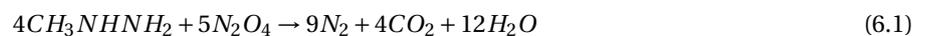


Figure 6.2: Schematic of liquid-propellant rocket

The required mixture ratio of 1.65 at 17 [bar] is derived from Equation (6.1). Ignition is almost instantaneous (rise time < 50 [ms]) with temperatures of up to 3385 [K], so a heat shield on the engine is required. Densities of the fuel (MMH) is 874 [kg/m<sup>3</sup>] and of the oxidizer (N<sub>2</sub>O<sub>4</sub>) is 1442 [kg/m<sup>3</sup>] results in mass percentages of 60.6 % and 39%. The chemical MMH is toxic in small amounts. However it is easily stored in outer space and the fuel tanks of the system are low in volume due to the high density of the liquid. Therefore they easily fit into both Spilaio and Noor. The combustive equation is as follows:



To achieve a high landing accuracy (100x100 [m<sup>2</sup>]) special adaptable thrusters are required. The high performance lightweight European Apogee Motor (EAM) with all-in-one combustion chamber and nozzle of 500 [N] provides the best performance in its class worldwide ( $I_{sp}$  of 325 [s])<sup>4</sup>. In addition 200 [N] Automated Transfer Vehicle (ATV) thrusters which control attitude and change the S/C velocity simultaneously are used. A physical presentation of the thrusters is shown in Figure 6.3a and Figure 6.3b. They use the same fuel, oxidizer and pressurizer (Helium) so fuel tanks can be shared.

The mass flow for each engine can be calculated since the specific impulse and the thrust is known. This done by making use of Equation (6.2). Results are shown in Table 6.3.

$$\dot{m} = \frac{F}{I_{sp}g_0} \quad (6.2)$$

<sup>4</sup>500 [N] EAM bi-propellant thrusters - <http://cs.astrium.eads.net/sp/spacecraft-propulsion/apogee-motors/500n-apogee-motor.html>

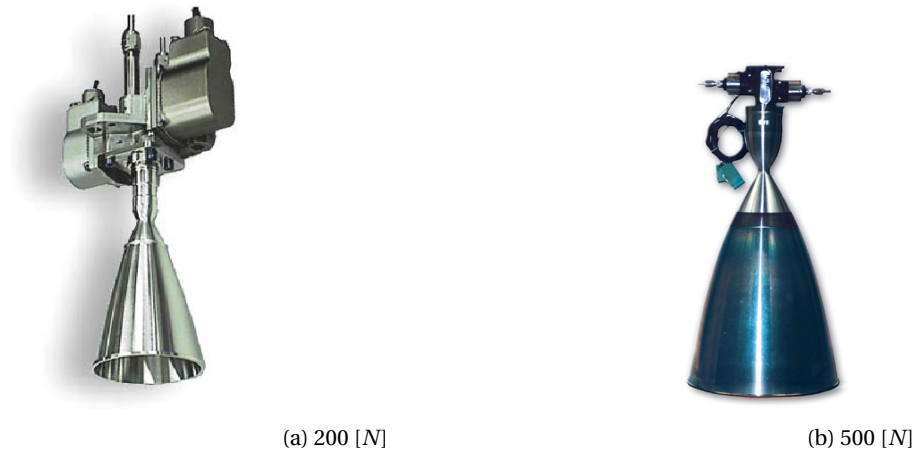


Figure 6.3: Chemical propulsion thrusters [16]

Thrust [N]	$I_{sp}$ [s]	Mass [kg]	Mass flow [kg/s]	Amount of thrusters	Nozzle $\phi$ [mm]	Overall height [mm]
200	280	2	0.0728	6	200	500
500	325	5	0.1568	5	382	803

Table 6.3: Thrusters characteristics

In total six 200 [N] and five 500 [N] thrusters are used for landing. These numbers are based on an iterative process computed by using Matlab. This topic is elaborated on in Section 6.2.2. These thrusters shall be placed inside the lunar module. For the lunar capture burn two additional thrusters are needed which shall be placed inside Spilaio.

### 6.2.2. LANDING

This section deals with the landing trajectory to achieve a high precision ( $100 \times 100 [m^2]$ ) landing. The total propellant mass needed for the entire landing manoeuvre is derived from this. Noor is modelled as a point mass. Instead of a fuel-efficient direct descent trajectory the satellite will enter a lunar parking orbit because it is extremely challenging to time a direct descent from Earth and anomalies are complicated to model [17]. From the parking orbit the landing area can be scanned beforehand, which is helpful in achieving the desired accuracy and high reliability. The navigation associated with landing is discussed in Chapter 11.

#### TRAJECTORY AND ASSUMPTIONS

The landing process itself consists of four main phases. First, during the de-orbit phase an impulse is given to get out of the 100 [km] parking orbit and enter the Hohmann transfer that will take Noor to an altitude of 15 [km]. Secondly, Noor cruises until the 15 [km] orbit is reached. Thirdly, the braking phase is subdivided into a full braking and an approach phase. Finally the terminal vertical descent phase reduces the velocity to its final value before a small free-fall. A schematic presentation is given in Figure 6.4.

The entire trajectory is presented visually in Figure 6.5. The phases are denoted in Figure 6.5 as [AB], [BC - 1], [BC - 2] and [CD].

In order to calculate the trajectory as a point mass in 2D, several assumptions need to be made. The equatorial velocity of the moon is equal to 4.6 [m/s]. Accounting for this is neglected because it only accounts for 0.3% of the fuel consumption during landing. Gravity perturbations due to the Earth and Sun and irregularities in the Moon's gravitational field are neglected as well.

#### CONSERVATION OF LINEAR MOMENTUM AND IMPULSE

The principle of linear momentum and impulse has been used to define both the path as well as the time associated with the manoeuvre. From the parameter time, changes in velocities and travelled distances can be derived [19]. Equation (6.3) conserves impulse.

$$\sum F_{av} = \frac{1}{t_2 - t_1} \int \sum F dt \quad (6.3)$$

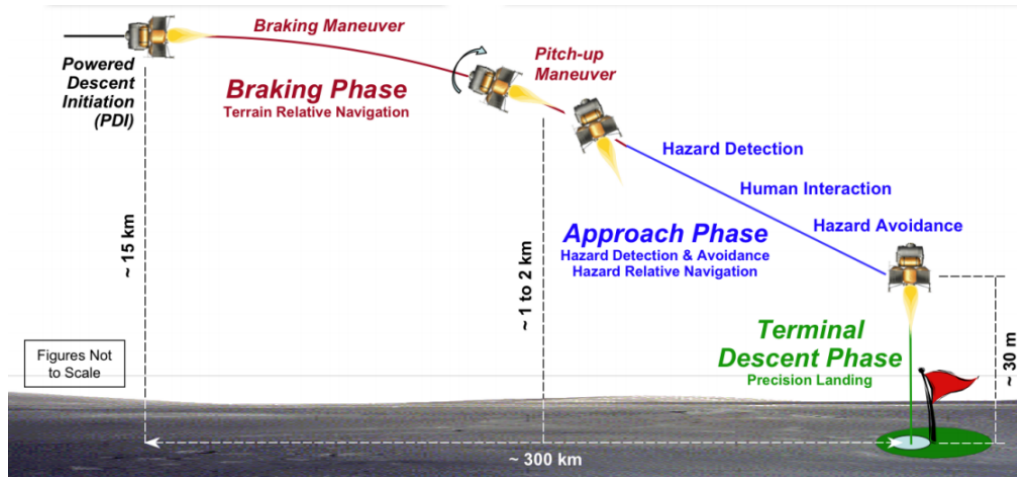


Figure 6.4: Braking phase [BC] [18]

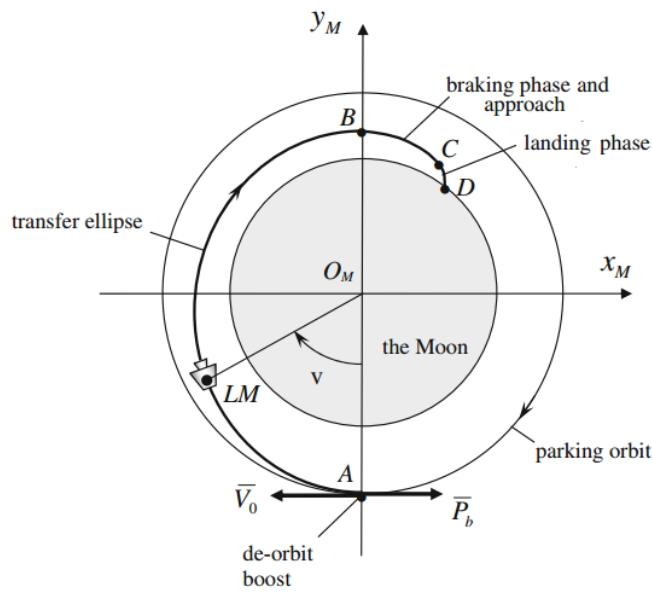


Figure 6.5: Landing mission profile [16]

In this equation  $\sum F_{av}$  is the average thrust delivered by the thrusters. The starting time  $t_1$  is equal to zero and for convenience  $t_2 = t$ .

$$t \sum F_{av} = \sum F dt \quad (6.4)$$

The total force equals the product of its mass and the rate of change of its linear momentum according to Newton's second law.

$$t \sum F_{av} = m_2 v_2 - m_1 v_1 \quad (6.5)$$

The mass  $m_2$  is a function of time due to mass flow rate of the thrusters.

$$t \sum F_{av} = m_2(t) v_2 - m_1 v_1 \quad (6.6)$$

The mass  $m_2$  can be determined by subtracting the change in mass from the initial mass.

$$m_2(t) = m_1 - \dot{m}_i t \quad (6.7)$$

Combining eq. (6.6) and eq. (6.7) gives eq. (6.8).

$$t \sum F_{av} = (m_1 - \dot{m}_i t) v_2 - m_1 v_1 \quad (6.8)$$

Rearranging eq. (6.8) provides an eq. (6.9) for time.

$$t = \frac{m_1(v_2 - v_1)}{\dot{m}_i v_2 + \sum F_{av}} \quad (6.9)$$

Time is the most crucial parameter that needs to be found in order to determine propellant mass and volume and the distance travelled in both horizontal and vertical direction. From the total mass used as propellant the volume of the oxidizer and fuel tanks can be determined. For every phase ([AB], [BC] and [CD]) the total used propellant mass shall be calculated. The total propellant mass needed per phase is calculated by simply multiplying the propellant mass flow by the burn time (Equation (6.10)). Subtracting the total mass change (Equation (6.11)) from the start mass gives the start mass for the up-following phase (Equation (6.12)). Notice that in Equation (6.11) a correction factor of 5 % is introduced in order to account for the pressurizing helium needed and fuel that might get trapped [20] [21].

$$m_p = \dot{m}_p \cdot t_{burn} \quad (6.10)$$

$$\Delta m_i = 1.05 \cdot m_{p_i} \quad (6.11)$$

$$m_{end_i} = m_{start_i} - \Delta m_i = m_{start_{i+1}} \quad (6.12)$$

#### DE-ORBIT PHASE AB

Figure 6.5 shows the different landing phases. Phase [AB] is the de-orbit phase. A burn of several seconds is needed to transfer from a 100 [km] circular orbit into a Hohmann transfer with an apogee of 100 [km] and a perigee of [15km]. The semi-major-axis of this ellipse is equal to:

$$a = \frac{r_{apo} + r_{peri} + 2 \cdot r_{moon}}{2} = 1.7956 \cdot 10^3 [km] \quad (6.13)$$

The thrust delivered during this manoeuvre shall be the maximum available thrust. In this equation [n] represents the number of engines and [T] the thrust. Equation (6.14) shows the total thrust produced by the engines.

$$T = n_1 \cdot T_1 + n_2 \cdot T_2 = 6 \cdot 200 + 5 \cdot 500 = 3700 [N] \quad (6.14)$$

The velocity at a circular orbit is calculated using Equation (6.15) in which  $r = r_{orbit} + r_{moon}$ . The velocity of the elliptical orbit is calculated using equation Equation (6.16).

$$V_{circ} = \sqrt{\frac{\mu_{moon}}{r}} \quad (6.15)$$

$$V_{elliptical} = \sqrt{\mu_{moon} \left( \frac{2}{r} - \frac{1}{a} \right)} \quad (6.16)$$

The circular velocity at an altitude of 100 [km] is equal to 1.6332 [km/s]. The elliptical velocity at 100 [km] orbital height is equal to 1.6136 [km/s]. Therefore the total Delta-V needed for this manoeuvre is equal to  $(\Delta V) = 19.4$  [m/s]. The total burn time can be calculated by using the principle of linear momentum and impulse discussed in Section 6.2.2. Recall Equation (6.9) and fill in the values for the velocities (Equation (6.15) and Equation (6.16) and thrust (Equation (6.14)). The burn time is found to be  $t_{AB} = 26.7$  [s]. A summary of all the characteristics is given in Table 6.4

The total propellant mass used is equal to  $m_{prop} = 17.21$  [kg]. The total weight of propellant and helium  $\Delta M_{AB}$  needed for phase [AB] is found to be 18.07 [kg]. A mass table for phase [AB] is presented in Table 6.5.

After the de-orbit burn is initiated and completed Noor enters into a cruise phase until the 15 [km] altitude is reached. The transfer time is calculated by multiplying the general Hohmann transfer orbit time equation by half and subtracting the de-orbit burn time [Equation (6.17)].

Type	Magnitude
Start velocity	1.6332 [km/s]
End velocity	1.6136 [km/s]
Thrust delivered	3700 [N]
Burn time	26.7 [s]

Table 6.4: Phase [AB] characteristics

Type	Mass [kg]
Start	1050.47
Propellant	17.21
Mass change	18.07
End	1032.40

Table 6.5: Phase [AB] mass table

$$t_{cruise} = \pi \sqrt{\frac{a^3}{\mu_{Moon}}} - t_{burn_{de-orbit}} \quad (6.17)$$

The total cruise time is found to  $t_{cruise} = 56.45 \text{ min}$ .

#### FIRST BRAKING PHASE BC-1

The braking phase is divided into two main phases. For phase [BC – 1] the horizontal velocity is slowed down to 100 [m/s]. For phase [BC – 2] the horizontal velocity is completely brought back to zero. From that moment on the approach phase starts which will be discussed in Section 6.2.2. The attitude control thrusters will make sure that at the start of the braking phase the velocity vector of Noor is in horizontal direction with respect to the Moon's surface. The thrusters will be ignited and Noor will switch to an angle of 10° downwards with respect to the horizontal velocity. The way in which the thrust is oriented is shown in Figure 6.6. Notice that the reaction of the thrust is directly opposite relative to the thrust vector shown in the figure. The x- and y-axis shown in figure Figure 6.6 are considered to be the positive directions throughout the calculations.

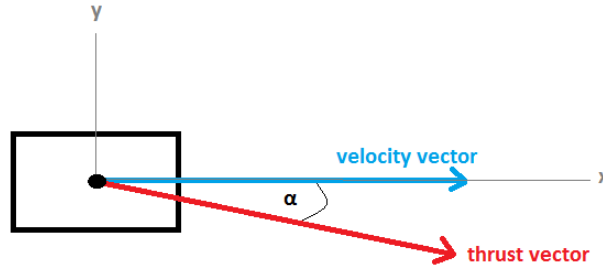


Figure 6.6: Thrust orientation [BC]

The reason for thrusting at an angle is due to the fact that part of the vertical velocity caused by attraction of the Moon's gravity has to be lowered in order to avoid impact with the surface. The thrust delivered during phase [BC – 1] shall be the maximum available thrust. Noor shall still be considered as a point mass. The total thrust delivered in horizontal direction can be calculated using Equation (6.18). In this equation [n] represents the number of engines and [T<sub>x</sub>] the thrust in horizontal direction. The angle  $\alpha$  is the angle between the velocity vector and the thrust vector.

$$T_x = [n_1 \cdot T_1 + n_2 \cdot T_2] \cdot \cos(\alpha) = [6 \cdot 200 + 5 \cdot 500] \cdot \cos(10) = 3643.8 [N] \quad (6.18)$$

In a similar manner the vertical thrust vector can be calculated. This is done in Equation (6.19).

$$T_y = [n_1 \cdot T_1 + n_2 \cdot T_2] \cdot \sin(\alpha) = [6 \cdot 200 + 5 \cdot 500] \cdot \sin(10) = 642.5 [N] \quad (6.19)$$

The starting velocity at an altitude of 15 [km] is calculated using Equation (6.16). The value of the semi-major-axis is identical to the one calculated in Equation (6.13). By means of Equation (6.9) the total burn time for phase [BC – 1]

is found to be equal to  $t_{BC-1} = 400.56$  [s]. The starting mass is  $m_{BC-1_{start}} = 1032.40$  [kg]. The velocity in horizontal direction is found to be equal to  $1.692$  [km/s]. The horizontal required velocity at the end of the first braking phase is  $100$  [m/s]. The vertical velocity right at the start of the braking phase is  $0$  [m/s]. However, due to gravity attraction this speed will change over time. The end velocity in vertical direction can be calculated using Equation (6.20):

$$V_{yBC-1} = -g_m \cdot t_{BC-1} + \frac{T_y \cdot t_{BC-1}}{m_{BC-1_{start}} - T_y \cdot t_{BC-1}} \quad (6.20)$$

The end velocity in vertical direction is equal to  $-20.11$  [m/s]. A summary of all the characteristics is given in Table 6.6.

Type	Magnitude
Start velocity (x)	1.692 [km/s]
End velocity (x)	0.1 [km/s]
Start velocity (y)	0 [km/s]
End velocity (y)	-0.0201 [km/s]
Thrust delivered (x)	3643.8 [N]
Thrust delivered (y)	642.5 [N]
Burn time	400.56 [s]

Table 6.6: Phase [BC – 1] characteristics

The total propellant mass used is equal to  $m_{prop} = 375.78$  [kg]. The total weight of propellant and helium  $\Delta M_{BC-1}$  needed for phase [BC – 1] is found to be  $394.57$  [kg]. A mass table for phase [BC – 1] is presented in Table 6.7.

Type	Mass [kg]
Start	1032.40
Propellant	375.78
Mass change	394.57
End	637.83

Table 6.7: Phase [BC – 1] mass table

The average accelerations in x- and y-direction can also be computed (Equation (6.21) and Equation (6.22)). From that, the distances travelled in both x- and y-direction can be computed using Equation (6.23) and Equation (6.24), respectively. The findings are presented in

$$a_{xBC-1} = \frac{-(V_{x-start_{BC-1}} - V_{x-end_{BC-1}})}{t_{BC-1}} \quad (6.21)$$

$$a_{yBC-1} = \frac{-(V_{y-start_{BC-1}} - V_{y-end_{BC-1}})}{t_{BC-1}} \quad (6.22)$$

$$d_{xBC-1} = V_{x-start_{BC-1}} \cdot t_{BC-1} + 0.5 \cdot a_{xBC-1} \cdot t_{BC-1}^2 \quad (6.23)$$

$$d_{yBC-1} = V_{y-start_{BC-1}} \cdot t_{BC-1} - 0.5 \cdot g \cdot t_{BC-1}^2 + 0.5 \cdot a_{yBC-1} \cdot t_{BC-1}^2 \quad (6.24)$$

The results are presented in Table 6.8.

Type	DIS [km]
X-direction	245
Y-direction	-8.4

Table 6.8: Phase [BC – 1] distance table

### APPROACH PHASE BC-2

For the approach phase [BC – 2], the procedure is identical to the one outlined in Section 6.2.2. The main differences are that: the  $500$  [N] thrusters are now switched-off and the angle  $\alpha$  is set to  $60^\circ$ . The characteristics, the masses and the travelled distances are presented in Table 6.9, Table 6.10 and Table 6.11, respectively.

Type	Magnitude
Start velocity (x)	100 [km/s]
End velocity (x)	0 [km/s]
Start velocity (y)	-0.0201 [km/s]
End velocity (y)	-0.0937 [km/s]
Thrust delivered (x)	848.5 [N]
Thrust delivered (y)	848.5 [N]
Burn time	63.01 [s]

Table 6.9: Phase [BC – 2] characteristics

Type	Mass [kg]
Start	637.83
Propellant	84.53
Mass change	88.77
End	549.06

Table 6.10: Phase [BC – 2] mass table

Type	DIS [km]
X-direction	60
Y-direction	-6.56

Table 6.11: Phase [BC – 2] distance table

### TERMINAL DESCENT PHASE CD

The final phase is the terminal descent phase. During the phase Noor will descent the last 40 [m]. The situation is shown in figure Figure 6.7.

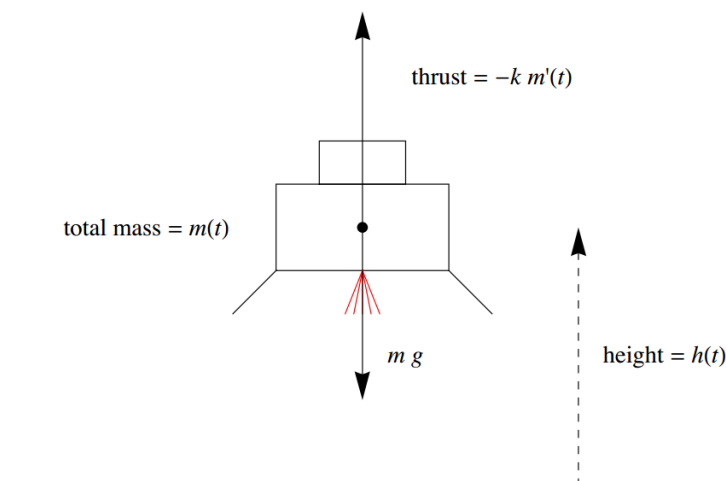


Figure 6.7: Terminal landing phase for lunar landing [22]

The final descent phase is set to take  $t_{CD} = 28$  [s]. During this phase six 200 [N] thrusters and five 500 [N] are used. The characteristics and the masses are presented in Table 6.12 and Table 6.13 respectively.

From a height of 3 [m] the chemical propulsion is switched-off and the landing module is released into a free fall. The reason for choosing to free fall from this altitude rather than land on the moon with a velocity of 0 [m/s] is because due to plume effects caused by thrusters the module might get damaged by lunar dust. NASA has extensively studied this phenomena during the Apollo missions using different methodologies [23]. The Apollo lunar modules were dropped from an altitude of 12 [m]. However, the engines used for those missions were much more powerful than the ones used for the LOFARside mission. Based upon weight fractions derived from the Apollo 11 lunar module

Type	Magnitude
Start velocity (y)	-0.0937 [km/s]
End velocity (y)	0 [km/s]
Thrust delivered (y)	3700 [N]
Burn time	28 [s]

Table 6.12: Phase [CD] characteristics

Type	Mass [kg]
Start	549.06
Propellant	49.60
Mass change	52.09
End	496.97

Table 6.13: Phase [CD] mass table

and the LOFARside module, a safe distance for a free fall is estimated to be 3 [m] [23]. In Section 14.3 the loads at touchdown are calculated and designed for.

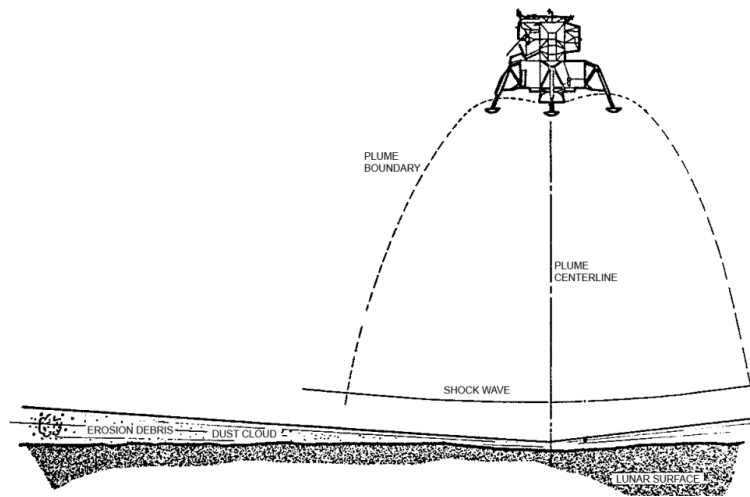


Figure 6.8: Shock waves during landing phase for lunar landing [23]

### 6.2.3. HOVERING

A possible component of the landing maneuver is the hovering phase. This phase uses a lot of fuel and should be as short as possible. However, hovering for a certain amount of time might be necessary for hazard detection. In the case of landing on a crater rim, precise maneuvering is necessary. A way of estimating propellant fuel needed for hovering is derived in this section. In the derivation specific impulse ( $I_{sp}$ ) depends on the propulsion system,  $g_0$  and  $g_m$  are the gravitational accelerations of the Earth and Moon, respectively. The term  $t$  is the hovering time. During hovering the thrust ( $F_T$ )<sup>5</sup> is equal to the gravitational force ( $F_G$ ) exerted on the lander by the Moon:

$$F_T = F_G = -\frac{dm}{dt} \cdot I_{sp} \cdot g_0 = m \cdot g_m$$

The above expression can be rearranged to put the  $dm$  and  $dt$  terms on opposing sides.

$$-\frac{dm}{m} = \frac{g_m \cdot dt}{I_{sp} \cdot g_0}$$

This expression can then be integrated:

<sup>5</sup>General Thrust Equation - <http://www.grc.nasa.gov/WWW/k-12/airplane/thrsteq.html>

$$-\ln\left(\frac{m}{m_0}\right) = \frac{g_m \cdot t}{I_{sp} \cdot g_0}$$

After solving for the begin-to-end mass ratio ( $m/m_0$ ) and subtracting this from 1, an expression is found for the propellant fuel fraction necessary for hovering, Equation (6.25).

$$\frac{m_{hover}}{m_0} = 1 - \frac{m}{m_0} = 1 - e^{\left(-\frac{g_m \cdot t}{I_{sp} \cdot g_0}\right)} \quad (6.25)$$

The begin mass ( $m_0$ ) is in this case the begin mass of the lander at a certain hovering height after the main landing burns.

By assuming  $I_{sp} = 325$  [s] and using a 90 [s] hovering time estimate necessary for possible hazard avoidance and maneuvering, a propellant mass fraction was estimated. It was found to be 0.0269. Multiplying this value with the eventual estimated landed dry weight gives a hover fuel weight of 12.8 [kg].

#### 6.2.4. MASS AND TIME BUDGETS

The total overview of mass change during the different phases and the associated time is presented in Table 6.14.

Phase	Start mass [kg]	Propellant [kg]	End mass [kg]	Time [s]
De-orbit [AB-1]	1010.52	18.07	1032.40	26.7
Cruise [AB-2]	1032.40	0	1032.40	3387
Brake [BC-1]	1032.40	394.57	637.83	400.5
Approach [BC-2]	637.83	88.77	549.06	63.0
Terminal Descent [CD]	549.06	52.09	496.97	28.0
Hover	496.97	12.8	484.17	90
Total	-	566.3	-	518.2

Table 6.14: Mass and time table landing phase

#### 6.2.5. VOLUME TANKS

Besides the landing phase, chemical propulsion is needed for controlling the attitude during the transfer and a brake burn to maintain the parking orbit around the moon. For these manoeuvres, 20.63 [kg] (Section 8.5.2) and 71.9 [kg] (Table 3.3) fuel is need, respectively. The total weight of propellant mass needed during the entire mission is equal to 650.27 [kg]. However, two main systems will be used; both pressurized with their own helium tank. The largest one, used for landing, will contain 570.24 [kg] (see Table 6.14). The second tank will be placed in the mothership and will contain 92.53 [kg] of fuel. The volumes of the pressurizer and fuel tank can be calculated based upon the densities of the liquids. The results are presented in Table 6.15. From these results it can be concluded that liquids are more or less the same volume-wise. For the sake of symmetry, the highest value of the volume is taken and that volume is used for both the oxidizer and the fuel. This is done for both the transfer tanks as well as the lander tanks. A representation of how the tanks fit into the VEGA is given in Appendix A.

Phase	Propellant [kg]	Oxi. [kg]	Fuel [kg]	Volume oxi. [m3]	Volume fuel [cm3]
Transfer	92.53	56.07	36.46	0.039	0.0417
Landing	570.24	345.57	224.67	0.239	0.257

Table 6.15: Propellant volume tanks

For the tanks the aluminium alloy 7075 is used as a material. It is compatible with the chosen fuel type as well as the oxidizer. Furthermore its strength to weight ratio is high and the alloy is quite resistant to corrosion [21]. Figure 6.9 shows an example of a propellant tank as described.

For every 1.2 [kg] of propellant, 3 [g] of helium is needed for proper flow of the liquids. This means that in total 1.43 [kg] of helium is needed. This helium is contained in a pressurized tank of 17 [bar] at a temperature of 278 [K]. Using the Ideal Gas Law (Equation (6.26) <sup>6</sup>), the volume for both helium tanks can be computed. The individual gas constant ( $R$ ) for helium is equal to 2.08.

$$p = \rho \cdot R \cdot T \quad (6.26)$$

<sup>6</sup>Ideal Gas Law - [http://www.engineeringtoolbox.com/ideal-gas-law-d\\_157.html](http://www.engineeringtoolbox.com/ideal-gas-law-d_157.html)



Figure 6.9: Propellant fuel tank (example) [20]

The density at the mentioned conditions is found to be  $\rho = 2.803 \cdot 10^3 [kg/m^3]$ . The volume tank results for helium are presented in Table 6.16.

Phase	Helium needed [kg]	Tank volume [cm <sup>3</sup> ]
Transfer	0.232	83
Landing	1.426	509

Table 6.16: Volume of the helium tanks

### 6.2.6. VALIDATION & VERIFICATION

The results obtained in this chapter can be validated and verified by using similar missions and comparing results. The conceptual design of the ESA Lunar Lander is a mission that is comparable to the LOFARside mission. The ESA Lunar Lander is using the same number of engines and the eventual mass landed is double the weight that Noor will land. However, the amount of chemical propellant is also double the amount which means that relatively spoken the values seem to match. Also the time span corresponds to the time allocation of the ESA Lunar Lander. A comparison can be obtained from Figure 6.10 and Table 6.17.

	#	TRAJECTORY PHASE	TIME ALLOCATION
De-orbit Maneuver	1	Orbit	N/A
Powered Descent Maneuver	2	Coast	~ 55 min
Pitch Up Maneuver	3	Braking	~ 6.5 min
Vertical Descent Maneuver	4	Approach	~ 30 - 120 sec
Touchdown	5	Vertical Descent	~ 30 sec
Total Time Allocation			~ 1 hour

Figure 6.10: Time allocation ESA Lunar Lander [18]

#	TRAJECTORY PHASE	TIME ALLOCATION
1	Orbit	N/A
2	Coast	57 min
3	Braking	6.7 min
4	Approach	63 sec
5	Vertical Descent	28 sec

Table 6.17: Time allocation LOFARside landing

## ELECTRICAL POWER SUBSYSTEM

The electrical power subsystems (EPS) aboard Spílaio and Noor produce and provide the right amount of power to the instruments and the other subsystems. In the following sections, the power budgets for the mission phases are estimated (Section 7.1) and the power generation (Section 7.2) and secondary power source options (Section 7.3) are described. Lastly, the power management and distribution (Section 7.4) are explained.

### 7.1. POWER BUDGETS

In the next subsections, the initial estimations for the power consumption per mission phase are presented and explained. The power budgets are for the most part based on historical data and if needed, scaled to increase compliance with the LOFARside mission.

#### 7.1.1. TRANSFER PHASE

In order to determine the area and mass of the solar array of Spílaio, an estimation of the total required power  $P_{SA}$  must be made. In Table 7.1, the power budget for Spílaio is given. For proper functioning of the subsystems, excluding the propulsion subsystem, the required power is estimated to be  $P_{bus} = 970$  [W].

Subsystem or power consumer	Power Budget [W]	
	Normal	Eclipse
Data Handling	30	30
Attitude Control	475	410
Communications	25	20
Thermal [3, pp. 332]	190	50
Power Conditioning	120	40
Battery Charging	130	0
Electric Propulsion	8500	0
Total Power	9430	550

Table 7.1: The power budget for the transfer from LEO to LLO. Given for normal and eclipse operations.

The numbers for data handling, communications and power conditioning are directly taken from the SMART-1 power budget [24]. The amount of power required for attitude control is computed by scaling up the SMART-1 value with the mass ratio between LOFARside and SMART-1. The power budget in eclipse mode is derived from the ratios used for SMART-1 [24]. To charge the batteries, the minimum power required can be calculated by dividing the total required battery capacity by the time available for charging. This is done with Equations (7.1) and (7.2).

$$C_r = \frac{P_e T_e}{(DOD)Nn} \quad [Whr] \quad (7.1)$$

In Equation (7.1),  $P_e$  denotes the power required in eclipse mode,  $T_e$  is the time duration of the longest occurring eclipse,  $DOD$  is the Depth-of-Discharge,  $N$  is the number of batteries and  $n$  is the transmission efficiency. From STK eclipse simulation, the longest eclipse time equals  $T_e = 2.2$  [hrs]. The corresponding orbital period equals  $T_{orbit} = 14.7$  [hrs]. The DOD is approximated to be 85% [24] and the transmission efficiency 90% [3, pp. 422]. The number of batteries is set to  $N = 1$  to calculate a total battery capacity of  $C_r = 1580$  [Whr]. In conclusion, the total amount of power that must be produced by the solar array is equal to  $P_{SA} = 9430$  [W].

$$P_{charge} = \frac{C_r}{T_{orbit} - T_e} = \frac{1580}{14.7 - 2.2} = 127 \quad [W] \quad (7.2)$$

### 7.1.2. LANDING, DEPLOYMENT AND OPERATION PHASE

For Noor, an estimation of how much power,  $P_{SA}$ , the solar array must provide during an illuminated period and a power profile was made. Noor's power subsystem is supposed to power the spacecraft (S/C) during landing and deployment as well as the surface operations. The landing profile provided four phases, which are important for the sizing of the power subsystem and these are presented in Table 7.2. The power subsystem will be designed for the average power needed during the operational phase, since this segment has the highest power demand besides the landing. The landing will rely on the secondary power source because the solar panels will not be operational during this phase. Furthermore, any peak loads will be handled by the secondary power source.

Subsystem	Landing Phase A [W]	Landing Phase B [W]	Deployment Phase [W]	Operations Phase [W]
Telemetry, Tracking and Command 9	0	0	5	55
Command and Data Handling 10	20	20	20	20
Power [3, pp. 334]	50	12.5	27.5	33.8
Attitude and control [3, pp. 316]	20	5	0	0
Thermal [3, pp. 316]	10	2.5	5.5	6.8
Structures and mechanisms 14	0	0	0	0
Guidance and navigation 11	120	10	0	0
Propulsion [3, pp. 318]	0	0	0	0
Rover 12	0	0	52	0
Antennas 3	0	0	0	12.1
Extra instruments 3	0	0	0	7.4
<b>Total</b>	<b>220</b>	<b>50</b>	<b>110</b>	<b>135.1</b>
<b>Margin 10%</b>	<b>22</b>	<b>5</b>	<b>11</b>	<b>13.5</b>
<b>Average Power</b>	<b>242</b>	<b>55</b>	<b>121</b>	<b>148.6</b>

Table 7.2: Power budget for Noor during the different segments of the mission.

To determine the  $P_{sa}$  Equation (7.3) was used [3] was used. Where  $P_e$  and  $P_d$  are the spacecraft's power requirements during eclipse and daylight respectively. The terms  $T_e$  and  $T_d$  are the lengths of these periods per orbit in hours. The parameters  $X_e$  and  $X_d$  are the efficiencies of the paths from the solar arrays through the batteries to the different loads of the subsystems and the path directly from the arrays to the loads. The efficiency values for eclipse and daylight depend on the type of power regulation, which will be discussed in Section 7.4. For Noor a peak-power tracker will be used to regulate and control the power subsystem and therefore  $X_e = 0.6$  and  $X_d = 0.8$  [3, pp. 413]. In Section 5.2 the eclipse and daylight periods were determined to be 7 and 4.5 days, respectively. This leads to  $T_e = 168$  [hr] and  $T_d = 108$  [hr], so the total required power during daylight is found to be  $P_{sa} = 572.5$  [W].

$$P_{SA} = \frac{\frac{P_e T_e}{X_e} + \frac{P_d T_d}{X_d}}{T_d} \quad [W] \quad (7.3)$$

## 7.2. GENERATION

Over the years, different ways of generating power have been developed. Each of them having their benefits and drawbacks depending on the mission. The most common power sources used in space are listed in Table 7.3, on which a quick elaboration and trade-off is presented in this section.

### 7.2.1. TRANSFER PHASE

As can be seen in Table 7.1, the propulsion subsystem of Spílaio consumes an enormous amount of power during the transfer phase. Since power generation can be a very costly matter and the total budget of 500M € is a solid top level requirement, the specific cost should be low. Another criterion for the trade-off is a high specific power, so that the mass of the power generator is minimized.

The power sources listed in the latter three columns of Table 7.3 are respectively radioisotope thermoelectric generators (RTG), nuclear reactors and fuel cells. They are specifically used for interplanetary missions, when there is a lack of solar flux. Also, these power sources very high priced compared to the other two, more conventional power sources. To give an estimation of what the costs would be when the power is generated by RTG's: the required power for this mission equals approximately 9.5 [kW] and the cheapest RTG generates one Watt of power to 16K \$. This means that the total costs for only the power generation would exceed 150M \$ or 130M €. This already takes up one-fourth of the total budget, while it should not exceed 6%. The other two power sources are even more expensive. Furthermore, one of the requirements formulated by the client is not to use nuclear power sources. Therefore, the use of RTG's, nuclear reactors and fuel cells is not suitable for this mission.

The remaining options, solar photovoltaic and solar thermal dynamic can be weighed against their respective specific power. From Table 7.1, the minimum mass of a solar thermal dynamic power source would be about 630 [kg] for the required power, whereas the maximum mass of a solar photovoltaic power source would be about 380 [kg]. Also the use of solar photovoltaic cells is well-known and reliable [25]. From this, the conclusion can be drawn that a solar photovoltaic power source, hence an array of solar cells, is the best option for this mission.

EPS Design Parameters	Solar Photovoltaic	Solar Thermal Dynamic	RTG	Nuclear Reactor	Fuel Cell
Power Range [kW]	0.2-300	5-300	0.2-10	5-300	0.2-50
Specific Power [W/kg]	25-200	9-15	5-20	2-40	275
Specific Cost [\$/W]	800-3000	1000-2000	16K-200K	400K-700K	50K-100K
Principal Applications	Earth-orbiting	Earth-orbiting	Interplanetary	Interplanetary	Interplanetary

Table 7.3: Trade-off data and principal applications of the most common power sources used in space. [25, pp. 659]

### 7.2.2. LANDING, DEPLOYMENT AND OPERATION PHASE

The main selection criteria for the primary power source used on Noor are low mass and low life-cycle cost. This is largely effected by the required power output and the mission lifetime. Figure 7.1 provides four options that might be suitable for the power subsystem of Noor, considering a lifetime of 5 years. These four are: dynamic or static nuclear reactors, RTG's and solar photovoltaic power generators. The first two options are disregarded due to the client's request not to use nuclear energy. Given the fact that an RTG uses radioactive material and that its price range is much higher than the price range for solar cells, as discussed earlier and shown in Table 7.3, this power source was rejected as well. Hence, solar photovoltaic power was chosen.

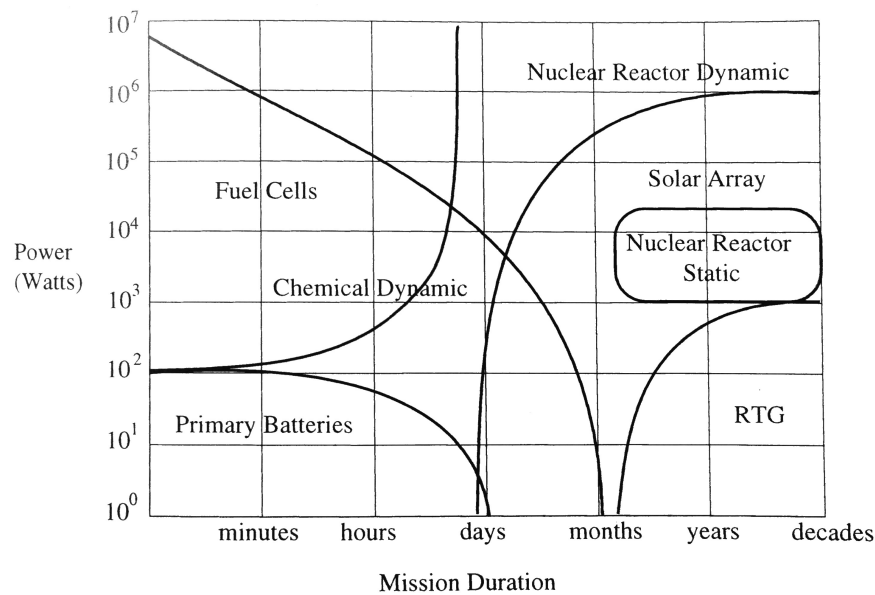


Figure 7.1: Options for primary power sources with respect to required output power and mission duration [26].

### 7.2.3. SOLAR CELL AND EFFICIENCY

In the previous subsection, the choice for a solar photovoltaic power source was justified. A solar array consists of multiple solar cells connected in series and in parallel. The largest space application solar cell manufacturer of Europe is the German company Azur Space. Their expertise lies within the development of multi-junction GaInP/GaAs solar cells and assemblies, of which an overview<sup>1</sup> is given in Table 7.4.

To select the most optimal solar cell, a trade-off is done by multiplying the normalized specific power by the normalized power density. Both factors have equal weight. The results of the trade-off are shown in Table 7.5. The winner option in Table 7.5 is the triple-junction 3G30C-Advanced. For this particular solar cell, three sizes are available with basically the same performance. The reason for the (L) version to end up last in the ranking is the higher coverglass thickness compared to the (M) and the (S) version. This results in a much lower specific power. The solar cell consists of gallium indium phosphide (GaInP), gallium arsenide (GaAs) and is fabricated on a germanium (Ge) wafer. In

<sup>1</sup><http://www.azurspace.com/index.php/en/products/products-space/space-solar-cells>

Solar Cell/Assembly <i>Azur Space</i>	Area [cm <sup>2</sup> ]	Cell Area [cm <sup>2</sup> ]	Average weight [mg/cm <sup>2</sup> ]	Thickness [mm]	V <sub>oc</sub> [mV]	I <sub>oc</sub> [mA]	V <sub>mp</sub> [mV]	I <sub>mp</sub> [mA]	P <sub>max</sub> [W]	Efficiency [-]
Triple Junction Solar Cell 3G28C	32.00	30.18	86	0.150	2667	506	2371	487	1.155	0.280
Triple Junction Solar Cell 3G30C-Advanced (S)	32.00	30.18	86	0.150	2700	520	2411	504	1.216	0.295
Triple Junction Solar Cell 3G30C-Advanced (M)	64.00	60.36	86	0.150	2700	1041	2411	1007	2.428	0.294
Triple Junction Solar Cell 3G30C-Advanced (L)	72.00	68.76	130	0.230	2700	1186	2411	1147	2.765	0.294
Silicon Solar Cell S32	23.61	23.61	32	0.130	628	1081	528	1025	0.541	0.169
Triple Junction Solar Cell Assembly 3G28A	32.18	30.18	116	0.280	2690	520	2409	503	1.211	0.293
Triple Junction Solar Cell Assembly 3G30A	32.18	30.18	116	0.280	2662	505	2365	487	1.152	0.280

Table 7.4: Specifications for Azur Space solar cells at AM0 spectrum,  $S_r = 1367 [W/m^2]$  and  $T = 28^\circ$ . In order to make a distinction for the 3G30C cells, (S), (M) and (L) denote the size of the respective solar cell.

Figure 7.2a, a schematic of the winner cell is depicted. In Figure 7.2b, the electrical characteristics are represented by an I-V curve. The efficiency is equal to  $\eta_{cell} = 0.295 [-]$ . The efficiency loss caused by mounting the solar cells onto a panel is covered in Section 7.2.6.

Solar Cell/Assembly <i>Azur Space</i>	Specific Power [W/g]	Power Density [W/cm <sup>2</sup> ]	Normalized P/m [-]	Normalized P/A [-]	Score [-]	Ranking #
Triple Junction Solar Cell 3G30C-Advanced (S)	0.469	0.040	0.654	1.000	0.654	1
Triple Junction Solar Cell 3G30C-Advanced (M)	0.468	0.040	0.653	0.998	0.652	2
Triple Junction Solar Cell 3G28C	0.445	0.038	0.621	0.949	0.590	3
Silicon Solar Cell S32	0.716	0.023	1.000	0.569	0.569	4
Triple Junction Solar Cell Assembly 3G28A	0.346	0.040	0.483	0.996	0.481	5
Triple Junction Solar Cell Assembly 3G30A	0.329	0.038	0.459	0.947	0.435	6
Triple Junction Solar Cell 3G30C-Advanced (L)	0.309	0.040	0.432	0.998	0.431	7

Table 7.5: Trade-off for Azur Space solar cells. In order to make a distinction for the 3G30C cells, (S), (M) and (L) denote the size of the respective solar cell.

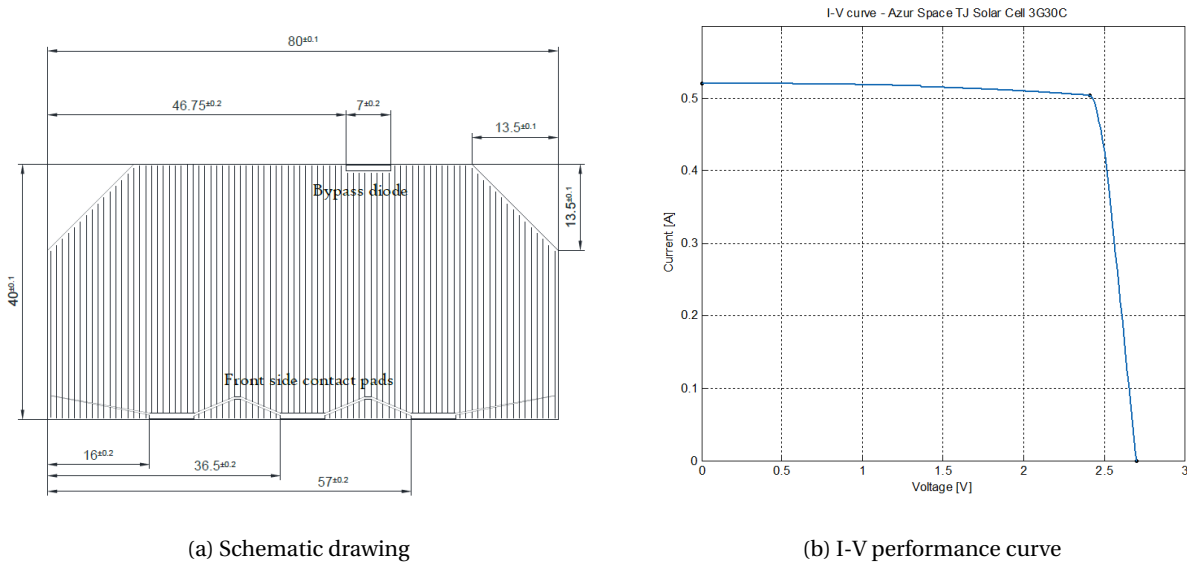


Figure 7.2: Azur Space TJ Solar Cell 3G30C.

## 7.2.4. SOLAR FLUX

The solar cells extract energy from the Sun's radiation and convert it to useful electric energy. The amount of energy received by a solar array depends on its area and distance from the Sun. The solar flux  $S_r$  in  $[W/m^2]$  at a certain distance  $r$  from the sun is given by Equation (7.4).

$$S_r = S_0 \left( \frac{r_0}{r} \right)^2 [W/m^2] \quad (7.4)$$

### TRANSFER PHASE

Where  $S_0$  denotes the average solar flux in Earth orbit equal to  $1377 [W/m^2]$  and  $r_0$  is the average distance between the Sun and the Earth, which equals  $1.496(10)^{11} [m]$ . [27, pp. 22] To calculate the minimum solar flux the solar

array will receive during the transfer phase,  $r$  must be equal to the maximum distance (*worst case scenario*) reached between the Sun and solar array of Spílaio. From Figure 7.5, it can be seen that the maximum achieved distance between the Earth and S/C is  $4.1(10)^8$  [m]. Adding this distance to the average distance between the Sun and the Earth and then filling in Equation (7.4) yields a minimum solar flux of  $S_r = 1370$  [ $W/m^2$ ].

#### LANDING, DEPLOYMENT AND OPERATION PHASES

For the operational phase,  $r$  must be equal to the maximum distance reached between the Sun and solar array located on the lunar South pole, which is about  $1.5(10)^{11}$  [m]. Then using Equation (7.4) the minimum solar flux is determined to be  $S_r = 1370$  [ $W/m^2$ ] as well.

#### 7.2.5. INCIDENCE ANGLE

The Sun incidence angle,  $\theta$ , will determine how much power output is generated by the solar array. It is defined to be the angle between the vector normal to the surface of the array and the Sun line [3, pp. 417]. If the Sun line is perpendicular to the surface of the solar array, the maximum power output is generated.

#### TRANSFER PHASE

During the transfer phase, the solar array attitude will constantly be corrected, so that the Sun line is pointing normal to the array. These corrections are conducted by the ADCS Section 8.5.2. The S/C will be able to rotate about the axis coinciding with the line of thrust. The accuracy for this rotation is  $1^\circ$ . Also, the rod to which the solar arrays are attached will be able to rotate about its axis, see Section 14.2. The error in this action may be assumed the same as the accuracy of the sun sensors, which is negligible. Concluding, the maximum incidence angle occurring during the transfer phase is  $\theta = 1^\circ$ .

#### LANDING, DEPLOYMENT AND OPERATION PHASES

For the chosen landing location the Sun's elevation must be obtained to calculate the Sun incidence angle. The Moon's axis of rotation has a small inclination with respect to the ecliptic, which causes the variations of the Sun's elevation to be limited to about  $1.54^\circ$  over one year [4]. Using this information [11] evaluated the elevation variations over one lunar rotation at the Connecting ridge close to Shackleton Crater, which is the desired landing location. In Figure 7.3 the results are presented, where the coloured lines represent the movement of the Sun over one year. Each coloured line, moving from right to left, indicates a different month. The elevation moves upward till the maximum is reached, then down again (dashed lines). Figure 7.3 provides the range of the Sun elevation of  $-2^\circ$  to  $2^\circ$ . Although the results obtained by [11] are determined for the Connecting Ridge, for the purpose of this project it was assumed that the Sun elevation range is similar at the Shackleton Crater, which is only 10 [km] away.

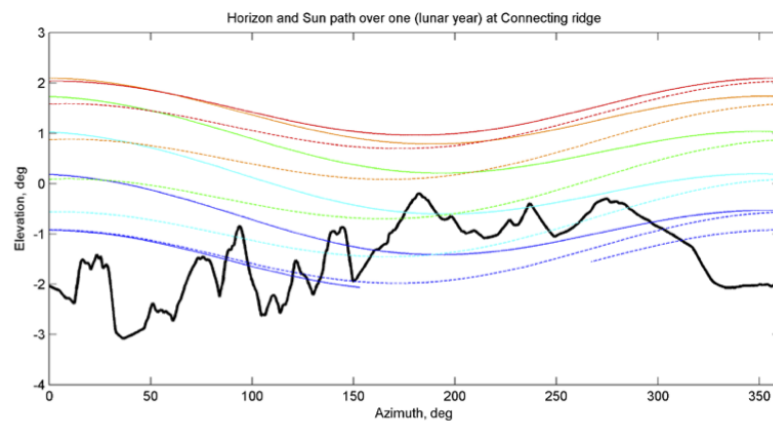


Figure 7.3: Local horizon (bold black line) and path of the Sun centre over one year (coloured lines), as seen from the Connecting Ridge. [11].

In Section 7.5 the configuration of the solar cells, which will be placed on the truncated cone, is explained. The angle of incidence will be affected by this configuration, since the solar array will not be placed perpendicular to the lunar surface. The angle of the truncated cone is calculated to be  $73.82^\circ$  with respect to its local horizontal. Using the elevation range and this angle the Sun incidence angle can be computed. The incidence angle was calculated to be between  $14.18^\circ$  and  $18.18^\circ$ . To minimize the cosine loss the Sun incidence angle should be as low as possible [3, pp. 417]. This means that the worst case of cosine loss happens when  $\theta = 18.18^\circ$ . The solar array should be designed for this situation.

### 7.2.6. INHERENT DEGRADATION

Solar cells assembled in a solar array have a lower efficiency than a single cell. This decrease in BOL performance is referred to as inherent degradation  $I_d$  and is caused by design and assembly losses, possible shadowing by appendages and temperature effects. For this mission, a nominal value of  $I_d = 0.72$  [-] is applied [25, pp. 645] for the design of the solar array for the transfer phase as well as for Noor.

### 7.2.7. LIFE DEGRADATION

#### TRANSFER PHASE

During the mission the efficiency of the solar array will further decrease. This accumulated degradation is caused by multiple factors. Statistically, the most severe damage is done by natural radiation, consisting of electrons and protons. High concentrations of energetic charged particles are found in the Van Allen belts: two donut-shaped radiation clouds encircling the Earth. The inner belt is characterized by large amounts of high energy protons and stretches from 1275 [km] to 13000 [km] (most dense concentrations between 1275 - 5000 [km]), with respect to the surface of the Earth. Heavy concentrations of electrons are encountered in the outer belt, which is located at 13000 [km] and ends at 38000 [km] (most dense concentrations between 13000 - 20000 [km]). In Figure 7.4, a schematic is depicted of the extent of the Van Allen radiation belts. [27, pp. 31–34] [28] Other possible factors contributing to the degradation of the solar array are ultraviolet radiation, thermal fluctuations, impacts from micrometeoroids or debris and exhaust gasses from the engines. However, for a maximum cislunar<sup>2</sup> environment exposure of 1 year, these factors may be neglected. [27, pp. 170]

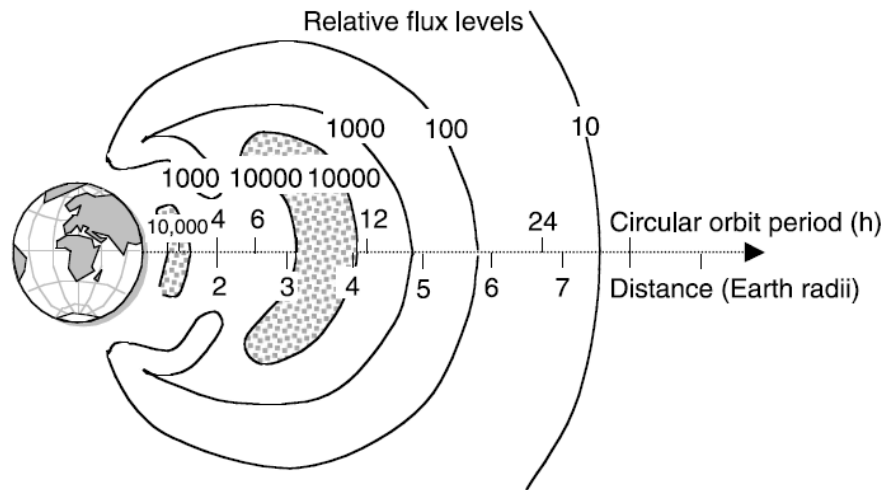


Figure 7.4: Schematic of relative flux levels corresponding to distance from Earth. Van Allen radiation belts indicated by grey-dotted areas. Based on NASA's AP-8 environment. [27]

Since the S/C conducts a low-thrust transfer from Earth to the Moon, the time spent in the Van Allen belts is considerable. A detailed study of the total radiation dose received by the solar array and its damaging effect must give insight into the degradation due to natural radiation. The ionized particles in the cislunar region are at a wide range of different energy levels, expressed in [MeV]. If the damaging effect per energy level is known, the total electron fluence [ $e/cm^2$ ] can be normalized to an equivalent energy level of 1 [MeV].

To determine the total amount of equivalent electron fluence received, the SPace ENVironment Information System (SPENVIS) is used. This is a tool developed by ESA and it provides information on the space environment. Since the tool is not (yet) capable of simulating a transfer orbit, the conducted spiral trajectory of the S/C must be divided into segments. The boundaries of these segments are defined by two altitudes with respect to the Earth's surface. The real transfer time between these two altitudes will be the input for the segment simulation time, which is not allowed by SPENVIS to exceed 30 days. The orbit in each segment will be elliptic with its periapsis and apoapsis respectively at the lower and higher altitude. [29, pp. 49–54] In Figure 7.5, the altitude with respect to the Earth's surface is given as a function of time.

In Table 7.6, the segmentation of the transfer orbit is presented. The total trajectory is divided into 16 segments, with respective simulation times between 19 and 30 days (maximum). Since SPENVIS is only able to handle 10 segments at a time, the total transfer is split up into a trajectories from LEO parking orbit to the outer boundary of the outer

<sup>2</sup>situated between the Earth and the Moon.

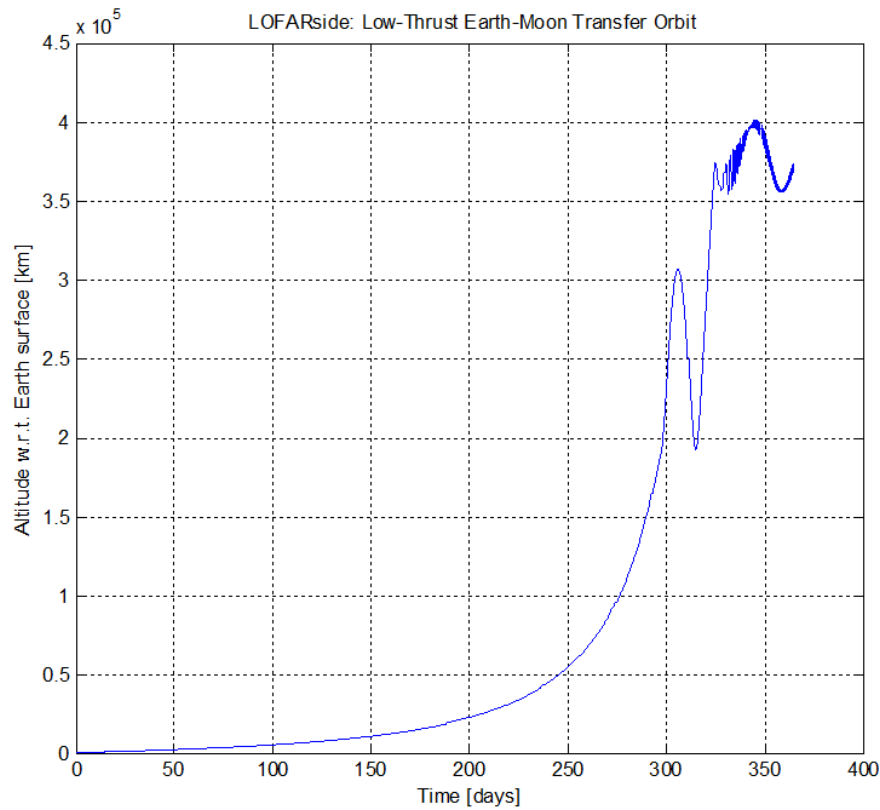


Figure 7.5: The altitude of the low-thrust transfer orbit from LEO to LLO given as a function of time.

radiation belt and from there to LLO parking orbit. The first trajectory is divided as such, so that the segmentation specifically accounts for the Van Allen belts. As can be seen, the first segment covers the altitude range from LEO parking orbit to the inner boundary of the inner radiation belt. The elliptic orbits in segment 2 through 7 take place in the inner Van Allen belt, an area dominated by ionized protons. The orbits in the outer belt are simulated in segment 8 through 10. Segments 11 through 16 cover the second trajectory.

With the generated segmented transfer orbit, the NASA's space environment models AP-8/AE-8 can be used to approximate the total radiation dose received from LEO parking orbit to LLO. This is done with SPENVIS. The damage equivalent fluences normalized to 1 [MeV] are obtained for coverglass thicknesses ranging from 0 to 1524 [ $\mu\text{m}$ ]. This is presented in Table 7.7. The coverglass is made of silicon dioxide ( $\text{SiO}_2$ ) and has a density of  $\rho = 2.32$  [ $\text{kg}/\text{m}^3$ ].

The more thick the coverglass, the more resistant the solar cell is against radiation damage. However, the mass of the solar array will increase as well. The optimum coverglass thickness is found at the point where increasing the thickness would only add more mass to the solar array than it would save mass. In Figure 7.6, a diagram of the 1 [MeV] fluence as a function of coverglass thickness is depicted. For the LOFARside mission, a coverglass thickness of 250 [ $\mu\text{m}$ ] is chosen. This corresponds to a 1 [MeV] electron front side fluence of  $2.55(10)^{15}$  [ $\text{e}/\text{cm}^2$ ]. The fluence through the rear side of the solar panel is estimated to be 10% of the front side fluence<sup>3</sup>. The total 1 [MeV] electron power irradiation endured by the solar panels throughout the transfer orbit therefore equals  $2.81(10)^{15}$  [ $\text{e}/\text{cm}^2$ ].

In Figure 7.7, the normalized maximum power is given as a function of total 1 [MeV] fluence. In order to determine the life degradation due to radiation damage, the normalized maximum power must be obtained at a 1 [MeV] fluence amount of  $2.81(10)^{15}$  [ $\text{e}/\text{cm}^2$ ]. This results in  $L_d = 0.79$  [-], hence a life degradation of 21%.

#### LANDING, DEPLOYMENT AND OPERATION PHASE

Since one of the requirements is given to be scientific operations of 5 years, Noor should provide enough power output for those 5 years. During the operational period the solar panel performance will decrease due to different reasons. The factors that cause this degradation must be considered to calculate the life degradation  $L_d$ .

<sup>3</sup>Remco van der Heijden (AD&S), personal communication, January 14, 2015

Segment #	Orbit Altitude [km]		Real time [days]		Simulation time [days]	Note
	Perigee	Apogee	Start	End		
1	300	1275	0	28	28	LEO
2	1275	2260	28	50	22	Inner heavy radiation belt
3	2260	3500	50	73	23	Inner heavy radiation belt
4	3500	5000	73	95	22	Inner heavy radiation belt
5	5000	7000	95	117	22	Inner radiation belt
6	7000	9600	117	140	23	Inner radiation belt
7	9600	13000	140	162	22	Inner radiation belt
8	13000	20000	162	192	30	Outer heavy radiation belt
9	20000	27400	192	212	20	Outer radiation belt
10	27400	38000	212	231	19	Outer radiation belt
11	38000	60000	231	253	22	Cislunar region
12	60000	100000	253	275	22	Cislunar region
13	100000	190000	275	297	22	Cislunar region
14	190000	303000	297	321	24	Cislunar region
15	303000	400000	321	346	25	Lunar Capture
16	360000	400000	346	365	19	LLO

Table 7.6: The segmentation of the transfer orbit from LEO to LLO. Used to model the damaging effect of radiation in SPENVIS.

Coverglass thickness [ $\mu\text{m}$ ]	Total 1 MeV Fluence [ $e/cm^2$ ]		
	$P_{max}$	$V_{oc}$	$I_{sc}$
0	6.90E+18	4.64E+18	6.87E+18
25.4	9.19E+16	7.51E+16	7.38E+16
76.2	1.56E+16	1.55E+16	1.05E+16
152.4	5.47E+15	5.85E+15	3.35E+15
304.8	1.88E+15	2.12E+15	1.06E+15
508	7.56E+14	8.93E+14	3.95E+14
762	3.96E+14	4.79E+14	2.03E+14
1524	1.28E+14	1.60E+14	6.18E+13

Table 7.7: The damage equivalent fluences normalized to 1 [MeV] for a triple junction AZUR 3G28C, similar to a 3G30C, given for different coverglass thicknesses.

The lunar environment is dominated by four radiation types: low energy Solar Wind Particles (SWPs), high energy Galactic Cosmic Rays (GCRs), sporadic high energy particles released during Solar Energetic Proton (SEP) events and secondary radiation caused by interactions of these previously mentioned sources with the lunar surface [30]. Furthermore, interactions with the plasma can influence the EPS and may cause problems like charging, arcing, electrical breakdown of dielectrics and shifts in electrical potential [26].

For an estimation of the life degradation an evaluation of the total radiation received by the solar array and the damage it will cause was conducted. As mentioned earlier the lunar environment consists of a range of different ionized particles, which all have different energy levels. A similar approach, as explained in Section 7.2.7, was used to determine the degradation for mission lifetime of Noor. For the calculations the average lunar apogee and perigee for the years 2022 - 2027 were used [4]. The average lunar apogee and perigee were calculated to be 405378 [km] and 362565 [km] respectively. The total fluence for 90 days was found to be  $1.25(10)^{13} [e/cm^2]$ , which leads to a value for the fluence for 5 years of  $2.534(10)^{14} [e/cm^2]$ . This corresponds with a degradation of 4% over 5 years of operations.

Then the degradation caused by other factors than radiation needs to be determined. The contribution of the radiation to the total life degradation is obtained from [25, pp. 647]. Generally, the degradation caused by radiation is 60%. This means that the total degradation for a mission duration of 5 years is 6.7%, which will provide for a value of  $L_d$  of 0.933.

### 7.2.8. TEMPERATURE EFFECT

The temperature of the spacecraft and the solar panels fluctuates throughout its mission. An increase in temperature decreases the performance of the solar cells and thus the solar panels. The amount of performance decrease can be

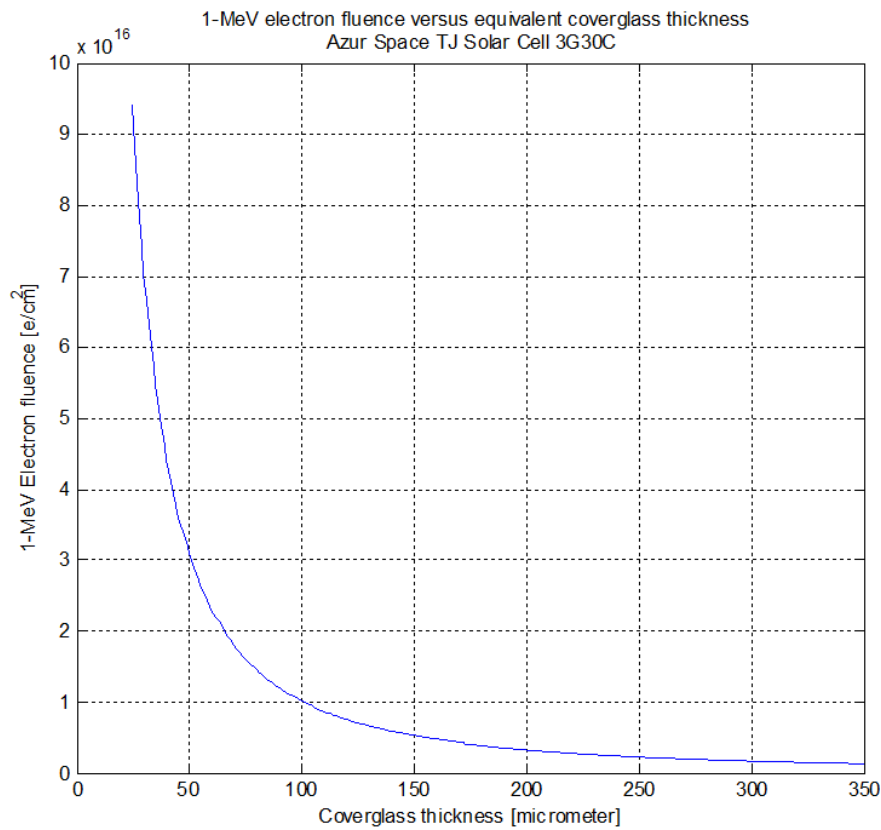


Figure 7.6: 1 [MeV] electron fluence versus equivalent coverglass thickness

estimated with the temperature coefficient  $\gamma_T$  [%/°K]. This coefficient is a function of 1 [MeV] fluence  $e$ . In Table 7.8, the effect of 1 [MeV] electron irradiation on the temperature coefficient of 3G30C solar cell can be seen. The results for the temperature coefficient  $\gamma_T$  are more or less the same for each level of irradiation: in the range of -0.25 to -0.23 [%/K].

1 [MeV] $e$ [ $e/cm^2$ ]	$P_{max}$ [W]	$\gamma_{T,P}$ [mW/°K]	$\gamma_T$ [%/K]
1E+14	1.187	-2.7	-0.23
2E+14	1.159	-2.8	-0.24
5E+14	1.128	-2.8	-0.25
10E+14	1.086	-2.7	-0.25
30E+14	0.953	-2.3	-0.24

Table 7.8: The effect of 1 [MeV] electron irradiation on the temperature coefficient. [31]

### TRANSFER PHASE

As was discussed in Section 7.2.7, the total 1 [MeV] electron fluence captured by the solar panels throughout the transfer phase equals  $2.81(10)^{15}$  [ $e/cm^2$ ]. From Table 7.8, the corresponding temperature coefficient is then estimated to be -0.245 [%/°K]. The temperature range, the solar panels have to endure at EOL are between 88 [K] and 344 [K] (Chapter 13). The reference performance of the solar cell is measured at an average temperature of 301 [K]<sup>4</sup>. The efficiency at maximum temperature is then calculated with Equation (7.5) to be  $\eta_{T,max} = 0.89$  [-].

$$\eta_{T,max} = 100 + (T_{max} - T_{ref})\gamma_T = 100 + (344 - 301)(-0.245) = 89\% \quad (7.5)$$

<sup>4</sup>[http://www.azurspace.com/images/products/0003384-01-01\\_DB\\_3G30C\\_advanced.pdf](http://www.azurspace.com/images/products/0003384-01-01_DB_3G30C_advanced.pdf)

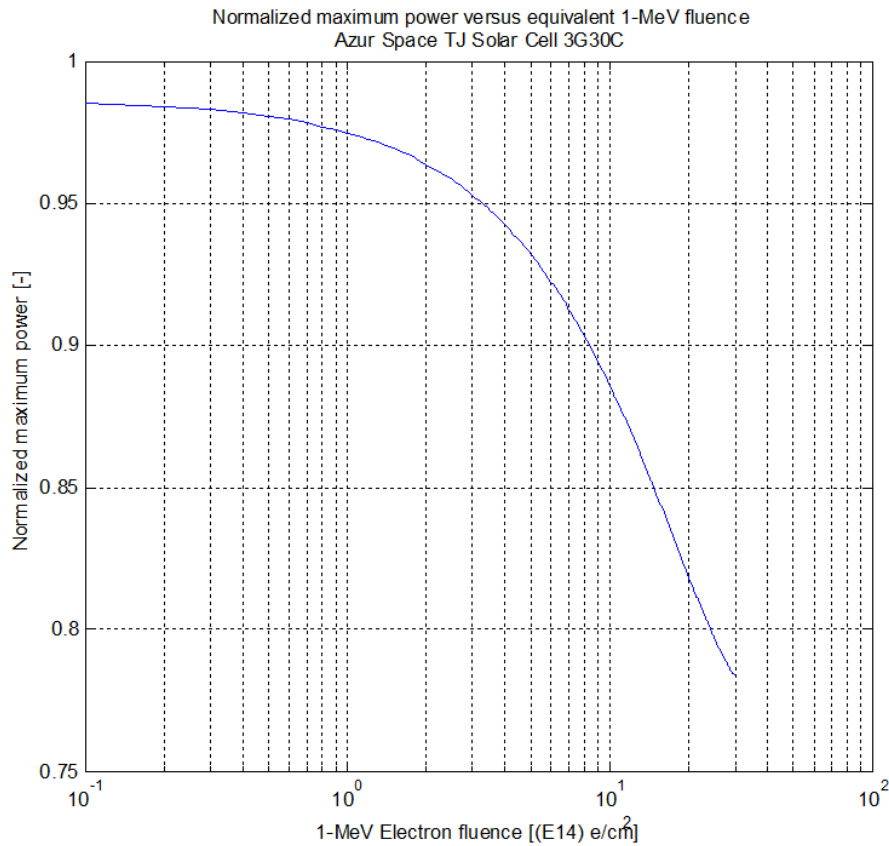


Figure 7.7: Normalized maximum power versus equivalent 1 [MeV] electron fluence.

#### LANDING, DEPLOYMENT AND OPERATION PHASE

For the remaining phases, the temperature fluctuations at the Shackleton crater rim are evaluated. These range from 90 [K] to 135 [K], hence do not exceed 301 [K]. Therefore the efficiency at maximum temperature equals  $\eta_{T,max} = 1.00$  [-]

#### 7.2.9. POWER PRODUCTION CAPABILITY: BOL AND EOL

For sizing of the solar array the average power requirement and mission life are two key design considerations. The solar array system must be designed to meet the power requirements at the EOL and therefore the array will be oversized for BOL [27]. As stated in Section 7.1, the total power production capability of the solar array at EOL must be 9430 [W] for the transfer phase and 535 [W] for the mission operation phase. Using Equation (7.6),  $P_{BOL}$  can be computed for both phases. The excess power that results from subtracting  $P_{EOL}$  from  $P_{BOL}$  equals approximately 2500 [W] and 38 [W] for the transfer and mission operation phase respectively. This is summarized in Table 7.9. Note that the large amount of excess power produced at the start of the transfer phase may inflict thermal problems. This excess power must be diverted with shunt modules (Section 7.4).

$$P_{BOL} = \frac{P_{EOL}}{L_d \eta_{T,max} \cos \theta} \quad [W] \quad (7.6)$$

Mission Phase	$P_{BOL}$ [W]	$L_d$ [-]	$\eta_{T,max}$ [-]	$\theta$ [°]	$P_{EOL}$ [W]	$P_{Excess}$ [W]
Transfer	13420	0.790	0.89	2	9430	3990
Noor	644	0.934	1.00	18.18	571	73

Table 7.9: Overview on  $P_{BOL}$  and  $P_{EOL}$  for the transfer and mission operation phase.

### 7.2.10. AREA, MASS AND COST OF SOLAR ARRAY

The solar array area required to deliver the end-of-life power amount  $P_{EOL}$  is determined with Equation (7.7). For Noor this value of  $A_{sa}$  has to be multiplied with  $\pi$  because of the given configuration of the solar cells, which will be explained in more detail in Section 7.5. The corresponding mass can be calculated using Equation (7.8), where  $\rho_{A,sa}$  is the area density equal to  $5.5 [kg/m^2]$ <sup>5</sup>. The total cost of the solar array can be estimated with Equation (7.9), where  $c_{sa}$  is the specific cost equal to  $2500 [€/W]$ <sup>6</sup>. The parameters used to fill in these equations are obtained throughout this chapter and are summarized in Table 7.10, along with the numbers found in this section.

$$A_{sa} = \frac{P_{EOL}}{S_r \eta_{cell} I_d L_d \eta_{T,max} \cos \theta} \quad [m^2] \quad (7.7)$$

$$m_{sa} = \rho_{A,sa} A_{sa} \quad [kg] \quad (7.8)$$

$$C_{sa} = c_{sa} P_{BOL} \quad [euro] \quad (7.9)$$

Parameter	Symbol	Mission Phase	
		Transfer	Noor
Power beginning-of-life	$P_{BOL} [W]$	13420	644
Power end-of-life	$P_{EOL} [W]$	9430	571
Solar flux	$S_r [W/m^2]$	1370	1370
Solar cell efficiency	$\eta_{cell} [-]$	0.295	0.295
Inherent degradation	$I_d [-]$	0.72	0.72
Life degradation	$L_d [-]$	0.79	0.934
Thermal efficiency	$\eta_{T,max}$	0.89	1.00
Incidence Angle	$\theta [^\circ]$	1	18.18
Solar array area	$A_{sa} [m^2]$	46	7
Solar array mass	$m_{sa} [kg]$	253	38.5
Solar array cost	$C_{sa} [€]$	34M	1.6M

Table 7.10: Overview on the parameters calculated and defined to calculate the area, mass and cost of the solar array.

## 7.3. ENERGY STORAGE

The secondary power system is designed to provide power in case no solar radiation is available. For both power subsystems this will occur during eclipse periods. Furthermore, the energy storage system is also designed for peak power demands. A number of different design options are available. The most common secondary power sources used in space technology are batteries. However, other interesting technologies, like flywheels and regenerative fuel cells, also find application on S/C. However, one of the given requirements is to use off-the-shelf products for the LOFARside mission. Therefore, as well as for other reasons not necessarily mentioned here, these technologies were rejected and secondary batteries were chosen.

### 7.3.1. BATTERY TYPES

Secondary batteries are different from primary batteries in that the chemically stored energy which is used during discharge can be returned when the battery is recharged. After the discharge period, the battery can be recharged by the primary power source of the S/C. Each battery consists of a number of electrochemical cells that are assembled in series to obtain the required voltage and current [27]. The batteries themselves can also be connected in series to increase the voltage and connected in parallel to increase the current output. This will result in an increase of the capacity [Whr] [3]. In Table 7.11 different types of batteries are given as well as their properties.

For the LOFARside mission Lithium ion (Li-ion) batteries will be chosen due to a couple of reasons. The technology for Li-ion batteries offers a better performance than Nickel Cadmium (NiCd), Nickel Hydrogen (NH<sub>2</sub>) and Nickel Metal Hybrid (NiMH). The Li-ion batteries have a higher energy and volume density, which gives a 50% mass and

<sup>5</sup>Remco van der Heijden (AD&S), personal communication, January 20, 2015

<sup>6</sup>Anonymous, personal communication, January, 2015

Characteristic	NiCd	NiH2	NiMH	Li-ion
Specific Energy [Whr/kg]	35	49 IPV 60 CPV	60	85-175
Energy Density [Whr/l]	45	25 IPV 40 CPV	86	160
Operating Temperature [Celsius]	- 40 / +70	- 5 / + 20	- 5 / + 20	- 40 / + 70

Table 7.11: Characteristics of different secondary batteries. Note, IPV means individual pressure vessel and CPV means common pressure vessel [32, pp. 657].

65%. Moreover, the higher recharge efficiency of Li-ion will provide advantages for the thermal control system. Lastly the Li-ion technology has a low self discharge rate of 5% per year [25].

The most renowned manufacturers for batteries used in space applications are Saft and Eagle Picher. Both companies are known for their Li-ion batteries <sup>7</sup>. To select the most optimal battery amongst the options, a trade-off is conducted by adding the normalized energy, specific energy and the normalized weight. Both factors have equal weight. The normalized values are added to see which battery type performs best in the two characteristics which are important for the LOFARside mission. Furthermore, note that during normalizing the weight of the batteries, the highest score was denoted to the lowest weight. The results of the trade-off are shown in Table 7.12. The winner battery type for this mission was found to be the VES 180 from Saft.

Battery type	Energy [Whr]	Normalized Energy [-]	Specific Energy [Whr/kg]	Normalized Specific Energy [-]	Score	Ranking
VES 180 (Saft)	180	0.479	165	1	1.479	1
SLC-21060-001 (Eagle Picher)	256	1	131.7	0.238	1.238	2
VL48E (Saft)	170	0.411	150	0.657	1.068	3
SLC-16050 (Eagle Picher)	204	0.644	121.3	0	0.644	4
SLC-027-01 (Eagle Picher)	112	0.014	139	0.405	0.419	5
VES 140 (saft)	140	0.205	126	0.108	0.313	6
SLC-028-01 (Eagle Picher)	110	0	125	0.085	0.085	7

Table 7.12: Trade-off for Li-ion batteries in order to decide which battery is the best option. Note, the different manufacturers are denoted under the battery type.

### 7.3.2. BATTERY SIZING

To size the batteries the total energy,  $C_r$ , of the battery system is calculated using Equation (7.1). Below, this equation is stated again. Where  $P_e$  denotes the required power during eclipse time,  $T_e$  is the time duration of the longest eclipse in hours during the mission,  $DOD$  gives the Depth-of-Discharge,  $N$  is the number of batteries and  $n$  is the battery-to-load transmission efficiency. For both systems a transmission efficiency of 90% is assumed [3, pp. 422].

$$C_r = \frac{P_e T_e}{(DOD) N n} \quad [Whr]$$

Using the specifications of the SAFT VES-180 battery, which are an energy of 180 [Whr] and a specific energy of 165 [Whr/kg], the number of batteries and mass can be determined.

<sup>7</sup>Brochures can be found at <http://www.saftbatteries.com/battery-search/mp-vl-batteries-other-space-vehicles> and <http://www.eaglepicher.com/lithium-ion-8>

## TRANSFER PHASE

As previously calculated in Section 7.1.1, the total energy of the batteries equals  $C_r = 1580$  [Whr]. The minimum number of VES-180 batteries needed to power the S/C in eclipse mode can then be obtained with Equation (7.1) and is  $N = 9$ . Since the specific energy is 165 [Whr/kg], the corresponding total mass is computed to be 9.6 [kg].

## LANDING, DEPLOYMENT AND OPERATIONS PHASES

The energy storage system of Noor must provide for the required power of the operational phase during eclipse, the total power needed for both the landing phases and the necessary power for deployment. The batteries must provide power for the latter if midway the deployment or during the entire time an eclipse period occurs.

The first step is to determine the DOD for the batteries of Noor. In Figure 7.8 the illumination fraction at the landing site is given. All these peaks represent a life cycle for the Li-ion battery inside, so counting these peaks results in an estimate of 150 peaks every 6 months, which leads to a total of 1500 life cycles. This corresponds to a DOD of 85% for the VES 180 from Saft<sup>8</sup>. Although this value seems very high, the battery will rarely be completely discharged because of the irregular illumination conditions as explained in Section 5.2.

Using Equation (7.1) the total energy,  $C_r$ , for the landing, deployment and operation phases can be calculated. The results are presented in Table 7.13. The operational phase is the most demanding segment for the energy storage system. If the system is designed for this phase, it can provide enough power during the other phases. For  $C_r = 303$  [Whr] Noor will need 2 batteries. Note, that this is a non-redundant design. Using the specific energy of the VES 180 the mass of the battery system is calculated to be 1.8 [kg].

Segment	$C_r$ [Whr]
Landing Phase A	4
Landing Phase B	0.2
Deployment Phase	44.3
Operational Phase	303

Table 7.13: Overview of the total energy,  $C_r$ , needed for the landing, deployment and operation phases.

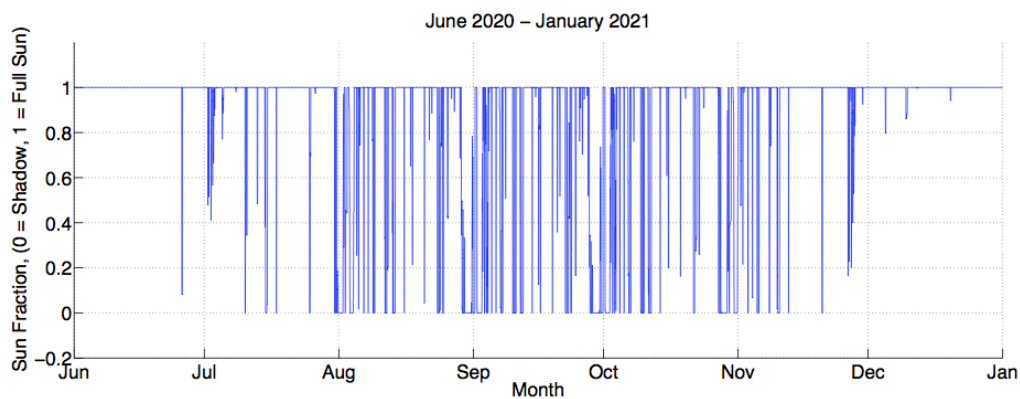


Figure 7.8: Estimated Sun illumination fraction near the Shackleton Crater rim, for Jun 2020 - January 2021. The Sun illumination fraction is defined as the fraction of the Solar illumination and eclipse [33]

### 7.3.3. REGENERATIVE FUEL CELLS

For the design of Noor's secondary power source the use of regenerative fuel cells (RFCS) was considered. RFCS are interesting for application on lunar base scenarios, particularly on the South pole, where these systems can result in a significant mass reduction in comparison with a battery system [13]. Results obtained in [13] show that even with a significantly oversized solar array, a battery system is heavier than a reasonably-sized solar array combined with a RFCS system. However, the use of RFCS was rejected because mass is not the only factor to be considered. Other important things to consider are reliability, flight experience and Technology Readiness Level (TRL). The RFCS systems are not yet space proven, which is the most important objection, since one of the requirements of the LOFARside mission is to use products that will have a TRL of 5 at the beginning of the mission. Moreover, RFCS become very interesting when the S/C has high power demands ( $>1$  [kW]) which is not the case for Noor. It actually as a relatively low power demand.

<sup>8</sup><http://www.saftbatteries.com/battery-search/mp-v1-batteries-other-space-vehicles>

## 7.4. POWER MANAGEMENT AND DISTRIBUTION

Within the S/C all instruments and components have different operating voltages and power demands. The power management and distribution subsystem (PMAD) is responsible for managing the alternating loads within the S/C. That is, high loads when the solar panels provide power and low loads in eclipse periods, when the subsystems are powered by the batteries.

### 7.4.1. POWER DISTRIBUTION

Without a proper power distribution the EPS is prone to power losses. These losses occur in the regulation devices and conductors when the current gets to high. Power is the product of voltage and current, so the voltage should increase proportionally with the power to keep the current at a low level [27]. To match product requirements of space agencies and manufacturers the S/C bus voltages are often chosen from standardized values. These are: 28, 50, 70, 100, 120 and 160 [V] [27]. When choosing the bus voltage Equation (7.10) [27, pp. 56] can be used. The value obtained for the optimum voltage is then shifted to the nearest standard voltage. One of the top level requirements for the LOFARside mission indicates that the use of off-the-shelf products is preferred. This means that the S/C bus voltage for the transfer and for Noor should preferably fall within the standard voltage bands.

$$V_{opt} = 0.025P_{req} \quad [V] \quad (7.10)$$

A power distribution system of a S/C can be organized in two ways, either centralized or decentralized. The positioning of the converters determines which type is used. The converters are located at each individual power load when using a decentralized method. The centralized system uses the main bus to regulate the distribution so the converters are located within the bus[3] [27].

#### TRANSFER PHASE

The total power requirement for Sp<sup>í</sup>laio equals 9430 [W]. Operating the electric engines requires the largest part of the budget, namely 8500 [W]. Since the electric propulsion subsystems consist of more components than just the electric thrusters, the total power distribution will be divided into two different voltage busses: one solely for the electric engines and one for the other components of the propulsion subsystem and the other subsystems.

To determine the optimum voltage for both busses, Equation (7.10) is applied. Using  $P_{req,engines} = 8500$  [W] and  $P_{req,bus} = 970$  [W], the resulting optimum voltages are 213 [V] and 25 [V] respectively. To benefit from the familiarity and availability of standard voltage busses, these optimum voltages are shifted towards their closest standard voltages. Thus, a 160 [V] voltage bus and a 28 [V] voltage bus will be used. The conversion between the two busses is done by a DC/DC unit in the Power Distribution Unit (PDU), which then distributes the power over the subsystems and batteries. This is depicted in Figure 7.9.

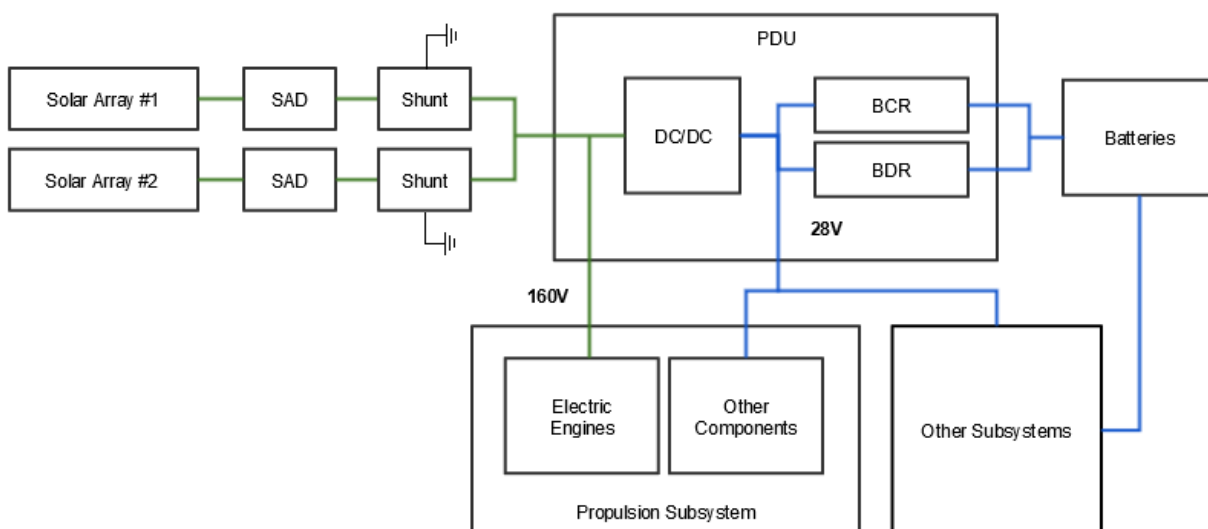


Figure 7.9: Electrical Block Diagram of Sp<sup>í</sup>laio EPS.

SAD = Solar Array Drive, PDU = Power Distribution Unit, BCR = Battery Charge Regulator, BDR = Battery Discharge Regulator

### LANDING, DEPLOYMENT AND OPERATION PHASE

For Noor the bus voltage was determined with Equation (7.10). The power requirement for Noor differs each phase. Therefore the bus voltage for all phases was calculated using the power requirements provided in Table 7.2. The bus voltage for all phase was found to be 28 [V], which is very convenient since this simplifies the power distribution. This value is confirmed by [3] and [26] where it is stated that S/C with low power demand ( $< 2000$  [W]) rely on a standard bus voltage of 28 [W] for the power distribution.

Noor will use a centralized approach, where the power is regulated from the main bus. This means that the power distribution subsystem will not need a customized EPS for the different subsystems. For smaller S/C that have relatively low power requirements, this approach is preferred[3]. In Figure 7.10 this centralized approach is shown. The power distribution unit (PDU) will regulated the power towards all the other subsystems.

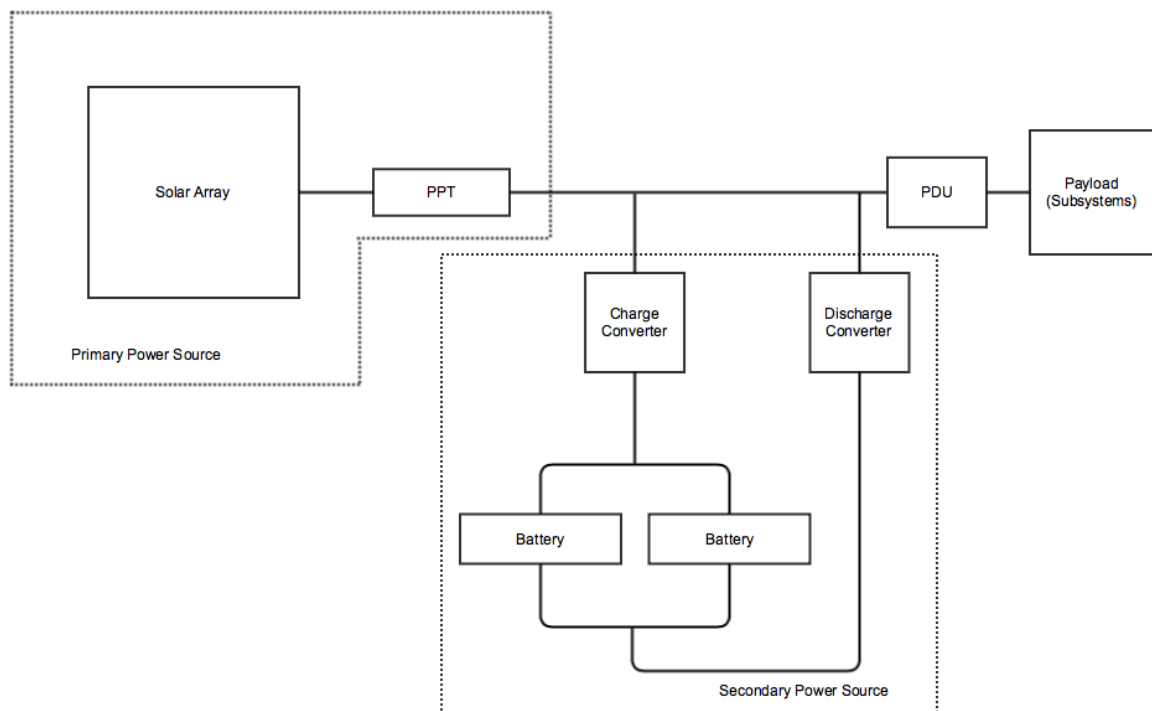


Figure 7.10: Electrical Block Diagram of Noor Power Subsystem. Note, PPT: Peak-Power Tracker and PDU: Power distribution Unit.

#### 7.4.2. POWER REGULATION

Three main parts can be distinguished within the power regulation subsystem, with respect to an EPS using a combination of a solar array and batteries. These three parts are: controlling the solar array, regulating bus voltage, and charging the battery [3]. In the same order these three parts of the regulation system will be discussed.

For controlling the power coming from the solar array two main methods are used, the peak-power tracker (PPT) and a direct-energy-transfer (DET). The PPT will, as its name suggests, track the peak power of the solar array and it will withdraw the power demands of the S/C as long as these do not exceed the peak power of the solar array. The DET on the other hand dissipates the power not used by the S/C [3] [27].

The bus voltage of the S/C can be regulated with three different regulation types, these are Sun regulated, quasi-regulated or fully regulated. For a Sun regulated S/C the bus voltage will be derived from the battery regulation and therefore vary significantly over time. A quasi-regulated S/C only regulates the bus voltage during charging but not during the discharge. The S/C will be fully regulated when the entire system needs regulation [3] [27].

Finally, the charging of the batteries is discussed. There are two ways for charging, either parallel or in series. A parallel system is often chosen because it is less complex and also lower in cost. There are also a couple of disadvantages, the system is more difficult to integrate within the S/C and due to temperature differences during charging the batteries might degrade faster. Therefore individual charging of the batteries is preferred for missions with a lifetime longer than 5 years [3] [27].

## TRANSFER PHASE

The power for Spílaio will be controlled by a direct-energy-transfer (DET) subsystem with a shunt regulator to divert the excess power. The advantages over a peak-power-tracker (PPT) is the higher efficiency at EOL, lower mass, lower complexity and lower cost. A disadvantage is that the total power generated by the solar arrays cannot be used to its full potential [3]. However, since the solar arrays are heavily oversized to comply with the EOL power requirements and the BOL power is abundant, this disadvantage can be disregarded. In Figure 7.9, the electric block diagram is presented.

## LANDING, DEPLOYMENT AND OPERATION PHASE

The first step is to determine which type of power control technique is going to be used. For Noor a PPT subsystem was chosen because this technique is more suitable when there are large variation in solar array input energy throughout the mission [27] [26]. At the landing site the illumination is very irregular and therefore the eclipse and daylight periods are irregular as well. A PPT makes the best use of the solar array at every moment of the mission [27] [26]. The PPT unit will be placed between the solar array and the batteries, as can be seen in Figure 7.10.

Secondly, a proper bus voltage controlling system was chosen. Noor requires a highly regulated bus, because of the different power demands during the different phases, as presented in Table 7.2. Given the irregular illumination pattern at the landing location, trickle charge of the batteries is necessary. Moreover, these power demands are relatively low. A fully regulated EPS might be very inefficient when used for S/C that have high power requirements [3]. For these reasons it was decided to use a fully regulated bus.

Lastly, it determined that Noor will charge the batteries in parallel, which is shown in Figure 7.10. This technique was chosen due to the lower cost, less complexity, as well as the mission duration which is 5 years. For mission longer than 5 years individual charging is preferred [3]

## 7.5. STRUCTURAL ELEMENT OF NOOR'S SOLAR ARRAY

For the solar array of Noor some considerations regarding its structural elements are presented in this section. First the location and configuration of the solar cells is discussed and then the protection of the solar cell during different phases of the mission is explained.

### 7.5.1. LOCATION AND CONFIGURATION OF THE SOLAR CELLS ON NOOR

Generally solar arrays are in three different configurations: planar, cylindrical or omnidirectional. The most common and well known type are flat panels that are pointed towards the Sun. Power output from this type of panels is proportional to area of the the panels pointing towards the Sun. Cylindrical arrays are very compatible with spin-stabilized systems, which will point the spin axis perpendicular towards the Sun [3]. This configuration is often used on small satellites. The cells will be mounted directly on the body of the S/C and therefor no honeycomb substrate is necessary. This will save substrate mass as well as gimbals. However, the obvious disadvantage is that the S/C will need about 57% more solar cells to provide for the same power requirements [27].

For Noor it was decided to mound the solar panels directly on the configuration of Noor because of a couple of reasons. Firstly, the illumination pattern at the landing site is very complex. If planar panels were used, then this pattern would get even more complicated since the eclipse periods caused by the orbital mechanics of the Sun-Earth-Moon system should be considered too. Furthermore, the panels should be designed to move around part of the body of Noor so they can account for the orbital movements of the Moon. This would mean more moving parts and complex structures. The second reasons is that with this configuration the solar array can be protected easily against loads caused by landing as well as the plume caused by the thrusters. The later will be explained in more detail in Section 7.5.2. Finally, body mounted solar cells mean that no extra deployment system is necessary and therefore less moving parts, so no risk of failure and a higher reliability. However, more solar cells are needed to provide for the same power demands. On the other hand, less mass is necessary for the the panel structure due to the fact that no honeycomb substrate, moving parts and deployment structures are used.

The decision to place the solar cells on the body will cause the total output power of the array to decrease. The cells will not always be orientated toward the Sun but the output of the array will be nearly proportional to the amount of solar energy intercepted [27]. The area of the configuration that intercepts solar energy is  $1/\pi$  times the total area of Noor. For this reason the array should have  $\pi$  times more solar cells to provide for the same amount of power. The solar cells are only placed on the top part, which has the cone shape.

### 7.5.2. PROTECTION OF THE SOLAR CELLS ON NOOR

Proper operation of the solar cells is essential for the success of the LOFARside mission because the EPS of Noor will provide, among others, for the power demands of the scientific operations. During different phases of the mission their functioning might be compromised. Therefore the protection of the solar cells during these periods will be discussed.

#### TRANSFER PHASE

The solar cells of Noor must be protected against the natural radiation, caused by charged particles in for example the Van Allen belts, where the S/C comes across during transfer. For this purpose a protection shield of a still to determine material will be used. This shield will be attached around the truncated cone of Noor. The bottom part of the shield is attached with hinges and the top part will use a spring system. Once Noor has landed the top part of the plate will be released using this spring system. The shield should fold open like a flower.

#### LANDING, DEPLOYMENT AND OPERATION PHASE

Lunar dust may cause problems for lunar exploration missions because of the highly charged dust particles. These particles are very 'sticky' and get attached to surfaces of equipment, optical systems, instrumentation and solar panels. Dust accumulation on the solar panel will mean that the total output power of the solar array will decrease. There are ways to actively remove the dust, which also prevents dust from accumulating on the solar cells. These systems use electrostatic and dielectrophoretic forces to remove dust from surfaces and to prevent the accumulation of dust on these surfaces [34] [35] [36]. In [34] and [35] these active removal and dust prevention systems were tested and simulated in lunar conditions. The results show that the transparent dust shield operates successfully under high vacuum, even with extreme dust loading that caused the solar cell performance to drop to 11-13% of the normal performance. The dust shield showed an improvement above 90% in solar cell performance. Furthermore, the solar cell performance did not appear to be influenced by the application of the dust shields. The use of an electrostatic and dielectrophoretic dust shield seems very promising to protect the solar cells of Noor against lunar dust.

## 7.6. VERIFICATION AND VALIDATION

Calculations in this chapter were based on physical methods and models provided in [3], [25], [27], [26] and [37]. After the different methods were applied and simulated for the LOFARside mission these were checked with numerical values and results obtained with analytical calculations. For validation of the applied approach the computed results were compared with existing data, for example the SMART-1 mission and the conceptual design of the ESA Lunar Lander.

The sizing of the EPS of Sp<sup>í</sup>laio was partly based on the SMART-1 mission. Especially the design of the power budget relied on SMART-1's, as explained in Section 7.1.1. The life degradation of the solar array due to irradiation during the transfer orbit was assessed with SPENVIS. This is a space environment modeling system, developed and extensively verified by ESA/ESTEC [37]. Validation was done by comparing to the life degradation of the SMART-1 solar array, which was 16%<sup>9</sup>. Compared to the 21% life degradation of the solar array of Sp<sup>í</sup>laio, this is a noteworthy difference. However, SMART-1 was launched into a geostationary transfer orbit, hence the amount of time spent in the Van Allen Belts was much less. Therefore, the value found for the life degradation of Sp<sup>í</sup>laio solar array is considered validated.

The design of Noor was compared with the ESA Lunar Lander ([38]) and the Low Cost Robotic Lunar Lander from NASA ([39]) because these two conceptual designs are similar lander concepts. The mass and solar array area, as computed in this chapter, of the EPS is found to be similar and in the same order of magnitude as the Low Cost Robotic Lunar Lander [39]. The difference can be explained due to the different landing locations and therefore the different configuration of the solar array as well as the different power requirements for eclipse periods. These are much lower for the Low Cost Robotic Lunar Lander as it will not be operational during eclipse [39]. The configuration of Noor was compared to the ESA Lunar Lander, which has the same landing location and will use the configuration of the solar array [38]. This comparison also showed values similar to the ones computed in this chapter.

<sup>9</sup><https://directory.eoportal.org/web/eoportal/satellite-missions/s/smart-1>

# ATTITUDE DETERMINATION AND CONTROL SUBSYSTEM

The Attitude Determination & Control Subsystem (ADCS) is crucial for the mission success since it helps to determine the inertial orientation and position of the S/C. It then feeds the information to the actuators allowing to ultimately control the S/C to suit the required mission's needs with the correct accuracy. This chapter discusses the ADCS requirements (Section 8.1), the appropriate equations of motion (Section 8.2) and the geometric properties of the S/C (Section 8.3). Furthermore, the different disturbance torques (Section 8.4) and the transfer phase ADCS design are explained (Section 8.5). This chapter concludes with the ADCS block diagram (Section 8.6) and an evaluation of the verification and validation procedures (Section 8.7).

## 8.1. ADCS REQUIREMENTS

Before designing the ADCS, all mission requirements and S/C capabilities must be defined. This subsystem will be most crucial through the transfer phase and landing, where small maneuvering will be required to maintain the planned mission trajectory. For the transfer phase, one of the most important requirements is that the S/C needs to be always 3-axis stabilized. This will help to control the orientation of the body once a torque is applied to obtain a desired attitude. Furthermore, from mission needs, during the transfer phase the electric propulsion thrust vector must always be pointing in the direction perpendicular to the Earth's gravitational acceleration. This can be sometimes naturally achieved through gravity gradient stabilization, depending on the S/C's geometric configuration.

The structure also requires a certain angular rate requirement to cope with the necessary pointing accuracy. Although pointing mechanisms should be avoided since they introduce complexity and unreliability, it will be necessary to adapt the design such that the solar arrays can remain pointing to the Sun whilst the S/C aligns with the local vertical. Since it will not be necessary to acquire any high precision measurements during the transfer phase, it was decided that the pointing accuracy of the S/C will suffice with  $\theta_a = 1^\circ$ .

## 8.2. EQUATIONS OF MOTION

In order to determine the S/C's attitude dependence on the external disturbance, the equations of motion describing the kinematics of the vehicle must be derived. The S/C's attitude is determined by Euler's equations for rotational dynamics. These equations define the conservation of angular momentum ( $H$ ), which in vector form using a body fixed reference frame takes form as in Equation (8.1)[40].

$$\dot{H} = T - \omega \times H \quad (8.1)$$

This relation states that the rotational motion of a body will continue unperturbed unless an external torque ( $T$ ) is applied. It is only defined when using it in the body's reference frame, where the vector product of the angular velocity with the angular momentum ( $\omega \times H$ ) can only alter the direction of the angular momentum. Therefore, the magnitude of the angular momentum in a system can only be increased/decreased by applying an external torque. The system's momentum can be found with the help of the S/C's moment of inertia and angular velocity ( $\omega$ ) as Equation (8.2) states [40].

$$H = I\omega + h \quad (8.2)$$

Where  $h$  is the angular momentum stored by any on-board rotating object such as a momentum wheel or gyroscope. In the absence of any rotating object, the Equation Equation (8.2) in matrix form becomes:

$$H = \begin{bmatrix} I_{xx}\omega_x - I_{xy}\omega_y - I_{zx}\omega_z \\ I_{yy}\omega_y - I_{yz}\omega_z - I_{xy}\omega_x \\ I_{zz}\omega_z - I_{zx}\omega_x - I_{yz}\omega_y \end{bmatrix} \quad (8.3)$$

Using this relation, the change in angular velocity can be found using:

$$I\dot{\omega} = T - \dot{I}\omega - \omega \times H$$

The term  $\dot{I}\omega$  describes the changes in the MOI and how it can affect the attitude dynamics (i.e. solar panels and antennas). In the absence of changes in the mass properties this term will then disappear. Knowing this, the equations of motion describing the change in angular velocities can be derived. From Newton's second law, a force can be related to the change in momentum as in Equation (8.4) [40].

$$F = m \frac{dV_G}{dt} + m\Omega_{bE} \times V_G \quad (8.4)$$

With  $V_G = [u \ v \ w]^T$  being the velocity vector and  $\Omega_{bE} = \omega = [p \ q \ r]$  the angular velocities with respect to the x, y and z axes (pitch, yaw, roll) of the body frame with respect to an inertial Earth fixed reference frame. Substituting these into Equation (8.4) the following is achieved:

$$F = m \begin{bmatrix} \dot{u} + qw - rv \\ \dot{v} + ru - pw \\ \dot{w} + pv - qu \end{bmatrix}$$

The forces acting on the S/C are the thrust acting directly through the body  $F_{Thrust}^b = [0 \ 0 \ T]^T$  as well as all other incoming disturbance torques from the environmental operating conditions, which are further explained in Section 8.4. Solving for the change in angular velocities, the kinematic equations of motion describing the attitude of the S/C result in Equation (8.5) [41]:

$$\begin{aligned} \dot{p} &= \frac{I_{zz}}{I^*} T_x + \frac{I_{xz}}{I^*} T_z + \frac{(I_{xx} - I_{yy} + I_{zz})I_{xz}}{I^*} pq + \frac{(I_{yy} - I_{zz})I_{zz} - I_{xz}^2}{I^*} qr \\ \dot{q} &= \frac{1}{I_{yy}} T_y + \frac{I_{xz}}{I_{yy}} (r^2 - p^2) + \frac{I_{zz} - I_{xx}}{I_{yy}} pr \\ \dot{r} &= \frac{I_{xz}}{I^*} T_x + \frac{I_{xx}}{I^*} T_z + \frac{(I_{xx} - I_{yy})I_{xz} + I_{xz}^2}{I^*} pq + \frac{(-I_{xx} + I_{yy} - I_{zz})I_{xz}}{I^*} qr \end{aligned} \quad (8.5)$$

These help sizing the actuators that can be used to achieve the required pointing accuracy. In Section 8.5, simplifications to the equations of motion for the transfer phase are made to decrease the computational complexity. For this purpose, first the moments of inertia need to be determined.

### 8.3. S/C GEOMETRIC PROPERTIES

The geometrical properties of the S/C influence greatly the attitude and the orientation control of the vehicle. The components inside the S/C shall all be distributed and placed as symmetric as possible with respect to the vertical axis of symmetry. For this purpose, the center of mass is first computed with Equation (8.6) below, using the axis coordinates from Figure 14.1 such that:

$$\begin{aligned} C_x &= \frac{\sum m\bar{x}}{\sum m} \\ C_y &= \frac{\sum m\bar{y}}{\sum m} \\ C_z &= \frac{\sum m\bar{z}}{\sum m} \end{aligned} \quad (8.6)$$

It is found that for the symmetrical S/C structure, both  $C_x$  and  $C_y$  lie in the axis of symmetry whereas  $C_z = 1.98 [m]$  from the separation plane between the VEGA and bottom of the S/C. The solar panels will be symmetrically placed

at this  $z$  location since it will decrease the stresses in the connection hinge when changing the attitude (hence they do not shift the center of mass in any way). The mass moments of inertia are calculated using Equation (8.7) by also adding the Steiner terms with respect to the center of mass:

$$I = \int_{m_i} r_i^2 dm + m_i d_i^2 \quad (8.7)$$

Where  $m_i$  is the mass of object  $i$  and  $d_i$  is the perpendicular distance from the center of mass of object  $i$  to the center of mass of the whole structure. In matrix form it results in Equation (8.8) where the Steiner terms are already added:

$$I_{CG} = \begin{bmatrix} I_{xx} & -I_{xy} & I_{xz} \\ -I_{xy} & I_{yy} & I_{yz} \\ -I_{xz} & -I_{yz} & I_{zz} \end{bmatrix} = \begin{bmatrix} I_{xx} & 0 & 0 \\ 0 & I_{yy} & 0 \\ 0 & 0 & I_{zz} \end{bmatrix} \quad (8.8)$$

The above matrix is simplified to a diagonal matrix containing the principal axes moment of inertia since the configuration of the S/C is symmetric with respect to both x and y axes. The results are summarized in Table 8.1.

Vehicle	$I_{xx}$ [ $kgm^2$ ]	$I_{yy}$ [ $kgm^2$ ]	$I_{zz}$ [ $kgm^2$ ]
Transport Vehicle	590.5	590.5	57.65
Lander Vehicle	16.2	16.2	59.3
Total	658.7	658.7	116.95
Total (+Solar Panels Deployed)	$2.42 \cdot 10^4$	$7.39 \cdot 10^3$	$1.69 \cdot 10^4$

Table 8.1: Moments of Inertia

## 8.4. DISTURBANCE TORQUES

External torques are divided into two types: disturbance torques and control torques. Disturbance torques are the environmental torques that the S/C will experience through the course of the mission, whereas control torques are the torques generated intentionally by thrusters to achieve the desired capability (note: reaction wheels do not change the total angular momentum because they are not external torques). In Space there are several disturbance torques that need to be taken into account for the design of the ADCS. Since the LOFAR mission will begin transfer phase at 300 [km] altitude, the atmospheric torque induced by the drag is neglected.

### 8.4.1. GRAVITY TORQUE

This disturbance torque is caused by the gravity field of the Earth and needs to be compensated by the actuators. This torque can be modelled using Equation (8.9) [40]:

$$\begin{bmatrix} T_{gx} \\ T_{gy} \\ T_{gz} \end{bmatrix} = \frac{3\mu}{2R^3} \begin{bmatrix} \|I_{zz} - I_{yy}\| \sin(2\phi) \cos(\theta)^2 \\ \|I_{zz} - I_{xx}\| \sin(2\theta) \cos(\phi) \\ \|I_{xx} - I_{yy}\| \sin(2\theta) \sin(\phi) \end{bmatrix} \quad (8.9)$$

With  $\mu = 3.986 \cdot 10^{14}$  [ $m^3/s^{-2}$ ] the Earth's standard gravitational parameter and  $R$  being the distance from the S/C's center of mass to the center of the Earth. Using the values from the orbit design and assuming a maximum deviation of  $45^\circ$  for both the roll and pitch angles  $\phi$  and  $\theta$  respectively, the gravity disturbance torques were evaluated. Only the maximum torques were taken into account for the choice of the actuators. The total gravity torque is then found with Equation (8.10), where the results can be found in Table 8.2:

$$T_g = \sqrt{T_{gx}^2 + T_{gy}^2 + T_{gz}^2} \quad (8.10)$$

### 8.4.2. SOLAR PRESSURE TORQUE

The incidence of the solar rays in the solar panels induce an extra disturbance torque on the S/C. This torque is found using Equation (8.11) [40].

$$T_s = \frac{\Phi}{c} A_s (1 + q) (C_{p_s} - C_m) \cos(\varphi) \quad (8.11)$$

Here,  $\Phi$  is the solar constant with an average value at 1AU of  $\Phi = 1,366 [W/m^2]$  [40] and  $c = 3 \cdot 10^8 [m/s]$  is the speed of light.  $A_s$  represents the lit surface area, which was taken to be a maximum when the whole S/C is under full sunlight. Furthermore,  $q$  represents the reflectance factor that varies from 0 for perfect absorption to 1 for perfect reflection. In this case a value of  $q = 1$  was taken since it will result in the biggest disturbance torque for which proper actuators will have to compensate. The difference between  $C_{p_s} - C_m$  represents the distance from the center of pressure of the solar radiation to the center of gravity of the S/C. The center of solar radiation pressure was taken to be at the geometric center of the solar panels since these panels present the biggest area away from the center of mass of the S/C. Lastly,  $\varphi$  is the angle of incidence of the Sun which was taken to be  $0^\circ$  in order to achieve a maximum solar torque.

### 8.4.3. MAGNETIC TORQUE

The Earth's magnetic field also induces a torque on the S/C that tries to align any local magnetic field. The torque induced due to this is found with Equation (8.12):

$$T_m = D \left( \frac{M}{R^3} \lambda \right) \quad (8.12)$$

With  $M = 7.8 \cdot 10^{15} [Tm^3]$  the polar magnetic field,  $R$  the distance from the center of the S/C to the center of the Earth (here the orbit altitude from Section 3.1.2 is used) and  $\lambda$  a unit-less function of the magnetic latitude (varying from 1 at the magnetic equator to 2 at the magnetic poles) [40]. All worst case scenarios have been taken into account to compute the maximum total disturbance torque.

### 8.4.4. TOTAL TORQUE

The total torque acting on the S/C is then found with the equation below. In Table 8.2 all contributing torques are presented. These are used as input disturbance to the equations of motion so that the required momentum unloading can be estimated.

$$T_{total} = \sqrt{T_g^2 + T_s^2 + T_m^2}$$

Disturbance Torque	Maximum Value [Nm]
Total Gravity Torque, $T_g$	$2.7 \cdot 10^{-3}$
Solar Pressure Torque, $T_s$	$1.33 \cdot 10^{-6}$
Magnetic Torque, $T_m$	$1.16 \cdot 10^{-6}$
Total Torque	$5.9 \cdot 10^{-3}$

Table 8.2: Maximum disturbance torques acting on the S/C

## 8.5. TRANSFER PHASE ADCS DESIGN

For the transfer phase, the S/C's thrust vector must be always pointing in the direction perpendicular to the gravity pull in order to conduct the spiraling out. "If one face of the S/C with no momentum bias is pointing down the vertical then no external torque is required to maintain this condition, given that the principal axis is aligned with the normal to the orbit plane" [40].

Since the moment of inertia around the z-axis of the connected transfer and lander vehicles is smaller than the other moments of inertia ( $I_{xx} = I_{yy} > I_{zz}$ ), the S/C will naturally tend to change its orientation so that z-axis is perpendicular to the gravity pull. This is known as gravity gradient stabilization and occurs when applying passive ADCS control means. As [41] expresses, "differential forces acting on an asymmetric S/C force the minor axis (minimum moment of inertia axis) to be perpendicular to the gravitational equipotential", which is exactly the required attitude control for this mode. Nonetheless, passive control means require active control systems to counteract disturbance torques. Furthermore, the Earth's gravity field is not uniform ( $J_2$  effect) and have to further ensure that the S/C's z-axis (thrust vector) is always perpendicular to the gravity. Simplifications to the equations of motion are made in this section.

### 8.5.1. SIMPLIFIED EQUATIONS OF MOTION

The y-axis of the body fixed reference frame (see Figure 14.1) is pointing in the direction of the gravity pull and the  $[x \ y \ z]'$  coordinates are simplified to:

$$e_t = \begin{bmatrix} x \\ y \\ z \end{bmatrix} = \begin{bmatrix} 0 \\ 1 \\ 0 \end{bmatrix}$$

If, for example, the S/C is rotated by  $\phi$  around the y-axis, the coordinates of the unit vectors also change and thus the Euler rotation matrix must be incorporated such that:

$$e_t = \begin{bmatrix} \cos\phi & 0 & -\sin\phi \\ 0 & 1 & 0 \\ \sin\phi & 0 & \cos\phi \end{bmatrix} \begin{bmatrix} x \\ y \\ z \end{bmatrix} \quad (8.13)$$

From this matrix it is visible that there is a component affecting two axis at the same time. For the solar panels, which are pointing along the y-axis, to be pointing in the local gravity vector, the S/C has to rotate around the x-axis (yaw) as well as the z-axis (roll) at the same time. The kinematic equations of motion are simplified using Equation (8.14).

$$\frac{d\vec{A}}{dt} = \vec{\Omega} \vec{A} \quad (8.14)$$

Where the attitude kinematics matrix becomes:

$$\vec{\Omega} = \begin{bmatrix} 0 & \omega_z & -\omega_y \\ -\omega_z & 0 & \omega_x \\ \omega_y & -\omega_x & 0 \end{bmatrix}$$

Note, that with the current S/C configuration, the moment of inertia around the x-axis and y-axis are equal ( $I_{xx} = I_{yy}$ ), which simplifies the Euler equations of motion to Equation (8.15).

$$\begin{bmatrix} \dot{\omega}_x \\ \dot{\omega}_y \\ \dot{\omega}_z \end{bmatrix} = \begin{bmatrix} T_x \\ T_y \\ T_z \end{bmatrix} - \begin{bmatrix} I_{zz} - I_{yy} \\ I_{xx} - I_{zz} \\ I_{yy} - I_{xx} \end{bmatrix} \begin{pmatrix} \omega_y \omega_z & 0 & 0 \\ 0 & \omega_z \omega_x & 0 \\ 0 & 0 & \omega_x \omega_y \end{pmatrix} \quad (8.15)$$

Assuming the conservation of momentum, the total angular momentum of the S/C is equal to the angular momentum of the reaction mechanisms such that:

$$H_{S/C} = H_{mw}$$

The Euler EOM has to be then integrated with respect to time:

$$H_{S/C} = \int M_{S/C} dt = I_{S/C} \omega_{S/C}$$

Where  $M_{S/C} = I_{S/C} \dot{\omega}$  represents Euler equations of motion. Combining both equations, the sizing of the reaction wheels can then be estimated with the simplified Equation (8.16), with subscript 'mw' meaning the momentum wheel.

$$I_{mw} \omega_{mw} = I_{S/C} \omega_{S/C} \quad (8.16)$$

### 8.5.2. ACTUATORS

Using the above equations, proper sizing of the actuators can be achieved. For the transfer phase, it has been decided that to minimize complexity and fuel weight, Control Momentum Gyroscopes (CMG) will be placed inside the transfer vehicle, which will control the attitude of the combined S/C vehicle. These CMG will also have to ensure that the S/C is 3-axis stabilized at all times. For mission purposes, the maximum disturbance torques were used as well as the moments of inertia taking into account the deployed solar panels. Airbus Defense & Space offers a package of 4 Control Momentum Gyroscope (CMG 15-45S)<sup>1</sup> that can address the required control of the LOFAR transfer phase. The mass of each CMG is  $m_{CMG} = 18.4$  [kg] with a diameter of  $D_{CMG} = 0.27$  [m]. The moment of inertia of each CMG is estimated with Equation (8.17)

$$I_{CMG} = m_{CMG} \frac{r^2}{2} \quad (8.17)$$

These CMGs are used for one tonne class satellites (as given in the specifications) and applying Equation (8.16) with the according input variables, it is found that at least 8 reaction wheels will be necessary. This entails that two boxes of  $310 \times 300 \times 150$  [mm] containing 4 reaction wheels each will be necessary.

The CMGs need momentum unloading which is performed with a thruster system. These will also be incorporated to ensure attitude control at all times. The procedure to size these begins with the accumulated momentum that needs to be released throughout the whole transfer time. The angular momentum ( $\Delta H$ ) that is unloaded per thruster activation is found with Equation (8.18), where  $F$  is the thrust per thruster,  $l$  is the arm from thruster location to center of gravity position (taken to be slightly larger than the S/C diameter) and  $\Delta t$  the thruster unloading time (estimated from reference papers to be  $\Delta t = 10$  [s]).

$$\Delta H = 2F l \Delta t \quad (8.18)$$

The angular momentum per orbit is calculated using the disturbance torques from Section 8.4 and is defined in Equation (8.19) [3].

$$H_{orbit} = T_D \frac{P}{4} (0.707) \quad (8.19)$$

Where  $P$  is the orbital period and is found using Equation (8.20). For the LOFAR, the orbital period was locally found using all the altitudes ( $h$ ) of the transfer phase as found in Section 3.1.2.

$$P = 2\pi \sqrt{\frac{h^3}{\mu}} \quad (8.20)$$

On the other hand, the angular momentum of the S/C using a maximum allowable motion of  $\theta_a = 1^\circ$  can also be computed from Equation (8.21) [3].

$$H_{orbit} = T_D \frac{P}{4} \frac{1}{\theta_a} \quad (8.21)$$

The maximum between these two values must be taken into account. For the thruster unloading, the daily accumulated momentum must be used Equation (8.22). Here,  $N$  is the number of orbital revolutions that the S/C undergoes per day, which is found by dividing the Earth's orbital period ( $T_E = 23h56m4s$ ) by the S/C's orbital period found in Equation (8.20). The function relating these variables is presented in Equation (8.23).

$$H_a = \sqrt{N} * H_{orbit} \quad (8.22)$$

$$N = \frac{T_E}{P} \quad (8.23)$$

The mass of the propellant required can now be computed, where the angular momentum ( $\Delta H$ ) that is unloaded per thruster activation was found using Equation (8.18) [3]. The number of dumps that the thrusters need to be activated

<sup>1</sup>CMG: <http://www.space-airbusds.com/en/equipment/cmg-15-45s.html>

per day is just the accumulated angular momentum ( $H_a$ ) divided by the angular momentum unloaded per thruster activation ( $\Delta H$ ), found as follows:

$$N_{dumps} = \frac{H_a}{\Delta H}$$

The propellant mass per dump is found with Equation (8.24), where  $g_0 = 9.81 [m/s^2]$  is the Earth's gravitational acceleration at sea level and  $I_{sp}$  is the thruster specific impulse.

$$m_{prop} = \frac{F\Delta t}{g_0 I_{sp}} \quad (8.24)$$

The total propellant mass is found by multiplying the number of dumps required per day by the duration of the transfer time (365 days) times the propellant mass per dump and thus:

$$m_{prop-total} = m_{prop} \times N_{dumps} \times T_{transfer} \quad (8.25)$$

Applying these equations to different thrusters, it is found that Airbus Defense & Space offers a 22 [N] bipropellant thruster<sup>2</sup> that can fulfill the attitude requirements with the least amount of propellant mass. In Table 8.3, all properties about the ADCS thrusters are presented. Only 10 thrusters will be incorporated into the design as can be seen in the CATIA V5 model. This is due to the fact that 4 thrusters are incorporated per axis for the x and y axes, whereas only two thrusters will be placed in the z-axis. During the transfer phase, the other two required thrusters for the z-axis are placed on the bottom of the transfer vehicle, which are the same as the thrusters used for braking. On the other hand, once the lander has decoupled, the thrusters used for landing will also be used for the attitude control. At least 4 per axis will be active at all times (two up and two down) to be able to adjust to any orientation required.

Thruster	10×22 [N]
<b>Total Mass [kg]</b>	6.5
<b>Propellant Mass Transfer [kg]</b>	20.63
<b>Propellant Mass ADCS Land [kg]</b>	3.05
<b>Total [kg]</b>	30.18

Table 8.3: LOFAR ADCS actuators

Table 8.3 presents just two candidates that were considered when selecting the thrusters. A few other European thrusters were considered during the calculations but did not provide results with enough confidence since data was incomplete. Further analysis shall be carried out to take into account other attitude modes that were not considered in this analysis.

### 8.5.3. SENSORS

Sensor selection is an important milestone in the ADCS design. These allow to determine the attitude and position of the S/C from an inertial perspective, which is of most importance for the computer to command the actuators. Sensors can be of two kinds; they can detect different types of celestial bodies or they can be gyroscopes which react to small angular accelerations of the S/C. For the LOFAR S/C two coarse bi-axis Sun sensors (BASS7)<sup>3</sup> from Airbus Defense & Space will be used. These will help to determine the position of the S/C with respect to the Sun so that the solar arrays can point, when possible, the panels at the maximum incidence angle. They have been used for several deep space missions and have a low mass of 65 g. Furthermore, it is a passive equipment that does not require any power consumption, which is ideal to keep the power budget within limits.

Sun sensors on the other hand cannot provide inertial positioning of the S/C by themselves and often need to be combined with other inertial sensors. For this mission, two star sensors from Ball Aerospace & Technologies Corp will be used; the CT-633 stellar attitude sensor<sup>4</sup> combined with the CT-602 star tracker<sup>5</sup>. The first provides attitude information to the S/C, whereas the latter gives the positioning of stars which is then used by the on-board computer. An Inertial Measurement Unit (IMU) will also be incorporated into the design of the ADCS sensors. An IMU has

<sup>2</sup>22 [N] Thruster: <http://cs.astrium.eads.net/sp/spacecraft-propulsion/bipropellant-thrusters/22n-thruster.html>

<sup>3</sup>BASS7: <http://www.space-airbusds.com/en/equipment/bass.html>

<sup>4</sup>CT-633: [http://www.ball Aerospace.com/file/media/D0399\\_CT-633.pdf](http://www.ball Aerospace.com/file/media/D0399_CT-633.pdf)

<sup>5</sup>CT-602: [http://www.ball Aerospace.com/file/media/D0540\\_CT-602.pdf](http://www.ball Aerospace.com/file/media/D0540_CT-602.pdf)

gyroscopes for attitude determination and contains accelerometers and an Inertial Navigation System (INS) which integrates velocity to relative position. Honeywell offers a Miniature Inertial Measurement Unit (MIMU)<sup>6</sup> which can be used for deep space missions and provides all 3-axis angular measurements. In Table 8.4 further properties of the selected sensors are given.

Sensor	Mass [kg]	Power [W]
2× Sun sensor (BASS7)	0.065	-
Stellar Attitude Sensor (CT-633)	2.49	8
Star Tracker (CT-602)	5.48	8
MIMU	4.44	22
Total	12.54	38

Table 8.4: LOFAR ADCS sensors

## 8.6. ADCS BLOCK DIAGRAM

The block diagram of the ADCS subsystem is presented in Figure 8.1. This is a very simplified model of the connected sensors and actuators but gives a good first impression of how the system will function. A more elaborate algorithm of the ADCS will be required in the continuation of the project.

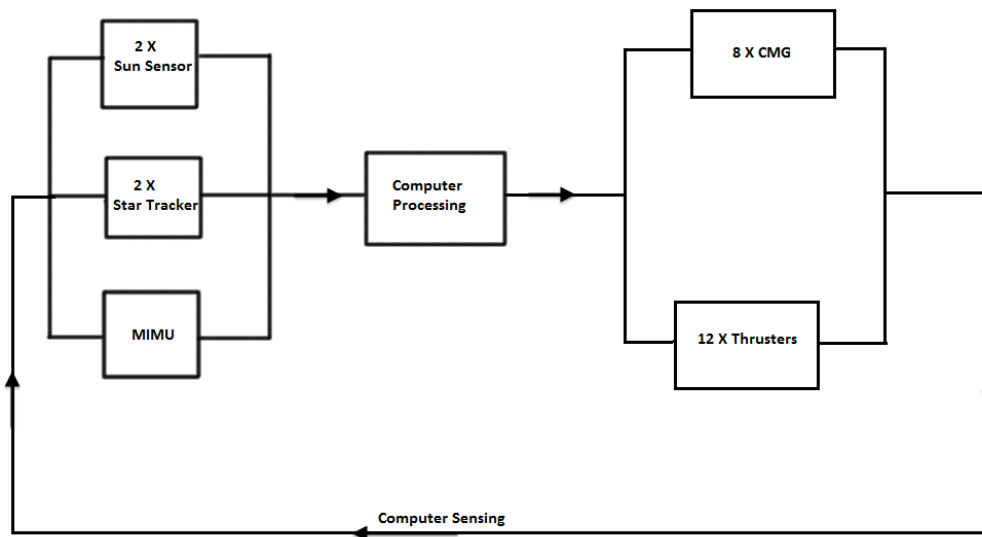


Figure 8.1: ADCS Block Diagram

## 8.7. VERIFICATION & VALIDATION

To verify that the ADCS delivers reasonable results, the different components were constructed into blocks. First, the input geometric properties are uploaded into a file which feeds these into the calculation of the center of mass. This was then verified by other team members who calculated these with other programs (*MS Excel*). The output of the center of mass is then used for the calculation of the moments of inertia. Furthermore, the disturbance torques were estimated from [40], [3] and delivered the same results when applied using Earth distances. The equations of motion were then built into a different block for the sizing of the reaction wheels as well as for the thruster selection. Block tests were then conducted using different input geometries and analysing the results. Then a system test was carried out which delivered the presented results. Validation procedures shall be carried out once the actuators and sensors have been properly modelled and control loops are integrated. Furthermore, testing of the components is of utmost importance to validate the results from the models and shall be performed as soon as the physical flight test model is constructed. This is left for the future considerations of the project since at this current stage, the lack of open data from other missions cannot give confident validation results.

<sup>6</sup>MIMU <http://www51.honeywell.com/aero/common/documents/myaerospacecatalog-documents/MIMU.pdf>

## TELECOMMUNICATION SUBSYSTEM

In this chapter the detailed design of the communication subsystem of the LOFAR mission is presented. First, an analysis for different mission phases (Section 9.1) is given, followed by the approach for designing the telecommunication subsystem (Section 9.2). Then the transfer phase (Section 9.3), Mission phase (Section 9.4) and system overview (Section 9.5) are described. The chapter ends with a explanation of the verification and validation (Section 9.6) procedures.

### 9.1. ANALYSIS FOR DIFFERENT THE MISSION PHASES

The communication subsystem is responsible for telemetry, tracking and command transmission (TT&C). In this section the elements of TT&C are explained and their implications on the design of the communication subsystem are introduced.

#### 9.1.1. TELEMETRY

Telemetry consists of housekeeping data, attitude data and the payload data. Housekeeping data tells the status of health of different subsystems. It is accomplished by reporting measured temperatures, pressures, voltages and currents, operational status of equipment, redundancy status, deployment status of mechanism [40] etc. This data has to be sent back to the Earth in order to foresee and avoid any possible malfunctions. Attitude data is gathered from the IMU, Star sensors and Sun sensors. Normally they are fed back to the Command and Data Handling subsystem where an appropriate command is sent to the actuators. However in case of software or hardware failure of the On-Board Computer (OBC), the attitude control might be carried out from the ground station and in this case the attitude data also needs to be transmitted back to the Earth. The payload data consists of the astronomical measurements made by the crossed dipole antennas and the additional instruments. The telemetry data rate greatly depends on the mission phase.

During the launch phase the S/C data is minimal and the data is usually sent down by the launcher [40], so this will not put driving constraints on the design of the communication subsystem of this mission. During the transfer phase telemetry consists housekeeping and attitude data. [3]. The housekeeping data transmission of this phase typically requires sampling of 30 [s] to 2 [min] which results in a few hundred [bit/s] [40]). According to [3] data rate for telemetry will be between 100 and 10000 [bit/s]. This estimation is based on previous missions and it does not include payload data. Since the spacecraft utilizes electronic propulsion, the pointing of the solar array towards the sun has to be continuous. To simplify antenna pointing, continuous coverage should be achieved. This can be done by one omnidirectional antenna (for example biconical antennas) [42]. However it is difficult to mount these antennas such that radiation pattern does not get too disturbed. Perhaps the easiest solution is two have two antennas with hemispherical coverage. No telemetry data is sent from the mothership after decoupling and from the lander during landing. During deployment telemetry data mostly consists of the status of the rover. Then the measurements begin and the data rate greatly increases up to 84 [Mbit/s]. Apart from that, housekeeping data could be transmitted and commands could be received from the ground station [40].

#### 9.1.2. COMMAND

The S/C for the LOFAR mission is designed to be autonomous. However, in some cases, for example, if a malfunction occurs, the control from the ground station might be desired. The typical commands of this mission's can be found in Section 10.1. One command that is expected to arrive via communication system is the electrical pointing of the antenna array station. Commands are usually sent in S-Band [40] and they can be transmitted during any of the phases of the mission except maybe during landing, since the relative velocities involved are too large and there is no time for intervention. Data rate for the command is estimated on previous Near-Earth mission from [3] and it's about 2000 ([bit/s]), although other sources have suggested lower data rates (such as 200 [bit/s] [43]).

### 9.1.3. TRACKING

Although tracking will be done autonomously by Microcosm Autonomous Navigation System, in case of failure, ranging and somewhat less accurate angle measurements can be done by sending and receiving the same signal to the ground station and measure its shift in frequency [3].

### 9.1.4. ELEMENTS OF COMMUNICATION SYSTEM

The communication subsystem generally consists of a receiver, transponder and High Power Amplifiers (HPA). The receiver is the antenna connected to a Low Noise Amplifier (LNA), a Local Oscillator (LO), a down-converter (DC) and a power supply [42] [25]. Transponder can be regarded as a transmitter and a receiver built together. They are responsible for modulation, separating the broadband signals into individual channels and fulfilling tracking functions. If the payload has high data rate, sometimes it is sent via a wideband transmitter instead of transponder [25]. HPA's can be either Travelling Wave Tube Amplifier (TWTA) or Solid State Power Amplifier (SSPA). TWTA's are more efficient they are capable of achieving higher gains than the SSPA's [40],[25]. On the other hand SSPA's have lower mass, higher reliability [40],[25].

## 9.2. APPROACH

The main tool of analysis is the budget link, which allows to determine the required transmitted power and antenna size for a given frequency band, data rate and modulation type. As it has been explained in Section 9.1, the requirements for the transfer phase and for the mission phase are quite different, and therefore the approach will differ slightly too. For the transfer phase it is really important to have global coverage area. Furthermore the data rate is low, so low gain antennas (LGA's) will suffice. That is why it is convenient to start with choosing the antenna type first (so that the global coverage will definitely will be achieved) and choose the frequency band later. This process is illustrated in Figure 9.1 and as it can be seen it is a highly iterative process. The process of designing the budget link of the mission phase starts with choosing a frequency band and then choosing the antenna later. It is because the biggest constrain on the design process is the high data rates, which is best solved by using high frequencies. The coverage area cannot be too small, however, because then the pointing mechanism has to be very accurate, which increases costs. Once the margin is closed, the parameters of the antennas will be known. Although antennas are usually custom produced, in this report already existing antennas were used (with slightly different parameters) to facilitate the mass and operation temperature range estimations. The other main components such as high power amplifiers (HPA) and transponders are usually off-the shelf products [25]. The choice of high power amplifiers will be determined by the output RF power and the used frequency [42]. To find the optimal transponder/wideband transmitter, data rate, frequency band, mass, power consumption, operating temperature range, supported modulation type, saturation power will be taken into account [42]. RF cables/waveguides, diplexers, RFDU will not be chosen, but their mass and power consumption will be roughly estimated according to [3].

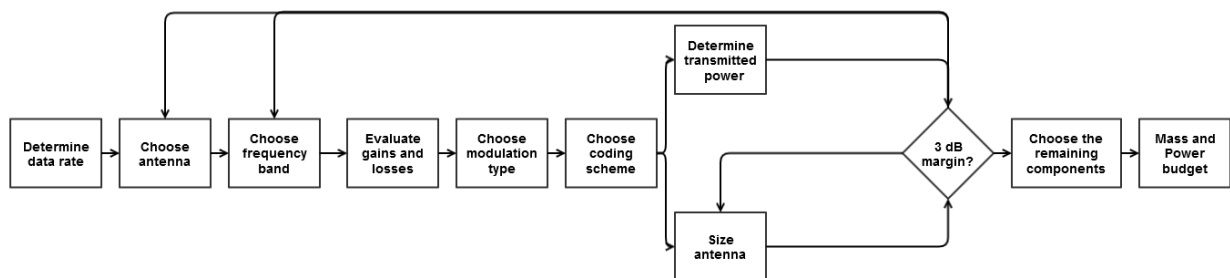


Figure 9.1: The approach of designing the telecommunication system for the transfer phase

## 9.3. TRANSFER PHASE

In this section the antenna used for the transfer phase is designed. First, possible options are discussed.

### 9.3.1. ANTENNA DESIGN OPTIONS

Full Earth coverage could be achieved with one omnidirectional antenna or two low gain antennas placed on opposite sites of the spacecraft. Omnidirectional antennas (turnstile, biconical horn) require an extra mounting device to avoid deflections from the body of the spacecraft. Using two different antennas would provide redundancy and interference problems can be overcome by using different polarizations for the antennas. Two antenna types were

considered; helical antenna and horn antenna. Helical antenna provides wide beamwidth below 4 [MHz] while the horn antenna does the same above 4 [MHz] [44]. These low gain antennas are relatively cheap and are easy to mount on the body of the spacecraft. To determine the required transmitted power and dimensions of the antennas, a budget link was set up for the transfer phase communication.

### 9.3.2. SETTING UP THE BUDGET LINK

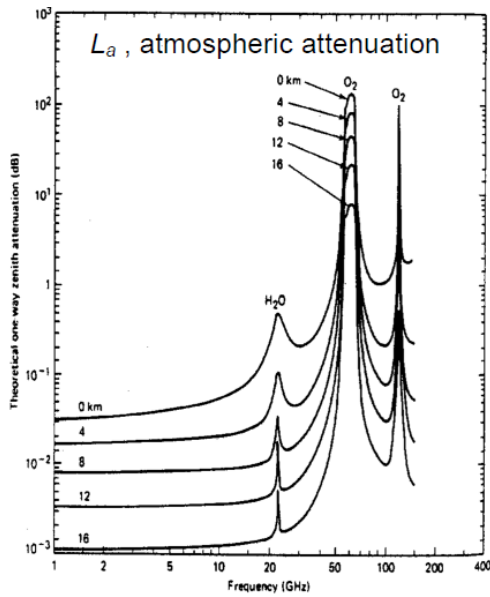
The link equation gives us the signal-to-noise ratio as a function of antenna gains, losses and system noise:

$$SNR = \frac{P \cdot L_t \cdot G_t \cdot L_{fs} \cdot L_a \cdot G_r \cdot L_s \cdot L_{pr} \cdot L_r}{R \cdot k \cdot T_{sys}} \quad (9.1)$$

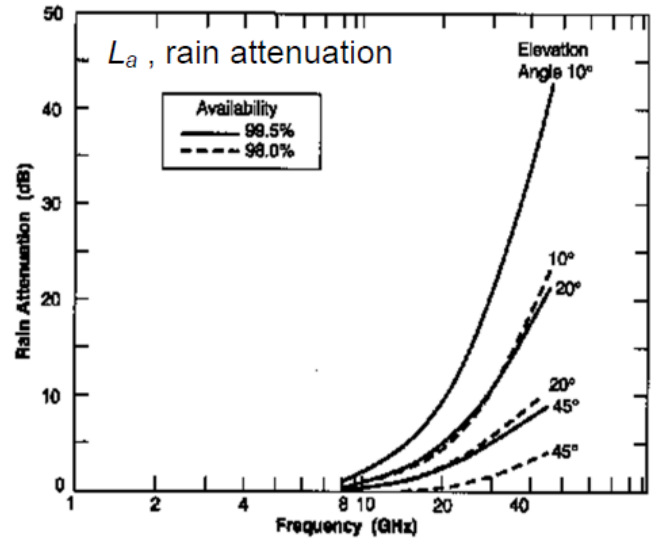
Where  $P$  is the transmitted power,  $L_t$  and  $L_r$  are the loss factor of the transmitter and receiver,  $G_t$  and  $G_r$  are the transmitter and receiver gain, respectively.  $L_{fs}$  is the free-space loss

$$L_s = \left(\frac{\lambda}{4\pi S}\right)^2 \quad (9.2)$$

Where  $S$  is the distance between the transmitter and the receiver antenna.  $L_a$  are the losses related with atmospheric attenuation and rain. Values for this parameter can be obtained from Figure 9.2a and Figure 9.2b.



(a) Atmospheric attenuation as a function of frequency



(b) Attenuation by the rain as a function of frequency

Figure 9.2: Losses related with atmospheric attenuation and rain [3]

$L_{pr}$  is the antenna pointing loss and it is given by the following expression in decibels [3]:

$$L_{pr} = -12 \left(\frac{e_t}{\alpha_{1/2}}\right)^2 \quad (9.3)$$

Where  $e_t$  is the pointing offset angle and  $\alpha_{1/2}$  is the half-power beamwidth and they have to be given in degrees.

The system noise is characterized by the system temperature ( $T_{sys}$ ). Normally, system noise is mainly determined by the noise figure of electronic components in the elements of the communication system (such as amplifier, receiver etc.). For a preliminary estimation the whole system noise can be estimated as a function of frequency used as it is shown in Figure 9.3

The gain of a helical antenna is given by

$$G_{hx} = 10.3 + 10 \cdot \log\left(\frac{\pi^2 D^2 L}{\lambda^3}\right) \quad (9.4)$$

The gain is given in decibels.  $L$  denotes the length of the helical antenna and the  $D$  means the diameter. The half-power beamwidth of the helical antenna is given by:

$$\alpha_{1/2,hx} = \frac{52}{\sqrt{\pi^2 D^2 L / \lambda^3}} \quad (9.5)$$

Noise Temperature	Frequency [GHz]					
	Downlink			Crosslink	Uplink	
	0.2	2-12	20	60	0.2-20	40
Antenna Noise [K]	150	25	100	20	290	290
(Cable Loss Factor) <sup>-1</sup> [dB]	0.5	0.5	0.5	0.5	0.5	0.5
Cable Loss Noise [K]	35	35	35	35	35	35
Receiver Noise Figure [dB]	0.5	1.0	3.0	5.0	3.0	4.0
Receiver Noise [K]	36	75	289	627	289	438
<b>System Noise [K]</b>	<b>221</b>	<b>135</b>	<b>424</b>	<b>682</b>	<b>614</b>	<b>763</b>

Figure 9.3: System noise estimation [3]

This equation gives the beamwidth in degrees. The gain of a horn antenna can be calculated by:

$$G_{hr} = 20 \cdot \log\left(\frac{\pi D}{\lambda}\right) \quad (9.6)$$

And the half-power beamwidth can be determined:

$$\alpha_{1/2,hr} = \frac{225}{\pi D/\lambda} \quad (9.7)$$

The previous equations also give results in decibels and degrees, respectively.

	Helical antenna	Horn antenna	Comments
<b>Main parameters</b>			
Frequency downlink [GHz]	2.2	4.10	S-Band for helical antennas and C-Band for horn antennas for ideal beamwidth
Frequency uplink [GHz]	2.025	4.00	Determined by the turnaround ratio of the transponder from [3].
Data rate downlink [bit/s]	10000	10000	Housekeeping and attitude data
Data rate uplink [bit/s]	2000	2000	From [3]
System noise downlink [K]	135	135	Based on preliminary estimation from [3]
System noise uplink [K]	614	614	Based on preliminary estimation from [3]
<b>Antenna parameters</b>			
S/C aperture [m]	0.055	0.115	The helical antenna has a length of 0.1 [m]
S/C antenna transmitted power [W]	1	1	
S/C antenna aperture efficiency [0]	0.7	0.52	From [3]
G.S. antenna aperture	15	15	Using Estrack G.S.
G.S. transmitted power	500	500	Estimation from [3]
G.S. antenna aperture efficiency	0.55	0.55	Parabolic antennas, from [3]
Pointing offset angle of S/C antenna [°]	0.8	0.8	Estimation from [3]
Pointing offset angle of G.S. [°]	0.8	0.8	Estimation from [3]
HPBW of S/C antenna [°]	43.47	89.46	Calculated from eq. (9.5) and eq. (9.7).
HPBW of G.S. [°]	0.16	0.16	Calculated from eq. (9.11)
<b>Budget link (downlink)</b>			
Transmitted power [dBW]	0	0	
Transmitter gain [dB]	11.86	5.21	Calculated from eq. (9.4) and eq. (9.6).
Transmitter loss [dB]	-0.97	-0.97	Estimation from SMAD [3]
Free-space loss [dB]	-212.10	-216.18	384 400 km is assumed for distance
Atmospheric loss [dB]	-0.03	-0.04	For S- and C-Bands it is almost negligible.
Pointing loss [dB]	-0.004	-0.001	Rain has no effect at all
Receiver loss [dB]	-0.97	-0.97	Almost negligible
Receiver gain [dB]	49.29	53.37	Estimation from [3]
System loss [dB]	-174.29	-174.29	Calculated from eq. (9.10)
			228.6-10log(T <sub>sys</sub> )-log(R <sub>b</sub> )

Signal to noise ratio [dB]	13.56	13.41	
Margin [dB]	3.26	3.11	Differential BPSK applied, so 10.3 dB is required
<b>Budget link (uplink)</b>			
Transmitted power [dBW]	26.99	26.99	Estimation from [3]
Transmitter gain [dB]	49.29	53.37	Calculated from eq. (9.10)
Transmitter loss [dB]	-0.97	-0.97	Estimation from [3]
Free-space loss [dB]	-212.10	-216.18	384 400 km is assumed for distance
Atmospheric loss [dB]	-0.03	-0.04	For S- and C-Bands it is almost negligible.
Pointing loss [dB]	-9.57	-24.49	Rain has no effect at all
Receiver loss [dB]	-0.97	-0.97	Almost negligible
Receiver gain [dB]	11.86	5.21	Estimation from [3]
System loss [dB]	-176.74	-176.74	Calculated from Equation (9.4) and Equation (9.6).
Signal to noise ratio [dB]	33.61	16.32	228.6-10log( $T_{sys}$ )-log( $R_b$ )
Margin [dB]	23.31	6.02	Differential BPSK applied, so 10.3 dB is required

Table 9.1: Budget link for the transfer phase of the mission

### 9.3.3. CLOSING THE BUDGET LINK

As it can be seen from Table 9.1, the budget link can be closed easily if a 3 dB margin is applied and if it is assumed that the maximum acceptable bit error rate is  $10^{-5}$  (as proposed by [3]). The transmitted data during the transfer phase will consist of housekeeping data and attitude data (downlink) and commands (uplink). The downlink and uplink data rate is estimated to be 10 [kb/s] and 2 [kb/s] respectively. These reference data rates are obtained from [3] and they are based on previous Near Earth missions. For the helical antenna S-Band has been chosen. This is because the data rates are low and there is no need for high antenna gain. Also selecting a lower frequency band minimises the free-space loss. As it has been previously mentioned the antenna coverage properties get better for horn antennas above 4 [MHz]. That is why the horn antenna would use the C-Band. Differential Binary Phase Shift Keying (D-BPSK) has been chosen for modulation. Since this eliminates the need for recovery of the reference carrier and consequently yields a simpler demodulator [44] (at the price of worse performance, however it does not matter in this case because it is fairly easy to get the 3[dB] margin with these low data rates). Also because of similar reasons, channel coding is not required, which further increases the simplicity and reliability of the system. From Table 9.1 one can see that the horn antenna requires a 11.5 [cm] aperture whereas the helical antenna needs to have only 5.5 [cm] wide aperture. The mass estimation of the antenna is based on statistical data from [3]. The relations for helical and horn antennas are, respectively Equation (9.8) and Equation (9.9).

$$m_{hx} = k_{hx} \cdot L \cdot D = 0.605 \quad [kg] \quad (9.8)$$

$$m_{hr} = k_{hr} \cdot \frac{D^3}{\lambda} = 1.05 \quad [kg] \quad (9.9)$$

where  $k_{hx}$  and  $k_{hr}$  are 11 [kg/m<sup>2</sup>] and 53.3 [kg/m<sup>2</sup>] respectively. Because the difference in mass and in volume the helical antenna is chosen. Although if one wants to choose the truly optimum solution, the radiation interference with the spacecraft body should be analysed as it could have a major consequence on the communication performance. But that kind of analysis is beyond the scope of this project.

Therefore it is concluded that the spacecraft shall have two, preferably European manufactured helical antennas mounted on its body on the opposite sides that has at least 5.5 [cm] aperture and at least a 10 [cm] length with at least 1 [W] transmitted power and at least 17.12 [°] half-power beamwidth. There are several antennas that meet these requirements. Swedish company RUAG manufactures S-Band conical helix antennas designed especially for TT&C. German company STT-SystemTechnic GmbH has a 5.4 [cm] diameter helical antenna with approximately 10 [cm] length (with the connector) and with 0.14 [kg] mass. Its operating temperature range is from -40 [C°] to +85 [C°]. Third option could be using S-Band quadrifilar helix antenna made by Surrey Satellite Technology. It weighs approximately 0.5 [kg] and it has a dimensions of 10 x 10 x 38.9 [cm] and its operating temperature range is from -20 [C°] to 50 [C°].

## 9.4. MISSION PHASE

In the Midterm report it was mentioned that the scientific data recorded on the Moon would be either transmitted by using laser or by radio frequency. In this section both two options will be analysed and then finally the most



Figure 9.4: Possible helical antennas for the transfer phase communications. From left to right: Surrey Satellite Technology, RUAG, STT

feasible option will be chosen. One of the options is to use a high-gain reflector antenna to transmit the data via radio frequency. This option was analysed with calculating the budget link. The budget link equation is the same as for the transfer phase (Equation (9.1)) and Equations (9.2) and (9.3) are also valid. However for parabolic antenna, the gain is computed as:

$$G_p = 17.8 + 20 \cdot \log(D) + 20 \cdot \log(f) \quad (9.10)$$

and the half-power beamwidth is

$$\alpha_{1/2} = \frac{21}{fD} \quad (9.11)$$

In the last two equation frequency has to be given in [GHz]. Equation (9.10) gives the answer in [dB] and Equation (9.11) in degrees. The downlink data rate consists of the data produced by the tripole antennas, the additional instruments.

$$R_{dl} = R_{ant} + R_{add} \quad (9.12)$$

The data rate produced by the additional instruments is negligible compared to the that of primary payload Chapter 18 and therefore it will be ignored from now on. First, a bandwidth must be assumed for the measured analog signal. The lunar crossed dipole antennas have been optimized to operate under 10 [MHz] and therefore:

$$B = 10 \cdot 10^6 \quad [Hz] \quad (9.13)$$

This analog signal needs to be sampled at least at Nyquist rate to avoid aliasing:

$$f_{nyq} = 2 \cdot B \quad (9.14)$$

Assuming that one sample will be represented with 2 bits, the data rate per antenna:

$$R = 2 \cdot f_{nyq} \quad (9.15)$$

Thus for  $n$  antennas, the data rate before correlation:

$$R_{ant, bc} = 4 \cdot B \cdot n \quad (9.16)$$

Based on a discussion with Professor Gurvitz the data rate will be approximately 10 times lower after correlation. Therefore

$$R_{dl} = 0.4 \cdot B \cdot n \quad (9.17)$$

Keeping in mind that 21 antennas will be used, Equation (9.17) gives 84 [Mbit/s] The uplink data rate  $R_{ul}$  consists of commands and it is approximated to be 2000 [bit/s] [3]. This is based on previous Near-Earth missions, which are tabulated in [3].

Because the downlink and uplink data rates are so different, it is convenient to use different frequency bands and different antennas. The budget link for the mission phase can be found in Table 9.2. For downlink data transmission, high-gain parabolic antenna has been chosen. When the data rates are relatively high, it is advantageous to use higher frequency bands, so higher gains can be achieved with smaller antennas. However higher frequencies will result in narrow beams, which will require really accurate pointing mechanism. That's why as a compromise X-Band has been chosen. As it can be seen in Table 9.2 the parabolic antenna has been sized to have 0.7 [m] diameter. Therefore the half-power beamwidth of the downlink signal is:

$$\alpha_{1/2} = \frac{21}{fD} = \frac{21}{0.7 \cdot 8.4} = 3.57 \quad [^\circ] \quad (9.18)$$

If a circular beam is assumed, then  $h$  diameter of the circle that the beam of the downlink radio signal covers from a distance  $R$  can be given:

$$h = 2 \cdot R \cdot \tan\left(\frac{\alpha_{1/2}}{2}\right) \quad (9.19)$$

Substituting 384 400 [km] (Moon-Earth distance) for  $R$  we get 23968.64 [km], which is much larger than the diameter of the Earth. Therefore, it is assumed that there is no need for pointing mechanism to point the high-gain antenna. For modulation Binary Phase Shift Keying will be used. The required signal-to-noise ratio could be even further decreased if concatenated encoding (Reed-Solomon combined with convolutional coding) was applied. However, according to [3] for high data rates it is not recommended to apply coding, because the decoding would get too complex.

	High gain antenna	Low gain antenna	Comments
<b>Main Parameters</b>			
Frequency downlink [GHz]	8.4	2.2	X-Band for HGA/ S-Band for LGA
Frequency uplink [GHz]	-	2.025	Determined by the turnaround ratio
Data rate downlink [bit/s]	$8.4 \cdot 10^7$	10000	from Equation (9.17) and from [3]
Data rate uplink [bit/s]	-	2000	from [3]
System noise downlink [K]	135	135	from fig. 9.3
System noise uplink [K]	614	614	from fig. 9.3
<b>Antenna parameters</b>			
Lander antenna aperture [m]	0.7	0.055	
Lander transmitted power [W]	8.5	1	
Lander aperture efficiency [-]	0.55	0.7	parabolic HGA/ helical LGA
Lander pointing offset angle [°]	0.5	0.8	Based on preliminary estimation from [3]
HPBW of Lander antenna [°]	3.57	47.87	HGA from eq. (9.11) LGA from eq. (9.5)
G.S. antenna aperture [m]	35	15	Using ESTRACK ground stations
G.S. transmitted power [W]	1000	500	Estimation from [3]
G.S. aperture efficiency [-]	0.55	0.7	From [3]
G.S. pointing offset angle [°]	-	0.5	Estimation from [3]
HPBW of G.S. antenna [°]	-	0.69	from eq. (9.11)
<b>Budget link (downlink)</b>			
Transmitted power [dBW]	9.29	0	
Transmitter gain [dB]	33.20	11.01	HGA from eq. (9.10) LGA from eq. (9.4)
Transmitter loss [dB]	-0.97	-0.97	Estimation from [3]
Free-space loss [dB]	-222.63	-210.99	384 400 [km] is assumed for distance From fig. 9.2a and fig. 9.2b
Atmospheric loss [dB]	-0.05	-0.03	From eq. (9.3)
Pointing loss [dB]	-0.2352	-0.0034	Estimation from [3]
Receiver loss [dB]	-0.97	-0.97	From eq. (9.10)
Receiver gain [dB]	67.18	48.18	228.6-10*log( $T_{sys}$ )-log( $R_{dl}$ )
System loss [dB]	-167.3	-167.3	From eq. (9.1)
Signal to noise ratio [dB]	12.9	13.56	For HGA BPSK is used, so 9.6 [dB] is required For LGA D-BPSK is used, so 10.3[dB] is required
Margin [dB]	3.21	3.26	
<b>Budget link (uplink)</b>			
Transmitted power [dBW]	-	0	
Transmitter gain [dB]	-	47.46	From eq. (9.10)
Transmitter loss [dB]	-	-0.97	Estimation from [3]
Free-space loss [dB]	-	-210.27	384 400 [km] is assumed for distance From fig. 9.2a and fig. 9.2b
Atmospheric loss [dB]	-	-0.03	From eq. (9.3)
Pointing loss [dB]	-	-6.28	Estimation from [3]
Receiver loss [dB]	-	-0.97	from eq. (9.10)
Receiver gain [dB]	-	9.94	228.6-10*log( $T_{sys}$ )-log( $R_{dl}$ )
System loss [dB]	-	-167.71	From eq. (9.1)
Signal to noise ratio [dB]	-	33.6	For HGA BPSK is used, so 9.6 [dB] is required For LGA D-BPSK is used, so 10.3[dB] is required
Margin [dB]	-	23.26	

Table 9.2: Budget link for the transfer main mission phase

Since the requirements for the mission phase uplink data transmission are exactly the same as for the transfer phase uplink data transmission, the very same antenna could be used. That is a helical antenna with 0.055 [m] diameter and 0.1 [m] length operating in S-Band and using Differential Binary Phase Shift Keying without utilizing coding.

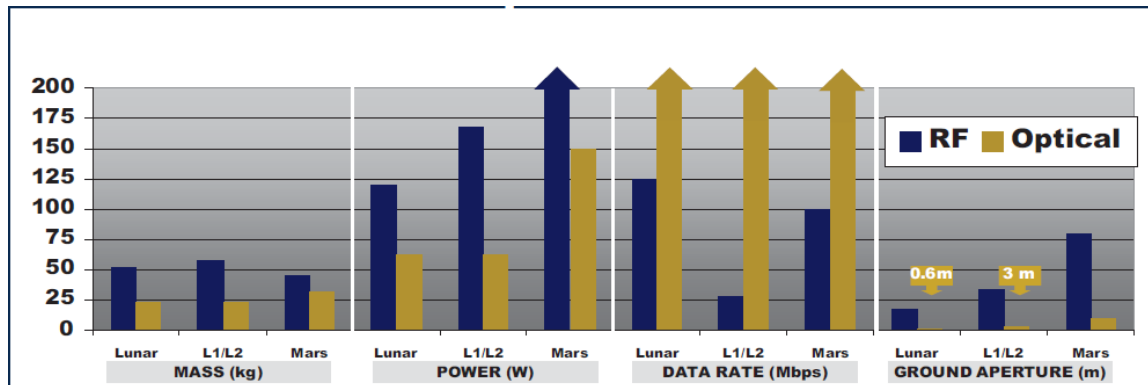


Figure 9.5: Difference between the performance of the laser and the radio frequency communication system for three different missions [45]

Another solution would be to use laser communications. As it is shown in Figure 9.5, by using laser communication, appreciable savings are possible in mass and power consumption. Moreover much higher data rates are possible. The biggest problem is that this technique is relatively new, and the development custom produced laser communication system, which is optimized for the LOFAR mission, would be too expensive, time-consuming and risky. The only possibility would be to use an already existing 'off-the-shelf' product. According to DSA's knowledge there is only one product like that.

Payload of the Lunar Atmosphere and Dust Environment Explorer (LADEE), the Lunar Laser Communication Demonstration (LLCD) can transmit up to 620 [Mbit/s] and it weighs 32 [kg] and consumes 137 [W] [46]. Lasercom produces a very narrow beam as it is illustrated in Figure 9.6. That is why it needs to have a very accurate pointing mechanism. This is accomplished by Magneto-hydrodynamic Inertial Reference Unit developed by Applied Technology Associates (ATA). It is assumed that this device would meet the requirements imposed by the LOFAR mission, as it has been designed for LADEE, which is an orbiter, and, therefore, it requires even stricter pointing accuracy. As one can see the LLCD weighs more and consumes more power than the RF system. This is probably because LLCD is too powerful for the LOFAR mission in terms of data rate. Therefore, the X-band radio frequency system is an obvious choice for transmitting the scientific data from Moon to Earth.

## 9.5. SYSTEM OVERVIEW

In this section the architecture of the communication subsystem is presented and based on that, the corresponding required power and mass is estimated. As it was described in Section 9.3, two S-Band helical antennas will be used for the transfer phase. Two concepts are proposed by [42] for the architecture of the communication system for TT&C applications. One would assign different frequency band for the antennas and two different transponders would be used, thus improving the redundancy of the system. Another approach would use switching techniques to select the appropriate antenna based on the spacecraft's orientation [42]. The received signal strength is shown by the transponder's Automatic Gain Control (AGC) levels. If the AGC level of the transponder is below a certain threshold value then the transponder switches to the other antenna. To fulfil the TT&C requirements a simple transponder is enough, for example the Integrated S-Band Transponder manufactured by ThalesAlenia<sup>1</sup>. Since its moderate weight (2.5 [kg]), it is decided to use two S-Band transponders. Because of the low RF power consumption and because of the choice of S-Band, Solid-state Power Amplifiers will be used (SSPA). Since both low gain antennas operate as receiver and transmitter, two diplexers have to be implemented as well.

For the mission phase the receiver and the transmitter antenna will be physically separated and they will also operate in different frequency bands. Because the scientific data transmission is only in one way, a simple wideband

<sup>1</sup>[https://www.thalesgroup.com/sites/default/files/asset/document/Platform\\_Solutions\\_ISBT\\_Integrated\\_Transponders.pdf](https://www.thalesgroup.com/sites/default/files/asset/document/Platform_Solutions_ISBT_Integrated_Transponders.pdf)

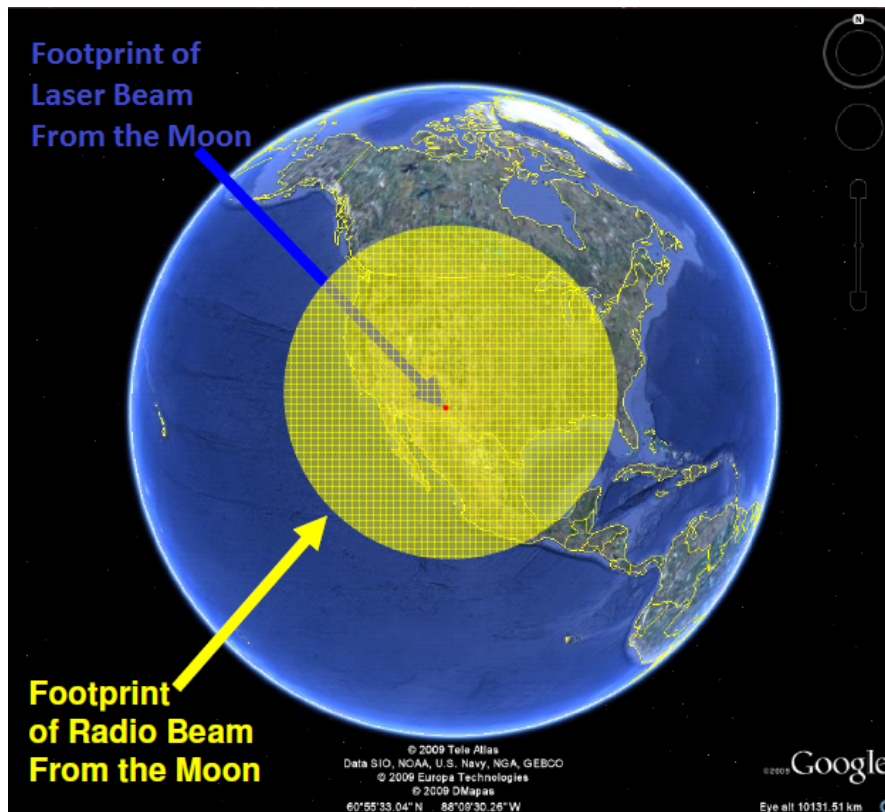


Figure 9.6: The difference between coverage area of K-Band radio communication (yellow) and laser from the Moon [45]

transmitter will be used instead of transponder. This way high data rates can be handled without increasing the complexity and mass and power consumption. For reference, the XT<sub>x</sub>400 X-Band Transmitter will be considered, developed by Surrey Satellite Technology<sup>2</sup>. It weighs 4 kg and it is capable of supporting 10-500 [Mb/s] data rate. Because of the high frequency bands and high RF power outputs TWTA's will be responsible for high power amplification. Because of the one-way communication, no duplexers will be needed. To implement redundancy, the communication subsystem will have two transmitters and two TWTA's. As it has been discussed in Section 9.4 the receiving of the commands can be accomplished by an antenna with the same characteristics as the one used for the transfer phase. It is decided that the very same antenna will be used. This means that there will be 3 antennas in total. Two low-gain helical antennas. One of them will be mounted on the lander part, while the other one will be on exactly on the other side, but on the mothership part. Consequently only one of the low gain antennas will be present on the Moon. The high gain antenna will be a parabolic reflector, inside the lander. After the landing, the parabola antenna will be deployed and it is going to be on the top of the lander. A simplified illustration can be found of the architecture of the communication system in Figure 9.7. The mass and power consumption of the communication system elements can be found in Table 9.3.

## 9.6. VERIFICATION AND VALIDATION

The budget link model used in this has been used in [3], [25], [44]. Also an example preliminary design calculation is tabulated in [25] at page 480, Table 16-13. The model used here was verified with the help of that table. The input parameters of model used in this project were changed to that of SMAD [25] and the results were compared. There were some minor discrepancies mainly because in SMAD the system noise was derived, whereas for the LOFAR mission this parameter was estimated. Derivation of the system noise can be done only in later phases of this mission, when the noise figures of each electrical component are known. The validation was performed by comparing the results of the model with existing missions (Huygens-Cassini, BepiColombo, LRO). The known parameters from those missions were the antenna diameter, frequency band and the distance. For Huygens-Cassini also the transmitted power was known [47]. The known parameters of the missions were fed into the used budget link model and assumptions were made for unknown parameters (such as coding type, modulation type, data rate). It was shown that it is possible to close the budget link with the known parameters and with reasonable margin. However it is realized that this procedure cannot be regarded as proper validation. In the later phases of the mission more information

<sup>2</sup><http://www.sstl.co.uk/getattachment/39811ce4-df75-4456-8ffd-71eb2c63f729/X-Band-Transmitter>

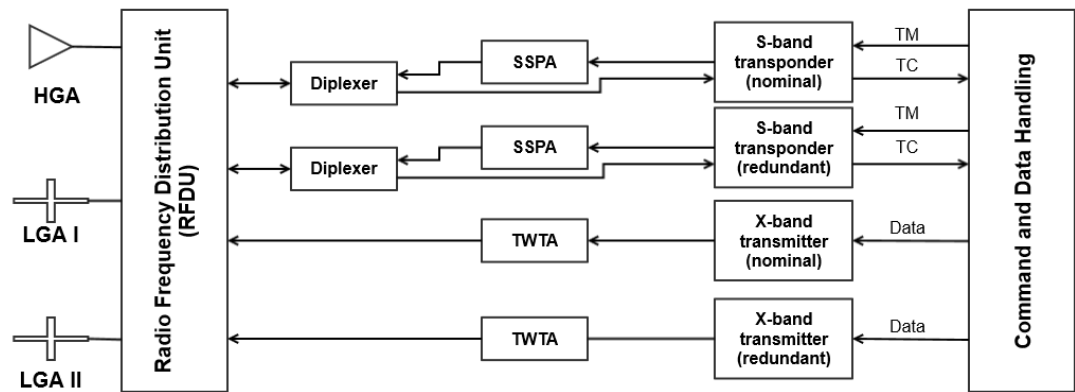


Figure 9.7: Communication system architecture

<i>Unit</i>	<i>Qty</i>	<i>Power Consumed</i> <i>[W]</i>	<i>Unit Mass</i> <i>[kg]</i>	<i>Total mass</i> <i>[kg]</i>	<i>Notes</i>
S-Band Transponder	2	Rx: 5 Tx: 25	2.6	5.2	Dimensions: 228x170x194 [mm] It includes the SSPA
S-Band Diplexer	2	0	0.2	0.4	Estimation from [3]
S-Band Antennas	2	0	0.5	1	Helical Antenna
S-Band cables	All	0	3	3	Estimation from [3]
X-Band Transmitter	2	50	4	8	Dimensions: 215x205x135 [mm] It includes the TWTA's Parabolic
X-Band Antenna	1	0	3	3	Estimation from [3]
X-Band cables	All	0	5	5	Estimation from [3]
RFDU	1	0	1	1	Estimation from [3]
<b>Total</b>		<b>Transfer : 30</b> <b>Mission: 55</b>		<b>26.6</b>	

Table 9.3: Mass and power consumption of the elements of communication subsystem

should be collected about the communication subsystem of previous missions (especially ones that included direct communication between lander and Earth) so that the model can be validated.

## COMMAND AND DATA HANDLING SUBSYSTEM

This chapter contains the design of the Command and Data Handling subsystem. An overview is given of the required commands and telemetry during different phases of the mission (Section 10.1). This gives a picture of what complexity is expected and what hardware components are needed. Furthermore, a preliminary power and mass estimation is also given in this chapter. Finally the requirements of the software are estimated based on the functions it needs to perform, and a processor is chosen based on those estimation as a benchmark design (Section 10.2).

### 10.1. COMMAND AND DATA HANDLING

The Command and Data Handling is responsible for receiving, validating, decoding and distributing commands, housekeeping and attitude data [3]. Therefore, every command and all the telemetry will be handled by this subsystem except the payload data, which after modulation and correlation will be directly sent to the ground station on Earth. This is possible because the storage of the scientific data is not necessary.

This subsystem for this mission can be divided into three parts from a mission phase point of view. One of them is responsible for the transfer, landing, deployment and the mission phase, while the second one is responsible for the controlled crash on the Moon and finally the third one manages the data and command flow on the rover. Since the latter has already been designed and tested by the NASA, it will not be considered further in this report. Although it might be worth to mention that its software probably requires minor modifications in a more mature phase of this project. The hardware of the transfer and deployment/mission phase C&DH will be placed in the lander. Furthermore, because of its complexity and high level of autonomy, it will require an On-Board Computer. During the transfer phase it is responsible for collecting housekeeping data (see Chapter 9) and attitude data (from the Sun sensors and the star sensors) and distributing commands to the CMG's and to the engines and to the thrusters for breaking and to the actuators of the solar arrays. During landing it has to collect information from the IMU's and generate commands based on the measured values and forward them to the thrusters of the lander. In the mission phase it collects housekeeping data mainly from the telecommunication system and from the payload. After decoupling, the transport vehicle has to perform a controlled crash. It is assumed that this is carried out with stored commands. This means that the C&DH, which is responsible for crashing does not need to have a separate OBC. The data storage system with the pre-written commands will have to be connected to the CMG's. This means that physically there is no big difference between the transfer/mission phase C&DH and the controlled crashing C&DH; it is basically the same system except that the 8 CMG's also have to be connected to a data storage. This data storage has to be placed in the transport vehicle. Before decoupling the wires between the bus and the CMG's, thrusters for breaking, 2 electrical propulsion engines have to be cut (possibly with a thermal knife) and the data storage system has to be turned on. This way the C&DH in the transport vehicle and the lander can operate separately after decoupling.

From a functional point of view C&DH subsystem can be divided into the command decoding and the data handling. Command decoding means to collect all the commands from the OBC and from the uplink, order them, format them and send them to the correct subsystem for execution. Data handling means to collect all the telemetry data, format them and send them to the ground station and/or to the OBC. The functions of the command decoder part of this subsystem are illustrated in Figure 10.3. The commands mostly arrive from the On-Board Computer (OBC) but in some special cases (OBC malfunction, etc.) they can also arrive from the ground stations through the low gain antennas and the S-Band transponders. The hardline test input is only for testing and it is inactive during the mission. The outputs of the command can be of two types: discrete and serial. Discrete commands have fixed amplitudes and they can be further grouped; High-Level Discrete Command, 28 [V], 10 to 100 millisecond pulses and Low-Level Discrete Command, an open collector or 5 [V] pulse typically interfacing with digital logic. High-level commands typically responsible for driving electromechanical RF switches or relays [40]. Therefore probably these kind of commands will trigger the decoupling of the lander from the transport vehicle, deployment of the high gain antenna after landing, turning on/off instruments, thrusters etc. Low-Level Discrete Commands are usually used to set or reset the bi-stable logic [40] and Serial Digital data is used to reprogramme the memory locations in OBC and to set up the

registers in the ADCS [40]. Typical commands are: to adjust the throttle setting of thrusters (both during landing and during transfer phase), change settings of the CMG's, sun sensors, to turn the solar arrays to the Sun, to decouple from the transport vehicle, to turn on the cameras and lidar for landing, to deploy the high gain antennas, to deploy the solar array after landing, to turn on the rover etc. In Figure 10.3 Command Source Arbitration is responsible for giving priority for commands arriving from the uplink. Typically a code consists of synchronization code, spacecraft address bits, command message bits and error check bits [3]. Commands must be validated before execution. The validation process consists of checking the previously mentioned code components. Both accepted and rejected commands are fed into the data handling system and sent downlink to provide operational feedback [3].

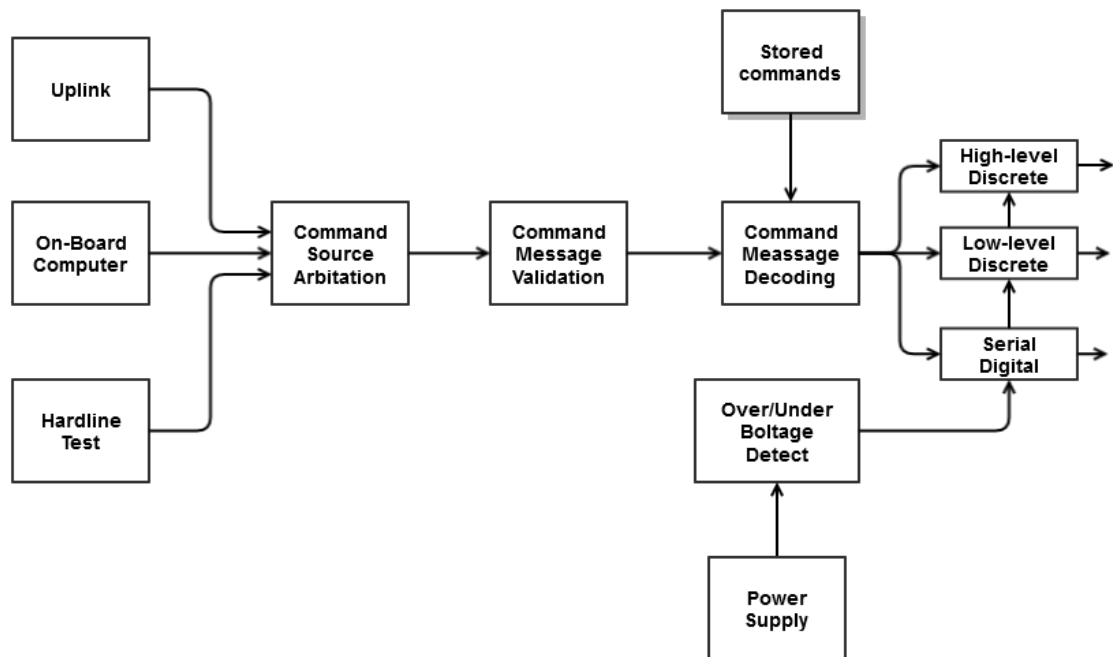


Figure 10.1: The functional block diagram of the command decoder. From [3]

A functional block diagram about the data handling operations of the C&DH system can be found in Figure 10.2. As it can be seen the signals can arrive in many forms. High-Level Analog does not require amplification, while Low-Level Analog and Passive Analog signals do [3]. Furthermore every analog signal has to be converted into digital before forwarding to the OCB or the S-Band transponders. The types of the incoming signals at this phase of the design are still unknown. The telemetry data (that is the data handled by this subsystem) will consist of housekeeping data and attitude data. The payload data will be directly send to the ground station and will not enter C&DH.

Physically the Command and Data handling system of the LOFAR mission consists of the following components [48]:

- Processor, Operating System (OS), internal clock
- Motherboard
- Network card, modem etc.
- Memory or data storage unit
- Data storage unit for stored commands
- Software
- Network (harness and connectors)
- Data acquisition unit
- Control unit

The first four components make up the On-Board Computer. Although it is quite common for spacecrafts to have a separate data storage units, but because the payload data will not be stored and because the connection time with the ground station is assumed to be almost continuous, the required storage capacity is going to be low and therefore the data storage unit will be integrated into the computer. The motherboard provides a platform for the processor to communicate with external units and memory with the means of electrical connections. The last two are sometimes referred to as Data Acquisition and Control Unit (DACU). Harness is a string of cables which are responsible transmitting power and information. The cables are usually bound together by clamps [48]. The data

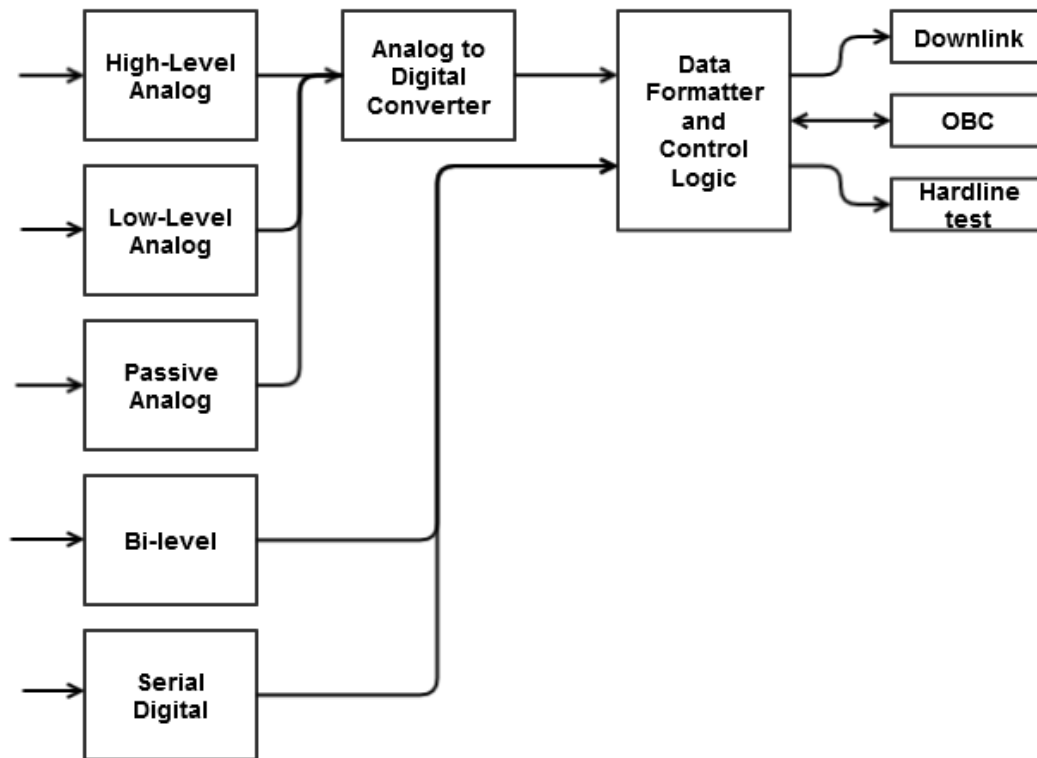


Figure 10.2: The functional block diagram of the data handling system. From [3]

acquisition unit, also called On-Board Data Handling unit (OBDH) is responsible for command source arbitration and command message validation and command message decoding and data formatting [48].

In Figure 9.7 the architecture of the Command and data handling system is presented. The On-Board Computer system is connected to the Data acquisition unit and the command processor and the other subsystem via a bus. This bus is realized with a two twisted pairs of wires [49]. One of them is the interrogation bus, through which the data is either sent to the CPU or one of the network cards or prepared for downlink transmission. The other one is the response bus, through which the data is sent from the CPU or from one of the network cards to subsystems. Besides that, there is an internal bus for the computer, where the different network cards and modems are connected with the Central Processing Unit (CPU). It is advised by [50] that for low data rates MIL-STD-1553 bus standard should be used and for the internal bus system the so-called Peripheral Component Interconnect (PCI). SSR stands for the Solid-State data storage system and it is needed for storing the software and also storing some commands that are meant to be executed later. H/K board is used for interfacing with the temperature, pressure and electric sensors so ensure the flow of the housekeeping data and also it is responsible for providing a clock. S-Band card prepares the data stream for BPSK modulation in the S-Band Transponder so that the telemetry data can be transmitted to the Earth. It also forwards the commands arriving from the ground station to the CPU. The I/O board is responsible for handling the High-Level Discrete commands. It is required that the C&DH is equipped with Computer Watchdog, it is tasked with monitoring the computer for software/hardware failures. This function is accomplished by having one or two countdown timers. These timers are reset by the OBC when timing-out. If the computer fails to reset them, then the watchdog system resets the OBC and temporarily the commands will be received from the ground station [3].

Command and Data Handling subsystems are usually derived from previously used systems with small changes in hardware [3]. Custom-made designs are rare. This way the reliability can be increased and extensive and expensive testings can be skipped. Since they are mostly off-the shelf products, the estimation for required power, size and mass of this subsystem can be based on statistical data obtained from [3]. Based on this estimation method the C&DH of the LOFAR mission will weigh about 5[kg] it will consume about 10[W] and it will consist of a 6000 [cm<sup>3</sup>] box and a smaller box for the stored commands.

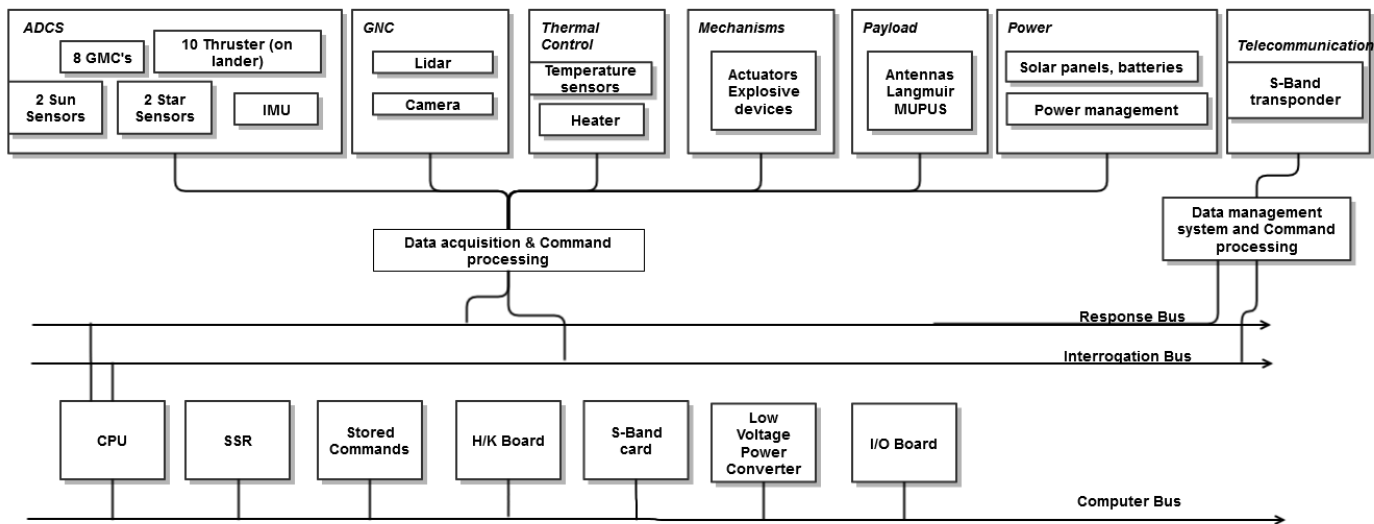


Figure 10.3: Architecture of the Command and Data Handling subsystem, loosely based on [3],[49] and [50]

## 10.2. ON-BOARD COMPUTER

The preliminary design of a computer system is really complex process and it is beyond the scope of this project. However, its feasibility can be demonstrated by estimating the required performance of the processor. Then an off-the-shelf processor can be chosen that meets the requirements. The design of the other components of the OBC hardware (such as modems, cards, ) will not be considered in this report, although they are taken into account in the mass and power estimation in Section 10.1. The estimation of the software requirements can be done by listing the required functions that it needs to execute and then estimating its Source Lines of Codes (SLOC) and its required instructions per second. Estimations are based on a performance of the 1750A general purpose processor and they are obtained from [3] and [25]. The results can be found in Table 10.1. To estimate for the required memory for the software one has to account 2-4 [kB] per every 1000 SLOCs [48]. This means that approximately 108-216 [kB] is needed. The selection of the processor is influenced by the required throughput and the rate of the ADCS and C&DH type functions [25]. The RAD750 processor has a similar instruction mix and it can operate with throughput higher than 400 [MIPS]. Furthermore it is a reliable product and it has been used for many space missions (such as Lunar Reconnaissance Orbiter, Mars Reconnaissance Orbiter, Deep Impact etc.)

Computer Software Component (CSC)	Source Lines of Code	Typical Execution Frequency [Hz]	Typical Throughput [KIPS]
<b>Executive</b>	1000	N/A	60
<b>Communication</b>			
Command Processing	1000	10	7.0
Telemetry Processing (with compression)	3500	10	3.0
<b>Attitude/Orbit Sensor Processing</b>			
Rate Gyro	800	10	9.0
Sun Sensor	500	1.0	1.0
Star Tracker (output quaternion)	2000	0.01	2.0
<b>Attitude Determination and Control</b>			
Kinematic Integration	2000	10	15.0
Kalman Filter	8000	0.01	80.0
Error Determination	800	10	12.0
Precession Control	3500	10	30.0
Ephemeris Propagation	2000	1	2.0
Orbit Propagation	3000	1	20.0
<b>Attitude Actuator Processing</b>			
CMG Control	1500	10	15.0
Thruster Control	1200	2	1.2
<b>Fault Detection</b>			
Monitor	4000	5	15.0
Fault Identification	2500	5	5.0
Fault Correction	5000	N/A	N/A
<b>Utilities</b>			
Basic Mathematics	800	N/A	0
Transcendental Mathematics	1500	N/A	0
Matrix Mathematics	1750	N/A	0
Time Management and Conversion	700	N/A	0
Coordinate Conversion	2500	N/A	0
<b>Other Functions</b>			
Momentum Management	3000	N/A	
Power Management	1200	1	1.0
Thermal Control	800	0.1	0.1
Mechanisms	800	0.1	0.1
<b>TOTAL</b>	54050		267.2
ADCS [%]	8.2		
C&DH [%]	45.6		

Table 10.1: Estimation of software requirements based on [3]

# GUIDANCE AND NAVIGATION SUBSYSTEM

In this chapter the design of the Guidance and Navigation Subsystem is presented. This subsystem is responsible for determining and controlling the position of the spacecraft and estimating the time of arrival [48]. The guidance and navigation system for the transfer phase (Section 11.1 & Section 11.2) and the design for the landing phase (Section 11.3) is described in the following sections.

## 11.1. TRANSFER NAVIGATION

The navigation system determines the velocity and position of the spacecraft. There are many off-the-shelf navigation methods. To avoid high development and testing costs, it is enough to choose one of them, rather than develop a new one. There are two ground-based methods proposed by SMAD [3]; Ground tracking and TDRS tracking. Ground-based tracking is based on measuring a frequency shift of a sent and received signal produced by one of the S-Band transponders. There are numerous autonomous navigation methods as well, such as GPS, GLONASS, MANS, Space Sextant etc. [3]. Autonomous navigation methods are recommended if the spacecraft has an On-Board Computer (OCB). Utilising such a system can reduce life-cycle costs and and risks [3]. Since the spacecraft will be equipped with OBC (see Chapter 10) and because only MANS is capable of operating beyond GEO orbits [3], it is decided that MANS will be used for primary navigation. Microcosm Autonomous Navigation System (MANS) uses the observations of the Earth, Moon and Sun to determine the position of the spacecraft [3]. MANS flight software can make use of star sensors, sun sensors and Internal Measurement Unit (IMU) [3]. The size of the hardware of MANS is negligible as it mainly uses the sensors of the ADCS [3]. To implement redundancy, in case of system failure the navigation system is switched to ground tracking.

## 11.2. TRANSFER GUIDANCE

The S/C needs orbital control for targeting the Moon [3]. It needs to follow the pre-determined orbit as described in Section 3.1. Since low thrust propulsion is used, the S/C has to constantly check if it is on course and if not, adjust the attitude to point the thrust vector in the right direction. The guidance can be done either autonomously or using ground control. Due to the intensive guidance required for low thrust trajectory and since the S/C already has a computer On-Board the guidance will be done autonomously and the commands for the ADCS are computed on the S/C itself. An advantage of autonomous guidance is that the S/C can be guided when it is out of contact with the Earth when it flies at the far side of the Moon. Autonomous guidance also reduces the operational costs and risks mentioned in Section 11.1. [3] If for some reason this autonomous guidance does not work. The system can be switched to ground controlled guidance where the commands for the S/C are computed on ground and sent to the S/C this can be done using the transponders available on the S/C.

## 11.3. LANDING NAVIGATION

In this section the navigation during landing will be discussed. To be able to land in an area of approximately 600 by 200 [m] as mentioned in Section 5.1, high precision determination of the position of the lander is necessary. This kind of precision can not be achieved solely with an inertial navigation system (INS). An inertial navigation system uses accelerometers to estimate velocity which is integrated to estimate position. Accelerometers and other sensor components always have a bias, because of integration the position error greatly increases with time if the system is not reset. This will give errors of 1.6 [km] after approximately one hour for Marine & Navigation Grade inertial systems <sup>1</sup>, which are the very best commercially available inertial sensors. Therefore some form of terrain relative navigation (TRN) will be needed. TRN estimates the lander position relative to a local lunar terrain map from lunar

<sup>1</sup><http://www.vectornav.com/support/library/inertial-sensor-market>

mapping missions. Knowing the position of the local map determines the absolute position of the lander. In practice TRN is combined with other systems, like INS, to improve performance.

The landing can be split up into the orbital coast and the powered descent (Phase BC). Powered descent can further be divided into sub-phases: braking, approach, and terminal descent. This is elaborated in Section 6.2.2 and depicted in Figures 6.4 and 6.5. During approach, using closed loop control and the estimated position of the lander relative to the landing site, the thrust will be varied. TRN will play its most important part during the braking and approach phases.

First, in Section 11.4 various TRN methods are discussed. After this a trade-off between the methods is performed in Section 11.5. In Section 11.6 the chosen TRN method is placed in a block diagram and interfaces with other sensors, processor and actuators are given. Section 11.7 briefly discusses considerations for hazard avoidance and detection for the terminal landing phase. Next, in Section 11.8 implications of navigation on the trajectory are considered. Finally, in Section 11.9 presents strategies for testing of the landing navigation system.

## 11.4. TERRAIN RELATIVE NAVIGATION METHODS

In [12] an overview is given of available TRN methods. They can also be found in Table 11.1 where each method is given an identifier (ID). What all methods have in common is that they compare terrain measurements to rendered maps of the Lunar terrain. These maps are based on measurements done by previous missions, like the Lunar Reconnaissance Orbiter (LRO), Kaguya and Chandrayaan-I. The LRO [51] was launched in 2009 taking with it the Lunar Orbital Laser Altimeter (LOLA) and the Lunar Reconnaissance Orbiter Camera (LROC). LOLA made digital elevation models (DEM) of the lunar surface and the LROC made high resolution images of the lunar surface. Focusing on certain areas at the poles (the Shackleton Crater among others), the instruments have made high resolution maps (0.5 [m] to 2 [m] pixel scale).

The TRN methods are divided in two ways, first by the types of sensors used: passive imaging and active range sensing. Passive imaging uses cameras, active range sensing uses Light Detection And Ranging (LiDAR) [52] or radar. However, radar can not provide high resolution and is therefore limited to the use as an altimeter (ID 9 in Table 11.1), whereas LiDAR does offer high precision because of the shorter wavelengths used. Secondly, there is a subdivision defined by the type of algorithm that is used to compare the surface measurements with a map: correlation and pattern matching approaches. A correlation approach acquires patches of the surface with a sensor. The correlation algorithm then compares the patch with every location on the on-board map of the region of interest. It gives high scores to areas with similar values, the area with the highest score is chosen as the patch location. The difference in perspective is rectified with the attitude and altitude (for passive imagers). Pattern matching approaches use predefined landmarks such as craters. Landmark characteristics are for example crater diameter, and distances and angles between craters. Surface data is collected and again landmarks are extracted. Subsequently, landmarks are compared to look for matches. In Section 11.5 a trade-off of the TRN methods is presented.

## 11.5. TRN TRADE-OFF

In this section the advantages and disadvantages of the TRN methods in terms of trade-off criteria will be listed and quantified where possible. Based on this a trade-off is performed that is presented in Section 11.5. The trade-off is done keeping in mind that the landing location will be a rim of the Shackleton crater.

### Mass

LiDAR has the disadvantage of being relatively heavy. Airborne systems offered by companies such as Optech, Riegl and Leica Geosystems have masses varying around 100 [kg]. For example the Optech Pegasus HA500<sup>2</sup> has a mass of 111 [kg] and the Leica ALS80<sup>3</sup> a mass of 80 [kg]. For comparison, the Optech CS-10000 Aerial Digital Camera System weighs approximately 20 [kg]. Because of limited mass available in the lander, mass is given a weight of 5.

### Altitude

Passive optical systems can be used from relatively high altitudes. Some cameras can provide the resolution necessary for far range TRN from orbit. LiDAR has a limited range, the best option Optech has to offer in terms of operating altitude, the Pegasus HA500, can be used from 5 [kg] high maximum. Performances of LiDARs from other companies are inferior in terms of altitude performance. Higher operating altitude gives more flexibility, a limited altitude sets high constraints on the landing profile. Altitude is given a weight of 3.

<sup>2</sup><http://www.optech.com/wp-content/uploads/PEGASUS-Specsheet-140624-WEB.pdf>

<sup>3</sup>[http://www.leica-geosystems.com/downloads123/zz/airborne/ALS80/brochures/Leica%20ALS80%20BRO\\_en.pdf](http://www.leica-geosystems.com/downloads123/zz/airborne/ALS80/brochures/Leica%20ALS80%20BRO_en.pdf)

ID	Sensing Method	Sensor	Approach	Required inputs	Output estimate	Strengths	Limitations
1	Passive visible	Camera	Crater Pattern Matching for Position Estimation	descent image; crater landmark database	absolute position (and attitude)	insensitive to changes in illumination; does not require attitude or altitude measurements	requires solar illumination; requires cratered terrain
2			Scale Invariant Feature Transform (SIFT) Pattern Matching for Position Estimation	descent image; SIFT landmark database	absolute position (and attitude)	general representation should work for all terrains including ones without craters; does not require attitude or altitude measurements	requires solar illumination; illumination changes between image and map not well tolerated; large rotations degrade performance
3			Onboard Image Reconstruction for Optical Navigation (OBRON) - Surface Patch Correlation for Position Estimation	multiple overlapping orbital images to construct map; descent image; lander attitude; lander altitude	absolute position (and attitude update)	general representation should work for all terrains including ones without craters; built in accommodation of illumination changes and terrain relief	requires: solar illumination; multiple overlapping images of landing site; rendering of landing site map prior to landing; attitude and altitude estimate
4			Image to Map Correlation for Position Estimation	map image; descent image; lander attitude; lander altitude	absolute horizontal position	general representation should work for all terrains including without craters; requires one orbital image and no 3D modeling for re-rendering	requires solar illumination; possibly sensitive to large illumination changes and terrain relief
5			Descent Image Motion Estimation Subsystem (DIMES) - Consecutive Image Correlation for Velocity Estimation	3 descent images; 3 attitude estimates, 3 altitude estimates	average horizontal velocity	general representation should work for all terrains	requires solar illumination, need overlap between consecutive images
6			Structure From Motion - Consecutive Image Correlation for Velocity and Attitude Rate Estimation	2 descent images; 2 altitudes	average velocity (and angular rate) between images	does not require attitude estimate, general representation should work for all terrains; fast implementation and very accurate	requires solar illumination; need overlap between consecutive images
7	Active ranging	Imaging LIDAR	Shape Signature Pattern Matching for Position Estimation	range image; motion correction data; shape signature data based from 3D map	absolute position (and attitude)	general approach solves for position and attitude without prior knowledge of these measurements; independent of lighting conditions;	long processing time; more general than needed; requires significant terrain relief; LIDAR less mature than camera
8			Range Image to DEM Correlation for Position Estimation	range image or scans; motion correction data; absolute attitude estimate; digital elevation map	absolute position	independent of lighting conditions; more robust than Altimeter to DEM correlation	Requires scanner , gimbal or imaging array; LIDAR is less mature than camera.
9		Altimeter	Altimeter to DEM Correlation for Position Estimation	altimetry swath; motion correction data; absolute attitude estimate; digital elevation map	absolute position	independent of lighting conditions; sensors likely to work at higher altitude possibly up to 100km	requires long contour; LIDAR is less mature than camera.
10			Imaging LIDAR	Consecutive Range Image Correlation for Velocity Estimation	2 range images; motion correction data; 2 attitudes	average horizontal and vertical velocity	independent of lighting conditions;

Table 11.1: Overview of TRN methods

### Cost

Because high resolution cameras have been around for a long time, they are readily available on the market and hence cheaper than LiDAR systems, which are relatively new. A LiDAR from Optech costs approximately 1.3 million. High resolution cameras that can be used for landing purposes vary greatly in price: from tens of thousands to a hundreds of thousands, but stay well below the 1 million mark. Since the costs mentioned here are relatively low compared to overall mission costs, the criterion has a weight of 1.

### Reliability

Passive optical systems can be very simple and they have been used in space for years, making them very reliable. LiDAR has also been used in space successfully, but is relatively new and not as robust as cameras. The kind of algorithm used for TRN also has an effect on reliability. Correlation approaches work relatively fast compared to pattern matching, but for correlation the images or range measurements taken by the sensor have to be transformed to the same reference frame as that of the database map to be correlated. For this, accurate knowledge of the attitude and sometimes altitude are necessary, meaning that coupling of errors between attitude, altitude and position estimate can occur. This rectification is absent for pattern matching and so is the coupling of errors. Methods that estimate velocities by comparing measurements (IDs 5,6 and 10) are very robust. Reliability is given a weight of 4.

### Lighting

The main disadvantage of passive optical systems is that they need sunlight to function. Some systems are also very sensitive to large variations in illumination. Active ranging systems can be used in all lighting conditions, even in complete darkness. Relying on lighting conditions sets constraints on mission components such as the lunar transfer, which further propagates to lower-level components. This criterion has a weight of 4.

### Precision

Both optical systems can have a high variety in resolutions. However, the TRN estimates can only be as precise as their reference maps. The LRO mapped the lunar surface with the LOLA and LROC, the LOLA DEMs have a 25 [m] per pixel resolution on the South pole. The methods that compare images or range data for velocity estimates (IDs 5, 6 and 10) have lower precision. Because the landing precision requirement is so strict, precision is given a weight of 5.

### Power

The main discriminator in terms of power is the acquisition of data. Power consumption of a LiDAR system is around 900 <sup>4</sup> [W] while the Optech CS-10000 <sup>5</sup> camera system consumes 120 [W] (with gimbal). Power use has a weight of 3.

	Mass	Altitude	Precision	Cost	Reliability	Lighting	Power	Total score
<b>Weight criterion</b>	<b>5</b>	<b>3</b>	<b>5</b>	<b>1</b>	<b>4</b>	<b>4</b>	<b>3</b>	
<b>1</b>	4	4	4	4	3	3	4	92
<b>2</b>	4	4	4	4	2	2	4	84
<b>3</b>	4	4	4	3	3	2	3	84
<b>4</b>	4	4	4	4	3	2	4	88
<b>5</b>	4	4	1	4	5	3	4	85
<b>6</b>	4	4	1	4	5	3	4	85
<b>7</b>	2	2	3	2	3	5	2	71
<b>8</b>	2	2	4	2	3	5	2	76
<b>9</b>	2	5	2	4	2	5	3	76
<b>10</b>	2	2	2	2	4	5	2	70

The method that won is the crater pattern matching method using a camera (ID 1). Near the Lunar South Pole the amount of craters is very high, so the method benefits from that. However, the camera needs to have a minimum amount of craters in vision for the algorithm to give reliable results, [53, pp. 419-430] suggests at least 4. This will have implications for the approach, at higher altitudes waypoints can be detected more frequently because more craters are visible. Therefore at lower altitudes the absolute navigation by pattern matching will be aided by an optical velocity estimation method to accurately determine positions between waypoints. These methods compare two images to estimate the velocity and position change of the lander and use the same sensor, the camera. This kind of velocity estimate is much more accurate than an INS. Structure From Motion (ID 6) is chosen for this, which avoids the need for an attitude input. Using method 6 instead of method 5 (see Table 11.1) avoids the propagation

<sup>4</sup><http://www.optech.com/wp-content/uploads/PEGASUS-Specsheet-140624-WEB.pdf>

<sup>5</sup>[http://www.optech.com/wp-content/uploads/specification\\_cs-10000.pdf](http://www.optech.com/wp-content/uploads/specification_cs-10000.pdf)

of attitude error into the velocity estimate. The velocity estimate from this method will be fed into the INS and integrated for a relative position estimate.

## 11.6. NAVIGATION ARCHITECTURE

In this section a block diagram is given to show the interfaces of the various sensors, processors and actuators that work together during lunar landing. In Figure 11.1 this is depicted schematically. The architecture uses three sensors. The first is a star tracker to determine attitude. Secondly, an Inertial Measurement Unit (IMU) is used for attitude and position relative to the last determined absolute position. One of the components of the IMU is an Inertial Navigation System (INS), which integrates velocity since the last valid waypoint. Using both the star tracker and the IMU for attitude determination can avoid error propagation from attitude to position estimate and offers redundancy. The third sensor is the TRN-sensor, in this case the camera. Using the crater database extracted from 3D maps and the lander's INS position estimate since the last waypoint, a 2D projection of the terrain with craters is created. This process generates an image as would be seen from a virtual camera with the lander's current position and attitude. The craters extracted from the actual camera are then matched with the 2D projection. The crater filter subsequently discards matches that are faulty based on certain criteria. It can also feed through data that has a probability to be faulty. This information will be shared with the navigation filter. The position relative to a crater is then estimated, the higher the resolution of database maps and images, the higher the precision of this estimate. Absolute position is estimated by determining the location of the crater in the global map and fed into the navigation filter. The navigation filter also receives data from the IMU which contains an INS. Combining this data with the information from the crater filter, the navigation filter makes a decision and sends a control input to the thrusters. A control law determines the optimum trajectory to the landing site and defines the thrust setting.

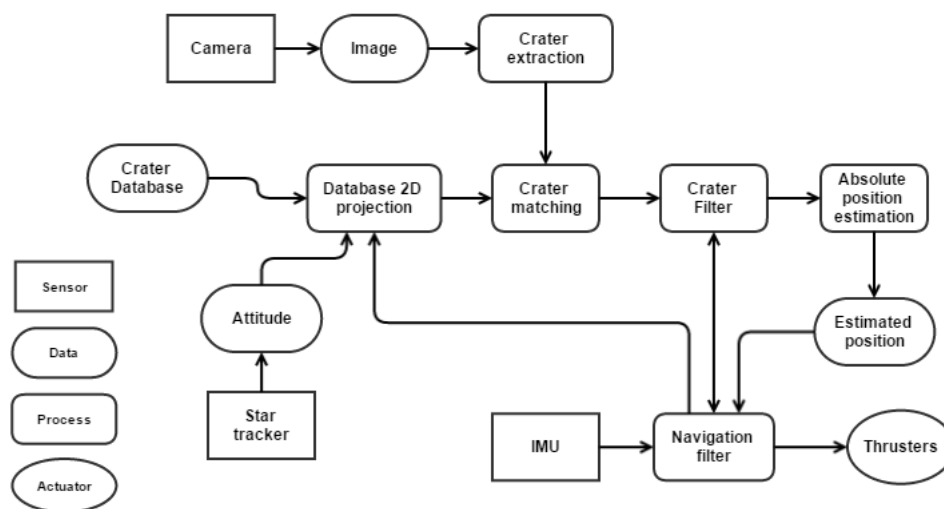


Figure 11.1: Schematic representation of the navigation architecture during landing

## 11.7. HAZARD DETECTION AND AVOIDANCE

Hazards during landing can lead to mission failure. Hazard detection and avoidance (HDA) methods will be implemented to prevent this. The Shackleton Rim has relatively smooth terrain as explained in [11] where an assessment of the amount of boulders at the landing site has been performed. It is important to determine what is considered a hazard, [11] suggest boulders of 0.5 [m] high and slopes of more than 15°. However the lander will be designed to be able to land on a slope of 30° as will be explained in Section 14.3. During the final 100 [m] of the descent the lander's navigation will switch from TRN to Hazard Relative Navigation (HRN). It will scan the surface for hazards, if it encounters one at its landing site it will calculate a new terminal landing trajectory. Redundancy in fuel is necessary for this. How much fuel precisely can be determined in a later design phase when time needed for scanning, processing and recalculating a trajectory can be pinpointed accurately. For now, 90 [s] is assumed to calculate the needed fuel, this is presented in Section 6.2.2.

On the Moon, objects can cast very long shadows. The crater pattern matching method used for TRN can distinguish crater edges during the lunar day using a camera. However, down at boulder size, certain terrain features can obscure

possible hazards with their long shadows. Considering this, a short-range LiDAR system will be used for HDA. These systems are much lighter than their long-range counterparts [54].

### 11.8. TRN IMPLICATIONS ON TRAJECTORY

As suggested in [53], at least four craters have to be in sight to accurately determine the position with a crater pattern method. Considering the swath angle of the camera and the amount of identifiable craters near SR1, a height can be determined at which the lander has to approach the landing site. After this the lander will descend vertically.

The landing ellipse semi-major axis is much smaller than its semi-minor axis (which is uncertainty in lateral position) and is neglected. Because the landing site is elongated (Section 5.1) and this elongation stretches roughly along  $0^\circ$  longitude (or  $180^\circ$  depending on perspective), the lander will have to approach the site from the right direction. This configuration occurs every two weeks.

### 11.9. VERIFICATION AND VALIDATION

To verify the TRN method that has been chosen, simulations can be performed. Simulated lunar terrain has been made in relatively high detail [12]. A possible strategy is to let the simulated lander determine its position in the simulated map, then this estimate can be checked with the actual position to determine the position error. A different strategy is to do a real life test with a UAV carrying the same sensors and algorithm on board and let it fly over terrain that mimics lunar terrain. It must be kept in mind that the UAV shall not experience nearly the same velocities that occur during a lunar landing. However its performance might be extrapolated to get an estimate of performance during lunar landing.

# 12

## MOON ROVER SUBSYSTEM

Using a trade-off the rover was selected as the most optimal deployment method. The design of the rover used is based on NASA's Axel v3 rover, which uses a "rappelling robot concept" consisting of "two wheels connected by a central cylindrical body, a caster arm, and an actively controlled tether passing through the caster arm... The caster arm provides a reaction force against the terrain needed to generate forward motion when traveling on flat ground." [8, pp. 16] In this chapter an analysis is made of how this rover must be adapted for the LOFARside mission including considerations on the power required, cable design, sensing, the size and mass of the rover and thermal control. The following section describes the power requirements for deployment (Section 12.1), cable design considerations (Section 12.2), and the sizing of the rover (Section 12.3).

### 12.1. POWER REQUIRED FOR DEPLOYMENT AND END-OF-LIFE DISPOSAL

The Axel v3 rover makes use of two 120 [W] engines to power its wheels, and two 120[W] engines to power the tether drum and arm actuators. The desired wheel torque is 120 [Nm] at a speed of 10 [cm/s] and for the tether drum and arm actuators it is 64 [Nm] at 5 [cm/s] but in opposite direction to each other to match the wheel torque and speed [55, pp.670]. In this section, a simple model of the rover on the moon is derived and together with an analysis of Shackleton crater used to adapt the rover design to the mission's specific needs.

#### 12.1.1. LAGRANGE EQUATIONS OF MOTION FOR SINGLE WHEEL ON SLOPE

The rover descending and ascending down a slope is modelled as a single wheel as seen in Figure 12.1.

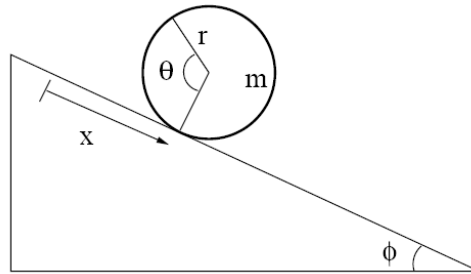


Figure 12.1: Simplified axel rover model on a slope

The Lagrangian of the system is given by the difference in potential (V) and kinetic energy (K) in Equation (12.1). The Euler-Lagrange equation is given in Equation (12.2). T represents outside forces acting on the system, in this case the torque on the wheel.

$$\mathcal{L} = K - V \quad (12.1)$$

$$\frac{\partial \mathcal{L}}{\partial x} - \frac{d}{dt} \frac{\partial \mathcal{L}}{\partial \dot{x}} = T \quad (12.2)$$

The kinetic and potential energy of the wheel when rolling uphill are given in Equations (12.3) and (12.4).

$$K = \frac{1}{2} m \dot{x}^2 + \frac{1}{2} J \dot{\theta}^2 \quad (12.3)$$

$$V = mgx \sin(\phi) \quad (12.4)$$

Recognizing that  $X = R\theta$ , substituting in the Euler-Lagrange equation and solving it yields Equation (12.5).

$$\frac{3}{2}m\ddot{x} + mg\sin(\phi) = T \quad (12.5)$$

Assuming a constant velocity, like in the Axel rover experiments [8, pp.34], an expression for the power required to roll uphill is given in Equation (12.6).

$$P = T \cdot w = mg\sin(\phi) \cdot \dot{\theta} \quad (12.6)$$

### 12.1.2. VALIDATION OF THE MODEL

Peak values of the power occur when the slope is completely vertical, or if the wheel has to lift its entire weight over an obstacle, like a rock. Power consumption data of the first Axel rover on a straight obstacle course with paddle wheels shows peak values of 210 [W] [8, pp.34] at 6.5 [RPM]. For mountain bike tires values reduce to 60 [W]. This difference can be explained by the fact that, due to the paddles, the rover has to effectively lift itself over obstacles of a height the mountain bike tire cannot traverse. This lifting of its own weight corresponds to the most extreme situation in the mode, a vertical slope. For this case, the above model predicts peak values of 167 [W]. The difference could be attributed to the engine efficiency, which for a DC electrical engine is in the range of 80-90%, corresponding to a predicted peak value range of 185-209 [W]. It is therefore concluded that the model is able to provide an initial estimate of the total power required for the rover used. For further analysis, three-dimensional equations of motion for a two wheel rover can be derived and combined with data of obstacles, which will provide a more detailed image of the power consumption.

### 12.1.3. APPLICATION TO SHACKLETON CRATER

On its descent into the crater the rover will descend a 30 degree slope over 8.4 [km] and travel 1.6 [km] on an uneven mound like feature that has a central peak of 200 [m] height [8, pp.50]. On both slopes the rover has to be able to traverse obstacles and backtrack its path in case of too large rocks or if it has entered a smaller crater. This means that the peak value of power consumption will be reached frequently. Most importantly, the rover has to be able to deliver this peak power with its tether alone, as it might be in a situation where its wheels lose contact with the ground. Similarly, the actuators on the rover wheels need to be able to deliver this peak power in case of forward obstacle traversal. In the case of none or small obstacles the rover will require significantly less power.

Shackleton crater's walls are smoother than the bottom of the crater and have a RMS surface roughness of <1 within 5 [m], whereas the surface has a RMS roughness of >1. It is an "ancient, unusually well-preserved simple crater whose interior walls are fresher than its floor and rim." [56, pp.381-383]. This indicates that the crater walls can be traversed relatively easy, while the bottom of the crater could pose more difficulty. Regardless, it is not possible to determine the amount of obstacles and their size that the rover will encounter at a relevant scale. Power test data for the Axel rover suggests a near sinusoidal distribution [8, pp.34] during obstacle traversal, so an average power of half the peak value is assumed. For end-of-life disposal consisting of retracting the antennas the rover will require more power, but since the speed at which this is done is not important, and peak values will not change, no additional power capability is considered for this case.

Axel v3 can operate for 8h on 4 Thunder Power 22-V 8-A h lithium polymer batteries which can be trickle charged so that for eclipse periods of the landing module the rover retains its functionality. For the LOFARside mission eclipse periods are below 8 hours so it is suggested to remove two batteries to save weight. Axel v3 rover weighs 39 [kg], but for deployment from a lander a 15 [kg] target can be envisioned [55, pp.672]. For this mission a mass estimate used for cable design in Section 12.2 is 25 [kg] for the rover and 50 [kg] for cables. This translates to a peak power value of 125 [W] and an average power of 62.5 [W]. However, as the cable is deployed the mass of the rover and so the power required reduces, so that the average power over the complete deployment is 42.12 [W] In case of a smooth surface of the crater walls the rover might not require power at all to descend, but this is impossible to ascertain at the moment. Further investigation of lunar crater walls is recommended.

## 12.2. CABLE DESIGN AND TENSION CONSIDERATIONS

In this section the design for the cable that is used as tether and data/power connection is presented. Data rate and power transmission are discussed first and based on preliminary mass estimations. Only tensile forces are considered for the cable. Preliminary investigations at the baseline level revealed that a combination of fiber optic cables with a dedicated power cable is the best option.

### 12.2.1. POWER AND DATA RATE IMPLICATIONS

From Section 3.4.1 and Section 12.1 the power consumption during mission operations is 30 [W] and for deployment 62.5 [W], whereas the data rate during mission operations is 840 [Mbit/s]. Single fiber links can support data rates well in excess of 840 [Mbit/s]. Temperatures in Shackleton crater don't exceed 100 [K] and can be as low as 40 [K] [55, pp.673]. For copper a resistivity of  $5 \cdot 10^{-6}$  [Ohm · km] is used and the required power is 62.5 [W]. Calculations for a copper wire to transmit power are shown in 12.1.

Surface area of cable [mm <sup>2</sup> ]	Cable diameter [mm]	Resistance [Ohm/km]	Power loss at 28V [W]	Power loss at 440V [W]	Cable mass [kg/km]
0.1	0.178	500	2531.25	10.25	0.90
0.3	0.309	166,7	843.75	3.42	2.69
0.5	0.399	100	506.25	2.05	4.48
0.7	0.472	71,4	361.61	1.46	6.27

Table 12.1: Copper cable dedicated wiring results

A single harsh environment fiber optic cable with polyurethane as protective material that can withstand the temperature range of the Shackleton crater weighs 3.6 [kg/km] (based on inquiry at Timbercon). Embedding a copper wire with a 0.25 [mm] diameter (resulting in a loss of 4 [W]) adds 1.76 [kg/km]. The wire then weighs 53.6 [kg] for the 10 [km] length. This excludes tensile strength considerations.

### 12.2.2. CABLE TENSION CONSIDERATIONS

An extensive tension analysis is detailed both theoretically and experimentally in [8], and its conclusions are that a 100 [lb] rover causes peak tether tensions of 170 [lbf], when it is failing to climb a cliff. In this situation a composite tether weighing 1 [kg/km] that can hold up to 1000 [lb] is used. The rover with cables and antennas weighs 88.6 [kg] which corresponds to 332.1 [lbf] tether tension using the above results. This indicates that a similar composite tether as strength member is required to ensure the tensile strength of the cable. The overall cable mass is now 63.6 [kg].

### 12.2.3. CABLE ENVIRONMENT

The cable has to be able to operate to the specifications at temperatures below 100 [K] in the crater and up to 400 [K] outside of the crater. The copper cable has been sized for 100 [K] and the fiber optic cable functions irrespective of temperature, and has been designed for ranges of temperature of -200 to +200 degrees Celsius. The tensile strength of the composite tether does not change significantly with respect to room temperature conditions when tested at 100 [K] for carbon fiber [57]. This is depending on the type of composite used, however, it should be investigated further in detailed design. Furthermore, at the rim of the crater, a part of the cable will experience a large number of thermal cycles throughout the mission lifetime. The effect of such strains needs to be investigated as well.

## 12.3. SIZING OF THE ROVER

In this section the required size of the Axel rover is determined. First, the volume of the cables and antennas when rolled up on the rover is determined. The size of the rover follows from this.

The cable with embedded copper wire and strength member has a diameter of 2.3 [mm]. Approximating the cable on the spool by a square cross section, the thickness of the spool can be calculated as in Equation (12.7).

$$V = \frac{\pi}{4}(D_o^2 - D_i^2) \cdot width = length \cdot \frac{\pi d^2}{4} \quad (12.7)$$

Here d is the cable diameter,  $D_o$  is the outer diameter of the spool,  $D_i$  is the inner diameter of the spool (the diameter of the axis) and L is the length of the cable. Solving for the outer diameter yields Equation (12.8).

$$D_o = \sqrt{\frac{4Ld^2}{w\pi} + D_i^2} \quad (12.8)$$

The initial Axel rover has a width of 81.28 [cm] and an axis diameter of 15.24 [cm], whereas Axel v3 has a width of 1.52 [m]. The outer spool diameter for the first design is 32.57[cm] and for the third version it is 25.9 [cm]. Almost doubling the width reduces the spool thickness by about 6.6 [cm]. It is important to increase the wheel diameter

to ensure that obstacles can still be traversed. To this end, the wheel diameter of the third Axel rover of 84 [cm] will be used, but a width of 1 [m] is considered sufficient to ensure that the spool is not too thick, resulting in an outer diameter of 30.1 [cm]. Testing of the rover with 10 [km] cable on its spool should be performed to assess the changes in its ability to traverse obstacles. It should be noted that the wheels of the rover are foldable as is shown in Figure 12.2.

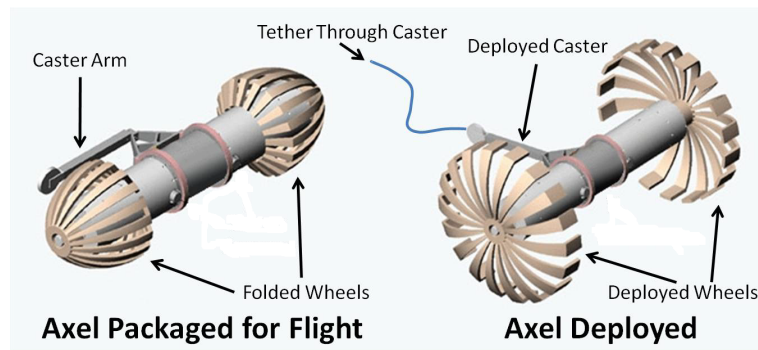


Figure 12.2: Axel rover foldable wheels [8, pp.16]

In the detailed design it should be investigated whether it is possible to wind and unwind the spool with antennas attached to the cable, or if a separate system is required that connects the antennas to the cable at the required position. The crossed dipole antennas before deployment have dimensions 4x4x4 [cm] [6, pp.62]. 21 such antennas will be placed inside the Shackleton crater. This means that a system can be envisioned where the spool is wound such that the antennas are at the top and outside of the spool and are deployed at regular intervals. The width of the spool fits the 84 [cm] width of a line of 21 antennas. Testing of such a system is required. Alternatively, if this system proves too complex or too unreliable, a polyimide film antenna could be considered [58, pp.6-7]. This antenna of 8 [m] length could be folded along the wire and be deployed by the rover further unwinding its tether.

### 12.3.1. ROVER NAVIGATION AND CONTROL

It is crucial for the success of the mission to ensure that the rover can avoid obstacles which it cannot traverse. Sensing and obstacle avoidance must be integrated into the design and control algorithms.

#### PROXIMITY SENSING

In the eternal darkness of the Shackleton crater a laser sensing system could be used to map the terrain ahead of the rover. LIDAR is a remote sensing technology that can be used to scan and map a surface. Lightweight close range LIDAR systems are available at very light weight (600 [g]) and low cost (8000 [\$])<sup>1</sup>. This system can map with an accuracy of 2 [cm] over a range of 100 [m] with 360 [°] horizontal and a 15 [°] vertical field of view. Testing and adaptation of the system to the space environment should be performed however.

#### CONTROL ALGORITHMS

Control algorithms will be designed with autonomy of the rover as the main goal. Motion planning algorithms for regions where the tether is not in tension exist [59]. For regions where the rover requires its tether to move a distinction can be made between ascent and descent paths. Ascending is much more difficult because of the need for grip of the wheels and the fact that obstacles are larger when approached from below. Shortest ascent and descent planning algorithms that have as input a map of the terrain can be implemented [8, pp.57-73].

### 12.3.2. THERMAL CONTROL

Due to the aforementioned extremely low temperatures in the Shackleton crater of 40-100 [K] and the fact that electronics generally do not work below -40 [°C] the rover requires thermal control. Apart from this, it is crucial to ensure that the heat of the rover does not contaminate any additional measurements taken. A preliminary thermal analysis assuming a multilayer insulation and operating power of 60 [W] concluded that the avionics operate at 28 [°C], which is not a problem [55, pp.676]. However, a more detailed thermal analysis that accounts for periods where the Axel rover doesn't use power such as during smooth descents and during the 5 year lifetime is required. The rover's ability to survive 5 years within the crater for possible end-of-life disposal needs to be assessed.

<sup>1</sup><http://velodynelidar.com/lidar/hdlproducts/vlp16.aspx>

### 12.3.3. ROVER CONFIGURATION

Based on the analysis of the previous sections the Axel rover design is adapted to fit LOFARside mission's specific needs. Results are presented in Table 12.2.

Axel Rover Design	
Peak power [W]	164.7
Average power [W]	52.02
Rover mass [kg]	25
Cable mass [kg]	63.6
Antenna mass [kg]	9.45
Peak tension [lbf]	369.54
DC Wheel actuator left [W]	100
DC Wheel actuator right [W]	100
DC Tether drum engine [W]	85
DC Arm actuator engine [W]	85
Operating temperature range [°Celsius]	-200 to +200

Table 12.2: Axel rover design results

A cross section of the axel can be seen in Figure 12.3.

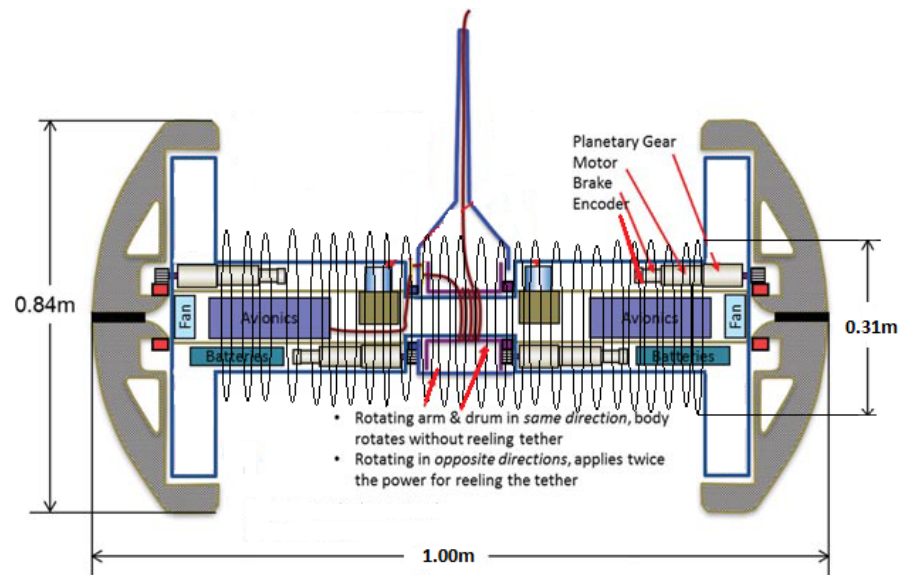


Figure 12.3: Cross section of the Axel rover with wire spool indicated [55, pp.673]

## THERMAL CONTROL SUBSYSTEM

In space, the range of temperatures of an object fluctuates abruptly. Most components sent to space have been developed and tested on the Earth and hence their operating conditions are similar to that of this mission. The LOFAR systems will be subject to two different environmental operating conditions presenting both different temperature control requirements; The transfer phase and the lunar stationing. This chapter will describe the required operating temperatures (Section 13.1), thermal control for the transfer phase (Section 13.2) and lunar station (Section 13.3). Lastly, an explanation of the verification and validation procedures (Section 13.4) is given.

### 13.1. REQUIRED OPERATING TEMPERATURE RANGE

Before designing and analysing the environmental temperature range that the S/C will experience, the operating temperatures of the systems on-board need to be first known. In Table 13.1, the minimum and maximum operating temperatures for the different subsystems are given. A proper thermal control can then be addressed to keep the S/C's temperatures within this range.

Subsystem	Minimum Temperature [K]	Maximum Temperature [K]
Batteries	253.15	333.15
Solar Arrays	123.15	373.15
Antenna	173.15	373.15
CMGs	253.15	328.15
Hydrazine fuel	288.15	313.15

Table 13.1: Required temperature range [3]

From the table it can be seen that the temperatures will have to be kept between 253[K] for a minimum temperature to 313[K] for the maximum temperature. Further local control will have to be undertaken for other specific subsystems such as the hydrazine fuel.

### 13.2. TRANSFER PHASE THERMAL CONTROL

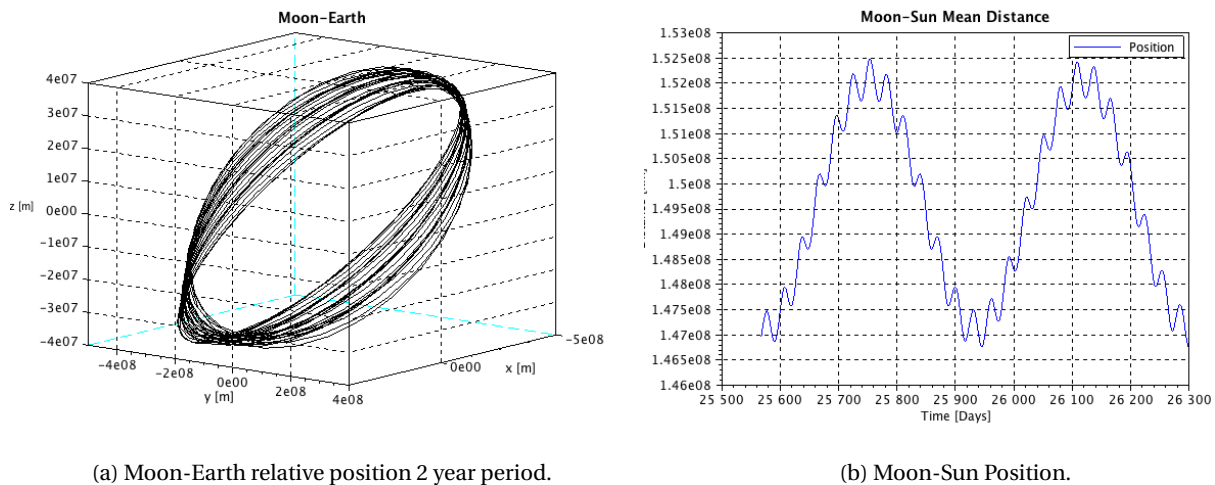
Due to vacuum and the lack of a continuum environment, the only way to receive or release energy in space is through radiation. Hence, convection and conduction with exterior sources cannot take place outside the atmosphere (only conduction within the S/C is possible) and hence the environmental radiation sources must be analysed.

#### 13.2.1. THERMAL ENVIRONMENT

The analysis of the thermal environment where the S/C is going to operate is of extreme importance since it determines how much heat from the different sources the spacecraft will receive. The spacecraft will not be subject to atmospheric drag (and thus no atmospheric drag heating) since the atmospheric pressure where it will operate, is typically less than  $10^{-7}$  [mb] and can be neglected [40]. Therefore, in order to properly determine the balance of heat, a thorough analysis of the radiation environment should be performed.

The main sources of radiation come from the direct Sun radiation, the Earth's albedo radiation (reflected radiation) and planetary radiation in the form of thermal energy (Infrared IR) directly from the Earth. For this purpose, first the position of the Moon with respect to the Earth for a 2 year period was calculated as can be seen from Figure 13.1a. Then the position of the Earth with respect to the Sun was calculated and finally the distance of the Moon with respect to the Sun could then be found as seen in Figure 13.1b. It is assumed that LOFAR is launched the 21st of November 2021 and the date was converted to Julian days (plotted in the x-axis). Only two years were used to see the

fluctuation of distance (which should be periodic) for the transfer of one year as well as for a one year stationing in the Moon.



### SOLAR RADIATION

The main source of incoming radiation is the Sun, where its intensity is inversely proportional to the square of the distance from the S/C to the Sun. A few important parameters when calculating this are the spectral distribution of the sun-light and the solar intensity. Furthermore, solar activity should also be taken into account since the Sun has periodic solar storms which emit millions of charged particles that influence directly on the spacecraft's state. The spectral distribution is considered constant around the solar system and entails that 99% of the solar energy lies between 150 [nm] and 10 [μm] with a maximum of around 450[nm] (yellow part of the visible spectrum) [40]. The solar radiation of the spacecraft can be calculated with Equation (13.1):

$$J_s = \frac{P}{4\pi d^2} \quad (13.1)$$

Where P is the Sun's power output  $P = 3.856 \times 10^{26}$  [W] [40] and d is the distance from the S/C to the Sun. For thermal control purposes, the maximum and minimum values of distance are of interest since those are the extreme locations where the S/C will have the greatest temperature change. Therefore, the solar radiation intensity was calculated using the Moon distance as can be seen from Figure 13.2, since the S/C will be closest to the Sun when the Moon is closest to the Sun and vice versa. This also helped decrease the required computational time since using the spiraling orbit position coordinates require more computational power without delivering any relevant results with respect to extreme temperatures. The figure presents the expected results since the solar radiation is a maximum when the Moon is closest to the Sun whereas it has minimum values when the moon is on the opposite side of the Earth.

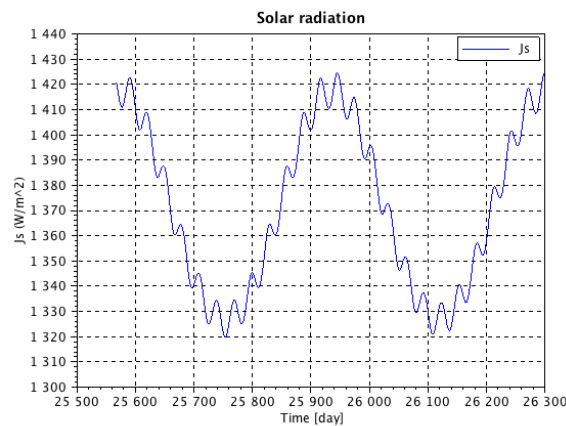
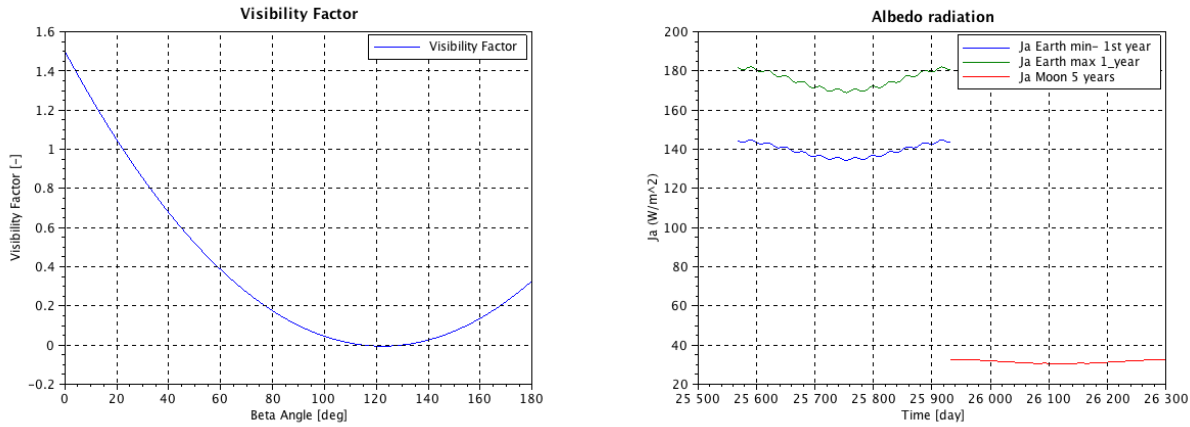


Figure 13.2: Solar radiation intensity versus time

### ALBEDO RADIATION

The albedo is the reflected radiation from the surface of the Earth due to the presence of reflecting bodies (i.e. snow, clouds or mountains). It is a complex function but can be expressed in terms of the visibility factor ( $F$ ) and the planetary albedo characteristic ( $a$ ) such that:

$$J_a = J_s a F \quad (13.2)$$



(a) Visibility factor interpolation.

(b) Albedo radiation intensity versus time.

The planetary albedo ' $a$ ' lies between 0.31-0.39 for Earth, depending on the amount of clouds in the atmosphere, whereas  $a=0.07$  for the Moon [40]. Thus only the maximum and minimum values will be taken into account, giving the maximum and minimum albedo radiation. The visibility factor ( $F$ ) was interpolated with the help of a Lagrange polynomial as can be seen from the Figure 13.3a. Plotting the interpolated function, we can achieve the visibility factor with respect to the angle between the local vertical and the Sun's rays ( $\beta$ ) [40]. The minimum and maximum albedo radiation intensity was taken as design driver since it gives the extreme case scenarios for the albedo radiation.

### PLANETARY RADIATION

Some planets in our solar system are active within the inside and emit heat in the form of radiation. The Earth radiates this heat in the infrared spectrum (IR) with wavelengths between 2 and 50 [ $\mu m$ ] [40]. The radiation that the S/C experiences comes mainly from the upper atmosphere plus the infrared contribution of the Earth's surface. Since the Earth presents many temperature changes across the surface, it is assumed that it radiates with a uniform intensity of  $P=237 [W/m^2]$  [40]. The planetary radiation can then be determined with Equation (13.3).

$$J_p = P \left( \frac{R_{rad}}{R_{orbit}} \right)^2 \quad (13.3)$$

$R_{rad}$  is the radius of the Earth's radiating surface and  $R_{orbit}$  is the distance from the S/C to the Earth. Substituting values in the above equation for the transfer phase and plotting versus the distance to the Earth results in Figure 13.4. This assumes that the transfer phase is carried out directly from the Earth to the Moon, without spiraling out. As stated previously, it is done this way in order to have the maximum and minimum values that the S/C will experience (closest and furthest away) so that thermal control can directly address the required temperature range.

### TOTAL INCIDENT RADIATION

Adding the three sources of radiation, we obtain the total incident radiations on the spacecraft. We can add all the minimums and all the maximum values to see the spacecraft minimum and maximum radiation range. Adding the three figures results in Figure 13.5.

#### 13.2.2. THERMAL EQUILIBRIUM

Once all incident radiations have been analysed, the thermal equilibrium of the S/C can be tailored. The thermal balance between the incoming radiation and the outgoing radiation must be evaluated, where the final heat of the satellite will be the difference between the received radiation and the heat radiated to Space. Therefore, the heat generated by the dissipation of the electronic components ( $Q$ ) inside the S/C has to be also taken into account. This

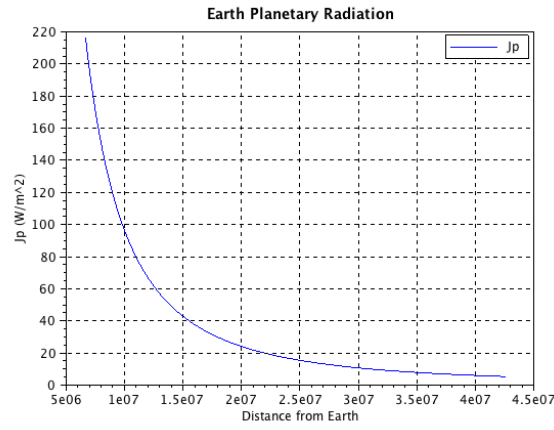


Figure 13.4: Albedo radiation intensity versus time

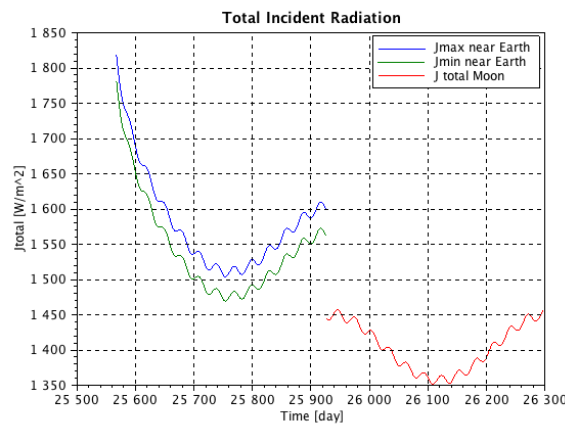


Figure 13.5: Total radiation intensity versus time

heat is transmitted via conduction due to direct contact between the different subsystems. There are various devices that generate heat such as the batteries, power converters, the propulsion subsystem and any active instruments. Thus the estimated internal heat generated is approximated with:

$$Q_{Internal} = Q_{Batteries} + Q_{Prop} + Q_{inst}$$

It is estimated to be 1% of the total power consumption during the transfer phase, which results in  $Q_{internal} = 85$  [W]. Using Equation (13.4), the thermal balance was calculated [40]:

$$T^4 = \frac{A_p}{A_{s/c}} J_p + \frac{Q}{A_{s/c} \sigma \epsilon} + \frac{A_s J_s + A_a J_a}{A_{s/c} \sigma} \frac{\alpha}{\epsilon} \quad (13.4)$$

$A_p$  is the surface where the planetary radiation acts,  $A_s$  represents the surface area of the acting solar radiation,  $A_a$  the albedo surface and  $A_{s/c}$  the total exterior surface of the spacecraft. For this case, maximum and minimum areas have been taken for different calculations. First it was assumed that only the bottom part of the S/C is under the influence of these radiations, which represents the minimum worst case scenario. On the other hand, half of the total S/C exterior surface was evaluated for the maximum worst case scenario. Furthermore,  $\sigma = 5.67(10^{-8})$  [ $W m^{-2} K^{-4}$ ] is Stefan-Boltzmann's constant whereas  $\alpha$  and  $\epsilon$  are the absorptance and emittance values of the exterior surface material. Changing the absorptance and emittance helps control the temperature range within the S/C.

### 13.2.3. THERMAL STRATEGY

The desired the thermal control can be achieved using passive control systems. The advantages of using passive thermal control is that no mechanical moving parts are required and also no power consumption is needed. Fur-

thermore, they are much easier to design and implement entailing low cost, low mass and high reliability. On the other hand, passive means to control thermal properties have low transport capabilities that usually need to be compensated with heat pipes. These control systems include paints, Multi-Layer Insulation (MLI) or Optical Solar Reflectors (OSR).

#### EXTERIOR MATERIAL PAINT

The paint used in the outer surfaces of the spacecraft has an important functionality since it will influence the absorptance and emissivity values in the equilibrium temperature phase. In the table below, typical values for colours used in space applications can be seen. These values hold for different wavelengths.

Material	Solar Absorptance (BOL), $\alpha$	Hemispherical Emissivity, $\epsilon$
Black paint	0.96	0.85
Aluminized Teflon foil 5mil	0.14	0.80
Silvered Teflon foil 5mil	0.09	0.80
Aluminized Kapton foil 2mil	0.42	0.72
White paint	0.24	0.82
Solar cell Si	0.75	0.82
Solar cell GaAs	0.91	0.81
CFRP	0.92	0.82
Aluminium 6061-T6	0.2	0.31
Gold	0.299	0.023
Steel AM350	0.357	0.111
White Epoxy	0.248	0.888
Quartz Over Silver OSR	0.07	0.79

Table 13.2: Absorptance and emissivity values for different materials

These materials have been implemented into the S/C configuration and are plotted in the Figure 13.6. The plots help visualize the variation in the maximum and minimum temperature ranges that the S/C will ever experience.

The black lines in the graphs represent the maximum and minimum allowable temperature limits which lie between 253[K] and 313[K]. From these, it is visible that no single material can ensure the control of these temperatures. The Aluminized Kapton can be used with only one layer ( $n=1$ ) as can be seen from Figure 13.6 but further optimization can be achieved by implementing several layers of one or several materials. These layers are required to maintain the levels within the stated limits, known as a Multi-Layer Insulator (MLI).

#### MULTI LAYER INSULATION

Multi-Layer Insulation of thin foils allow to achieve low emissivity values. It is made of thin layers which reduces the heat loss due to radiation. Many layers can be added to tailor the heat that needs to be kept inside the spacecraft. They act as radiation barriers and therefore decrease the heat flow and the heat dissipation. The Figure 13.7 below shows a typical MLI geometry to control heat input and output. The principle to work with multi-layer insulators is to stack  $n$  layers with low emissivity values ( $\epsilon$ ) and thus reduce the emissivity by  $n$  times. The stack of thin polymer foils can be done with materials such as kapton or mylar and from reference spacecraft it is found that typical  $n$  values range between 5 to 25 foils. For LOFAR purposes, simulations with 3, 5 and 7 layers of the same material were implemented.

As can be appreciated from Figure 13.8, the only material that can passively ensure the control of temperatures between  $T_{allow_{min}} = -20$  [°C] to  $T_{allow_{max}} = 40$  [°C] is the silver teflon 5mil with  $n=5$  layers of the same material. From the graph it is visible that this material can exactly keep the spacecraft temperature range between the required limits. Further optimization can be achieved by combining layers of different materials which could reduce the amount of stacked layers (and hence weight and complexity).

#### HEAT PIPES

The control of the temperatures within the spacecraft not only has to be carried out with a material selection but also a uniform temperature distribution must be achieved. In order to have the same temperatures in the S/C and to prevent big changes in temperatures from the illuminated and shadowed sides, heat pipes are incorporated. These heat pipes transport any heat difference and delivers it to the required region.

For the LOFAR mission a two-phase heat pipe using a continuous evaporation and condensation cycle at the saturation temperature of ammonia will be used. Airbus Defense and Space offer an axially grooved extrusion of an

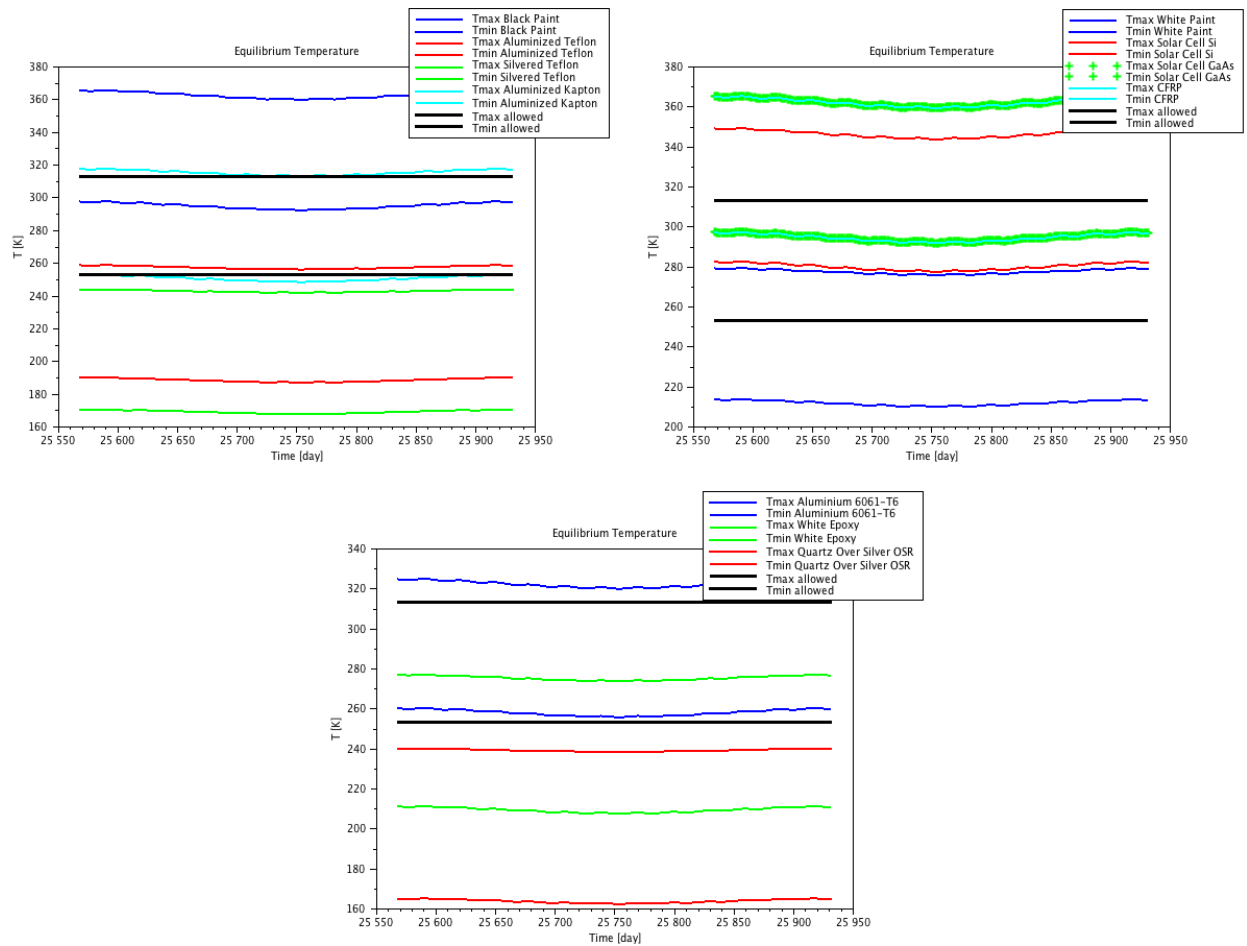


Figure 13.6: Equilibrium temperatures for different materials

aluminium alloy with as low as 4 [mm] in diameter<sup>1</sup>. It has a performance of up to 400[Wm] at 293 [K] with high endurance and lifetime. Further analysis will have to be carried out to determine the required dimensions and locations of the heat pipe system.

### 13.3. LUNAR STATION THERMAL CONTROL

Thermal control is also required once the S/C lands on the Moon, where the operating thermal environment at the lunar surface must also be understood. The batteries in the lander and other instruments will also have to be kept within their operating range. Note that some conduction between the lander and the lunar surface is likely and as the S/C temperature changes and becomes hotter than the surface, the Moon becomes a heat sink. Nonetheless, due to the low conductivity of the lunar soil and the vacuum conditions, only the radiation will be taken into account.

#### 13.3.1. LUNAR THERMAL ENVIRONMENT

In the polar regions of the Moon, temperatures vary from 120[K] to 160[K], whereas they take values as low as 40[K] in the shadowed polar craters [60]. For the Shackleton crater, the minimum temperature measured at the bottom floor was found to be 88[K] [61]. These extreme values come from the low mean heat flow incident from the solar flux, estimated to be between 12 to 21 [ $mW/m^2$ ] [62]. The temperatures in the Moon are modelled with Equation (13.5) [63]:

$$T_m = 373.9 \cos(\phi)^{0.25} \sin(\theta)^{0.167} \quad (13.5)$$

This equation is valid for different latitudes by considering the temperature only as a function of the angle between the Sun's rays and the normal outward vector of the lunar surface at a specific location. With  $\phi$  being the latitude of

<sup>1</sup>Heat Pipe: <http://www.space-airbusds.com/en/equipment/heat-pipes-3bv.html>

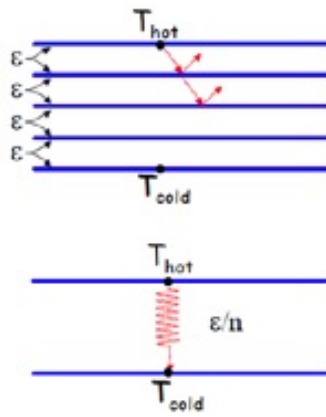


Figure 13.7: Multi-Layer Insulator representation

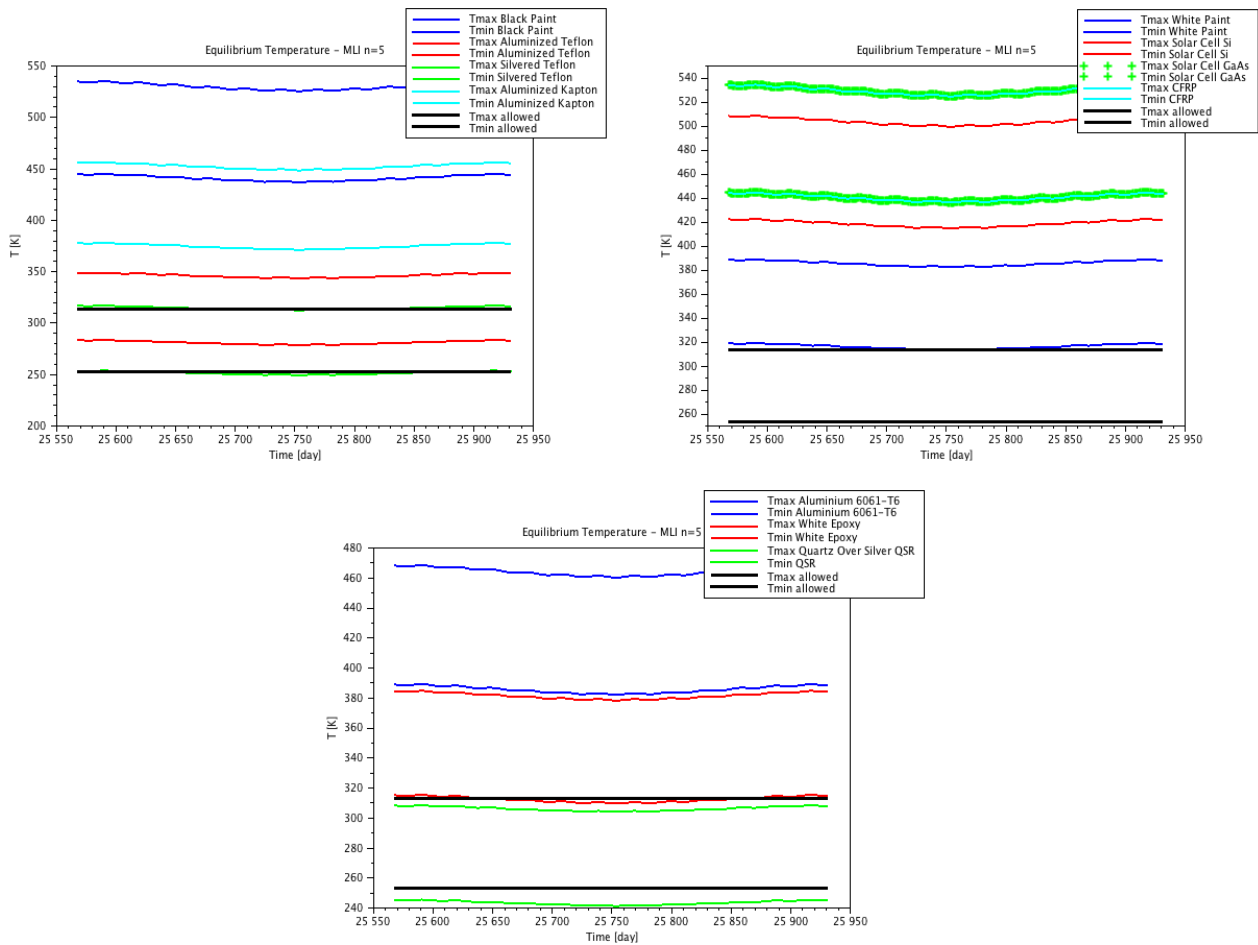


Figure 13.8: Equilibrium temperatures using MLI n=5 layers

the base position and  $\theta$  the Sun's angle above the lunar horizon. The Shackleton crater lies at a latitude of  $\phi = 89.9^\circ$  and taking  $\theta = 5^\circ, 45^\circ$  and  $90^\circ$  the following temperatures are estimated at this location:

$$T_{min_{5^\circ}} = 90.41[K]$$

$$T_{45^\circ} = 128.25[K]$$

$$T_{max_{90^\circ}} = 135.89[K]$$

These are very low temperatures that need to be taken into account for the thermal control of the mission. For the 1 degree case, this will never occur since the rays incidence will never be so low but it serves to evaluate any possible

combination. Furthermore, inside the crater temperatures will be very low throughout the whole mission due to the eternal darkness and therefore thermal control should also take this into account.

### 13.3.2. THERMAL STRATEGY

The antennas inside the crater are already designed to operate in those extreme conditions and therefore there is no need to insulate them nor protect them from their operating environment. The same holds for the cable connecting the antennas and it does not need to be thermally controlled. The only system that needs to be kept within a certain temperature range is the lander, which will house all electronic components required for the mission.

The lander has the same exterior material as explained previously with the same amount of layers since it was also designed to withstand the temperatures throughout the transfer phase. It will also have the chosen heat pipe system to transport the uneven distribution of heat from one side of the lander to the other; further thermal control is not required whenever the lander has any incident radiation from the Sun.

Nonetheless, it was calculated that the lunar base will be in the shadow for at most 7 days in a row and temperatures will be very low at this period. To ensure local heating on this moment, small heaters must be incorporated. MINCO<sup>2</sup> offers several types of heaters that can be used for our purposes. The lander will carry a polyimide film / FEP adhesive heater with a rated power density of  $52[W/m^2]$  and an operating temperature range between  $210[K]$  and  $473[K]$ . This is estimated to be sufficient for the 7 day eclipse time that LOFAR will experience. Further analysis of the placement of the heaters and their impact in the S/C must be carried out in the continuation of this project.

### 13.4. VERIFICATION & VALIDATION

The positioning of the Moon with respect to the Earth and Sun was found using built-in functions from CELESTLAB, an environment developed by the Centre Nationale d'Etudes Spatiales (CNES). On the other hand, the mathematical models used for the estimation of the radiation and thermal balance were found in [40]. These were coded into SCILAB which resulted in the above plots. To verify this, the distance from Earth to the Sun (1AU) was used and resulted in the same average incoming radiation that is experienced in the Earth. Verification was conducted in the sense that the mathematical models delivered reasonable results. Furthermore, the temperatures at the South Pole of the Moon were estimated with models from [62], [63]. These results were validated with results from other missions to the Moon from [61].

On the other hand, due to lack of time, experience and resources, Verification & Validation of the heat pipe system and of the incorporated heater could not be conducted. In the future development of the project this shall be addressed as early as possible to either improve or correct the model. Furthermore, the thermal cycles and the degradation in performance due to these has not been included in the analysis and further research shall be carried out in this regard.

---

<sup>2</sup>MINCO Heater: <http://www.minco.com/Heaters/Support-and-Tools/Heater-Configurator>

## STRUCTURES AND MECHANISMS SUBSYSTEM

In this chapter structural considerations are presented for the LOFARSide mission. The sections deals with loading cases for the integrated spacecraft (S/C) (Section 14.1), the solar panels (Section 14.2) and the landing struts (Section 14.3). An overview of the spacecraft with all its components can be found in Appendix A.

### 14.1. SPACECRAFT

In order to ensure that the spacecraft during the launch phase does not bend or buckle due to the high loads caused by the gravity gradient or vibrations, the investigation was made into that. This section discusses the structural characteristics of the spacecraft.

#### 14.1.1. S/C CONFIGURATION

Figure 14.1 shows the chosen configuration for the spacecraft. It consists of the Mothership (Spílaio) modeled as a cylinder and a lander (Noor) which geometrically is the combination of the cylinder and a truncated cone. The loads acting on both structures are translated to the inner cylinder via the four rods (see Figure 14.1 view (b)), thus the inner cylinder together with the rods takes up all the load that acts on the S/C during the launch. The dimensions are within the maximum allowable VEGA fairing dimensions which can be seen in Figure 14.2. Table 14.1 lists all geometric parameters of the S/C outer structure, but since the launch loads are taken by the inner structure of the S/C, Table 14.2 summarizes all relevant parameters which were used when calculating critical loads and stresses.

Spílaio is a cylinder with height of 1.2 [m] and outer diameter of 2.2 [m]. The inner structure of Spílaio consists of the inner cylinder (with height 1.2 [m] and diameter 0.5 [m]) and 8 rods: 4 at the top and 4 at the bottom, placed as can be seen in Figure 14.1 view (b). The rods dimensions can be seen in Table 14.2.

The 0.7 [m] vertical distance from the separation plane in Figure 14.1 is to shield the chemical and electric propulsion thrusters and the 0.8 [m] vertical distance from the bottom of Noor accounts for the clamp which will hold the two parts of the S/C together during the launch.

Noor consists of a cylinder (height 1.6 [m] and diameter 2.2 [m]) and a truncated cone (height 2 [m], bottom diameter 2.2 [m], top diameter 1.04 [m]). The angle between the slant of the cone and the height is 16.17 [°]. The inner cylinder inside Noor is 2.8 [m] high and has a diameter of 0.5 [m]. The cylinder is connected to the outer skin of Noor via 8 rods, 4 at the top of Noor and 4 at 1.6 [m] height from the bottom of Noor.

Parameter	Spílaio		Noor
		Cylinder	Truncated cone
Outer radius [m]	1.10	1.10	0.52
Thickness [m]	0.001	0.001	0.001
Height [m]	1.20	1.60	2.00
Cross-sec. area [m <sup>2</sup> ]	0.0069	0.0069	0.0033
Total volume of the skin [m <sup>3</sup> ]	0.0083		0.0212
Mass [kg]	<u>22.38</u>		<u>57.3</u>
Total mass [kg]		<b>79.68</b>	

Table 14.1: The parameters of the S/C outer structure



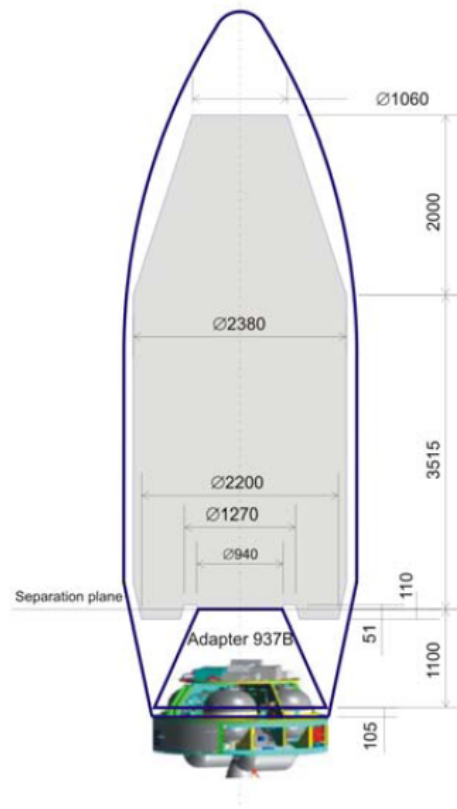


Figure 14.2: VEGA payload fairing [2]

- Instead of areas in Equation (14.1), the masses need to be taken into account as in Equation (14.2).

$$\bar{z}_{c.g.} = \frac{\sum Mz}{\sum M} \quad (14.2)$$

There are two requirements to be met regarding the c.g. position of the S/C:

- The longitudinal position of the c.g. of the entire S/C must not be higher than 2 [m] from the separation line (see Figure 14.2)
- The lateral position of the c.g. of the entire S/C must not deviate from the longitudinal axis of symmetry by more than 3 [cm]

The first requirement was checked using Equation (14.2) by calculating the centre of mass. It takes place 1.98 [m] from the separation line, which means that the requirement is met. As for the second requirement, as can be seen in the CATIA drawings, the payload is distributed more or less evenly, therefore it is reasonable to assume that the c.g. of the S/C will take place along the vertical symmetry axis.

#### SECOND MOMENT OF AREA

The moment of inertia (second moment of area) around the x-axis (similarly for y and z axis) is as follows:

$$I_{xx} = \int y^2 dA \quad (14.3)$$

The values of the MOI for the inner cylinders and rods of Spílaio and Noor are given in Table 14.2.

#### CROSS-SECTIONAL AREA

The cross-sectional areas in xy-plane of the inner and outer structure of Spílaio and Noor were calculated as follows; Equation (14.4) was used to calculate the cross-sec. area of a cylinder and Equation (14.5) was used to calculate the cross-sec. area of the rod ( $t$  - rod thickness and  $L$  - rod length in xy plane).

$$A_{cylinder} = \pi \cdot (R_{out}^2 - R_{in}^2) \quad (14.4)$$

$$A_{rod} = t_{rod} \cdot L_{rod} \quad (14.5)$$

Parameter	Spílaio		Noor	
	Cylinder	Rod	Cylinder	Rod
Outer radius [m]	0.25	NA	0.25	NA
Thickness [m]	0.001	0.001	0.001	0.001
Height [m]	1.20	0.01	2.80	0.01
Length [m]	NA	0.85	NA	0.85; 0.27
MOI around x-axis [ $m^4$ ]	$4.879 \cdot 10^{-5}$	NA	$4.879 \cdot 10^{-5}$	NA
MOI around y-axis [ $m^4$ ]	$4.879 \cdot 10^{-5}$	NA	$4.879 \cdot 10^{-5}$	NA
MOI around z-axis [ $m^4$ ]	$7.470 \cdot 10^{-5}$	NA	$1.743 \cdot 10^{-4}$	NA
Cross-sec. area [ $m^2$ ]	$1.57 \cdot 10^{-3}$	$8.5 \cdot 10^{-4}$	$1.57 \cdot 10^{-3}$	$8.5 \cdot 10^{-4}$ ; $2.7 \cdot 10^{-4}$
Total cross-sec. area [ $m^2$ ]	$8.4 \cdot 10^{-3}$		$6.04 \cdot 10^{-3}$	
Volume of the skin [ $m^3$ ]	$1.8 \cdot 10^{-3}$	$8.5 \cdot 10^{-6}$	$4.39 \cdot 10^{-3}$	$8.5 \cdot 10^{-6}$ ; $2.7 \cdot 10^{-6}$
Total volume [ $m^3$ ]	$1.9 \cdot 10^{-3}$		$4.43 \cdot 10^{-3}$	
Mass [kg]	<u>3.12</u>		<u>7.095</u>	
Total Mass [kg]	<b>10.21</b>			

Table 14.2: The parameters of the S/C inner load-carrying structure

Property	CFRP	Aluminum 6061 T-6
E-modulus [GPa]	70	68.9
Density [ $kg/m^3$ ]	1600	2700
Ultimate Tensile strength [MPa]	600	310
Ultimate Compressive strength [MPa]	570	310
Thermal expansion coefficient [ $K^{-1}$ ]	$21 \cdot 10^{-6}$	$22 \cdot 10^{-6}$ [64]
Cost per kg [€]	20	10

Table 14.3: Carbon fiber composite material and Aluminum 2024 T-4 mechanical properties

## VOLUME

The outer and inner structures of the complete S/C consists of a total of three different geometries: cylinder, rod and a truncated cone. Thus the volume equations used are briefly presented below.

- **Cylinder**

Spílaio and a part of Noor geometrically represent a hollow cylinder. The outer and inner volumes of these were calculated using Equations (14.6) and (14.7).  $H$  is the height of the corresponding cylinder which can be found in Table 14.2. Subtracting the two volumes, since the cylinders are hollow, gives the volume of the skin in Equation (14.8).

$$V_{out} = \pi \cdot R_{out}^2 \cdot H \quad (14.6)$$

$$V_{in} = \pi \cdot (R_{out} - t)^2 \cdot H \quad (14.7)$$

$$V_{skin} = V_{out} - V_{in} \quad (14.8)$$

- **Rod**

The inner S/C structure includes in total four webs that help to carry the lift-off (and other) loads. The volume of the web was calculated as follows:

$$V_{rod} = A_{rod} \cdot H_{rod} = t_{rod} \cdot L_{rod} \cdot H_{rod} \quad (14.9)$$

- **Truncated cone**

The part of Noor geometrically represents the truncated cone. The outer and inner volumes of which are calculated using Equations (14.10) and (14.11) and the skin volume - using Equation (14.12).

$$V_{out} = \frac{\pi \cdot h}{3} (R_{out}^2 + R_{out} \cdot r_{out} + r_{out}^2) \quad (14.10)$$

$$V_{in} = \frac{\pi \cdot h}{3} ((R_{out} - t)^2 + (R_{out} - t) \cdot (r_{out} - t) + (r_{out} - t)^2) \quad (14.11)$$

$$V_{skin} = V_{out} - V_{in} \quad (14.12)$$

	Mass [kg]	Cost [€]
S/C outer structure	79.68	796.8
S/C inner structure	10.21	204.2
Total structure	<u>89.89</u>	<u>1001</u>

Table 14.4: Total mass and cost of the S/C structure

## MASS

Knowing the volumes of the skin of both S/C parts (Spílaio and Noor), the mass for both was calculated using:

$$m = V_{skin}\rho \quad (14.13)$$

The mass values for all structural components can be found in Tables 14.1 and 14.2.

### 14.1.4. LOADS

The S/C will be subject to a set of different mechanical loads during its lifetime and even before [65]:

- Transportation
- Lift-off loads
- Engine/Motor generated acoustic loads
- Engine/Motor generated structure-borne vibration loads
- Wind and turbulence, aerodynamic sources
- Manoeuvring loads
- On board equipment operation

Since most of these are negligible with respect to the others, only the ones that drive the design will be evaluated one more level down.

#### LAUNCH LOADS

The stage at which the loads acting on the S/C are the most severe is the launch stage. The loads during the launch are the main criteria that drive the strength requirements for the design. During the lift-off, following loads/vibrations act on the structure:

- **Steady state accelerations**

The VEGA launcher has following acceleration loads [2]:

- The peak longitudinal acceleration does not exceed 5.5 g for a payload above 300 [kg]
- The highest lateral static acceleration is less than 0.9 g at maximum dynamic pressure and takes into account the effect of wind and gust encountered in this phase.

- **Low frequency vibrations**

The envelope of the sinusoidal vibration levels does not exceed the values given in Table 14.5.

Direction	Frequency band [Hz]		Sine Amplitude [g]	
Longitudinal	5-45	45-100	≤ 0.8	≤ 1.0
Lateral	5-25	25-100	≤ 0.8	≤ 0.5

Table 14.5: Sinusoidal vibration levels in the S/C

- **Broad band vibrations**

- Random vibrations

As stated in the VEGA manual [2], for payload above 300 [kg] (which is the case) the broadband vibrations are covered by acoustics.

- Acoustic vibrations in flight

Engine operation together with an unsteady aerodynamic phenomena during atmospheric flight introduce the acoustic pressure fluctuations. The envelope spectrum of the noise during flight can be found in the manual of the VEGA [2].

- **Load calculations**

Due to previously mentioned longitudinal maximum acceleration of 5.5g, the S/C inner load-carrying structure needs to be sized accordingly to make sure to sustain the applied compression loads. Figure 14.1 shows

the final dimensions of the inner structure. The following calculations make use of the values summarized in Tables 14.1 and 14.2.

– *Compressive stress*

First of all, due to the 5.5g gravitational acceleration there is a compressive force acting on the S/C during the launch. The applied force equals:

$$F_{app} = 5.5mg \cdot F.S. \quad (14.14)$$

Where F.S. is the safety factor and equals 1.5. Spílaio and Noor's inner structures were both sized separately and using Equation (14.14) the respective total masses that were used are summarized in the Table 14.6.

	Mass [kg]
Spílaio	1231
Noor	1049
Total spacecraft	2280

Table 14.6: The mass of the Noor and the Spílaio at lift-off

The applied compression force causes compressive stresses in the structure, which were calculated as shown in Equation (14.15) by substituting the values and  $A$  being the cross-sectional area. The compressive stresses acting on Spílaio and Noor are, respectively:

$$\sigma = \frac{F_{app}}{A} \quad (14.15)$$

$$\sigma_S = 20.1 \quad [kPa] \quad (14.16)$$

$$\sigma_N = 17.1 \quad [kPa] \quad (14.17)$$

– *Critical buckling load*

Next to the compressive stresses, the critical buckling load of the beam (hollow cylinder) that the structure can withstand has to be checked due to compression. Following equation was used to determine the critical buckling load:

$$P_{cr} = \frac{n^2 \pi^2 EI}{L^2} \quad (14.18)$$

$I$  - area moment of inertia,  $L$  - length of the beam (height of the cylinder in this case) and  $n$  - a scalar depending on whether the structure is simply supported or clamped.  $n = 1$  for the simply supported and  $n = 2$  for clamped structure. To ensure a safe lift-off the simply supported structure is assumed. After substituting the values into the according equation, the critical buckling loads for the inner cylinder of Spílaio and Noor become:

$$P_{crS} = 23.4 \quad [MN] \quad (14.19)$$

$$P_{crN} = 4.3 \quad [MN] \quad (14.20)$$

– *Vibrational loads*

One of the requirements is that for structural purposes the natural frequency of the S/C in the lateral direction must be equal at least 15 [Hz] which is the worst case scenario, and 20-45 [Hz] in the longitudinal direction.

Lateral direction

The next equations are used to find the expression of the deviation from the symmetry axis. The double derivative of the displacement  $\ddot{x}$  is the acceleration, which in the worst case scenario equals 5.5g. The maximum deviation from the symmetry can thus be calculated.

$$x = A \sin(2\pi f t) \quad (14.21)$$

$$\dot{x} = 2A\pi f \cos(2\pi f t) \quad (14.22)$$

$$\ddot{x} = -A(2\pi f)^2 \sin(2\pi f t) \quad (14.23)$$

$$A_{max} = \frac{\ddot{x}}{(2\pi f)^2} = \frac{5.5 \cdot 9.81}{(2\pi \cdot 15)^2} = 6.1 \quad [mm] \quad (14.24)$$

From the frequency requirement, the stiffness requirement for each inner cylinder can be drawn as follows, assuming that it is acceptable at this stage of the design to model the S/C as a single degree of freedom undamped mass-spring system. The stiffness of the structure was calculated using the Equation (14.26).  $L$  being the length of the beam (height of the cylinder in this case):

$$k_{req} = \omega^2 \cdot m \cdot F.S. = (2\pi f)^2 \cdot m \cdot F.S. \quad (14.25)$$

$$k = \frac{3EI}{L^3} \quad (14.26)$$

#### Longitudinal direction

To satisfy the requirement of having a natural frequency in the longitudinal direction of at least 20 [Hz], the following calculations were made. Again, modeling the S/C as an undamped mass-spring system:

$$A_{max} = \frac{\ddot{x}}{(2\pi f)^2} = \frac{0.9 \cdot 9.81}{(2\pi \cdot 20)^2} = 0.56 \quad [mm] \quad (14.27)$$

$$k_{req} = \omega^2 \cdot m \cdot F.S. = (2\pi f)^2 \cdot m \cdot F.S. \quad (14.28)$$

The actual stiffness of the structure in the longitudinal direction was calculated as follows:

$$k = \frac{EA}{L} \quad (14.29)$$

#### – Buckling with a cut-out

One of the requirements is to have the centre of gravity as close to the vertical line of symmetry (z-axis) as possible. The heaviest part of the scientific payload is the rover (100 [kg]). Thus, the idea is to put the rover as close as possible to the centre of Noor. To do that, while still making sure that the inner cylinder at the centre of Noor can sustain the lift-off loads, the cut was made inside the cylinder. It needs to be checked for both the compressive stresses and buckling loads during the launch. It was cut in such a way that the cross-sectional area is halved. Thus the compressive stresses acting on the structure using Equation (14.15) become:

$$\sigma_N = 34.2 \quad [kPa] \quad (14.30)$$

Change in the cross-sectional area changes the moment of inertia of the cylinder, thus it needs to be checked for buckling at the cut-out. The critical buckling load of the structure becomes:

$$P_{cr} = \frac{n^2 \pi^2 EI_{cut}}{L^2} = 2.15 \quad [MN] \quad (14.31)$$

All above calculated applied load values are much lower than the ultimate mechanical properties of CFRP 70 in Table 14.3. This means that the design will withstand all previously mentioned loads and stresses.

#### THERMAL LOADS

The outer structure of the S/C during different phases is subjected to certain temperature variations. This temp. variation introduces thermal stresses inside the structure which have to be withstood by the outer skin of the S/C. Knowing the maximum temperature variation and using the properties of the corresponding materials from Table 14.3, the thermal stress was calculated using following equation:

$$\sigma_{th} = \alpha E \Delta T \cdot F.S. \quad (14.32)$$

$\Delta T$  - the temperature variation,  $E$  - Young's modulus and  $\alpha$  - thermal expansion coefficient of the material. The maximum worst case scenario temperature variation occurs during the transfer phase, when the temperature changes from 210 to 320 K. This means that the maximum  $\Delta T = 110$  K. Filling in the numbers into the thermal stress equation and assuming F.S. to be 1.5:

$$\sigma_{th} = 250 \quad [MPa] \quad (14.33)$$

Comparing this result to the ultimate mechanical properties of Aluminum 6061 T-6 in Table 14.3, the structure will be able to withstand the thermal stresses.

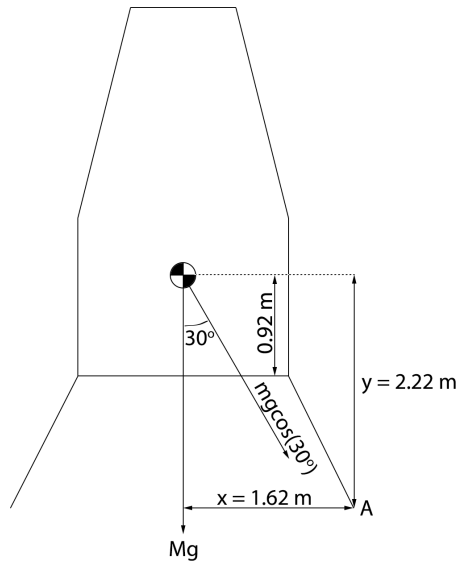


Figure 14.3: The forces acting on the Noor as rover begins to exit

### ROVER DEPLOYMENT LOADS

Once Noor has landed, the first step of performing the scientific mission is to deploy the rover. The rover gets deployed by cable which is attached to Noor at its centre of gravity, as can be seen in Figure 14.3.

Since it weighs a significant amount of kilograms, there is a possibility that as the rover gets out of Noor, the weight of the rover will make Noor tip over. To avoid this happening, the following calculations are made.

Noor will land on its four legs (for more details see Section 14.3). In the worst case scenario, the weight of the rover will exert a force (with respect to the legs) in the direction as shown in Figure 14.3. Note that depending on whether Noor will or not tip over as the rover exits Noor, the location at which the cable will be attached to the rover will be decided upon. As usual, the worst case scenario was taken into account: the cable is attached to Noor at the location of the c.g.

Position A where one of Noor's legs touches down is taken as a reference point. The sum of the moments about that point counter clock-wise positive (as shown) must be larger than zero. The force applied on Noor and the moment about point A can be calculated as follows:

$$F = m_{rover} \cdot g \cdot \cos(30^\circ) \quad (14.34)$$

$$\sum M_A = m_{Noor} \cdot g \cdot x + F \cdot \cos 30^\circ \cdot x_1 - F \cdot \sin 30^\circ \cdot y > 0 \quad (14.35)$$

$$m_{Noor} \cdot g \cdot x > m_{rover} \cdot g (\cos 30^\circ \cdot y \cdot \sin 30^\circ - x_1 \cos^2 30^\circ) \quad (14.36)$$

$$m_{Noor} \cdot x > m_{rover} \left( \frac{\sqrt{3}}{4} y - \frac{3}{4} x_1 \right) \quad (14.37)$$

The mass of Noor after touch-down excluding the rover is roughly 310 [kg], the horizontal component of the length of the leg is  $x$  and equals 1.62 [m], the horizontal distance between the point A and the point where the cable is attached to Noor is  $x_1$  (which equals  $x$  in case the cable is connected to Noor at the c.g. location) and equals 1.62 [m]. The vertical distance  $y$  between the c.g. and the point A equals 2.22 [m]. See for all dimensions.

Substituting all values into the equation, the following is true. Therefore, it can be concluded that deploying the rover once Noor has successfully landed is safe.

$$544.9 > 0 \quad (14.38)$$

#### 14.1.5. VERIFICATION AND VALIDATION PROCEDURES

All critical load and stress calculations were performed by making use of the Equations 12.1 - 12.34. The program *MS Excel* was used for that, since the equations are quite straight forward, there was no need for a more advanced program.

To validate whether the results produced by DSA match the real life data, there is only way one - to build the prototype and test it.

## 14.2. SOLAR PANELS

In this section the solar panel configuration is determined and checked for failure during lunar orbit insertion where a retrograde burn will be applied, Section 2.3. A solar array wing has several panels of equal length and thickness that can be folded onto one another. One wing has to have an area of  $23 \text{ [m}^2\text{]}$ . To use as much as possible inside the VEGA the panels have decreasing width towards a wing tip. The folded array can then fit within the cylindrical side of the VEGA payload fairing. In Figure 14.4 a schematic representation is shown. The shorter a panel's length, the more panels are present and the more efficiently the space is used. However, having a lot of panels of short length is more complex and takes a lot of space in the radial direction of the S/C cylinder (since the panel thickness remains constant). Considering these facts a compromise has been made and a solar array wing with 15 panels with each a length of  $1.2 \text{ [m]}$  has been chosen. The choice was made by creating a Matlab script describing the problem above.

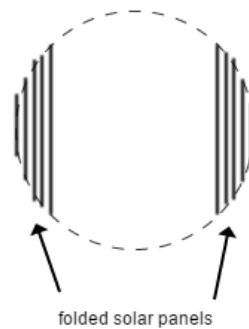


Figure 14.4: Schematic depiction of the solar panel in folded configuration.

The S/C will spiral out from LEO towards the lunar sphere of influence (LSOI) using electric propulsion. When it enters the LSOI an impulsive retrograde burn with chemical propulsion will make sure the S/C remains captured by the Moon. During this impulsive burn the solar panels and their connecting hinge will undergo a load, Figure 14.5 depicts the situation, the solar array wing is drawn as a single panel for simplicity and a symmetric configuration is assumed. The thrust ( $T$ ) causes a backward acceleration on the S/C, the solar panels keep moving in the same direction, so relative to the body the panels experience a forward acceleration and cause a moment. Assuming the panels do not bend, this moment can be calculated. This is a conservative approach because bending of the panels will reduce the relative acceleration since energy is used to deform the panels. In discussion with the client, it came forth that based on experience the hinge of the panels fails before the panels fail. This hinge can take a moment of  $500 \text{ [Nm]}$ , if the root moment exceeds this, several steps can be taken: the hinge can be reinforced, the configuration of the panels can be changed to be less wide or the insertion thrust can be lowered (which would mean insertion would take longer).

A Matlab script was made to calculate the root hinge moment and test for possible failure. The script divides a wing into the chosen number of panels. Thrust is multiplied with a dynamic amplification factor, also based on discussion with the client. The configuration passed the test.

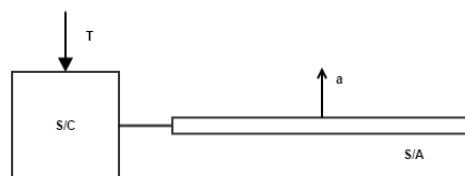


Figure 14.5: Depiction of loads on panels and hinge during lunar orbit insertion

## 14.3. LANDING STRUTS

In Section 11.7 hazards that can be encountered at the Shackleton Rim (SR1) are discussed. In the current section the implications of the hazards on the Noor's landing struts are determined. The baseline configuration uses four

landing struts. During the final phase of landing the LiDAR can offer a resolution of 0.1 [m] [11]. Next to small craters, hazards that should be avoided are assumed to be boulders that are more than 0.5 [m] in height and slopes of more than 15° [66]. The struts should provide enough clearance, so at least 0.5 [m]. An additional 0.9 [m] is taken for extra clearance because the length of the thrusters that stick out from the bottom of the Noor is 0.8 [m] and the LiDAR resolution is 0.1 [m]. If Noor would land on a slope of 15°, the struts will have to prevent Noor from tipping over. A sufficient angle between the Noor's vertical axis and the strut's longitudinal axis is needed for this. This angle is  $a$  in Figure 14.6. The height of the center of gravity (CoG) of the Noor is assumed to be at half the overall Noor's height, which is 1.4 [m] (this is a conservative estimate, the actual CoG of the Noor is lower because most heavy components are at the bottom). where the situation has been depicted. In the limiting case the line of action of the gravity force goes through the rotation point  $S$  and by using basic geometry  $a$  can be calculated. For the limiting case a negative angle was found, meaning that lander is wide enough and the CoG is low enough not to tip over over with vertical legs on a 15° slope. But it is possible for Noor to bounce off of the surface and rotate over  $S$  making it tip over. As a safety margin the slope angle that Noor has to be able to cope with was set to 30°, resulting in  $a = 20.3^\circ$ . Below a derivation of this angle is shown,  $r_L$  is the radius of Noor body cylinder, the other variables can be found in Figure 14.6. The length of a strut can then be calculated with Equation (14.42).

$$B = H_{cg} \tan(30) \quad (14.39)$$

$$C = B - r_L \quad (14.40)$$

$$a = \arctan\left(\frac{C}{h}\right) \quad (14.41)$$

$$L_{strut} = \frac{h}{\cos(a)} = \frac{1.3}{\cos(19.4)} = 1.38 \text{ [m]} \quad (14.42)$$

In Section 6.2.2 a free-fall height has been determined to prevent the thruster plume from blowing up too much regolith, this height ( $y$ ) is 3 [m]. At this height Noor is assumed not to be moving. Its potential energy is completely converted to kinetic energy just before Noor touches down. At touchdown the lunar surface exerts a force on the landing struts which performs work to decrease the kinetic energy to zero. Rearranging Equation (14.43) gives an expression for this force, here  $d$  is the distance over which Noor is stopped. To decrease the load on the struts, an energy absorber will be used in the struts which increases  $d$ . Some kind of pneumatic or hydraulic system could be used for this. However, this might give problems with leakage and pressure containment since temperatures vary greatly in space. A good and simple alternative is an aluminum honeycomb column that is installed into the hollow legs. Aluminum honeycomb can be greatly compressed, some by 70% of original length length<sup>3</sup>, the crushing is also very predictable and can be guided by surrounding material. To prevent one strut of being much shorter than the other ones (in case of a landing scenario where one strut hits the surface first),  $d$  is limited to be 0.3 [m]. The mass of Noor ( $m$ ) in Equation (14.43) can be found in Section 6.2.2 and is 455 [kg] just before touchdown, and  $g = 1.62 \text{ [m/s}^2\text{]}$ .

This leads to  $F = 7371 \text{ [N]}$ , the component of this force along the strut axis is:

$$E_{pot} = E_{kin} = mgy = W = Fd \quad (14.43)$$

$$F_{compr} = F \cos(a) = 7371 \cdot \cos(20.3) = 6915 \text{ [N]} \quad (14.44)$$

It is possible that just one strut hits the surface first, so a single strut must be able to take the load. The strut's length is much longer than its other dimensions, therefore it will fail due to buckling first. If it can take the compressive landing load without buckling it will also be able to withstand other loads.

A strut is assumed to be simply supported. This means that the buckling load can be found with Equation (14.18).

Because it is unknown at which direction a landing strut will hit the lunar surface, it is unknown around which axis the strut will bend or buckle. For this reason a circular cross section of the landing struts is chosen. The moment of inertia of a circular cross-section is found with Equation (14.45)

$$I = \frac{\pi}{4} (r_o^4 - r_i^4) \quad (14.45)$$

Where  $r_o$  is the outer radius and  $r_i = r_o - t$  is the inner radius, where  $t$  is the thickness. A minimum thickness of 3 [mm] was taken as smaller thicknesses are difficult to manufacture and assemble. The material chosen is a titanium alloy often used in space applications, Ti-6Al-4V. This material has a Young's Modulus of 115 [GPa] and a density of

<sup>3</sup>[http://www.plascore.com/energy\\_absorbers\\_crushlite.php](http://www.plascore.com/energy_absorbers_crushlite.php)

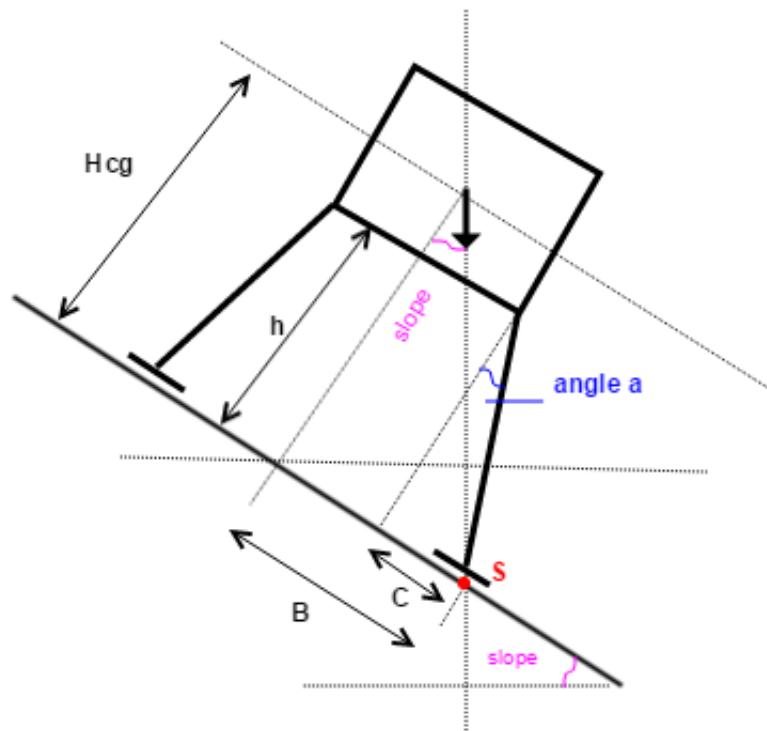


Figure 14.6: Depiction of Noor on a slope, the thick arrow is the gravity force. This situation is the limiting case where the gravity force line of action goes through the rotational point.

$4420 \text{ [kg/m}^3\text{]}$ . Using Matlab, the lightest cross-section per unit length that can withstand the buckling load has been found by varying  $r_o$  and  $r_i$ . For this cross-section  $r_o = 135 \text{ [mm]}$  and  $t = 3 \text{ [mm]}$ . Four struts then have a mass of  $4.6 \text{ [kg]}$ . At the base of the struts Noor will have a widened surface that is meant to prevent the strut from penetrating the soil. One leg might sink into the soil deeper relative to others, which could unbalance Noor. The exact dimensions of these surfaces is not determined, this should be done in the future by doing tests with a material that is comparable to the lunar soil.

## PERFORMANCE ANALYSIS

In this chapter the performance of the mission concept with respect to the system requirements is analyzed. The following sections provide an overview of the performance parameters (Section 15.1), compliance matrix and feasibility analysis (Section 15.2), and the sensitivity analysis (Section 15.3).

### 15.1. PERFORMANCE PARAMETERS

Key performance parameters for the mission are transfer time, mission lifetime, mass and power budget, mission cost, baseline and number of antennas. These values give an indication of the overall performance of the mission concept. A summary of these values is given in Table 15.1.

Performance Parameter	Required Value	Actual Value
Transfer time [years]	1	1
Mission lifetime [years]	5	5+
Mission cost [M€]	max 500	480
Baseline [km]	10-100	10
Number of antennas	max	21
Total Mass budget in LEO [kg]	2280	2280
Total mass budget lunar parking orbit [kg]	1496	1433.5
Dry mass on lunar surface [kg]	455	
Transfer Power Normal [W]	9430	9430
Transfer Power Eclipse [W]	550	550
Landing Phase A Power [W]	242	220
Landing Phase B Power [W]	55	50
Deployment Phase Power [W]	121	110
Operations Phase Power [W]	135.1	148.6

Table 15.1: Performance parameters

### 15.2. COMPLIANCE MATRIX & FEASIBILITY ANALYSIS

The compliance matrix showing which requirements have been met is presented in Figure 15.1. Some requirements have been altered with respect to the baseline report, while some are no longer relevant. These are marked with N/A.

One requirement that has not been met is SYS-QUA-6.2. It states that no single point of failures should be present in the design. However, some single point of failures are allowed if the parts in question have high reliability. For example, only one Marmen clamp is used for decoupling of the lander and transfer orbiter. The high-gain parabolic antenna of the telecommunication system is also a single point of failure. It has a diameter of 0.7 [m], weighs 3 [kg] and requires some actuators for pointing. Because of volume constraints and the fact that it is a very reliable flight proven component it was decided not to take a spare antenna. Another single point of failure is the tether of the rover. It has, however, been designed for the maximum loads it will encounter, uses tough outer material to protect it and because the tether is on the rover itself it is not dragged down into the crater. Including a second cable for redundancy would mean an increase in mass of 63.6 [kg], which would increase the loads the rover will endure and so the cables might need to be strengthened accordingly. Because of the large increase, it was decided not to take

Functional requirements	Check?	Environmental requirements	Quality factors requirements	Support requirements	Sustainability requirements	Physical requirements	Verification requirements
SYS-FUNC-1.1 The S/C shall be able to get to a 100 [km] polar lunar orbit within 1 year using a spiral transfer orbit.	Y	SYS-PHY-4.4 The payload shall have a lateral eigenfrequency of at least 15 [Hz].	SYS-ENV-5.1 Maximum orbit inclinations per altitude shall comply with the capabilities of the VEGA launcher, as described in the VEGA user manual.	SYS-ENV-5.2 The S/C shall be able to cope with a 0.9 [g] lateral static acceleration.	SYS-ENV-5.3 The S/C shall be able to cope with a 5.5 [g] longitudinal acceleration.	SYS-ENV-5.4 The payload shall be able to cope with a quasi-static load of 5.8-Mpayload/1000 +- 0.9 [g].	SYS-VER-9.1 All requirements shall be verified at subsystem, module and system level.
SYS-FUNC-1.2 The S/C shall be launched using the VEGA launcher.	Y	SYS-ENV-5.5 The S/C structure shall be able to withstand frequencies in TBD frequency range without being damaged.	SYS-ENV-5.6 The lunar lander structure shall be able to withstand the impact force of a 3 [m] drop	SYS-ENV-5.7 The S/C shall be able to withstand the conditions of space for the duration of the six year lifetime and Earth-Moon transfer.	SYS-ENV-5.8 Safety factors used shall comply with the safety factors defined by the VEGA user manual.	SYS-ENV-5.9 The S/C shall perform its mission with sufficient redundancy to ensure that no single point of failures are present.	SYS-VER-9.2 Subsystem requirements shall be SMART and so easily verifiable.
SYS-FUNC-1.3 The S/C propulsion system shall be preferably based on electric propulsion. Hybrid electric-chemical propulsion systems shall also be considered.	Y	SYS-ENV-6.1 The overall reliability of the S/C shall be no less than TBD.	SYS-ENV-6.2 The overall project risk shall conform to TBD acceptance criteria.	SYS-ENV-6.3 The S/C shall be able to cope with a 0.9 [g] lateral static acceleration.	SYS-ENV-6.4 The launch site shall be the Guiana Space Centre (CSG). The S/C shall be supported by a ground station for its six year lifetime.	SYS-ENV-6.5 The lunar lander shall be able to relay data for its six year lifetime with a baud rate of at least 100 [Smbit/SS].	SYS-VER-9.3 Subsystem requirements shall be SMART and so easily verifiable.
SYS-FUNC-1.4 A landing module shall be able to mechanically disconnect from the S/C in a lunar orbit.	Y	SYS-ENV-6.6 The S/C shall be able to cope with a 5.5 [g] longitudinal acceleration.	SYS-ENV-6.7 The S/C shall be able to cope with a 5.5 [g] longitudinal acceleration.	SYS-ENV-6.8 The S/C shall be able to cope with a 5.5 [g] longitudinal acceleration.	SYS-ENV-6.9 The S/C shall be able to cope with a 5.5 [g] longitudinal acceleration.	SYS-ENV-6.10 The S/C shall be able to cope with a 5.5 [g] longitudinal acceleration.	SYS-VER-9.4 Subsystem requirements shall be SMART and so easily verifiable.
SYS-FUNC-1.5 The landing module shall be placed on the lunar surface by means of a soft and precise landing.	Y	SYS-ENV-6.11 The S/C shall be able to cope with a 5.5 [g] longitudinal acceleration.	SYS-ENV-6.12 The S/C shall be able to cope with a 5.5 [g] longitudinal acceleration.	SYS-ENV-6.13 The S/C shall be able to cope with a 5.5 [g] longitudinal acceleration.	SYS-ENV-6.14 The S/C shall be able to cope with a 5.5 [g] longitudinal acceleration.	SYS-ENV-6.15 The S/C shall be able to cope with a 5.5 [g] longitudinal acceleration.	SYS-VER-9.5 Subsystem requirements shall be SMART and so easily verifiable.
SYS-FUNC-1.6 The landing module shall have the capability to deploy a LOFAR antenna system with a baseline of at least 10 [km].	Y	SYS-ENV-6.16 The S/C shall be able to cope with a 5.5 [g] longitudinal acceleration.	SYS-ENV-6.17 The S/C shall be able to cope with a 5.5 [g] longitudinal acceleration.	SYS-ENV-6.18 The S/C shall be able to cope with a 5.5 [g] longitudinal acceleration.	SYS-ENV-6.19 The S/C shall be able to cope with a 5.5 [g] longitudinal acceleration.	SYS-ENV-6.20 The S/C shall be able to cope with a 5.5 [g] longitudinal acceleration.	SYS-VER-9.6 Subsystem requirements shall be SMART and so easily verifiable.
SYS-FUNC-1.7 The landing module shall contain a lunar station that has the power and capability of transferring the collected data to the lunar orbiter with a data rate of 64 [Mbit/s]	N/A	SYS-ENV-6.21 The S/C shall be able to cope with a 5.5 [g] longitudinal acceleration.	SYS-ENV-6.22 The S/C shall be able to cope with a 5.5 [g] longitudinal acceleration.	SYS-ENV-6.23 The S/C shall be able to cope with a 5.5 [g] longitudinal acceleration.	SYS-ENV-6.24 The S/C shall be able to cope with a 5.5 [g] longitudinal acceleration.	SYS-ENV-6.25 The S/C shall be able to cope with a 5.5 [g] longitudinal acceleration.	SYS-VER-9.7 Subsystem requirements shall be SMART and so easily verifiable.
SYS-FUNC-1.8 Mission control shall receive data from the moon LOFAR system via a TBD relay system.	Y	SYS-ENV-6.26 The S/C shall be able to cope with a 5.5 [g] longitudinal acceleration.	SYS-ENV-6.27 The S/C shall be able to cope with a 5.5 [g] longitudinal acceleration.	SYS-ENV-6.28 The S/C shall be able to cope with a 5.5 [g] longitudinal acceleration.	SYS-ENV-6.29 The S/C shall be able to cope with a 5.5 [g] longitudinal acceleration.	SYS-ENV-6.30 The S/C shall be able to cope with a 5.5 [g] longitudinal acceleration.	SYS-VER-9.8 Subsystem requirements shall be SMART and so easily verifiable.
SYS-FUNC-1.9 The lunar station shall be equipped with 200 [MHz] processing power to do preliminary data processing.	Y	SYS-ENV-6.31 The S/C shall be able to cope with a 5.5 [g] longitudinal acceleration.	SYS-ENV-6.32 The S/C shall be able to cope with a 5.5 [g] longitudinal acceleration.	SYS-ENV-6.33 The S/C shall be able to cope with a 5.5 [g] longitudinal acceleration.	SYS-ENV-6.34 The S/C shall be able to cope with a 5.5 [g] longitudinal acceleration.	SYS-ENV-6.35 The S/C shall be able to cope with a 5.5 [g] longitudinal acceleration.	SYS-VER-9.9 Subsystem requirements shall be SMART and so easily verifiable.
SYS-FUNC-1.10 The lunar station shall be able to generate and store power to perform its functions during eclipse times.	Y	SYS-ENV-6.36 The S/C shall be able to cope with a 5.5 [g] longitudinal acceleration.	SYS-ENV-6.37 The S/C shall be able to cope with a 5.5 [g] longitudinal acceleration.	SYS-ENV-6.38 The S/C shall be able to cope with a 5.5 [g] longitudinal acceleration.	SYS-ENV-6.39 The S/C shall be able to cope with a 5.5 [g] longitudinal acceleration.	SYS-ENV-6.40 The S/C shall be able to cope with a 5.5 [g] longitudinal acceleration.	SYS-VER-9.10 Subsystem requirements shall be SMART and so easily verifiable.
SYS-FUNC-1.11 The landing module shall be equipped for a mission duration of at least 6 years.	Y	SYS-ENV-6.41 The S/C shall be able to cope with a 5.5 [g] longitudinal acceleration.	SYS-ENV-6.42 The S/C shall be able to cope with a 5.5 [g] longitudinal acceleration.	SYS-ENV-6.43 The S/C shall be able to cope with a 5.5 [g] longitudinal acceleration.	SYS-ENV-6.44 The S/C shall be able to cope with a 5.5 [g] longitudinal acceleration.	SYS-ENV-6.45 The S/C shall be able to cope with a 5.5 [g] longitudinal acceleration.	SYS-VER-9.11 Subsystem requirements shall be SMART and so easily verifiable.
SYS-FUNC-1.12 The S/C shall be able to determine its position during transfer and lunar orbit within 1 degree of pointing accuracy.	Y	SYS-ENV-6.46 The S/C shall be able to cope with a 5.5 [g] longitudinal acceleration.	SYS-ENV-6.47 The S/C shall be able to cope with a 5.5 [g] longitudinal acceleration.	SYS-ENV-6.48 The S/C shall be able to cope with a 5.5 [g] longitudinal acceleration.	SYS-ENV-6.49 The S/C shall be able to cope with a 5.5 [g] longitudinal acceleration.	SYS-ENV-6.50 The S/C shall be able to cope with a 5.5 [g] longitudinal acceleration.	SYS-VER-9.12 Subsystem requirements shall be SMART and so easily verifiable.
SYS-CONF-2.1 The S/C shall accommodate the lunar landing module and a lunar orbiter.	Y	SYS-ENV-6.51 The S/C shall be able to cope with a 5.5 [g] longitudinal acceleration.	SYS-ENV-6.52 The S/C shall be able to cope with a 5.5 [g] longitudinal acceleration.	SYS-ENV-6.53 The S/C shall be able to cope with a 5.5 [g] longitudinal acceleration.	SYS-ENV-6.54 The S/C shall be able to cope with a 5.5 [g] longitudinal acceleration.	SYS-ENV-6.55 The S/C shall be able to cope with a 5.5 [g] longitudinal acceleration.	SYS-VER-9.13 Subsystem requirements shall be SMART and so easily verifiable.
SYS-CONF-2.2 The landing module shall be able to carry a minimum of 21 antennas.	Y	SYS-ENV-6.56 The S/C shall be able to cope with a 5.5 [g] longitudinal acceleration.	SYS-ENV-6.57 The S/C shall be able to cope with a 5.5 [g] longitudinal acceleration.	SYS-ENV-6.58 The S/C shall be able to cope with a 5.5 [g] longitudinal acceleration.	SYS-ENV-6.59 The S/C shall be able to cope with a 5.5 [g] longitudinal acceleration.	SYS-ENV-6.60 The S/C shall be able to cope with a 5.5 [g] longitudinal acceleration.	SYS-VER-9.14 Subsystem requirements shall be SMART and so easily verifiable.
SYS-CONF-2.3 The S/C configuration shall allow bringing 30 [kg] of secondary science instruments to the Moon.	Y	SYS-ENV-6.61 The S/C shall be able to cope with a 5.5 [g] longitudinal acceleration.	SYS-ENV-6.62 The S/C shall be able to cope with a 5.5 [g] longitudinal acceleration.	SYS-ENV-6.63 The S/C shall be able to cope with a 5.5 [g] longitudinal acceleration.	SYS-ENV-6.64 The S/C shall be able to cope with a 5.5 [g] longitudinal acceleration.	SYS-ENV-6.65 The S/C shall be able to cope with a 5.5 [g] longitudinal acceleration.	SYS-VER-9.15 Subsystem requirements shall be SMART and so easily verifiable.
SYS-INT-3.1 The S/C shall be attached to the VEGA launcher in a manner that does not damage it and facilitates its separation from the launcher.	Y	SYS-ENV-6.66 The S/C shall be able to cope with a 5.5 [g] longitudinal acceleration.	SYS-ENV-6.67 The S/C shall be able to cope with a 5.5 [g] longitudinal acceleration.	SYS-ENV-6.68 The S/C shall be able to cope with a 5.5 [g] longitudinal acceleration.	SYS-ENV-6.69 The S/C shall be able to cope with a 5.5 [g] longitudinal acceleration.	SYS-ENV-6.70 The S/C shall be able to cope with a 5.5 [g] longitudinal acceleration.	SYS-VER-9.16 Subsystem requirements shall be SMART and so easily verifiable.
SYS-INT-3.2 The S/C shall be in contact with ground control for the duration of the mission except for eclipse periods.	Y	SYS-ENV-6.71 The S/C shall be able to cope with a 5.5 [g] longitudinal acceleration.	SYS-ENV-6.72 The S/C shall be able to cope with a 5.5 [g] longitudinal acceleration.	SYS-ENV-6.73 The S/C shall be able to cope with a 5.5 [g] longitudinal acceleration.	SYS-ENV-6.74 The S/C shall be able to cope with a 5.5 [g] longitudinal acceleration.	SYS-ENV-6.75 The S/C shall be able to cope with a 5.5 [g] longitudinal acceleration.	SYS-VER-9.17 Subsystem requirements shall be SMART and so easily verifiable.
SYS-PHY-4.1 The maximum payload (depending on the orbit type) shall not exceed the mass limit of 2280 [kg]	N	SYS-ENV-6.76 The S/C shall be able to cope with a 5.5 [g] longitudinal acceleration.	SYS-ENV-6.77 The S/C shall be able to cope with a 5.5 [g] longitudinal acceleration.	SYS-ENV-6.78 The S/C shall be able to cope with a 5.5 [g] longitudinal acceleration.	SYS-ENV-6.79 The S/C shall be able to cope with a 5.5 [g] longitudinal acceleration.	SYS-ENV-6.80 The S/C shall be able to cope with a 5.5 [g] longitudinal acceleration.	SYS-VER-9.18 Subsystem requirements shall be SMART and so easily verifiable.
SYS-PHY-4.2 The CoG height of the payload shall be less than 2 [Sm] above the separation plane.	Y	SYS-ENV-6.81 The S/C shall be able to cope with a 5.5 [g] longitudinal acceleration.	SYS-ENV-6.82 The S/C shall be able to cope with a 5.5 [g] longitudinal acceleration.	SYS-ENV-6.83 The S/C shall be able to cope with a 5.5 [g] longitudinal acceleration.	SYS-ENV-6.84 The S/C shall be able to cope with a 5.5 [g] longitudinal acceleration.	SYS-ENV-6.85 The S/C shall be able to cope with a 5.5 [g] longitudinal acceleration.	SYS-VER-9.19 Subsystem requirements shall be SMART and so easily verifiable.
SYS-PHY-4.3 The dimensions of the launcher payload shall comply with the available space in the VEGA launcher as described in the VEGA user manual.	Y	SYS-ENV-6.86 The S/C shall be able to cope with a 5.5 [g] longitudinal acceleration.	SYS-ENV-6.87 The S/C shall be able to cope with a 5.5 [g] longitudinal acceleration.	SYS-ENV-6.88 The S/C shall be able to cope with a 5.5 [g] longitudinal acceleration.	SYS-ENV-6.89 The S/C shall be able to cope with a 5.5 [g] longitudinal acceleration.	SYS-ENV-6.90 The S/C shall be able to cope with a 5.5 [g] longitudinal acceleration.	SYS-VER-9.20 Subsystem requirements shall be SMART and so easily verifiable.

Figure 15.1: System requirements compliance matrix Yes=Y, No=N, not relevant any more=N/A

a second cable. It is however recommended to test the current cable design on Earth extensively, to assure its ruggedness and tensile strength.

The second requirement that has not been met is SYS-PHY-4.1. However, this is with respect to VEGA as launcher, whereas by the time of launch VEGA C will be available, for which this value (2280 [kg]) increases to 2622 [kg]. Furthermore, it is expected that another design iteration will reduce the current mass, as some systems, like the structure of the satellite, have been overdesigned, and mass contingencies are used.

### 15.3. SENSITIVITY ANALYSIS

In this section the influence of key mission parameters on the feasibility of the mission is investigated. These parameters are the transfer time (1 year), the baseline of the array (10 [km]), the number of antennas (21) and the location of the radar array on the Moon (In a crater on the South Pole). An analysis of the effect in a change of these parameters and an indication of values for which feasibility is questionable are presented.

#### 15.3.1. SENSITIVITY TOWARDS TRANSFER TIME

The top-level requirement regarding transfer time dictates a maximum transfer time of 1 year. During the transfer time the solar panels are exposed to ionizing radiation in the Van Allen belts, which degrades the performance of the solar panels. However, an increased transfer time greatly reduces the power required of the solar panels. A two year transfer time would result in a total degradation of the solar panels of 30%, but only half the power is required. The solar array size is consequently reduced from 46 [ $m^2$ ] to 35 [ $m^2$ ]. This means an approximate mass reduction of 75 [kg]. However, the exposure to ionizing radiation can damage more systems besides the solar panels. The consequences of this need to be established before the transfer time is increased to save mass.

#### 15.3.2. SENSITIVITY TOWARDS ARRAY BASELINE

A change in the baseline of the radar array has an influence on the cable mass, power loss in the cables, the maximum tension, the power required of the rover, the time to deploy the array and the resolution of the radar array. The relations between changes in baseline and the respective parameters are given in Table 15.2. The power required for the rover depends on the mass of the rover plus cables. Cable mass increases linearly with distance, but also the mass of the rover and power loss in the cables have an influence on the power required, so the relation is almost linear.

Parameter	Relation with baseline
Cable mass	linear
Cable tension	linear
Power loss	linear
Rover power required	almost linear
Time to deploy the array	linear
Resolution of radar array	linear

Table 15.2: Relation of key parameters to changes in baseline

The baseline cannot be increased indefinitely. The cable mass is 6.36 [kg/km]. The maximum payload mass available for the complete array is 216 [kg]. Subtracting from this the rover and antenna mass leaves 179.24 [kg]. This corresponds to a maximum baseline of 28.18 [km]. Peak cable tension would increase to 671.8 [lbf], which is within the limits of the cable. The time to deploy the array would increase from 28 [hrs] to 78.4 [hrs] and so is not problematic. The average power required of the rover would increase to 104.75 [W], which is only slightly larger than the power required during mission operation to operate the array. The specific crater chosen (Shackleton) is however not big enough for a 28km baseline, but there are craters which are. They might be in a less favourable position with respect to sunlight, however. Regardless, the critical parameter for increasing the baseline is the cable mass. For baselines beyond 28km different deployment methods need to be considered.

#### 15.3.3. SENSITIVITY TOWARDS NUMBER OF ANTENNAS

A change in the number of antennas influences the power required of the antennas, the data rate, sensitivity of the array, integration time of the measurements and the radar array mass.

The sensitivity of the array and integration time of measurements are related to the specific science that can be done with the radar array. As such, combinations of baseline and amount of antennas as well as array configuration are

subject to scientist's opinions. Both the sensitivity and the integration time increase quadratically with changes in the amount of antennas.

The data rate increases linearly with an increase in the number of antennas. Due to the configuration of the satellite a radar dish larger than 1 [m] in diameter is improbable. Also the transmitted power of the antenna cannot exceed about 30[W] due to restrictions of the antennas. This means that a maximum data rate corresponding to the data from about 140 antennas can be transmitted using radar technology.

One antenna requires 0.576 [W] for operation and the configuration of the satellite allows for a maximum increase in solar array size to produce an additional 86W for the operation of the radar array. This means that in total a maximum of 170 antennas can be supplied with power.

The antennas weigh 0.56 [kg], the maximum payload mass is 216 [kg], of which 88.6 [kg] is the rover and cables (provided that they remain unchanged). This means that a maximum of 227.5 antennas could be taken to the moon.

It is clear from the above considerations that the critical value for the amount of antennas is at about 140. For numbers beyond this value different transmission solutions are required. These could be laser or THz communications.

#### 15.3.4. SENSITIVITY TOWARDS LOCATION ON THE MOON

In the midterm report the decision was made to place the array in a crater on the South Pole instead of in an equatorial region on the far side. The cost in mass budget of placing the antennas in a different location is considered in this section.

One of the main considerations for placement was that on the South Pole there are regions of almost continuous illumination, an adjacent crater provides eternal darkness for the measurements, and a direct communications link with Earth is possible so no relay satellite is needed. Moving the antennas out of the crater means that they can only be operated when they aren't illuminated, at which time they do not receive any energy, so they require batteries to operate. Operating the 21 antennas for the 2 week darkness period requires about 103 [kg] in mass for additional solar array, regulators/converters and batteries [3]. Losing the benefit of direct communications with Earth or Earth-orbiting satellites means that a data relay satellite is required. In the mid-term such a satellite was estimated at 248.2[kg] [7].

## FUTURE DEVELOPMENTS

This chapter contains a description of future activities that have to be undertaken to complete the LOFARside mission. The project design and development logic, as well as a mission Gantt chart (Section 16.1) are presented in the following section. The chapter ends with an explanation of the steps necessary to produce the complete spacecraft (S/C) (Section 16.2).

### 16.1. PROJECT DESIGN & DEVELOPMENT LOGIC

This section contains the project design and development of the LOFARside mission. In Figure 16.1 the chronological order of post-DSE activities is shown using a block diagram, and in Figure 16.2 the Gantt Chart with the scheduling of these activities is given.

These figures contain seven project phases that are based on standardization provided by the European Space Agency (ESA) [67]. Each block in Figure 16.1 contains the description of the activity to be performed. The end of the design synthesis exercises (DSE) will conclude in a feasibility study of the LOFARside mission and finalizing the Phase-A study. Once the design has been agreed upon and is demonstrated to be feasible, a more elaborate Preliminary Design can be initiated (Phase-B), which is the first activity after the DSE. This will end with the Preliminary Design Review which will be the milestone to initiate the Detailed Design (Phase-C). Here, not only will all the systems and subsystems be thoroughly analysed (to the last component), but also a parallel manufacturing, integration, assembly and testing (IA&T) plans should be determined. Once the detailed design has concluded and a Detailed Design Review is undertaken, the Qualification and Production Phase can begin (Phase-D) as well as the IA&T of the transfer S/C and the lander. Furthermore, the production of the VEGA launcher should start at this point. The logical next step is to integrate both elements, the transfer S/C and the lander, and test them. At the same time, the launch site shall be prepared, where the end of Phase-D will result in an integrated S/C with all components, ready to be launched. Once all systems and subsystems are ready to go, and the launching platform is ready to operate, the launch will be conducted (Phase-E), which will lead to the start of the mission. This will then initiate the LOFAR mission operations which will involve the whole ground station control to be ready for the mission tasks. At this point, the mission will involve decoupling of the lander, after which the disposal of the transfer S/C will take place. Finally, the mission will continue acquiring useful scientific data until termination of the 6 year contract, which will initiate the Disposal Phase (Phase-F).

### 16.2. PRODUCTION PLAN

In this section a production plan for the LOFARside mission is presented. This comprises the production of the mothership, lander, and the LOFAR systems itself. As usual in aerospace the required components will come from different contractors who offer the best combination of quality and cost for a certain part. The client is Airbus Defence & Space, a global leader in aeronautics, space and related services. It is therefore beneficial to keep production within the boundaries of the company as much as possible. Also preferably European contractors will be chosen.

The mothership and lander both have a primary structure that carries loads and to which the subsystems are connected. This is a part that can not be bought readily, a dedicated design of the primary structure is needed. Because all other subsystems are connected to the primary structure and have to be compatible with this part, production of these parts should start as soon as possible. Of both primary structures several prototypes will be made for testing. Tests will simulate launch loads and vibrations, maneuvering loads and landing loads for the lander. After testing prototypes will be updated if necessary. This has to be considered in the schedule. Concurrent with primary structure manufacturing the subsystems will be manufactured. Some products are off-the-shelf and therefore have a manufacturing time of zero (or very short) and can be quickly delivered. Because their dimensions and weights are known, a structural prototype of the S/C with subsystems can be made for testing early on. Off-the-shelf products for the LOFAR mission are:

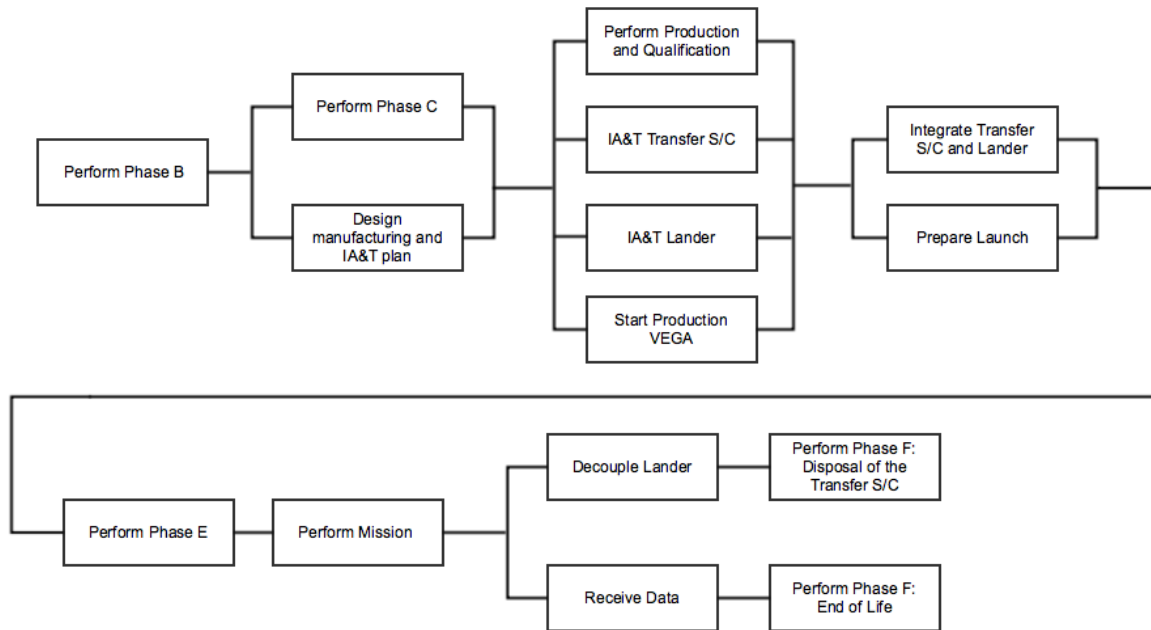


Figure 16.1: Block diagram for post-DSE phases of the LOFARside mission.

- Landing chemical thrusters
- Attitude thrusters
- Electric thrusters
- Batteries
- Inertial measurement unit
- Star trackers
- On-board processors
- Communication H/W (communication antennas usually not)
- Cables
- Payload (crossed dipole antennas, additional instruments)
- Processor

Legal issues concerning the purchase of these products do take time and have to be considered when scheduling. However, since all the products are manufactured in Europe, this should not be a problem.

Products that are dedicated to the mission will have some development and testing period. This can cause delays and therefore these products are identified:

- Communication antennas
- Software
- Solar panels (with deployment system)
- Rover

Software is tailored for the mission, for example subsystem control software (e.g. attitude control software) from previous systems can be reused, but the various parts have to be integrated and adjusted specifically for the mission. Attention has to be paid to the Terrain Relative Navigation (TRN) algorithms that have not been used earlier in flight. This software will use crater pattern matching and structure from motion algorithms that already exist but have never been used in the context of lunar landing. Development and integration into the system of the TRN software will be scheduled. The LOFAR rover is based on the Axel Rover design but has to be modified to be able to carry the payload antennas. The rover specifications will be dictated by its required performance to deploy the payload. Therefore its development can start at the start of the production. The solar panels will be developed by Airbus Defence & Space, their configuration is mission specific. Load testing and deployment of the panel will be scheduled. Figure 16.3 presents the schedule for production.

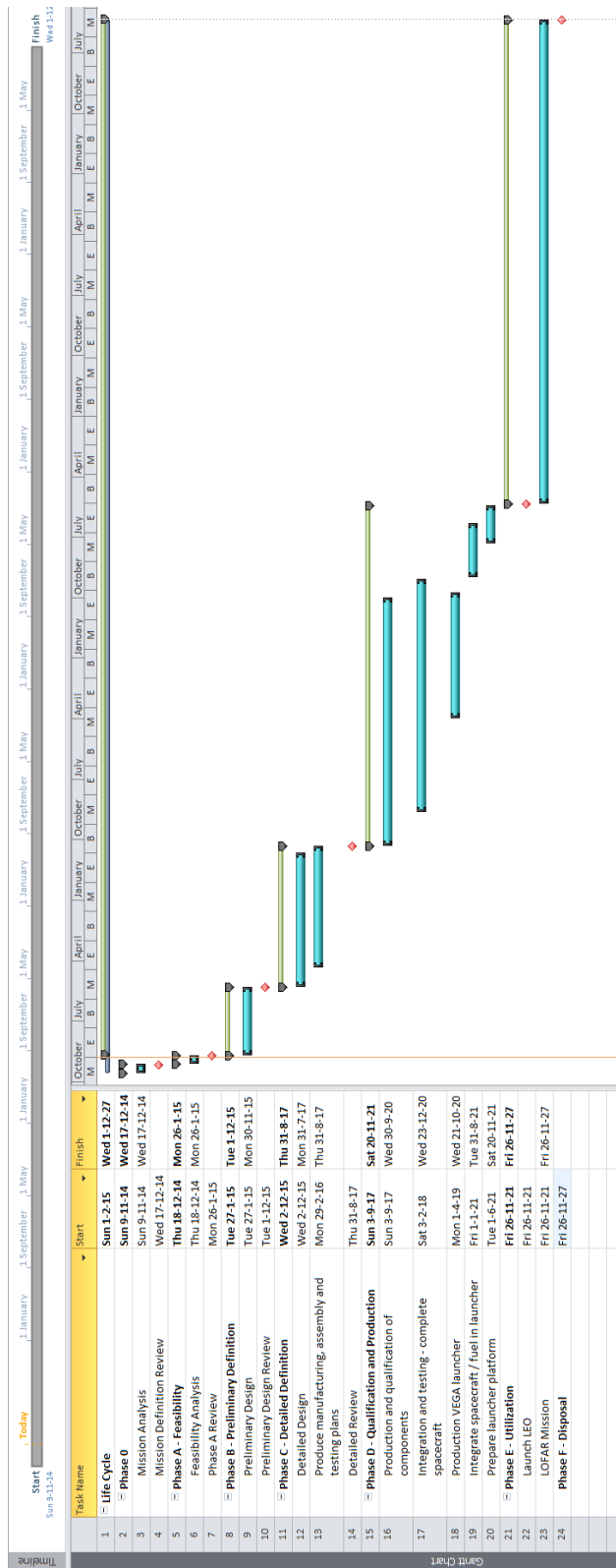


Figure 16.2: Project Gantt Chart

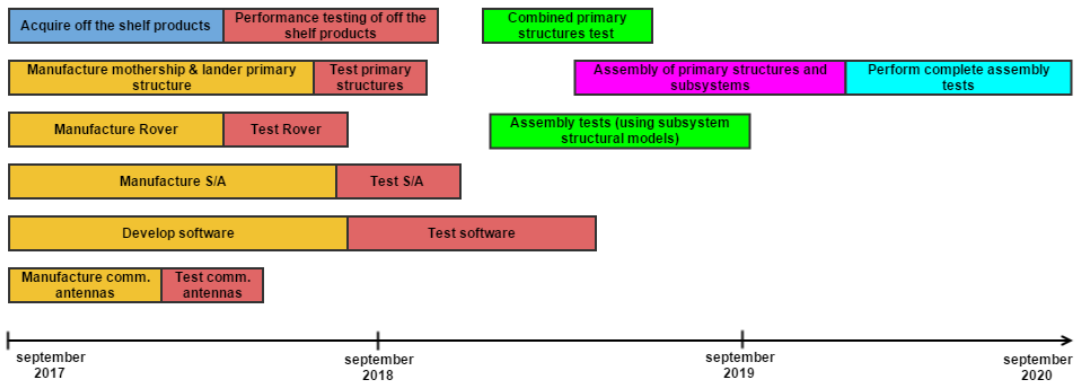


Figure 16.3: Production schedule

## PROJECT MANAGEMENT

This chapter will discuss the project management for the LOFARside mission. The resource allocation (Section 17.1), cost analysis (Section 17.2) and RAMS (Section 17.3) are discussed in the following chapters, as well as the risk management (Section 17.4).

### 17.1. RESOURCE ALLOCATION

To ensure that the technical resources shall not grow further than a certain margin, maximum values are established. Examples of technical resources are mass, electrical power and computing resources. The margin is based on a reserve/contingency value which has been carefully managed throughout the project. The most important parameters for space missions are [68, pp. 193]:

- Mass
- On-board computer capacity
- Electrical power
- Structural stiffness
- Pointing (error)
- Delta V
- Communication link
- Envelope/ size
- Production cost

To track the growth of the performance parameters and to avoid that these parameters grow out of the limits of constraints and requirements, Technical Performance Measurement (TPM) can be used. Past events show that the margin between the required value and the actual achieved value of technical resources tends to decrease during the execution of a project. Therefore TPM is used to define the discrepancies between the actual and required performance as early as possible. This is achieved by using known trends and past experience to model the development of the design. A better trace from predicted performance to non-compliance is enabled, which will indicate when discrepancies between design and requirements should be eliminated [68]. TPM tracks certain key parameters during the development process and sets a contingency for each parameter. The contingency gives a reserve as design difficulties are discovered. Contingency is dependent on the maturity of the design and on technology readiness level (TRL). As the project continues the design maturity increases and the contingency will reduce. For the chosen key parameters the following procedure is followed. First past missions are evaluated to extract information on the key parameters that are followed during the project development. The past missions are used to define trends. Then using this information a table specifying contingency allowance as a function of design maturity is defined for each, which is shown in Table 17.1.

<b>Design maturity</b>	Baseline review	Concept design	Preliminary design	Detailed design
Mass	25%	15%	TBD	TBD
On-Board computer capacity	40%	20%	TBD	TBD
Electrical power	30%	15%	TBD	TBD
Delta V	25%	10%	TBD	TBD
Communication link	40%	15%	TBD	TBD
Envelope / size	25%	20%	TBD	TBD
Production cost	30%	10%	TBD	TBD

Table 17.1: Contingency allowance in percentage

This step is followed by determining the actual, target and current value at the given evaluation moments during the project. Parameter information is given to the system engineer who monitors the development of the key parameters and compares them during the design process. The development will be represented in a graph to have a clear overview. When a problem arises, for example the actual value is higher than the target value of the mass, the systems engineer will communicate this to the group and allocate human resources for corrective action. Possible actions are decreasing uncertainty in the design, modifying the design and changing the specification value.

## 17.2. COST ANALYSIS

In this section a detailed cost analysis is performed for the different parts and phases of the LOFARside mission for the design and development year, which is 2015. Several cost estimation methods are available for estimations of conceptual design and phase A studies. For the LOFARside mission the Unmanned Space vehicle Cost Model and the NASA Instrument Cost Model provided in [25] were used in combination with the TRANSCOST model [69]. First the TRANSCOST model will be discussed and applied, followed by an explanation of the Unmanned Space Vehicle Cost Model and then the NASA Instrument Cost Model will be explained. This section will end with an overview of the total cost estimation of the LOFARside mission.

### 17.2.1. TRANSCOST COST ESTIMATION METHOD

The TRANSCOST cost estimation model is a parametric cost estimating method. This means it uses a mathematical relationships that relate cost to different performance parameters. This model uses statistical data, which include US, European and Japanese spacecraft and engine projects. It accounts for actual cost that also includes unexpected problems and delays. The main focus of the TRANSCOST model is on expendable and/or reusable space transportation systems [69].

For the LOFARside mission the TRANSCOST model was used to determine the cost for Spílaio because other cost estimation methods were found to be unsuitable due to the assumptions, on which they are based, or reference data they used. The TRANSCOST method, on the contrary, gives an approach for the estimation of Earth-Moon transportation [69, pp. 193]. The first step is to define the flight profile, which for the LOFARside mission is a transfer of payload from LEO to LLO by an expendable S/C. Then, using the payload mass delivered in LLO and the S/C mass in LEO the ManYear value of Spílaio can be determined using [69, pp. 202]. The obtained value of ManYear for Spílaio is 115. In Table 17.2 the used parameters and their values are summarized as well as the final obtained ManYear value.

Parameter	LOFARside Mission	Unit
Payload Capability LEO	2280	[kg]
Payload Capability LLO	1063	[kg]
ManYear	115	[-]

Table 17.2: Table with a summary of the parameters used to obtain the ManYear value for Spílaio.

### MANYEAR COST DEFINITION

The TRANSCOST model uses the ManYear value to indicate cost. The ManYear system is chosen because it provides a value which takes different currencies and fiscal years into account [69]. Before the actual cost of an estimation can be calculated the ManYear value should be converted to the desired currency and the current fiscal year to account for inflation. In [69, pp. 11] a history, from 1960 to 2002, of the cost of 1 ManYear is given in Euro among others. Using this data the ManYear value in 2015 can be extrapolated. The results of the computation are given in Figure 17.1. The value of 1 ManYear in 2015 was found to be 258600 euro, which means that the cost estimation of Spílaio is 29739 Million euro. Since the application of the LOFARside mission is completely different from past S/C and the TRANSCOST model is based upon S/C that use chemical propulsion, it was assumed that the calculated value does not include the solar panels.

### 17.2.2. UNMANNED SPACE VEHICLE COST MODEL

The Unmanned Space Vehicle Cost Model (USCM8) was developed by Telcolote Research for the US Air Force, Space and Missile Systems Center. The method is based on different Cost Estimating Relationships (CERs) statistically derived from a database of 44 satellites [25]. Although it concerns satellites, this method was found to be applicable for Noor because the system is mostly mass based and the masses of the different subsystems are in the same order of magnitude. However, at some points a higher value was assumed to account mismatches. Besides the S/C cost the

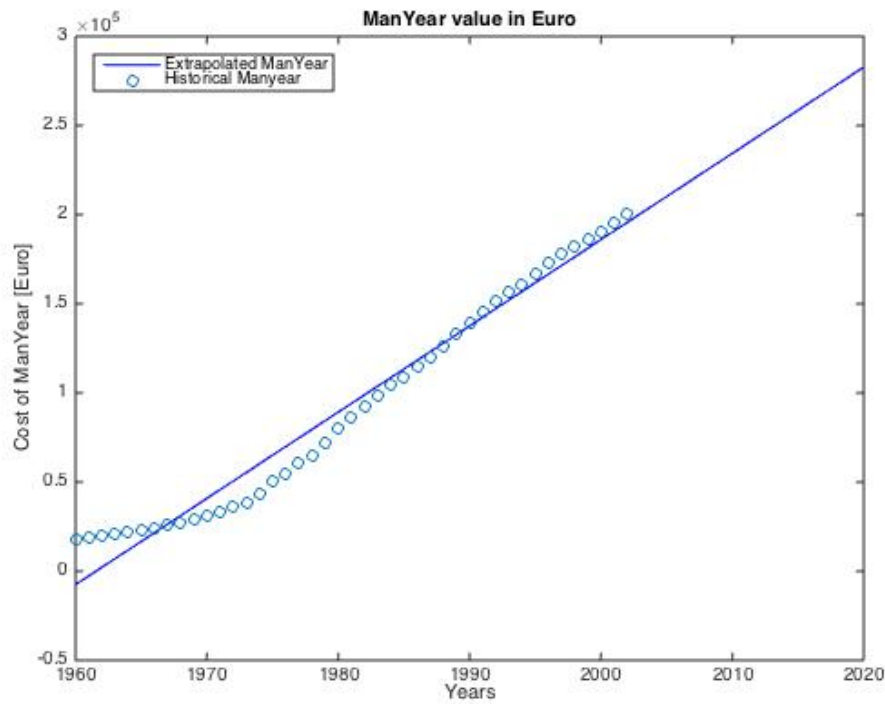


Figure 17.1: ManYear value from 1960 to 2002 [69] and the extrapolated data for the European aerospace industry.

USCM8 includes development, integration, testing, production, launch operations, software development, ground and payload equipment and ground operation cost [25].

The USCM8 as given in [25] gives all the values in thousand dollars for the fiscal year 2010 (*FY10*). This is indicated by the unit [*FY10K*\$] in the rest of this report. Once all the costs were obtained the *FY10K*\$ values were converted to the fiscal year 2015, indicated by [*FY15K*\$]. This conversion was done based on the inflation factors given in [25, pp. 316]. To estimate the cost for fiscal year 2015 the calculated cost should be divided by 0.867 [25, pp. 316]. Then these values were changed into euro using the exchange currency where 1 dollar is equal to 0.86 euro<sup>1</sup>.

#### COST ESTIMATING RELATIONSHIPS FROM USCM8

The USCM8 method was applied for different parts of the LOFARside mission. The following CERs were used to come to the total cost estimation that is shown in Table 17.4. Note, in the title above each CERs are numbers, which match the numbers provide in Table 17.4. Furthermore the values of all the different parameters used are summarized in Table 17.3.

##### 1.2.1 Structure & Thermal Subsystem

For an estimation of the non-recurring and recurring costs for the structure & thermal subsystem (S&TS) Equation (17.1) and Equation (17.2) were used respectively. Where the variable  $X_1$  is a combination of the structural and thermal subsystem masses given in [*kg*].

$$Y = 646X_1^{0.684} \quad [\text{FY10K}\$] \quad (17.1)$$

$$Y = 22.6X_1 \quad [\text{FY10K}\$] \quad (17.2)$$

##### 1.2.2 Attitude Determination and Control Subsystem

For an estimation of the non-recurring and recurring costs for the attitude determination and control subsystem (ADCS) Equation (17.3) and Equation (17.4) were used respectively. Where  $X_1$  is the mass of the ADCS, provided in [*kg*].

$$Y = 324X_1 \quad [\text{FY10K}\$] \quad (17.3)$$

$$Y = 795X_1^{0.593} \quad [\text{FY10K}\$] \quad (17.4)$$

##### 1.2.3 Electrical Power Subsystem

For an estimation of the non-recurring and recurring costs for the electrical power subsystem (EPS) Equation (17.5)

<sup>1</sup><http://www.xe.com> Last checked on 20-01-2015.

and Equation (17.6) were used respectively. Where  $X_1$  is the mass of the EPS, given in [kg].

$$Y = 64.3X_1 \quad [FY10K\$] \quad (17.5)$$

$$Y = 32.4X_1 \quad [FY10K\$] \quad (17.6)$$

### 1.2.4 Propulsion Subsystem

For an estimation of the non-recurring and recurring costs for the propulsion subsystem Equation (17.7) and Equation (17.8) were used respectively. Where in Equation (17.7)  $X_1$  is the volume of the fuel tank used for the chemical propulsion in [ $cm^3$ ]. In Equation (17.8)  $X_2$  is the mass of the chemical propulsion thrusters in [kg] and  $X_3$  is the burn time in [seconds].

$$Y = 20X_1^{0.485} \quad [FY10K\$] \quad (17.7)$$

$$Y = 29X_2 + 0.024X_3 \quad [FY10K\$] \quad (17.8)$$

### 1.2.5 Telemetry, Tracking and Command Subsystem

For an estimation of the non-recurring and recurring costs for the telemetry, tracking and command subsystem (TT&C) Equation (17.9) and Equation (17.10) were used respectively. Where  $X_1$  is the mass of the telemetry, tracking and command subsystem in [kg] and  $X_2$  the orbit type. The USCM8 only provides values for geostationary (GEO) orbit (1) or no GEO orbit (0). However, the no GEO orbit type indicates an orbit around Earth [25, pp. 300]. Therefore a value of twice GEO orbit,  $X_2 = 2$ , was assumed for Noor.

$$Y = 26916 \quad [FY10K\$] \quad (17.9)$$

$$Y = 883.7X_1^{0.491} 1.13^{X_2} \quad [FY10K\$] \quad (17.10)$$

### 1.4 Integration, Assembly, and Testing

For an estimation of the non-recurring and recurring costs for integration, assembly and testing (IA&T) Equation (17.11) and Equation (17.12) were used respectively. Where in Equation (17.11)  $X_1$  is the S/C total non-recurring cost in [FY10K\$], which means the total non-recurring cost for the all its subsystems. In Equation (17.12)  $X_2$  is the total S/C and payload recurring cost in [FY10K\$], where the total S/C recurring cost indicates the recurring cost of all the subsystems. Note, that for the correct value of  $X_1$  and  $X_2$  the estimation explained in Section 17.2.3 is necessary.

$$Y = 0.195X_1 \quad [FY10K\$] \quad (17.11)$$

$$Y = 0.124X_2 \quad [FY10K\$] \quad (17.12)$$

### 3.0 Software Development

For an estimation of the non-recurring and recurring costs for the software development Equation (17.13) and Equation (17.14) were used respectively. Where  $X_1$  is the total S/C and IA&T non-recurring cost [FY10K\$] and  $X_2$  gives the total S/C, payload and IA&T recurring cost in [FY10K\$]. Also for this calculation the correct value of  $X_1$  and  $X_2$ , as explained in Section 17.2.3 are necessary.

$$Y = 0.414X_1 \quad [FY10K\$] \quad (17.13)$$

$$Y = 0.32X_2 \quad [FY10K\$] \quad (17.14)$$

### 4.0 Launch Operations & Orbital Support

For an estimation of the recurring cost for the launch operations & orbital support (LOOS) Equation (17.15) was used.

$$Y = 5850 \quad [FY10K\$] \quad (17.15)$$

### 5.0 Aerospace Ground Equipment

For an estimation of the non-recurring cost for the Aerospace Ground Equipment (AGE) Equation (17.16) was used. Where  $X_1$  is the total S/C non-recurring cost and  $X_2$  is the S/C type. The USCM8 provides two S/C types, which are communication satellites (1) and non-communication satellites (1) [25, pp. 298]. For Noor the value of 1 was chosen. The correct value of  $X_1$  will use the estimation provided in Section 17.2.3.

$$Y = 0.421X_1^{0.907} 2.244^{X_2} \quad [FY10K\$] \quad (17.16)$$

Mission Segment	Variables		
	$X_1$	$X_2$	$X_3$
1.2.1	65 [kg]		
1.2.2	111.5 [kg]		
1.2.3	65 [kg]		
1.2.4	637,800 [cm <sup>3</sup> ]	55 [kg]	71 [sec]
1.2.5	22 [kg]	2	
1.4	117,664 [FY10K\$]	24,046 [FY10K\$]	
3.0	114,464 [FY10K\$]	27,028 [FY10K\$]	
5.0	91,519 [FY10K\$]	1	

Table 17.3: Table with the input variables for the USCM8 Cost Estimating Model.

### 17.2.3. NASA INSTRUMENT COST MODEL

The NASA Instrument Cost Model (NICM), developed by the Jet Propulsion Laboratory, was used to estimate the cost of the scientific payload. The CERs are based on a database of 154 instruments [25]. The model estimate includes development, unit and contractor cost [25]. For a proper estimation the CERs that is developed for optical planetary payload was used. The NICM also provides the cost in FY10K\$. For the conversion of FY10K\$ to the proper fiscal year and currency the same approach as in Section 17.2.2 was used.

#### 1.3.3 Scientific Payload

For an estimation of the non-recurring and recurring costs for the scientific payload without Colb $\acute{I}$  (TT&C) Equation (17.17) was used. Where  $M$  is the total mass of the scientific instruments in [kg],  $P$  is the maximum power in [W] and  $DL$  is the life time in months. For the LOFARside mission the following values were used:  $M = 42.8$ ,  $P = 19.5$  and  $DL = 60$ .

$$Y = 328M^{0.426}P^{0.414}DL^{0.375} \quad [FY10K\$] \quad (17.17)$$

### 17.2.4. COST ESTIMATION OVERVIEW

In Table 17.4 an overview of all mission segments and their cost is provided. For the total estimation a combination of the TRANSCOST and USCM8 model was used, but also available pricing for some components. The later are concerning the cost of the solar panels for Sp $\acute{I}$ lao, which were computed in Chapter 7. Also, the cost of Colb $\acute{I}$  and the cables were calculated based on available pricing information<sup>2</sup>. Furthermore the launch cost for the VEGA are readily available [2]. Once the total cost of the mission was determined a reserve factor of 20% was included based on the NASA Marshall Space Flight Center Cost-Adjustment Factors for Technology Development. Given the fact that the mission uses some new technology and that the Delft Space Agency has experience in aerospace engineering but not to the extent of this mission the margin of 20% was chosen [70, pp. 259]. In Figure 17.2 three pie charts are given to show the contribution in percentages of the different mission segments to the total cost. First an overview of the segments contributing to the transfer phase are given. Note, that it is not normal for the solar panels to have such a high contribution to the costs, but given the size and function of these panels it seems a proper estimate. Secondly, all parts contributing to the total cost of Noor are shown. The last pie chart gives an overview of the entire mission and all the mission segments.

## 17.3. RAMS

The LOFAR mission shall strictly follow the Reliability, Availability, Maintainability and Safety (RAMS) characteristics to any space mission. All subsystems must demonstrate with enough confidence their reliability. At the beginning of the mission, they must have all been flight proved, even if today they can have by requirement a technology readiness level (TRL) of 5. This entails that all the subsystems must be already available in the market by the launch date.

For this purpose, and to ensure safety of all subsystems throughout the whole mission, redundant subsystems will be implemented. This will be the case for the most critical subsystems, where failure of these would jeopardize the whole mission. For example, the thermal control subsystem will carry at least one redundant active control means (Heaters). Furthermore, the power generation subsystem will also carry redundant energy storage systems in case failure of the principal ones occurs. Another example are the redundant thrusters for AOCS control which will give a high reliability in terms of attitude control and maneuvering. Other possible redundant systems will be evaluated once a further iteration in the detailed design takes place. Nonetheless, care shall be given when implementing

<sup>2</sup>Private conversation with Jet Propulsion Laboratory.

<b>Mission Segment</b>	<b>Cost [K euro]</b>
<b>1.0 Spacecraft</b>	<b>223,199</b>
<i>1.1 Transfer Phase</i>	63,739
1.1.1 Spílaio	29,739
1.1.2 Solar Cells	34,000
<i>1.2 Noor Lander</i>	114,634
1.2.1 S&TS	12,594
1.2.2 ADCS	48,743
1.2.3 EPS	6,235
1.2.4 Propulsion	15,257
1.2.5 TTC	31,805
<i>1.3 Payload</i>	22,530
1.3.1 Colbí	172
1.3.2 Cables	172
1.3.3 Scientific Payload	22,186
<i>1.4 IA&amp;T</i>	22,296
<b>2.0 Launch</b>	<b>32,000</b>
<b>3.0 Software Development</b>	<b>48,192</b>
<b>4.0 LOOS</b>	<b>5,031</b>
<b>5.0 AGE</b>	<b>25,698</b>
<b>Total Estimated Cost</b>	<b>334,120</b>
<b>Total Estimated Cost With 20% Reserve</b>	<b>400,944</b>

Table 17.4: Cost Estimation of the LOFARside mission in FY15 K Euro.

these redundancies since they will increase the overall mass of the mother S/C, which directly translates to a reduced useful payload mass and an increase in costs. Therefore, reliability considerations shall provide just sufficient confidence that the LOFAR system will perform its tasks irrespective of failure of one particular subsystem (Fail-Safe philosophy).

This confidence can also be achieved by carrying out maintenance procedures of any subsystem when possible. Maintenance of any system in space is very hard (if not impossible) since it is physically impossible to reach any malfunctioning problem. Therefore, the problem can only be tackled if it can be remotely repaired from Earth or if the system is capable of autonomously fixing any arising issue. The first case is only possible for malfunctions in the software, where new software could be transmitted and implemented through the communications link, depending on the malfunction. The latter case would entail that the system is already designed to prevent and repair the malfunctions. This would surely have to be part of the detailed design process and will be evaluated at that stage of the project.

## 17.4. RISK MANAGEMENT

This chapter covers an evaluation of the risk management procedures implemented towards mitigating high-risk elements, a continued and updated risk assessment at system and project level using a risk map and risk trend tables. For remaining high-risk elements risk management procedures are detailed.

### 17.4.1. MIDTERM RISK MANAGEMENT EVALUATION

Risk assessment and mitigation was done at both project- and system level. Initial management procedures to mitigate risks were defined and their implementation is analyzed in this section.

Project level risk elements that were identified as high-risk elements at the midterm level were additional work/costs, mistakes in assumptions or references and unavailable information.

- Additional work has largely been prevented by the implementation of more detailed planning and strict deadlines. Especially towards the end of the project time this turned out to be a valuable mitigation strategy.
- An in-depth cost analysis revealed main cost drivers and their respective sensitivity. Cost estimation results can be used to formulate financial risk mitigation strategies.

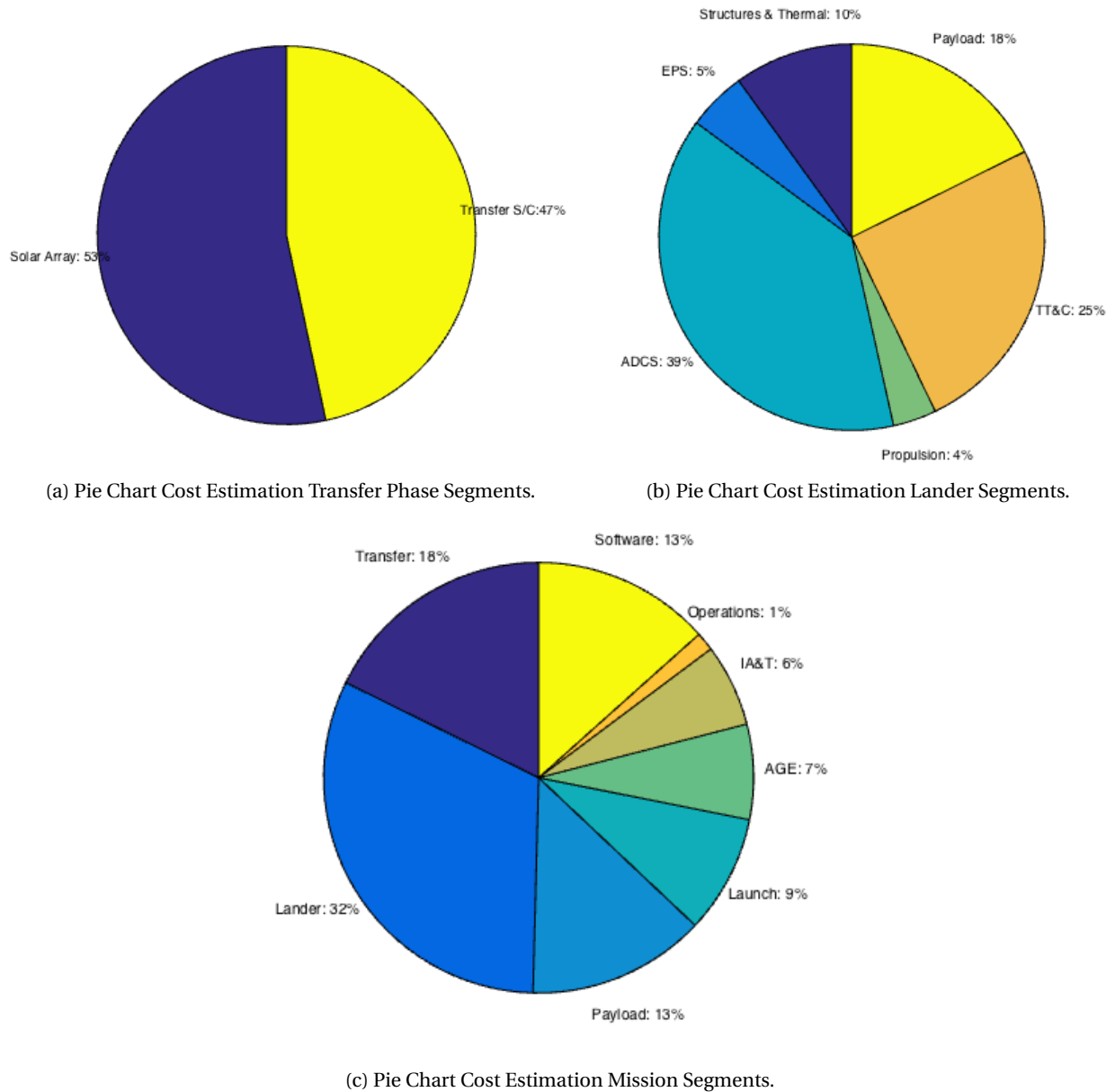


Figure 17.2: Pie Chart Cost Estimation in Percentages.

- The risk of having mistakes in assumptions or references is reduced by peer-reviewing the individual contributions of the team members.
- Time spent waiting on expert information or guidance has been reduced in some instances only.

At system level the identified high-risk elements were damage to payload, the electrical propulsion system, the identification of the landing site, the antenna deployment system, the concentration node & data processing unit and the Moon to Earth data relay unit.

- Preventing damage to the payload during launch and velocity changes of the satellite requires understanding of the loads and vibrations that occur. During launch the payload must be able to withstand a certain lateral and longitudinal acceleration, a certain quasi-static load, and must have a certain lateral and longitudinal Eigenfrequency. During landing on the lunar surface certain loads will occur. Structural design will ensure the satellite's compliance with all structural and environmental requirements. Models used can be validated using existing flight designs.
- The electrical propulsion system risk is reduced by using an existing design that has been verified and validated. It is not yet flight proven, however, so some independent testing is recommended to track the risk.
- The identification of the landing site and required precision during landing (100x100 [m]) have been investigated in some detail. Different terrain relative navigation (TRN) methods, navigation algorithms as well as hazard detection and avoidance are considered to ensure a successful precise landing. By the time of launch

(2020+) this technology will be flight proven.

- The antenna deployment system, mainly Colbí, has been designed for the Shackleton crater specifically, but some aspects will be solved during detailed design. Colbí used is based on a non-flight design, however.
- The concentration node & data processing unit consists of a flight proven computer chip that will be radiation shielded and not subjected to temperatures outside of its operational range.
- The Moon to Earth data relay unit has been designed to deliver the required capability using existing flight tested radar technology.

### 17.4.2. RISK ASSESSMENT

Risks are assessed for the project itself and for the satellite mission at system level. Risk events and elements are updated with respect to the midterm level. Specific subsystem risk assessment, as well as acceptance criteria thereof, are reserved for the detailed design. Project risk events are detailed in Table 17.5 and system level risks are given in Table 17.6.

Project Risk Events			
1	Additional work	5	Mistakes in assumptions or references
2	Additional costs	6	Loss of data
3	Risk too high	7	Change in top-level requirements
4	Change in trade-off criteria	8	Unavailable information

Table 17.5: Project risk events

System Risk Element			
1	VEGA launcher	10	Robotic antenna deployment
2	Damage to structure of satellite	11	Concentration node & data processing
3	Damage to payload	12	Solar array & power distribution
4	Satellite AOCS	13	Thermal control of lander & Colbí
5	Electrical propulsion system	14	Ground control segment
6	Transfer phase power generation	15	Coronal mass ejection
7	Terrain relative navigation	16	Meteorite strike
8	Lunar landing precision	17	Lunar dust disturbance
9	Lunar landing impact	18	

Table 17.6: System level risk elements

### 17.4.3. PROJECT RISK ANALYSIS

Risks related to the completion of the project are analysed in this section. Additional work and costs can occur for a variety of reasons, but mainly due to unforeseen circumstances and/or inadequate planning. If risk mitigation strategies are unsuccessful the project might be terminated because of unacceptable levels of risk. If insufficient funding can be secured the project will not be continued beyond the DSE. Any mistakes made in assumptions and/or references can have far-reaching consequences, in any case making mistakes increases the risk of the project. Loss of data is another reason for time/cost budget overruns, but is separated because it can be avoided easily. Something that emerged during the conceptual design phase was that it can take quite a long time to get relevant information from experts. Also, if the top-level requirements, like scientific requirements, aren't subject to change, it takes a while to get agreement from experts as well as the project client. To this end, the requirements are now set. Any changes will be subject to approval by project management and may require additional funds to be implemented. Similarly, changes to the trade-off criteria after the conceptual design phase require re-evaluation of the trade-off and so this is not possible any more.

Project risks are analyzed based on likelihood of occurrence and level of influence on the project at the final report level. Negligible disturbances do not disrupt the project process. Minor disturbances lead to some level of time and cost budget overruns, while significant and major disturbances lead to unacceptable overruns. Critical

disturbances lead to immediate termination of the project. The results of the project risk analysis are presented in Table 17.7.

<b>Likelihood of occurrence</b>					
Very likely					
Probable					
Possible			5		
Unlikely			1,8	4,7,2	3
Very unlikely				6	
<b>Influence on the project</b>	Negligible	Minor	Significant	Major	Critical

Table 17.7: Project risk map

#### 17.4.4. PROJECT RISK MITIGATION

The high-risk events that have been assigned mitigation strategies are tracked throughout the project using risk trends as shown in Table 17.8. Project risks are defined to be mitigated if they are unlikely to occur. It can be seen that the risk mitigation strategies that were implemented have largely been successful. In some instances a lack of information led to time budget overruns. After investigation it turned out that in these cases the mitigative strategy of contacting multiple people was not implemented or only implemented partially. The risk therefore has not been mitigated, but the same mitigation strategy remains and must be implemented more thoroughly. It is summarized in Table 17.9.

<b>Severity of Project Risk</b>			
<i>Critical - very likely/probable</i>			
<i>Major - very likely/probable</i>	Additional Cost		
<i>Critical - possible/unlikely</i>			
<i>Major - possible/unlikely</i>		Additional Cost	
<i>Significant - probable</i>	Additional Work	Unavailable information	Unavailable information
		Additional work	
<i>Significant - possible</i>	Mistakes in assumptions/references	Mistakes in assumptions/references	
<i>Risk mitigated</i>			Additional Cost Additional Work Mistakes in assumptions/references
<b>Design maturity</b>	<i>Baseline</i>	<i>Mid-term</i>	<i>Final</i>

Table 17.8: Project risk trends

<b>High-risk event</b>	<b>Mitigation strategy</b>
Unavailable information	Establish multiple lines of contact to avoid dependance on a single person Define deadlines after which a different strategy must be pursued

Table 17.9: Risk mitigation strategies for high project risk events

#### 17.4.5. SYSTEM RISK ANALYSIS

System risk elements are assessed in this section. Consequences of failures are evaluated by their effect on the satellite's ability to perform its mission. A distinction is made between catastrophic failures (direct termination of the mission and loss of the satellite), critical failures (complete restriction of the satellite's ability to perform its mission), major failures (severe impairment) and significant failures (clearly noticeable reductions in performance). The likelihood of occurrence of certain failures is assessed based on the TRL of the system, its complexity, as well as the design detail. Note that for outside disturbances like coronal mass ejections the systems ability to cope is evaluated. Coro-

nal mass ejections (CME) result in 'bursts of particles and electromagnetic fluctuations'<sup>3</sup> that could induce electric currents in the satellite's electrical systems. However, both the location of the array in a crater and the possibility to switch off the systems if a CME is observed limit the severity of this risk. Meteorite strikes hit the moon with 'incredible energy' and even a 5 [kg] object can 'excavate a crater over 9 meters across', but lunar impact monitoring is not very advanced yet<sup>4</sup>. Clearly, the consequence of a meteor strike is catastrophic, but how likely it is to occur is uncertain. Protection against meteorites will be limited to ensuring redundancy in the array configuration. Because this is an inherent property of the system, a meteorite strike is not included in the risk map. It will be taken into account when reliability can be assessed in more detail, however. Furthermore, lunar dust 'can accumulate on sensitive power components, such as photovoltaic arrays and radiator surfaces, reducing their performance.' [71, pp.1]. Lunar dust has adhesive and cohesive properties and so 'the most practical dust defensive strategy appears to be the protection of sensitive components from the arrival of lunar dust by location, orientation, or barriers'[71, pp.1]. The updated system risk map is shown in Table 17.10.

<b>Technology level</b>					
Feasible in Theory					
Working Laboratory Model					
Based on Existing Non-flight Engineering				10	
Extrapolated from Existing Flight Design			2,3,11	5,8,15,17	7,9
Proven Flight Design			13,14	4,6,12	1
<b>Criticality of consequence</b>	Negligible	Significant	Major	Critical	Catastrophic

Table 17.10: System level risk map

#### 17.4.6. SYSTEM RISK MITIGATION

The high-risk system elements that have been assigned mitigation strategies are tracked throughout the project using risk trends as shown in Table 17.11. Risks were identified and assessed at each stage of the project, and so some risks were added or have been changed into others. For example, Lunar landing (soft) and Lunar landing (precise) are represented by Identification of landing site and damage to structure of satellite. Risks are defined to be mitigated if they are extrapolated from an existing flight design or based on a proven flight design.

Risk mitigation strategies and increased level of design detail have led to the mitigation of all risks except for the antenna deployment system. This is because Colbí that the design is based on is based on a non-flight design. This is usually the case for custom designed robotic capabilities of satellites. However, extensive testing of the system has already been done and Colbí has been designed with redundancy in mind. Regardless, further testing of the antenna deployment is required, and mitigation procedures are detailed in Table 17.12.

<sup>3</sup>[http://www.nasa.gov/mission\\_pages/sunearth/news/flare-impacts.html#.VIraeXuy6G8](http://www.nasa.gov/mission_pages/sunearth/news/flare-impacts.html#.VIraeXuy6G8)

<sup>4</sup>[http://www.nasa.gov/centers/marshall/news/lunar/program\\_overview.html#.VIrf2nuy6G8](http://www.nasa.gov/centers/marshall/news/lunar/program_overview.html#.VIrf2nuy6G8)

<b>Severity of System Risk</b>			
<b>Catastrophic</b> - feasible in theory	Lunar landing (soft)		
<b>Critical</b> - feasible in theory	Lunar lander decoupling system	Identification of landing site	
	Antenna deployment system	Antenna deployment system	
<b>Major</b> - feasible in theory	Lunar landing (precise)		
<b>Catastrophic</b> - Lab model/non-flight design			
<b>Critical</b> - Lab model/non-flight design	Lunar data collection/transfer unit	Moon to Earth data relay unit	Antenna deployment system
		Electrical propulsion system	
<b>Major</b> - Lab model/ non-flight design	Damage to payload	Damage to payload	
		Concentration node & Data processing	
<b>Significant</b> - feasible in theory /working lab model			
<b>Significant</b> - non-flight design	Damage to structure of satellite	Damage to structure of satellite	
		Thermal control	
<i>Risk mitigated to extrapolation from existing or proven flight design</i>		Decoupling system	Identification of landing site Moon to Earth data relay unit Electrical propulsion system Damage to payload Concentration node &data processing Damage to structure of satellite Thermal control
<b>Design maturity</b>	<i>Baseline</i>	<i>Midterm</i>	<i>Final</i>

Table 17.11: System risk trends

<b>High-risk element</b>	<b>Mitigation strategy</b>
Antenna deployment system	Develop detailed configuration of crossed dipole antennas connected to the cable Consider implementation of polyimide film antenna Set up tests to determine reliability of the system

Table 17.12: Risk mitigation procedures for identified high-risk elements

## MARKET ANALYSIS

In contrast to telecommunications missions, scientific missions do not provide investors with a return on investment. All funding is usually provided by governments pledging a certain percentage of their GDP to scientific exploration of space and by educational institutions who hold an interest in the scientific output of the mission. As such, cost budget constraints are a forceful driving requirement for any scientific mission. Furthermore, placing a constellation of satellites in a Lagrange point orbit at the far side of the Moon to observe low frequency radiation free from Earth's influence is likely a cheaper solution than placing antennas on the Moon's surface. However, "a lunar location is much preferred from a scientific point of view... [and] explorational point of view" [72] because of better shielding, the possibility of expanding the mission in the future and addressing additional science. In response to this situation, the DSA team will investigate the option of taking on secondary scientific payloads in return for funding or resources. This will also increase the versatility of the mission and enhance the output value of the project. An investigation of different possible instruments (Section 18.1) and a trade-off to select the optimal combination (Section 18.2) as well as prospective monetary gains (Section 18.3) are presented in this chapter. Based on the selected instruments companies and educational institutions can be contacted to gauge their interest and ability to support the mission with funds.

### 18.1. SECONDARY INSTRUMENTS

DSA has conducted research of useful scientific instruments with the aim to prevent doing science that has been done before and complicating the mission unnecessarily. Based on the characteristics of different instruments found in scientific literature (see Table 18.1), the trade-off criteria were set up and the trade-off itself was conducted, as can be seen in Table 18.2.

#### SEISMOMETER

A seismometer enables identification of potential resources and securing the environment for manned exploration and will reveal information about the core, mantle and crust structure of the Moon. The Apollo missions performed extensive seismological experiments but not at the South Pole. In lumination periods a seismometer requires 2.6 [W], while the night mode allows a reduction of power consumption down to 1.6 [W]. The mass of the seismometer depends on its sensor configuration but is around 8.4 [kg][73]. The data rate after compression is about 3.15 [Gbit/s] [73]. The technological readiness level (TRL) of this seismometer is 5-6 [73] and the cost is roughly 30 [€M].

#### HEAT FLOW PROBE

The Heat Flow and Physical Properties Package is an experiment to make measurements to a depth of 3 [m] by means of an electro-mechanical hammering mechanism. The instrument consists of the temperature sensors and heaters that measure the thermal gradient and thermal conductivity, motion and tilt sensors that determine the position of the instrument in the ground, and electrical sensors which determine relative permittivity of the regolith [73]. The heat flow experiment was conducted on the Moon by missions Apollo 15 and 17, but not at the South Pole. Deployment can be done by a robotic arm or a dedicated unfoldable boom. Such a system weighs approximately 2 [kg] and is capable of a 3 [m] deployment distance [73].

The masses of the complete mole system and of a dual-mole system are 1.8 [kg] and 3.4 [kg] both, respectively [73]. Maximum power consumption occurs during the hammering phase - 12.2 [W] and minimum during the monitoring phase - 3.4 [W]. The data rates are quite low: 27.8 [bit/s] during hammering and 2.22 [bit/s] during thermal conductivity measurements and monitoring [73]. The technological readiness level (TRL) of the heat flow probe is 5-6 and the cost is roughly 11 [€M] [73].

#### MULTI PURPOSE SENSOR PACKAGE (MUPUS)

The MUPUS package was specifically designed for the Rosetta lander Philae [74]. It measures the physical parameters in the near-surface layers. It consists of a penetrator with its subsystems, the radiometer and the anchor sensors.

The main electronics are integrated into the common electronics box on the lander [74]. The main scientific objectives of MUPUS are to understand the energy balance at the surface and its variation with time and depth and to investigate the mass flow at the surface and its evolution with time.

The most complex instrument in the MUPUS package is the thermal probe (penetrator). The thermal probe being a hollow rod of 35 [cm] length needs to be placed outside of the lander's shadow. The penetrator will be inserted 30 [cm] into the ground about 1.5 [m] away from the lander by a deployment arm and an electromagnetic hammering mechanism. The penetrator is equipped with a depth sensor, thermal sensors that measure the temperature profile and a thermal diffusivity/conductivity profile [74].

The total mass, volume and the power consumption (including electronics) of the whole package are 2.35 [kg], 565 x 160 x 188 [mm], 2.2 [W], respectively [74]. Table 18.1 shows the mass and power of the MUPUS package.

#### ELECTROMAGNETIC SOUNDER

The EMS instrument uses high-heritage electric and magnetic field sensors. The EMS developed by the Southwest Research Institute (US) and the University of California, Berkeley (US) consists of the sensors designed to survive the full lunar temperature range and are heated by their own power dissipation [73]. Electromagnetic sounding experiments of the Moon were performed during the Apollo program and provided constraints on core size, mantle composition, and interior temperature.

EMS technical characteristics are: mass of 7.4-8.6 [kg] (depending on number of electrodes), power consumption of 4.0 [W], cost of 15 [€M] and data rate of 431.58 [bit/s]. The TRL of this instrument is a 6 [73].

#### LANGMUIR PROBE

Langmuir probe is a simple flight proven instrument for measuring plasma parameters. It consists of one or more voltage-biased electrodes placed in the plasma bulk. Depending on the number of electrodes, Langmuir probes can be subdivided in four categories: single, double, triple and quadruple probes. A Langmuir probe is mounted directly on the lander.

Plasma measurements have never been done before on the lunar surface and could explain an important part of the lunar environment. The electric fields can affect the behavior of instruments and equipment, and may cause charged dust to rise from the surface [75].

The mass, power consumption and data rate of such an instrument are approximately 5 [kg], 4 [W] [76] and 0.256 [bps] NASA<sup>1</sup>, respectively. Table 18.1 lists the mass and power.

Instrument	Mass [kg]	Power [W]	Cost [€M]	Data rate [bit/s]	TRL
Seismometer	7.4-8.4	2.60	30	2471.75	5-6
Heat flow probe	1.8-3.4	12.20	11	27.8	5-6
MUPUS	2.83	2.64	NA	50	NA
EMS	7.4-8.6	4.00	15	431.58	6
Langmuir probe	6	4.80	NA	0.256	NA

Table 18.1: Scientific instrument properties [73],[74], [77]

## 18.2. ADDITIONAL INSTRUMENTS TRADE-OFF

The following Table 18.2 shows the criteria chosen to trade-off different options as well as weights given to those criteria (5 - most important, 1 - least important). Also it shows the scores of each instrument (5 - the best, 1 - the worst). Combinations of instruments will be considered as well.

Instruments are only allocated 20% of the payload mass budget and so mass is the most important criteria with a weight of 5. The deployment of an instrument can add substantial mass and cost and so it is given a weight of 4. Additional instruments have to operate within the satellite's limited power budget and so power consumption has been given a weight of 3. Each instrument measures a particular science and it is hard to tell which one is more important than the other. Therefore, higher scores are given to the instruments that have not yet been operational on the Moon. Also the trade space model [78, pp. 55-57] is taken into account when allocating scores. Almost all instruments are flight proven designs and so TRL is given a score of 1.

<sup>1</sup><http://nssdc.gsfc.nasa.gov/nmc/experimentDisplay.do?id=1981-070B-09>

	Mass	Power	TRL	Complexity	Science	
Weight	5	3	1	4	2	Total
Seismometer	2	5	5	2	1	40
Heat flow probe	5	1	5	2	2	45
MUPUS	4	4	3	1	5	49
EMS	1	3	5	2	2	31
Langmuir probe	3	2	3	5	5	54

Table 18.2: Trade-off scores for additional scientific instruments

As can be seen from the trade-off, the instrument that suits the mission best is a Langmuir probe. The major advantage is the simplicity of deployment - it will be mounted directly on the lander, so no additional deployment mechanism is needed.

### 18.3. REQUIRED FINANCIAL CONTRIBUTION

A more detailed market analysis involving contact with different companies and educational institutions will reveal their interest in supporting the LOFARside mission. The instruments of the previous section, specifically the Langmuir probe are DSA's preferred secondary payload so efforts will be focused on finding partners for these. However, other instruments/payloads are also allowed. So, the types and number of instruments that will be taken as an additional payload will strictly depend on the companies who are willing to pay for those. Approximately 2 [€M]<sup>2</sup> per kilogram will be charged for piggyback payloads. In total the 30 [kg] of mass budget can be sold to interested companies for 60 [€M]. Additional market analysis is required to determine the extent to which companies are interested, or able to contribute to the mission.

<sup>2</sup>Estimated based on a discussion with Daphne Stam, who is basing her assumptions on personal communication with Arno Wielders (ESA and Mars One)

## SUSTAINABLE DEVELOPMENT STRATEGY

In this chapter the sustainable project management approach (Section 19.1), implications on economic and social development (Section 19.2) and design choices (Section 19.3) related to sustainability are described.

### 19.1. SUSTAINABLE PROJECT MANAGEMENT

Three main principles of sustainable mission design are the use of low-impact materials, ensuring energy efficiency, and design for reuse and recycling.

The Delft Space Agency (DSA) strives to use technology with a Technology Readiness Level (TRL) of at least 5-6, and to use off-the-shelf technology. This prevents large spending on development costs, duplication of efforts and through batch production production costs are reduced. However, it should be noted that using only off-the-shelf readily implementable technology might not lead to the most optimum configuration. For example, state of the art high-efficiency solar panels are not mass produced, and might require some additional development efforts. But using these panels will reduce the required solar array area and so reduce the spacecraft's mass and costs. Similarly, the chemical fuel used for orbit insertion at the moon is Monomethylhydrazine (MMH) which is toxic and carcinogenic in small amounts. However, it provides moderate performance for very low fuel tank system weight. From production and development efforts to launch and mission operations the energy efficiency of the spacecraft (S/C) should be maximized. The energy used by the S/C itself should be optimal so the total power needed for the mission is minimized. Effective project management, process optimization and adherence to time and cost budgets are required to ensure the project is completed effectively. Reuse and recycling of the satellite itself is difficult, since returning it to Earth will actually costs extra resources. The radar array could be upgraded to be used for future missions. The part of the S/C that is not landed on the surface of the moon will be disposed of by means of a controlled crash. The possibility of gathering scientific data from this crash, for example by observing the debris that is hurled across the surface, or by looking for water vapour if it is crashed into a crater should be investigated in more detailed design.

### 19.2. ECONOMIC & SOCIAL DEVELOPMENT

Space exploration has been a catalyst for the development of renewable energy technologies and therefore has directly contributed to sustainable economic development. Mankind's knowledge and understanding of the Universe has expanded tremendously due to scientific missions which explore the Universe. The technologies developed for space exploration stimulate economic growth. All technology used in the design and later in the production of the satellite will be provided by European companies, therefore contributing to the European Space Program. The project management of the DSA focus on reducing mission costs and material usage so as to use resources efficiently as well as responsibly. Cost estimations for the conceptual configuration were derived and presented in Section 17.2.1. Project management will implement financial control strategies to use funds effectively.

Social development in the context of space exploration is related to scientific advancements and educational opportunities as well as corporate social responsibility. Taking on secondary scientific payload, which could be provided by other space related companies or institutes, will increase the scientific contribution of the mission. Moreover, further development of the mission could provide opportunities for collaboration with educational institutes. Social corporate responsibility is related to treatment of employees, their wages, job opportunities etc. Developing the LO-FARside mission will unlikely lead to the creation of new jobs, since there is a limited European budget for scientific missions. Furthermore, social security, welfare and employee rights within Europe are at regulated standards. However, project management should ensure that, in the case of outsourcing the production of certain parts or buying off the shelf technology produced in developing countries, that working conditions are acceptable.

### 19.3. SUSTAINABLE DESIGN CHOICES

This section contains the design choices that were influenced by sustainability. Where possible, sustainability was included as a criterion for trade-offs. The transfer orbit and electrical propulsion system were chosen to maximize the mass in lunar parking orbit. Similarly, the landing procedure was optimized to maximize the payload mass on the lunar surface. This demonstrates the energy efficiency of the mission, since high thrust trajectories and different propulsion methods require a different launcher and thus lead to higher launch costs. Also, the same ADCS and thermal control system are used to control the transfer orbiter and the lander to prevent carrying duplicate subsystems. The transfer orbiter is disposed of by means of a controlled crash, which can be used to do scientific research. The lander does not carry sufficient solar panels and batteries to last the longest eclipse periods it will experience, because it would be over-designed for the rest of the lifetime. A bit of operational time is sacrificed to prevent ineffective use of resources. The lander can also be used as a beacon for future missions to assist their landing procedure. The precision of the landing using terrain relative navigation in combination with other sensors has never been achieved before, and will help increase the TRL of this technology so it can be used for future manned missions to the Moon.

The radar array on the lunar surface can be upgraded with subsequent missions, so parts of it could be reused. The Shackleton crater is an extremely favourable spot for multiple moon missions, or possibly even a lunar base. The rover is capable of retracting the radar array at the end of the mission lifetime so that the area is kept as clean as possible. Apart from this, the LOFARside mission will function as a kind of pathfinder mission to explore the possibilities of conducting low frequency and very low frequency radio astronomy on the far side of the moon. Studies of subsurface reflections of radiation off the regolith, the effects of lunar dust and studies of the properties of the surface layer of moon material will contribute greatly to Moon science in general, and to the construction of a future very large radar array in particular. Moreover, companies and educational institutions are offered the possibility to piggyback their own instruments in return for funding, which increases the scientific value of the mission, and contributes to social development.

## CONCLUSIONS AND RECOMMENDATIONS

The purpose of this report is to present the design of the subsystems of the mission concept to place a LOw Frequency ARray (LOFAR) on the far side of the moon. The design options that were chosen through trade-offs at the midterm level are analyzed and worked out in detail. It is essentially a feasibility study of the chosen mission concept. In this chapter, conclusions (Section 20.1) related to the completion of the project, evaluations of the top-level requirements (Section 20.2) and recommendations (Section 20.3) on future work are detailed.

### 20.1. CONCLUSIONS

The goal of the project is to show that it is possible to place a LOFAR system on the far side of the Moon with a budget of 500 [M€]. The mission concept described in this report demonstrates this.

The satellite will be launched using ESA's VEGA-C launcher. The structural subsystem is designed to withstand launch loads and vibrations while complying with the specified frequency domain. After launch the satellite will use an electrical propulsion system to spiral out from its 300 [km] low earth orbit with inclination of 16.7° with the Earth's equator. 46 [m<sup>2</sup>] solar panels will provide the system with power during the transfer. Active and passive thermal control systems will regulate the temperature within the spacecraft and 8 reaction wheels and 16 chemical thrusters will control its orientation. During the transfer phase two helical antennas mounted on opposite sides of the body will provide continuous communications with Ground Control. Using a chemical thruster the satellite will be inserted into a lunar orbit, where it will spiral down with low thrust propulsion to a polar orbit at 100 [km]. The lander will decouple from the transfer orbiter, which will be crashed in a controlled manner on the Moon. The lander will land on the rim of the Shackleton crater at the south pole of the Moon with a very high accuracy of 100 by 100 [m] using chemical propulsion. This accuracy is achieved using terrain relative navigation in combination with multiple sensors. Landing struts designed for a drop from 3 [m] will be deployed for landing. The lander, situated at a position of almost continuous illumination and visibility with Earth, will deploy a tethered rover based on NASA's Axel rover design that will descend into the crater's eternal darkness. It will deploy 10 [km] of cable and 21 antennas over unequal distances powered by the lander's solar panels of 6.9 [m<sup>2</sup>]. Using a thermal knife the crossed dipole antennas will deploy and after calibration can start their surveys. The data gathered will be used through radar interferometry and aperture synthesis to create a virtual radar array with a baseline of 10 [km]. The data will be sent via a direct radar communications link to Earth for processing and analysis. A high-gain parabolic antenna with a diameter of 0.7 [m] operating in X-band will be used for the downlink data transmission of 84 [Mbit/s]. Uplink transmission for commands will be received using a helical antenna with a 0.055 [m] diameter and 0.1 [m] length operating in S-band.

Cost analysis has indicated that the project can be completed within the budget. A market analysis has shown that up to 60 [M€] could be supplied by companies and educational institutions in return for taking their instruments to the Moon. Risk management procedures have mitigated most risks, and additional mitigation procedures have been assigned to the remaining risks. A performance analysis has proved the system's compliance with almost all requirements. The system has some single point of failures, but high reliability components are used in these cases. Furthermore, the mass of the design at this moment exceeds the mass limit of the VEGA launcher. Further design iterations can reduce the mass, e.g. the structure of the satellite is overdesigned in size. Any mass savings lead to less required fuel mass, so additional mass is saved. In the case that the mass does not decrease sufficiently, it is possible to use the VEGA C launcher, which provides 15% more performance. Some design options have not been considered because they simply were not allowed (nuclear technologies) or because information was unavailable (laser communication). The analysis of different design options was subject to time constraints and the information available and as such it is possible that the solution presented is not the most optimum. The integration of the different subsystems in the configuration of the satellite requires optimization with respect to the respective positions of the subsystems, cabling and production and assembly methods. Sustainable development has been implemented in trade-offs where possible, a sustainable project development approach is presented and contributions to social and economic development are indicated. Again, time constraints prevented a more thorough analysis in the form

of a life cycle assessment.

## 20.2. EVALUATION OF TOP LEVEL REQUIREMENTS

In this section an evaluation of the effect of the top-level requirements on the mission's feasibility is given.

The required use of the VEGA launcher had implications on the mass budget, the starting orbit and the project budget. VEGA Launch costs (approx. 30 [M€]) are significantly lower than e.g. Ariane V launch costs (150 [M€]). In relation with the mission budget of 500 [M€] this is a logical choice of launcher. However, it resulted in a limited mass budget (approx. 2300 [kg] in Low Earth Orbit (LEO)) and the restriction to a LEO starting orbit. The use of an electrical propulsion system, as was preferred by the client, means that the satellite spirals out towards the Moon through the Van Allen belts. These are a cloud of ionizing radiation trapped by the Earth's magnetic field which causes a degradation of the solar panels of 20%. If the satellite is launched into a Geostationary Transfer Orbit (GTO) a large part of the Van Allen belts can be skipped and less thrust is required to stay within the 1 year transfer time requirement. This would lead to a reduction in size of the solar panels and so save mass and volume. Similarly, a longer transfer time would also result in mass and volume savings due to less required thrust. However, the effect of prolonged exposure to the ionizing radiation of the Van Allen belts on spacecraft systems is not very well known. A shared Ariane V (or Ariane 6 depending on launch time) launch into GTO is therefore recommended.

It is preferred by the client to make use of European manufacturers only. In some cases this lead to the choice of a suboptimal component, e.g. US electrical propulsion systems are more advanced than European ones, however this was not a large constraint on the mission design.

It was difficult to establish the scientific requirements, because different combinations of baseline and number of antennas are best suited for different science topic. Discussions with experts at first yielded different opinions, but a consensus was finally reached. Some time budget was spent on research into radar astronomy and these discussions, however.

The missions operation lifetime was required to be at least 5 years. The main science goals (21cm Cosmology and Extra-galactic surveys) can be achieved within 9 months, however. The client H. Crujssen estimated ground control segment costs at 10-15 [M€] so with respect to budget constraints a trade-off between scientific gains of the 5 year lifetime and financial costs could be considered. Solar panel degradation and battery efficiency loss over the 4 years do not drive the power system so in that respect no additional mass and power budget costs are incurred.

## 20.3. RECOMMENDATIONS ON FUTURE WORK

Recommendations on future work per subsystem and on the extension of the low frequency radar array are presented in this section.

### Orbit design

A more advanced model of the electrical propulsion orbit can be developed by including more precise propagators (ways to integrate orbit parameters), improving the Earth and Moon gravity models and by improving disturbance factor modelling (solar pressure, LEO drag). Also, the low thrust orbit could be modelled such that no chemical insertion into a Moon orbit is required which further reduces fuel mass.

### Landing procedure

The landing procedure needs to be integrated with new software for Terrain Relative Navigation (TRN) and hazard detection and avoidance. Algorithms like crater pattern matching and structure from motion could be tested in Unmanned Aerial Vehicles (UAVs) and simulations.

### Propulsion

Future work on the electrical propulsion system could be finding other manufacturers and the newest developments. The exact integration of the engine and fuel tank in the satellite configuration needs to be designed. If the thrust required can be reduced by changing the orbit, or the transfer time, then for the same power higher efficiencies can be achieved by selecting higher specific impulse engines.

The fuel mass estimate for the chemical propulsion system can be improved by using an algorithm that calculates the optimum trajectory based on the position of the satellite.

### Power

The cover glass thickness for the solar panels during the transfer phase needs to be established. The point where adding more cover glass adds more mass than the reduction in degradation saves on solar panel weight needs to be

calculated. The type of solar cells used should be optimized for 1 [MeV] fluence to more accurately determine the degradation.

The illumination periods and the peaks surrounding the landing terrain should be analyzed exactly to size the solar panels and batteries more accurately. The body mounted solar panels must be protected from degradation due to exposure to space and the Van Allen Belts by a mechanism that can unfold like a flower. The use of electrostatic and di-electrophoretic systems to actively remove dust and stop dust accumulation is recommended.

The mass estimation of the solar array used on the Moon includes shielding for the backside of the panels and a thick coverglass. However, the panels are attached to the body of the lander so shielding is not required and the actual radiation on the Moon is lower than during the transfer phase. The mass might be reduced by as much as 25% if these effects are considered.

The incidence angle for the solar cells on the Noor lander should be evaluated for the case when the Noor lander will land on a slope. The steepest slope on which the Noor lander will land is 15°. The solar radiation incident angle should be evaluated in more detail for such a situation.

### Telecommunication

Radar communication was chosen because of a lack of information about laser communication. It is recommended to find the price of the laser system and conduct the trade-off again. During the transfer phase the interference of the spacecraft body with antenna pattern and the interference of two antenna patterns should be analyzed. Also the effect of the lunar regolith on the data transmission should be established.

### Command & Data handling

Based on requirements for a C&DH system software needs to be developed.

### Attitude Determination & Control System

The equations of motion can be expanded to develop a more detailed model. Controllers need to be chosen for control loops, which need to be designed for gains. Further requirements for mission modes, e.g. accuracies along the body axes, need to be formulated and control for nutation needs to be implemented.

### Transfer Guidance & Navigation

The software that produces the guidance and navigation signals that are sent to the satellite needs to be developed.

### Deployment & Rover Design

How the antennas are connected to the cable and the tether spool is rolled up needs to be tested and the reliability of this established. Alternatively, a film antenna might be easier to deploy and should be considered as well. Including sinkage models and obstacle traversal can give a more detailed view of the power budget. What obstacles can be expected in the crater should be analyzed based on comparable lunar craters. Besides this, it is recommended to test the tether of the cable in a field test with obstacles to ensure its ruggedness and tensile strength.

### Thermal Control

Future work on the thermal control system includes going beyond a black box mode. An internal view model to establish the heat conduction within the spacecraft and the local heat distribution should be made to distribute heat pipes and local heating systems.

### Structures

The structural mass of the S/C takes approximately 7% of the total lift-off mass, whereas SMAD [3] estimates it to be 12%. The reason for such a difference in numbers is due to the simplifications made in the calculations. For instance, for vibrational analysis the structure of the S/C was modeled as an undamped mass-spring system to be able to use equations taught in course AE2135-II to investigate vibrations. DSA is however aware of the fact that this assumption might lead to rather lighter structure than actually needed, hence the recommendation in the next design phase to account for these assumptions. Also, the configuration should be optimized with respect to the respective positions of the subsystems, cabling and production and assembly methods. More detailed drawings and cross-sections are required for this.

The analysis of loads and stresses should be performed using Finite-Element methods to optimize and size the structure accordingly. An analysis of shocks during the different mission phases, transportation loads and their effect on the structure should be included.

### Ground Control Segment

Ground control requirements based on the Operations & Logistics concept description need to be set. On the basis of these, the Ground Control segment can be designed and a specific ground control station and equipment can be chosen.

### Cost analysis

As design detail progresses, a bottom to top approach for cost modelling is heavily recommended. Also the detail of the top to bottom cost modelling tools employed can be increased accordingly. Furthermore, a estimation for the cost spread over the development years should be made. Critical cost drivers should be identified and their sensitivity to changes in key system parameters must be analyzed. Financial risks should be assessed and mitigated as part of the overall risk management.

### Risk analysis

Calculating probabilities of failures at system and subsystem level enables a more detailed risk management. As design detail progresses, subsystem level risk events need to be assessed and mitigated. Risk management should ensure that risks are assessed continuously and new risks are identified quickly to prevent unmitigated risk items from failing.

### Market analysis

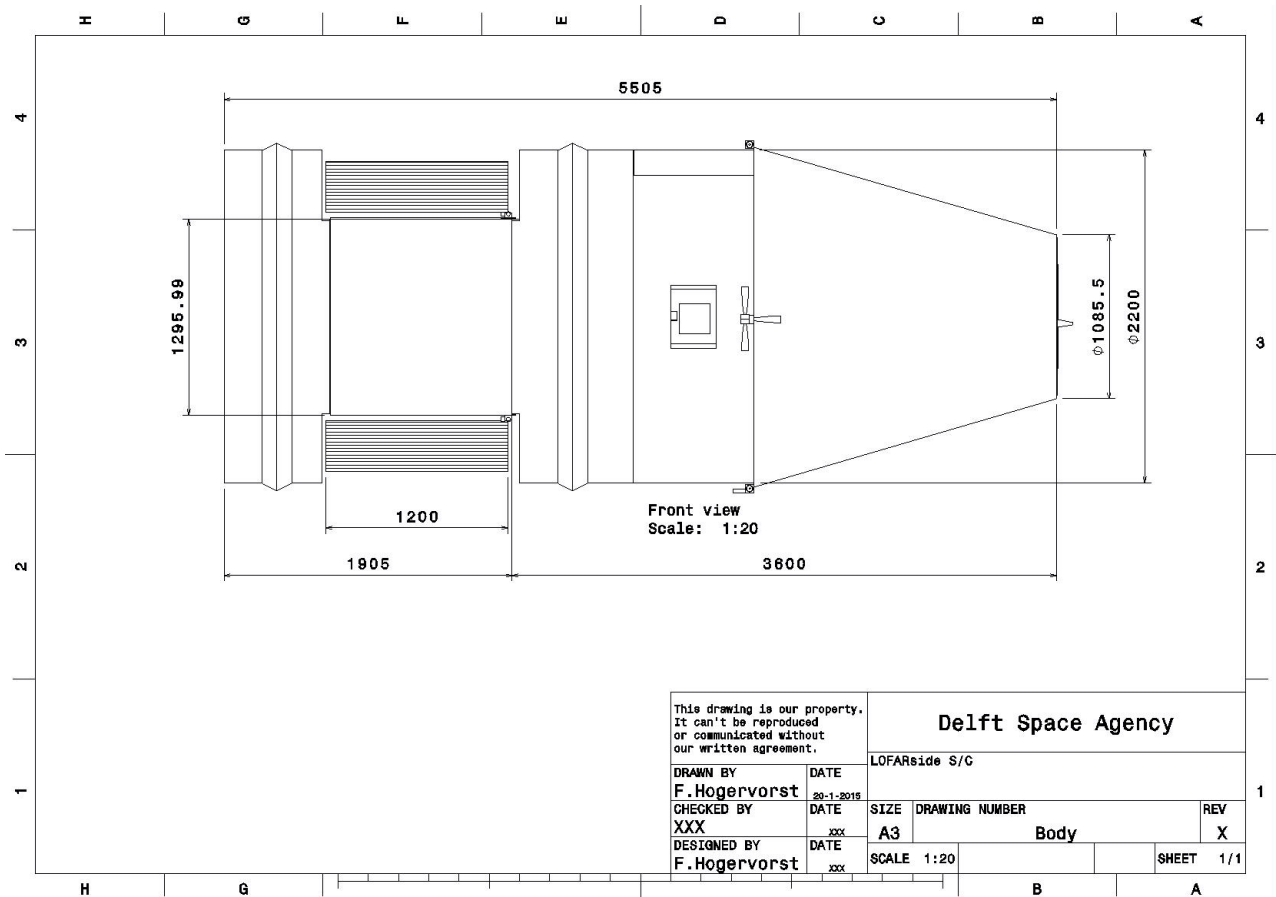
It is recommended to gauge industry interest and find companies/educational institutions willing to contribute additional instruments in return for funding. The Langmuir probe and MUPUS package should have a priority in this search, but companies can also contribute their own scientific payload. Implementation of these payloads into overall mass and power budgets must be done, as well as their compliance with the requirements ensured.

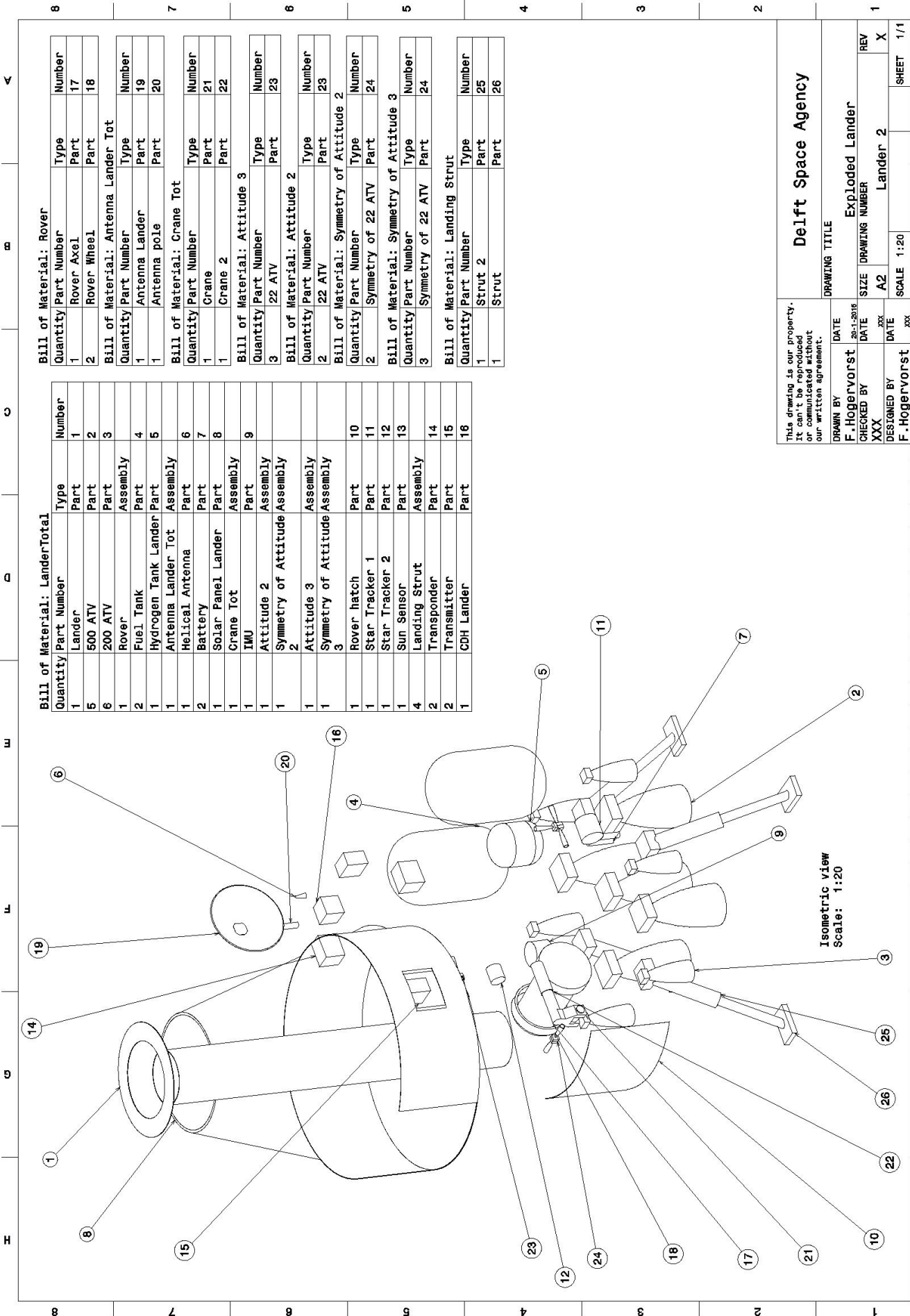
### Extension of LOFAR & Future Missions

There is a large scientific interest in conducting low frequency radio astronomy on the far side of the moon. An extension of the array by baselines up to 100 [km] and  $10^4$  to  $10^6$  antennas is required to observe scientific topics like exoplanets and the dark ages signal in detail [5]. Additional science conducted by the LOFARside mission will serve as a basis for such an extension.

# A

## CONFIGURATION





**Bill of Material: LanderTotal**

Quantity	Part Number	Type	Number
1	Lander	Part	1
5	500 ATV	Part	2
6	200 ATV	Part	3
1	Rover	Assembly	4
2	Fuel Tank	Part	5
1	Hydrogen Tank Lander	Part	6
1	Antenna Lander Tot	Assembly	7
1	Helical Antenna	Part	8
2	Battery	Part	9
1	Solar Panel Lander	Part	10
1	Crane Tot	Assembly	11
1	IMU	Part	12
1	Attitude 2	Assembly	13
1	Symmetry of Attitude Assembly 2	Assembly	14
1	Attitude 3	Assembly	15
1	Symmetry of Attitude Assembly 3	Assembly	16
1	Rover hatch	Part	17
1	Star Tracker 1	Part	18
1	Star Tracker 2	Part	19
1	Sun Sensor	Part	20
4	Landing Strut	Assembly	21
2	Transponder	Part	22
2	Transmitter	Part	23
1	CDH Lander	Part	24

**Bill of Material: Rover**

Quantity	Part Number	Type	Number
1	Rover Axle	Part	17
2	Rover Wheel	Part	18

**Bill of Material: Antenna Lander Tot**

Quantity	Part Number	Type	Number
1	Antenna Lander	Part	19
1	Antenna pole	Part	20

**Bill of Material: Crane Tot**

Quantity	Part Number	Type	Number
1	Crane	Part	21
1	Crane 2	Part	22

**Bill of Material: Attitude 3**

Quantity	Part Number	Type	Number
3	22 ATV	Part	23

**Bill of Material: Attitude 2**

Quantity	Part Number	Type	Number
2	22 ATV	Part	23

**Bill of Material: Symmetry of Attitude 2**

Quantity	Part Number	Type	Number
2	Symmetry of 22 ATV	Part	24

**Bill of Material: Symmetry of Attitude 3**

Quantity	Part Number	Type	Number
3	Symmetry of 22 ATV	Part	24

**Bill of Material: Landing Strut**

Quantity	Part Number	Type	Number
1	Strut 2	Part	25
1	Strut	Part	26

This drawing is our property. It shall be reproduced or communicated without our written agreement.

**Delift Space Agency**

**DRAWING TITLE**  
Exploded Lander

**DRAWN BY**  
F. Hogervorst

**CHECKED BY**  
XXX

**DESIGNED BY**  
F. Hogervorst

**DATE**  
20-1-2016

**DATE**  
2016

**DATE**  
2016

**SIZE**  
A2

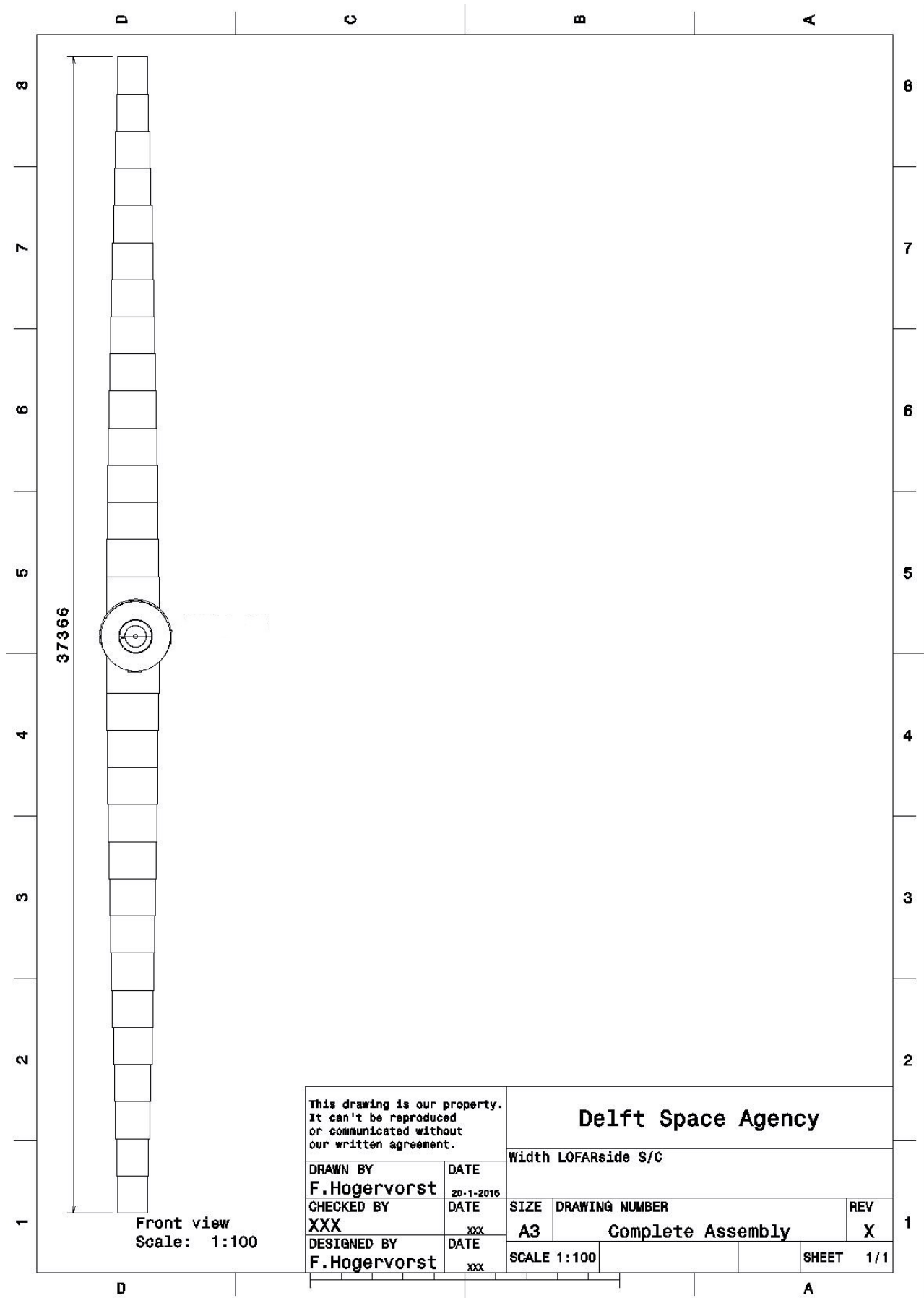
**DRAWING NUMBER**  
Lander 2

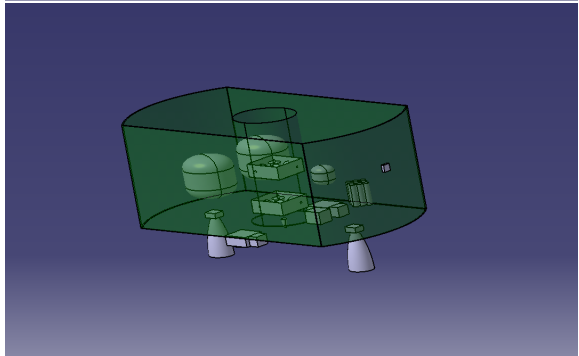
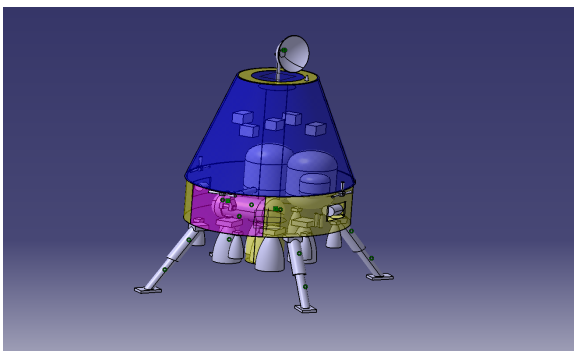
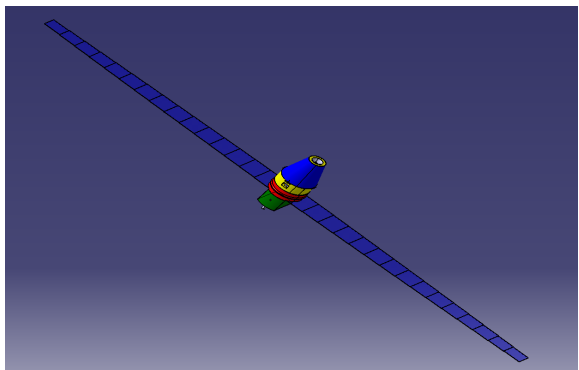
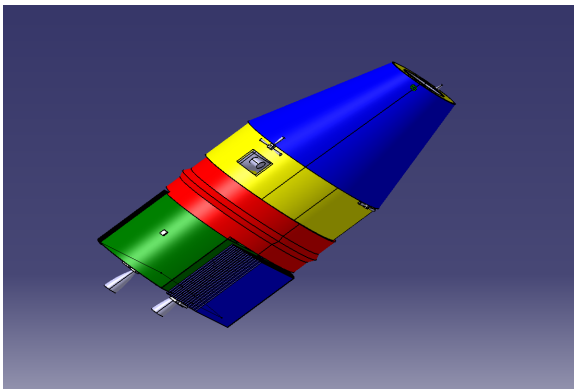
**SCALE**  
1:20

**REV**  
X

**SHEET**  
1/1

Isometric view  
Scale: 1:20







# BIBLIOGRAPHY

- [1] K. Bossenbroek *et al.*, *LOFAR on the far side of the Moon*, (2014), Baseline Report.
- [2] E. Perez, *VEGA User's Manual*, Arianespace, Évry-Courcouronnes (2006).
- [3] W. J. Larson and J. R. Wertz, *Space Mission Analysis And Design*, 8th ed. (Microcosm Press-Springer, New York, 1999).
- [4] R. Roncoli, *Lunar Constants and Models Document* (Jet Propulsion Laboratory, Pasadena, USA, 2005).
- [5] H. F. S. Jester, *Science with a lunar low-frequency array: From the dark ages of the universe to nearby exoplanets*, (2008).
- [6] L. Chen, *Design and study on moon-based very low frequency radio interferometer*, (2011), master thesis.
- [7] K. Bossenbroek *et al.*, *LOFAR on the far side of the Moon*, (2014), Midterm Report.
- [8] P. Abad-Manterola, *Axel rover tethered dynamics and motion planning on extreme planetary terrain*, (2012), PhD Thesis.
- [9] S. P. Hughes *et al.*, *Verification and Validation of General Mission Analysis TOol (GMAT)*, AIAA (2013).
- [10] R. H. Qureshi *et al.*, *Preparing General Mission Analysis Tool for Operational Maneuver Planning of the Advanced Composition Explorer Mission*, AIAA (2013).
- [11] D. D. Rosa *et al.*, *Characterisation of potential landing sites for the european space agency's lunar lander project*, Planetary and Space Science **74** (2012).
- [12] A. E. Johnson and J. F. Montgomery, *Overview of Terrain Relative Navigation Approaches for Precise Lunar Landing*, IEEEAC paper **1657** (2008).
- [13] J. Freeh, *Analysis of stationary, photovoltaic-based surface power system designs at the lunar south pole*, AIAA (2008).
- [14] D. B. J. Bussey *et al.*, *Illumination conditions of the south pole of the Moon derived using Kaguya topography*, Icarus (2010).
- [15] J. Fincannon, *Lunar south pole illumination: Review, reassessment, and power system implications*, AIAA (2007).
- [16] A. I. Kozynchenko, *Enhancing the manoeuvring capabilities of a lunar landing module using predictive guidance algorithms*. Acta Astronautica (2010).
- [17] A. M. Hawkins, *Constrained Trajectory Optimization of a Soft Lunar Landing from a Parking Orbit*, Tech. Rep. (2005).
- [18] B. Cohanin *et al.*, *Approach phase  $\delta v$  considerations for lunar landings*, (2014), technical report.
- [19] A. Bedford and W. Fowler, *Dynamics, Engineering Mechanics.*, si ed., edited by E. Morris (Addison-Wesley, Massachusetts, USA, 1987).
- [20] M. Riehle *et al.*, *Propulsion System for the European Lunar Lander - Development Status and Breadboarding Activities*, .
- [21] N. Feizal *et al.*, *Design of Nitrogen-Tetroxide/Monomethylhydrazine Thruster For Upper Stage Application*, .
- [22] M. Mureşan, *Soft landing on the Moon with Mathematica*, The Mathematica Journal (2012).
- [23] J. Marichalar *et al.*, *Study of Plume Impingement Effects in the Lunar Lander Environment*. (2009).
- [24] G. Racca *et al.*, *SMART-1 Mission Description and Development Status*, Planetary and Space Science **50** (2002).
- [25] W. J. Larson *et al.*, *Space Mission Engineering: The New SMAD*, 1st ed. (Microcosm Press, Hawthorne, CA, 2011).
- [26] A. Hyder *et al.*, *Spacecraft Power Technologies*, 1st ed. (Imperial College Press, London, United Kingdom, 2000).

- [27] M. R. Patel, *Spacecraft Power Systems*, 1st ed. (CRC Press, Boca Raton, Florida, 2005).
- [28] N. Yu Ganushkina *et al.*, *Locations of boundaries of outer and inner radiation belts as observed by Cluster and Double Star*, *Journal of Geophysical Research* **116** (2011).
- [29] C. R. Bos, *Conceptual System Design of a Solar Electric Propulsion Stage for Earth-Moon Cargo Transfer Missions*, (2013), MSc. Thesis.
- [30] J. Carpenter *et al.*, *Life sciences investigations for esa's first lunar lander*, *Earth Moon Planets* (2010).
- [31] J. Schneider *et al.*, *Qualification Test Report of 3G30C-Advanced Bare Solar Cell*, Azur Space (2012).
- [32] W. Larson *et al.*, *Human Spaceflight*, 1st ed., edited by M. Hollander (McGraw-Hill, 1999).
- [33] J. Fincannon, *Characterization of lunar polar illumination from a power system perspective*, AIAA (2008).
- [34] C. Calle *et al.*, *Active dust control and mitigation technology for lunar and martian exploration*, *Acta Astronautica* (2011).
- [35] C. Calle *et al.*, *Particle removal by electrostatic and dielectrophoretic forces for dust control during lunar exploration missions*, *Journal of Electrostatics* (2009).
- [36] G. He *et al.*, *Review of self-cleaning method for solar cell array*, *Precedia Engineering* (2011).
- [37] M. Kruglanski *et al.*, *Space Environment Information System (SPENVIS)*, Belgian Institute for Space Aeronomy and ESA/ESTEC (2010).
- [38] R. Fisackerly *et al.*, *The ESA Lunar Lander Mission*, AIAA (2010).
- [39] M. McGuire *et al.*, *COMPASS Final Report: Low Cost Robotic Lunar Lander*, NASA/TM (2010).
- [40] P. Fortescue *et al.*, *Spacecraft Systems Engineering*, fourth. ed. (Wiley, Croydon, United Kingdom, 2011).
- [41] J. R. Wertz *et al.*, *Spacecraft Attitude Determination And Control*, i ed., edited by J. R. Wertz (D. Reidel Publishing Company, USA, 1978).
- [42] R. Dybdal, *Communication Satellite Antennas* (McGraw Hill, New York City, USA, 2009).
- [43] Boeing, *Goes N data book* (Boeing Satellite Development Center, 2006).
- [44] G. Maral and M. Bousquet, *Satellite Communication Systems*, 5th ed. (Wiley, Chichester, West-Sussex, 2002).
- [45] NICT, *International workshop on ground-to-orbits laser communications experiments golce*, (2010).
- [46] B. L. Edwards *et al.*, *Overview of the laser communications relay demonstration project*, MIT Lincoln Laboratory (2012).
- [47] *Decanso desing and performance summary series article 3: Cassini orbiter/huygens probe telecommunications*, .
- [48] B. Zandbergen, *AE1222-II Aerospace Desing & Systems Engineering, Part: Spacecraft (bus) design and sizing* (TU Delft, Delft, The Netherlands, 2011).
- [49] A. Cruise *et al.*, *Principles of Space Instrument Design* (Cambridge Press University, Cambridge, New York, 2006).
- [50] Q. Nguyen *et al.*, *High*, American Institute of Aeronautics and Astronautics (2008).
- [51] G. Chin *et al.*, *Lunar Reconnaissance Orbiter Overview: The Instrument Suite and Mission*, *Space Science Reviews* **129**, pp 391 (2007).
- [52] A. Wehr and U. Lohr, *Airborne laser scanning—an introduction and overview*, *ISPRS Journal of Photogrammetry and Remote Sensing* **54**, pp 68–82 (1999).
- [53] M. Mammarella *et al.*, *Advances in Aerospace Guidance, Navigation and Control*, 1st ed., edited by F. Holzapfel (Springer Berlin Heidelberg, 2011).
- [54] *Velodyne lidar system*, Last access: 09 January 2015.
- [55] I. A. Nesnas *et al.*, *Axel and DuAxel Rovers for the Sustainable Exploration of Extreme Terrains*, *Journal of Field Robotics* (2012).

- [56] M. T. Zuber *et al.*, *Constraints on the volatile distribution within Shackleton crater at the lunar south pole*, Nature (2012).
- [57] M. B. Ruggles-Wrenn, *Effects of temperature and environment on mechanical properties of two continuous carbon-fiber automotive structural composites*, US Department of Energy .
- [58] J. Lazio *et al.*, *The Lunar Radio Array (LRA)*, LUNAR Consortium .
- [59] P. G. Xavier, *Shortest Path Planning for a Tethered Robot or an Anchored Cable*, International Conference on Robotics & Automation (1999).
- [60] B. Aldrin *et al.*, *The Lunar Base Handbook*, 2nd ed., edited by P. Eckhart (The McGraw-Hill Companies, New York, 2006).
- [61] J. Haruyama and others., *Lack of Exposed Ice Inside Lunar South Pole Shackleton Crater*, Science **332** pp **938-939** (2008).
- [62] Warren and Rasmussen, *Megaregolith insulation, internal temperatures, and bulk uranium content of the moon*. (Journal of Geophysical Research, Washington, USA, 1987).
- [63] Simonsen *et al.*, *Concepts and Strategies for Luner Base Radiation Protection* (SAE Paper 921370, USA, 1992).
- [64] BALSEAL, *Coefficient of thermal expansion for various materials at different temperatures*, (2004), technical report.
- [65] A. Calvi *et al.*, *Spacecraft Loads Analysis* ([http://www.ltas-vis.ulg.ac.be/cmsms/uploads/File/CALVI\\_Students\\_LIEGE\\_2011\\_6.pdf](http://www.ltas-vis.ulg.ac.be/cmsms/uploads/File/CALVI_Students_LIEGE_2011_6.pdf)), (2014), Last access: 13 December 2014.
- [66] B. Parreira *et al.*, *Hazard Detection and Avoidance in ESA Lunar Lander: Concept and Performance* , AIAA Guidance, Navigation, and Control (GNC) Conference (2013).
- [67] ESA, *Space Project Management: Project Planning and Implementation* (European Cooperation for Space Standardization, 2007).
- [68] National Aeronautics and Space Administration (NASA), *NASA Systems Engineering Handbook* (NASA Headquarters, Washington D.C., 2007).
- [69] D. Koelle, *Handbook of Cost Engineering for Space Transportation Systems with TRANSCOST 7.0* (TCSTransCost-Systems, OttoBrunn, Germany, 2000).
- [70] J. Wertz and W. Larson, *Reducing Space Mission Cost* (Microcosm Press, Torrance, USA, 1996).
- [71] C. M. Katzen *et al.*, *Lunar Dust Transport and Potential Interactions With Power System Components*, NASA contractor report (1991).
- [72] M. K. Wolt *et al.*, *A White paper for a low-frequency radio interferometer mission to explore the cosmological Dark Ages for the L2, L3 ESA Cosmis Vision program*, Tech. Rep. (Nijmegen, The Netherlands, 2013).
- [73] D. Mimoun *et al.*, *Farside explorer: Unique science from the farside of the moon*, (2011), proposal.
- [74] T. Spohn *et al.*, *Mupus – a thermal and mechanical properties probe for tge rosetta lander philae*, Space Science Reviews **128**, 339 (2006).
- [75] R. Mayerle *et al.*, *Langmuir Probes for the LUnar Surface (LPLUS)*, (2009).
- [76] G. Yi-bing *et al.*, *The design of the Langmuir probe onboard a seismo-electromagnetic satellite*, International Symposium on Photoelectronic Detection and Imaging (2011).
- [77] A. space, *Plasma Diagnostics: Langmuir Probes*, (2011).
- [78] D. W. M. Zachary James Bailey, *Mit master thesis: A trade space model for robotic lunar exploration*, (2010).